

**Some pages of this thesis may have been removed for copyright restrictions.**

If you have discovered material in AURA which is unlawful e.g. breaches copyright, (either yours or that of a third party) or any other law, including but not limited to those relating to patent, trademark, confidentiality, data protection, obscenity, defamation, libel, then please read our [Takedown Policy](#) and [contact the service](#) immediately

**ENVIRONMENTAL DEGRADATION OF  
POLYETHYLENE-BASED PLASTICS**

by

*Sukhvinder Kaur Chohan*

Doctor of Philosophy

THE UNIVERSITY OF ASTON IN BIRMINGHAM

May 1996

This copy of the thesis has been supplied on the condition that anyone who consults it is understood to recognise that its copyright rests with its author and that no quotation from the thesis and no information derived from it may be published without the author's prior, written consent.

# ENVIRONMENTAL DEGRADATION OF POLYETHYLENE-BASED PLASTICS

by Sukhvinder Kaur Chohan  
Ph. D. Thesis, 1996

## Summary

The criteria involved in the degradation of polyethylene-based degradable polymer samples have been investigated, with a view to obtaining a clearer mechanism of photo-biodegradation. The compatibility of degradable polymer samples during materials recycling was also studied.

Commercial and laboratory prepared degradable polymer samples were oxidised in different environments and the oxidation products formed were studied using various analytical chromatographic and spectroscopic techniques such as HPLC, FT-IR and NMR. It was found that commercial degradable polymer samples which are based on the ECO systems, degrade predominantly via the Norrish II process, whereas the other degradable systems studied (starch-filled polyethylene systems, transition metal systems, including metal carboxylate based polyethylene systems and the photoantioxidant-activator systems) photodegrade essentially via the Norrish I process. In all cases, the major photooxidation products extracted from the degradable polymer samples were found to be carboxylic acids, although, in the polymer itself a mixture of carbonyl containing products such as esters, lactones, ketones and aldehydes was observed.

The study also found that the formation of these hydrophilic carbonyl products causes surface swelling of the polymer, thus making bioerosion possible. It was thus concluded that environmental degradation of LDPE is a two step process, the initiation stage being oxidation of the polymer which gives rise to bioassimilable products, which are consequently bioeroded in the second stage, (the biodegradation step).

Recycling of the degradable polymer samples as 10% homogeneous and heterogeneous blends was carried out using a single screw extruder (180°C and 210°C) and an internal mixer (190°C). The study showed that commercial degradable polymer samples may be recycled with a minimal loss in their properties.

key words: degradable polyethylene, environmental degradation, photooxidation products, recycling,

*This Thesis is Dedicated to The  
Sweet Memory of My Loving Mother,  
Chanan Kaur*

## Acknowledgements

I would like to acknowledge, with gratitude, the guidance, advice and continuous encouragement given by my supervisor, Dr. Sahar Al-Malaika, during the tenure of this work.

I would also like to sincerely acknowledge the invaluable discussions and advice offered by Professor G. Scott and all members of the Polymer Processing and Performance Research Group.

I am grateful for the financial support supplied by the European Commission via BRITE-EURAM Project BE-3120-89, which allowed this research to be performed.

The following people must also be thanked in conducting the listed experimental work for this research:

Professor J. Lemaire and Dr. P. Dabin - molar mass measurements at Universit e de Clermont-Ferrand

Dr. M. Perry - for NMR analysis at Aston University.

Dr. P. Coe and Mr. G. Burns - for derivitisation work using DAST and SF<sub>4</sub> at University of Birmingham.

My thanks also go to Zahid Khan for his invaluable support, and kind help in processing experiments .

My appreciation must also be conveyed to my Father, S. Jagat Singh and Mother, Chanan Kaur and Sisters: Sarbjit, Paramjit, Karamjit and Harjinder and Brother, Satnam, for their love and encouragement throughout my academic career.

# CONTENTS

Title	1
Summary	2
Dedication	3
Acknowledgements	4
Contents	5
List of Tables	10
List of Figures	13
List of Diagrams	16
List of Schemes	17
<b>Chapter I: Introduction</b>	<b>20</b>
<b>1.1 General Introduction</b>	<b>21</b>
<b>1.2 Autoxidation of Hydrocarbons</b>	<b>22</b>
1.2.1 Initiation Reactions	22
1.2.2 Propagation	24
1.2.3 Termination	25
1.2.4 The Chain-Breaking Mechanism	26
1.2.5 Preventive Mechanism	26
1.2.6 Stoichiometric Peroxide Decomposers	27
1.2.7 Catalytic Peroxide Decomposers	27
<b>1.3 Photodegradation</b>	<b>29</b>
<b>1.4 Induced Oxidation and The Concept Of Photobiodegradable Plastics</b>	<b>31</b>
1.4.1 Biodegradable Plastics	32
1.4.1.1 Biodegradable Polymers in which the Macromolecular Backbone is Sensitive to Attack by Micro-Organisms	32
1.4.1.2 Polymers Containing Biodegradable Fillers	33
1.4.2 Photodegradable Plastics	34
1.4.2.1 Carbonyl Modified Polymers	35
1.4.2.2 Aromatic Ketones	36
1.4.2.3 Transition Metal Carboxylates and Related Metal Complexes	37
1.4.2.4 Antioxidant Photoactivators (APA)	38
<b>1.5 Characterisation of Oxidation Products in Polymers</b>	<b>41</b>
<b>1.6 Objectives</b>	<b>42</b>

<b>Chapter II: Experimental and Analytical Techniques</b>	<b>44</b>
<b>2.1 Materials</b>	<b>45</b>
<b>2.2 General Evaluation Techniques</b>	<b>45</b>
2.2.1 Determination of Mechanical Properties	45
2.2.2 Determination of Melt Flow Index	48
2.2.3 Determination of Molar Mass	50
2.2.4 Natural Weathering of Polymer Samples	50
2.2.5 Determination of Photo-Oxidative Behaviour on Exposure to UV Light	51
2.2.6 Determination of Thermal- Oxidative Behaviour	54
2.2.7 Thermal Oxidation in Aerated Water	54
2.2.8 Soil Analysis	54
<b>2.3 Polymer Processing and Recycling</b>	<b>55</b>
2.3.1 Laboratory Extrusion of PE Degradable Samples	55
2.3.1.1 Extrusion of the Polymer	55
2.3.2 Recycling of Commercial and Laboratory Extruded PE Degradable Samples by Multiple Extrusion using a Single Screw Extruder	56
2.3.3 Recycling of PE-based Photobiodegradable Polymer Film Samples (Commercial and Laboratory Extruded) by Multistep Processing using an Internal Mixer	60
2.3.4 Film Preparation	62
<b>2.4 Characterisation and Analytical Techniques</b>	<b>62</b>
2.4.1 Methodology for the Extraction of Photooxidation Products	62
2.4.1.1 Extraction using Water	62
2.4.1.2 Extraction using Sodium hydroxide Solutions	65
2.4.2 Derivatisation of oxidation products in degraded polymers	65
2.4.2.1 Reaction with Sulphur tetrafluoride (SF <sub>4</sub> )	67
2.4.2.2 Reaction with DAST	67
2.4.3 Infra-Red Spectroscopy	67
2.4.4 Analytical HPLC	69
2.4.5 Nuclear Magnetic Resonance Spectroscopy	69
2.4.6 Scanning Electron Microscopy	70
<b>Chapter III: Characterisation and Evaluation of Different Polyethylene Degradable Systems Based on Different Mechanisms of Degradation</b>	<b>84</b>
<b>3.1 Objectives and Methodology</b>	<b>85</b>

<b>3.2 Results</b>	89
3.2.1 Initial Physical Properties of Commercial Photodegradable Polymers	89
3.2.2 Initial Physical Properties of Laboratory Extruded Degradable Samples	90
3.2.3 Oxidation of Photodegradable Polymers	91
3.2.3.1 Initial Calculation of Carbonyl Area Index of Samples as Received	91
3.2.3.2 Photoxidation of Commercial Photodegradable Polymers Exposed in S/B UV Cabinet	92
3.2.3.3 Photoxidation of Laboratory extruded Photodegradable Polymers Exposed in S/B UV Cabinet	93
3.2.3.4 Photoxidation of Photodegradable Polymers Exposed for Natural Weathering	94
3.2.3.5 Effect of Heat on Photodegradable Samples Exposed in a Wallace Oven	95
3.2.3.6 Effect of Heat and Water on Photodegradable Samples	95
<b>3.3 Discussion</b>	96
3.3.1 Evaluation of Initial Properties of Photodegradable Samples	96
3.3.2 Effect of UV Irradiation on Photodegradable Samples	98
3.3.3 Effect of Heat on Photodegradable Samples at 70°C to Simulate Composting Environment	104
3.3.4 Overview of Results	104
<b>Chapter IV: Recycling of 10% Homogeneous and Heterogeneous Blends of Photobiodegradable Polymer Samples using a Single Screw Extruder and an Internal Mixer</b>	128
<b>4.1 Objectives and Methodology</b>	129
<b>4.2 Results</b>	135
4.2.1 Recycling of 10% Homogeneous Blends (In Virgin LDPE) of Photobiodegradable Polymer Samples (As Received) Using Single Screw Extruder	135
4.2.1.1 Melt Stability of Recycled Homogeneous Degradable-LDPE Blend Samples	135
4.2.1.2 Effect of Recycling on changes in Molar Mass	136
4.2.1.3 Effect of Recycling on Mechanical Properties	137
4.2.1.4 Effect of Recycling on the Subsequent Photoxidative Behaviour of Degradable Blends	137

4.2.2 Effect of Recycling on The Behaviour of 10% Homogeneous and Heterogeneous Degradable Blends (In LDPE) Reprocessed Using The Internal Mixer	139
4.2.2.1 Melt stability of Reprocessed Samples	139
4.2.2.2 Effect of Reprocessing on Mechanical Properties	140
4.2.2.3 Changes in Oxidation Products During Reprocessing	142
4.2.2.4 Photoxidative Behaviour After Reprocessing in an Internal Mixer.	144
<b>4.3 Discussion</b>	<b>145</b>
4.3.1 General Discussion	145
4.3.2 Effect of Recycling Temperature in a Single Screw Extruder on 10% Homogeneous Blends of Photobiodegradable Polymer films	145
4.3.3 Recycling of Photobiodegradable Polymer samples as 10% Homogeneous and Heterogeneous Blends in an Internal Mixer	148
4.3.4 Comparison of Recycled Homogenous Blends using a Single Screw Extruder and an Internal Mixer	154
4.3.5 Overview of Results	155
4.3.5.1 Number of Recycling Operations	155
4.3.5.2 Temperature	155
4.3.5.3 Photoxidation	156
<b>Chapter V: Characterisation of Photoxidation Products of Degradable Polymers and The Mechanism of Photo-Biodegradation</b>	<b>198</b>
<b>5.1 Objectives and Methodology</b>	<b>199</b>
<b>5.2 Results</b>	<b>202</b>
5.2.1 Photoxidation of Degradable Polymers	202
5.2.2 Extraction of Photoxidation Products using Water and dilute Alkali	202
5.2.3 Extraction of Photoxidation Products using 1M Sodium hydroxide	203
5.2.3.1 Treatment of Photoxidised unstabilised LDPE with 1M Sodium Hydroxide solution	203
5.2.3.2 Treatment of ECO Polymer With 1M Sodium Hydroxide	207
5.2.3.3 Treatment of Metal Carboxylate system with 1M sodium Hydroxide	210
5.2.3.4 Treatment of starch-filled PE system with 1M sodium hydroxide	213
5.2.4 Derivatisation of Photoxidation Products Still Bound in Polymer Backbone	216

5.2.5 Semi-Quantitative Analysis of Oxidation Products	218
5.2.6 Analysis of Extracted Photooxidation Products	220
5.2.6.1 FT-IR Analysis Of Extracted Products	220
5.2.6.2 Proton NMR Analysis	220
5.2.7 HPLC Analysis	223
5.2.8 SEM Analysis	224
<b>5.3 Discussion</b>	226
5.3.1 Photooxidation of Commercials degradable Polymers	226
5.3.2 Analysis of Extracted Photooxidation Products	230
5.3.3 Mechanism of Photo-Biodegradation	231
<b>Chapter VI: Conclusions and Recommendations For Further Work</b>	266
6.1 Conclusions	267
6.2 Recommendations for further work	269
<b>References</b>	272
<b>Appendix: Published work</b>	281
SC 1: A Comparative Study of the Degradability of Different Classes of Degradable Polyethylene.	
SC 2: Can Polyethylene be a Photobiodegradable Polymer?	
SC 3: Photooxidation and Biodegradation of Commercial photodegradable Polyethylenes.	

## LIST OF TABLES

Table	Page
<b>Chapter II</b>	
2.1: Classification of photobiodegradable polymer samples...	46
2.2: Summary of 'control' polymers used, their origin...	47
2.3: Experimental error calculated for MFI using sample Bso.	49
2.4: The average relative intensities calculated for uv cabinets...	53
2.5: Specifications of the Humboldt single screw extruder.	55
2.6: Conditions... for recycling using Humboldt extruder.	57
2.7: Summary of samples extruded in the lab. and their composition.	57
2.8: Conditions for recycling... at 180°C using Humboldt... extruder.	59
2.9: Conditions for recycling...at 210°C using Humboldt... extruder.	60
2.10: Samples reprocessed using the Torque Rheometer.	63
2.11: Conditions for HPLC analysis of the degradation products.	69
<b>Chapter III</b>	
3.1: Photobiodegradable polymer film samples.	86
3.2: Laboratory extruded degradable polymer samples...	87
3.3: Initial...properties...of commercial photobiodegradable...	89
3.4: Initial...properties...of laboratory extruded samples...	90
3.5: Determination of initial carbonyl area of degradables... as received.	92
3.6: Effect of photooxidation...on mechanical properties...	94
3.7: Embrittlement time...for thermal oxidation in air...	95
3.8: Embrittlement time and molar mass...at 70°C with air and water.	96

## Chapter IV

4.1: Commercial...samples used in the recycling experiments.	130
4.2: Laboratory extruded...samples...used in...this chapter.	131
4.3: Summary of photoxidised film samples used...as blends...	131
4.4: Summary of...degradable blends recycled in an internal mixer.	134
4.5: MFI of Homogeneous Blends...recycled...at 180°C and 210°C.	135
4.6: Changes in Molar mass of Blends...Recycled...180°C and 210°C	136
4.7: Mechanical properties of samples recycled...at 180°C and 210°C.	138
4.8: Control samples recycled in the internal mixer at 190°C.	140
4.9: MFI of recycled (internal mixer)...photobiodegradable samples.	141
4.10: Mechanical properties...of recycled degradable blends.	142
4.11: Changes in oxidation products after Recycling in an I.M.	143

## Chapter V

5.1: Photobiodegradable polymer film samples.	199
5.2: Time of exposure of photobiodegradable...samples.	200
5.3: Changes in FT-IR spectra of Bso at various stages of alkali...	205
5.4: Changes observed in solid state $^{13}\text{C}$ NMR of Bso...	206
5.5: Main absorptions in FT-IR spectra of A3 during alkali extraction.	209
5.6: Chemical shifts ( $^{13}\text{C}$ ) observed for A3 during alkali treatment.	209
5.7: Changes in FT-IR spectra of sample Bo1 during alkali treatment.	212
5.8: Chemical shifts for Bo1 at various stages of alkali treatment...	213
5.9: FT-IR analysis of C2 at different stages of alkali extraction.	215
5.10: Chemical shifts for C2 at various stages of alkali treatment...	215
5.11: Changes in FT-IR spectra of Bo1 and C2 after derivitisation...	217

5.12: Semi-quantitative analysis of photooxidation products...	219
5.13: The % of photooxidation products extracted...	220
5.14: FT-IR observations for the extracted photooxidation products...	221
5.15: Chemical shifts in proton NMR of extracted products...	221
5.16: Chemical shifts in the carbon NMR of extracted products...	222
5.17: Retention time and UV spectra of separated peaks...	223
5.18: Carbonyl oxidation products of LDPE based degradables...	226

## LIST OF FIGURES

Figure	Page
<b>Chapter II</b>	
2.1: FT-IR and UV spectra...of ECO polymer A3...	71
2.2: FT-IR spectrum of photodegradable...B 1...	72
2.3: FT-IR spectrum of photodegradable...Bo1...	73
2.4: FT-IR spectrum of photodegradable...B5...	74
2.5: FT-IR spectrum of photodegradable...B7...	75
2.6: FT-IR spectrum of biodegradables ...C2 and C3...	76
2.7: FT-IR spectra of biodegradable...C4...	77
2.8: FT-IR spectrum of extruded film of...Bso.	78
2.9: FT-IR of compression moulded unstabilised Polypropylene...	79
2.10: FT-IR spectrum of unstabilised...EPDM.	80
2.11: Accelerated S/B and sepap UV cabinets..	81
2.12: UV absorption spectra of polysulphone film...	82
2.13: Schematic representation of Humboldt...extruder.	83
<b>Chapter III</b>	
3.1: MFI, UTS, EB of commercial photobiodegradable samples...	106
3.2: MFI, UTS EB of laboratory extruded samples...	107
3.3: ...initial carbonyl area index of commercial degradables...	108
3.4: ...rate of photooxidation of commercial samples...	109
3.5: Changes in FT-IR spectra during exposure... of unstabilised LDPE...	110
3.6: Photooxidation of ...C2...	111
3.7: FT-IR... showing oxidation products of ...B1 during uv irradiation.	112

3.8: FT-IR... showing oxidation products of...A3 during uv irradiation...	113
3.9: ...photooxidation products formed during uv exposure for ...Bo1 &B5	114
3.10: Rate of photooxidation of starch-filled PE systems.	115
3.11: Photooxidation rate of laboratory extruded samples...	116
3.12: Decrease of EB of laboratory extruded...during uv exposure...	117
3.13: Photooxidation rate of samples exposed in natural conditions.	118
3.14: Thermal oxidation rate of samples...at... 70°C with air...	119
3.15: Thermal oxidation at... 70°C with air and water...	120
3.16: Heterogeneity index of degradable polymer samples...	121
3.17: FT-IR spectrum of expanded carbonyl region of Bso...	122
3.18: Photooxidation of laboratory extruded...mutual sensitisation...	123
3.19: ...decrease of ketone absorption...	124
3.20: Build up of vinyl and decrease of vinylidene...of A3, Bo1 and Bso.	125
3.21: ...time taken for vinyl content to reach a value of 1.00...	125
3.22: Comparison of extent and rate of...A3, Bo1 and Bso...	126
3.23: The effect of air and water on rate of thermal oxidation at 70°C...	127
 <b>Chapter IV</b>	
4.1: MFI of blends...recycled at 180°C using an extruder...	157
4.2: MFI of blends...recycled at 210°C using an extruder...	158
4.3: The effect of temperature on MFI of homogeneous blends...	159
4.4: Changes in molar mass of blends...recycled at 180°C...	160
4.5: Changes in molar mass of blends...recycled at 210°C...	161
4.6: The effect of temperature on the molar mass of recycled blends...	162
4.7: Changes in UTS of homogeneous blends...recycled at 180°C...	163

4.8: Changes in EB of 10% homogeneous blends...recycled at 180°C...	164
4.9: Changes in UTS of homogeneous blends...recycled at 210°C...	165
4.10: Changes in EB of 10% homogeneous blends...recycled at 210°C...	166
4.11: Effect of temperature on...rate of photooxidation...	167
4.12: Melt stability of...blends recycled at 190°C using an I.M...	168
4.13: Comparison of UTS of recycled...blends of sample A3...	169
4.14: Comparison of EB of recycled...A3 with control samples...	170
4.15: Comparison of UTS of recycled...blends of sample Bo1...	171
4.16: Comparison of EB of recycled...blends of sample Bo1...	172
4.17: Comparison of UTS of recycled...blends of sample B5...	173
4.18: Comparison of EB of recycled...blends of sample...	174
4.19: Comparison of UTS of recycled...blends of sample C2...	175
4.20: Comparison of EB of recycled...blends of sample C2...	176
4.21: Comparison of UTS of recycled...blends of sample C4...	177
4.22: Comparison of EB of recycled...blends of sample C4...	178
4.23: Increase in initial carbonyl content...of blends recycled in an I.M...	179
4.24: Decrease in the vinylidene content of...blends recycled in an I.M...	180
4.25: Overlay of...hydroxyl area of recycled...series I...	181
4.26: Overlay of...carbonyl area of recycled...series I...	182
4.27: Overlay of...vinyl and vinylidene areas of recycled...series I...	183
4.28: Overlay of...hydroxyl area of recycled...series II...	184
4.29: Overlay of...carbonyl area of recycled...series II...	185
4.30: Overlay of...vinyl and vinylidene areas of recycled...series II...	186
4.31: Overlay of...carbonyl area of recycled...series III...	187
4.32: Overlay of...carbonyl area of recycled...series IV...	188

4.33: Overlay of...carbonyl spectra... recycled degradables series V...	189
4.34: Photoxidation rates...recycled blends in I.M. at 190°C...	190
4.35: Comparison of the rates of photoxidation...recycled blends...	191
4.36: Evidence of crosslinking reactions during processing at 190°C...	192
4.37: Evidence of crosslinking reactions during processing at 210°C...	193
4.38: Changes in oxidation products for Series I...recycling in I.M...	194
4.39: Changes in oxidation products for Series II...recycling in I.M...	195
4.40 Changes in oxidation products for Series III...recycling in I.M...	196
4.41: Comparison of MFI...internal mixer and single screw extruder...	197

## Chapter V

5.1: Photoxidation...of Bso, A3, Bo1 and C2...	236
5.2: Photoxidation products of commercial degradable samples...	237
5.3: FT-IR spectra of photoxidised...LDPE...water extraction.	238
5.4: FT-IR spectra...of photoxidised...Bso...0.01M NaOH extraction.	239
5.5: FT-IR spectra of photoxidised...Bso-B...1M alkali extraction.	240
5.6: Solid state <sup>13</sup> CNMR spectra of Bso...1M alkali extraction.	241
5.7: FT-IR spectra of...Bso and insoluble precipitate...	242
5.8: FT-IR spectra of ECO polymer...1M alkali extraction.	243
5.9: Solid state <sup>13</sup> CNMR spectra of ECO polymer...1M alkali extraction.	244
5.10: FT-IR spectra of...Bo1... 1M alkali extraction.	245
5.11: Solid state <sup>13</sup> CNMR spectra...Bo1...1M alkali extraction.	246
5.12: FT-IR spectra...C2...1M alkali extraction.	247
5.13: Solid state <sup>13</sup> CNMR spectra of ...C2...1M alkali extraction.	248
5.14: FT-IR spectra...Bo1 derivitised with DAST...SF4 for 10 hours.	249

5.15: FT-IR spectra...C2 derivitised with DAST...SF4 for 10 hours.	250
5.16: FT-IR spectra...Bo1 derivitised with DAST for 24, 48 and 72 hours.	251
5.17: Area of photoxidation products...A3 and Bo1...	252
5.18: FT-IR spectra extracted photoxidation products...	253
5.19: Proton NMR spectra of extracted photoxidation products...	254
5.20: <sup>13</sup> Carbon NMR spectra of extracted photoxidation products...	255
5.21: HPLC chromatogram of the extracted photoxidation products...	256
5.22: UV spectra of the ten chromatographic peaks...of sample Bo1.	257
5.23: UV spectra of fumaric acid	258
5.24: SEM of A3 during abiotic oxidation	259
5.25: SEM of A3 during biotic oxidation	260
5.26: SEM of Bo1 during abiotic oxidation	261
5.27: SEM of Bo1 during biotic oxidation	262
5.28: SEM of C2 during abiotic oxidation	263
5.29: SEM of C2 during biotic oxidation	264
5.30: SEM of Bso during abiotic and biotic oxidation	265

## LIST OF DIAGRAMS

Diagram	Page
2.1: ...the shape and size of test specimens for mechanical properties...	48
2.2: Diagram showing typical stress/strain curve for polyethylene.	48
2.3: Distribution of the spectral intensity output of uv radiation...	52
2.4: Diagram showing the calculation for carbonyl content	68

## LIST OF SCHEMES

Scheme	Page
<b>Chapter I</b>	
1.1: Autoxidation of hydrocarbons.	22
1.2: Types of chain breaking mechanisms.	26
1.3: Mechanism of action of aromatic ketones.	36
1.4: Photoreduction of Ferric Acetylacetonate.	37
1.5: Mechanism of action of APA systems.	40
<b>Chapter II</b>	
2.1: Recycling of homogeneous blends using Humboldt extruder.	58
2.2: Recycling of blends using an internal mixer.	61
2.3: Extraction of photoxidation products using water.	64
2.4: Extraction of photoxidation products using alkali.	66
<b>Chapter III</b>	
3.1: Overview of methodology adopted in chapter 3.	88
<b>Chapter IV</b>	
4.1: ...methodology adopted for recycling of blends using extruder.	132
4.2: ...methodology adopted for recycling blends using internal mixer.	133
4.3: Formation of radicals in PE during processing.	148
4.4: Degradation of PP during processing.	150
4.5: Decomposition of hydroperoxides during processing of PE.	152
4.6: Competing reactions in PE during processing.	154

## Chapter V

5.1: ...overall methodology adopted for analysis of degradables...	201
5.2: Flowchart of methodology adopted for analysis of Bso.	204
5.3: Flowchart of methodology adopted for analysis of A3.	208
5.4: Flowchart of methodology adopted for analysis of Bo1.	211
5.5: Flowchart of methodology adopted for analysis of C2.	214
5.6: Flowchart of methodology adopted for SEM analysis...	225
5.7: Formation of photooxidation products during uv irradiation.	228
5.8: Formation of dicarboxylic acids during uv irradiation.	232
5.9: Mechanism of Photobiodegradation.	235

# CHAPTER I

## INTRODUCTION

## CHAPTER I

### INTRODUCTION

#### 1.1 GENERAL INTRODUCTION

Degradable polymers have been engineered to address the problems of plastics waste and litter, which has risen dramatically over the last three decades [1-5]. The problem of plastics waste and litter is not only an aesthetic one in areas of natural beauty, but, may also result in potential health threats to wildlife and humans [6-7]. Recently, due to the concern over the increasing plastics waste and litter, plastic manufacturers have produced exaggerated claims to their plastics being "environmentally friendly" or "biodegradable" [8].

To the 'green' consumer the terms environmentally friendly or biodegradable appear to be an ecologically satisfactory solution to the problems of plastics waste and litter. However, to the scientific community, the term biodegradable has no exact meaning [4]. Several recent international conferences of eminent scientists in this field have tried to clarify the definitions of degradability (photo and biodegradable) [9-10].

One of the main problems is distinguishing the fundamental principles underlying the processes of photodegradation (initiated by agents such as water, oxygen, heat and sunlight) and biodegradation (by microorganisms). In addition, it has frequently been stated that degradable plastics interfere with other waste management procedures such as composting, incineration and most importantly materials recycling [11-12].

## 1.2 AUTOXIDATION OF HYDROCARBONS

All organic compounds are susceptible to attack by molecular oxygen. The conversion of polyolefins to finished products is usually accomplished by subjecting the polymer to high temperatures and high shear stresses. Furthermore, a small concentration of oxygen is always present during the processing stage (either dissolved in the polymer or trapped in the polymer feed) which leads to oxidative degradation of the polymer. The degradation process continues during the service life of the polymer product when it is subjected to other environmental factors such as heat and light. The modern theories of free radical autoxidation mechanism of polyolefins are based on earlier studies carried out by Bolland and co-workers at the British Rubber Producers Association in the field of natural rubber during the 1940's [13-16]. Scheme 1.1 shows the basic free radical autoxidation processes involved in polymer oxidation [13-14].

### INITIATION



### PROPAGATION



### TERMINATION



Scheme 1.1: Autoxidation of hydrocarbons [13-14].

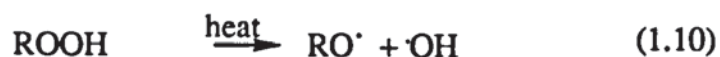
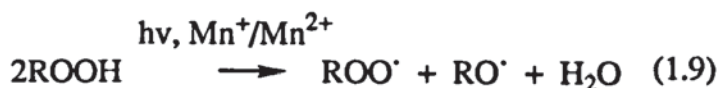
### 1.2.1 Initiation Reactions

The free radical mechanism of polymer oxidation is initiated by thermal energy, uv light, high energy radiation or mechanical stress. Commercial hydrocarbon polymers often contain chemical impurities such as small

amounts of oxygen containing species, unsaturation, peroxides and metal ions as catalyst residues. When polymer bonds are ruptured under any of the above conditions, alkyl and alkylperoxyl radicals are formed which in the presence of oxygen start the autoxidation process. As oxidation continues and the concentration of hydroperoxides increases in the substrate, the free radical decomposition of hydroperoxide becomes the predominant initiating reaction [17].

The rate of hydroperoxide decomposition is influenced by many factors:

1) the hydroperoxide concentration, 2) induced decomposition by self generated free radicals, 3) acid catalysed decomposition and 4) metal catalysed decomposition [17]. Metal catalysed decomposition shows the most pronounced effect; the pro-oxidant effect of transition metal ion via the redox reactions 1.7 and 1.8 is well established [17-19].



The most effective ions are those which are capable of undergoing a one electron oxidation/reduction between two states of comparable stability e.g.  $Fe^{3+}/Fe^{2+}$  or  $Co^{2+}/Co^{3+}$  [17]. It is recognised that catalysis occurs by a redox mechanism in which reactions 1.7 and 1.8 together bring about the breakdown of hydroperoxides to free radical products [17]. The activation energy for metal catalysed decomposition is lower ( $\sim 42.5\text{-}85 \text{ kJ mol}^{-1}$ , reaction 1.9) than that for thermal decomposition of hydroperoxides ( $\sim 170\text{-}191 \text{ kJ mol}^{-1}$ , reaction 1.10) [17]. Reactions 1.7 and 1.8 regenerate the metal

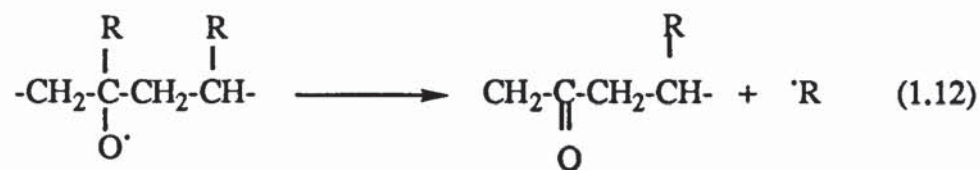
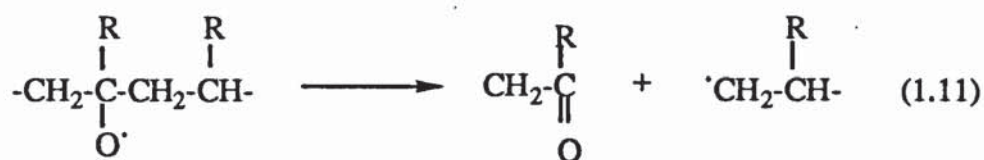
catalyst, and therefore only a small amount of metal is required to accelerate the decomposition of hydroperoxides.

### 1.2.2 Propagation

The macroalkyl radicals formed during the initiation stage react with oxygen to give peroxy radicals (see reaction 1.2) which can abstract a hydrogen from another polymer molecule to form hydroperoxides, and thus propagate the chain reaction. Reaction 1.3 which requires a higher activation energy, since it involves the breakage of an activated carbon-hydrogen bond, is the rate determining step [17]. In aliphatic hydrocarbons, intermolecular hydrogen abstraction predominates whilst in branched hydrocarbons (e.g. polypropylene) intramolecular propagation predominates [20].

The nature of the substrate structure has a profound effect on the rate of propagation. In addition, peroxy radicals are quite selective in hydrogen abstraction- abstracting principally a tertiary hydrogen in preference to secondary or primary hydrogen.

The formed hydroperoxide can undergo homolytic cleavage (reaction 1.10) to give very reactive alkoxy and hydroxyl radicals which can react with additional polymer molecules and thus initiate new oxidative chains; hence, as hydroperoxides accumulate and decompose into radicals the rate of oxidation accelerates. It can either undergo a  $\beta$ -scission process resulting in the fragmentation of the polymer chain together with the formation of carbonyl groups and alkyl radicals (reaction 1.11) or lead to the formation of an in-chain ketone and an alkyl radical, (reaction 1.12) [14, 21].



### 1.2.3 Termination

The rate at which oxidation proceeds for most organic compounds is generally not dependent on oxygen pressure. Under normal oxygen pressures and moderate temperatures the chain reaction terminates predominantly by reaction 1.6. However, at very low oxygen pressures or when the alkyl radical is stable towards oxygen, reaction 1.4 becomes more important [22-23].

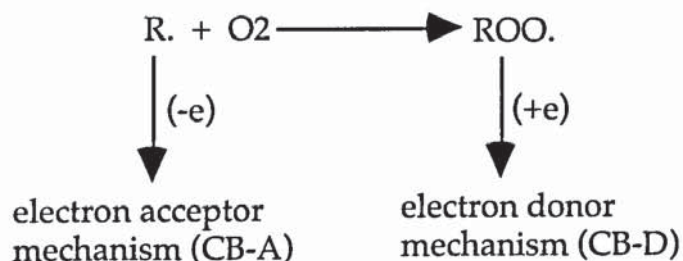
The free radical chain mechanism of autoxidation can be interrupted with the use of antioxidants [24-27]. Antioxidants act via two main mechanisms which are [26-27]:-

1) **Chain Breaking (CB) Mechanism:-** removes the two most important propagating species ( $\text{R}\cdot$  and  $\text{ROO}\cdot$ ).

2) **Preventive Mechanism:-** prevents the introduction of chain initiating radicals ( $\text{ROOH}$ ) into the system or removes them by a reaction which does not give radicals. The degradable systems discussed in this work operate by preventive mechanisms, hence, greater detail will be presented for this mechanism.

### 1.2.4 The Chain-Breaking Mechanism.

The chain-breaking mechanism can be further sub-divided into two groups, which are summarised in scheme 1.2 [28].

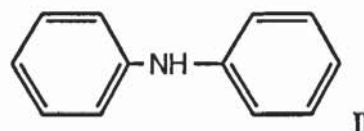
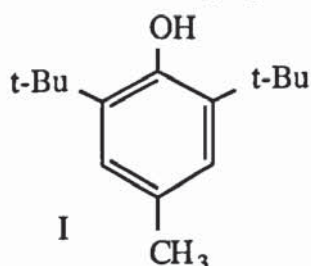


Scheme 1.2: Types of chain breaking mechanisms [28].

The chain-breaking electron acceptor mechanism (CB-A) involves the removal of the alkyl radical by an oxidation process. Examples of CB-A are nitro compounds [29-32] and stable free radicals such as Galvinoxyl [33]. The chain breaking donor mechanism (CB-D) involves the reduction of the alkylperoxyl radical to give a hydroperoxide [28] as shown in reaction 1.13.



The two best known classes of this type are the hindered phenols, I and the aromatic amines, II [34].



### 1.2.5 Preventive Mechanisms.

Preventive mechanisms include the introduction of agents which prevent the initiation of autoxidation mechanism by removing sources of free

radicals. Preventive mechanisms include metal ion deactivators, uv light deactivators and decomposition of hydroperoxides to non radical products [27]. The first two mechanisms merely retard rather than inhibit the formation of free radicals from hydroperoxides. The decomposition of hydroperoxides to non radical products (peroxidolytic mechanism) is the most important of the preventive mechanisms. There are two types of the peroxidolytic antioxidants:-

- 1) Stoichiometric (hydro)peroxide decomposers (PD-S)
- 2) Catalytic (hydro)peroxide decomposers (PD-C)

### 1.2.6 Stoichiometric Peroxide Decomposers

The most widely used PD-S antioxidants are the phosphite esters, which act mainly by reducing hydroperoxides to alcohols and the corresponding phosphate esters in a stoichiometric reaction (one molecule of peroxide is decomposed by one phosphite molecule), see reaction 1.14 [27].

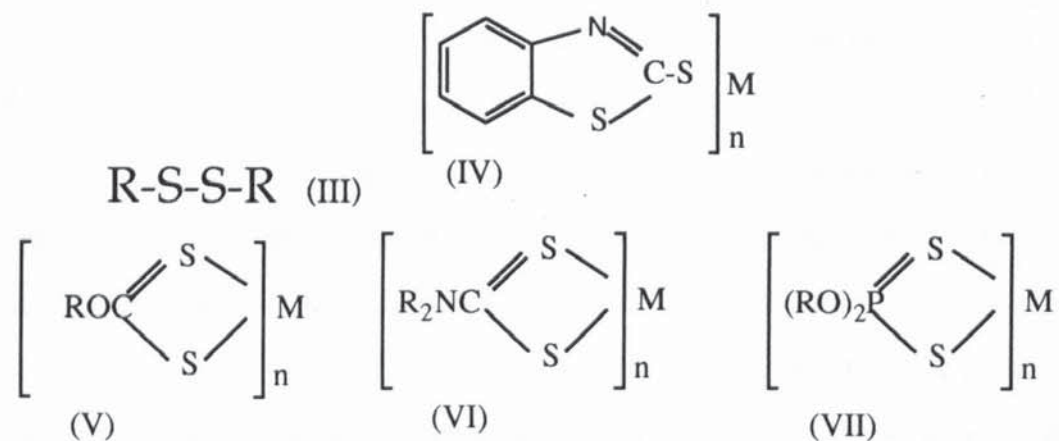


### 1.2.7 Catalytic Peroxide Decomposers

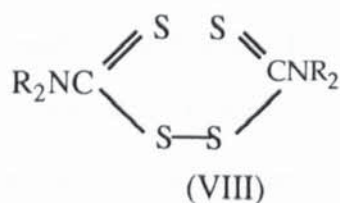
The pioneering studies of Denison [35] and Kennerly and Patterson [36] led to the recognition of a variety of sulphur-based peroxidolytic agents which function by a catalytic mechanism. It was later found that these sulphur based antioxidants have three features in common [37-38]:

- 1) the effective antioxidant is not the parent sulphur compound but an oxidation product formed from it.
- 2) the effective antioxidant is a catalyst for the ionic decomposition of hydroperoxides.
- 3) the antioxidant stage is frequently preceded by a prooxidant stage which varies in intensity depending on the structure of the sulphur compound.

Examples of catalytic peroxide decomposers include the dialkyl sulphides (III), metal mercapthiazolates (IV), metal xanthates (V) and metal dithiolates (which include dithiocarbamates (VI) and dithiophosphates (VII) [27].



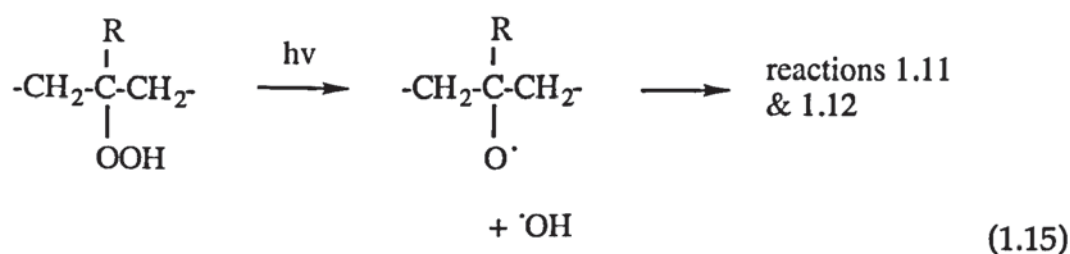
Metal complexes of dithioic acids (for example dithiocarbamates, DRC) were the earliest systems to be investigated because of their importance in rubbers and plastics, and in this work degradables containing iron and nickel dithiocarbamates are studied. Al-Malaika and co-workers [39-46] have extensively studied their mechanisms. They re-iterated earlier findings that these compounds undergo a series of oxidation reactions involving free radicals with sulphur acids as the main catalysts for the final catalytic ionic decomposition of hydroperoxides. The initial oxidation products formed for Fe and Ni DRC are disulphides (VIII). Metal dithiolates are, therefore, the precursors of the effective catalytic peroxide decomposers. This fact has been exploited in the development of highly effective thermal and uv stabilisers for polyolefins.



## 1.3 PHOTODEGRADATION.

'Pure' polyolefins contain only C-C and C-H bonds and therefore should be immune to oxidation reactions in the presence of sunlight. However, it has been recognised for many years that unsaturation and many oxygen-containing impurities are introduced into polyolefins (such as PE) during the manufacturing or fabricating stages. These impurities may absorb uv wavelengths and thus act as initiators for photooxidation [47]. In addition, the hydroperoxides formed in the autoxidation process by thermal and mechanoxidation (the primary products of oxidation) may also act as photoinitiators. Scott and co-workers found that in LDPE as the concentration of peroxides increased with processing time, increased initial rates of photooxidation were observed [48].

Photolysis of hydroperoxides can result in the formation of carbonyl compounds such as ketones, as shown in reaction 1.15 [49].

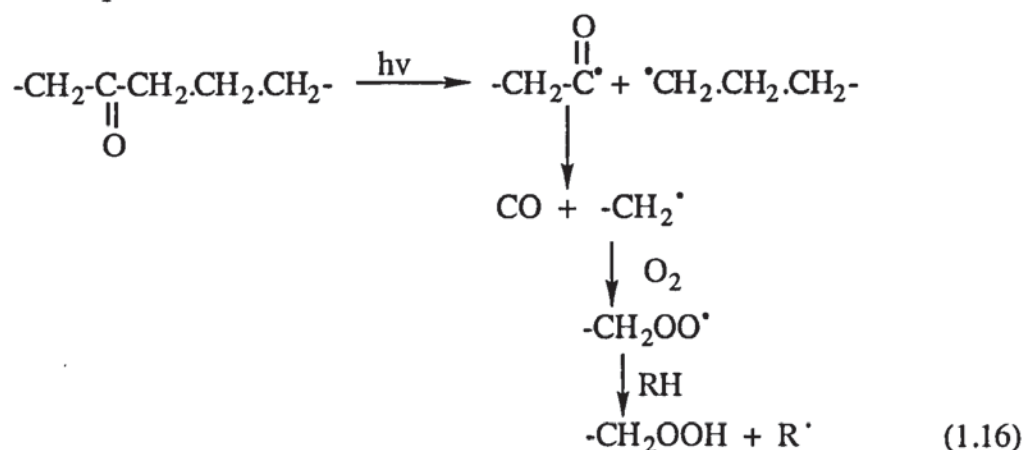


For example, Norrish and others have shown that at 313 nm tert-butyl hydroperoxide and cumene hydroperoxide decompose with the formation of acetophenone [49-50].

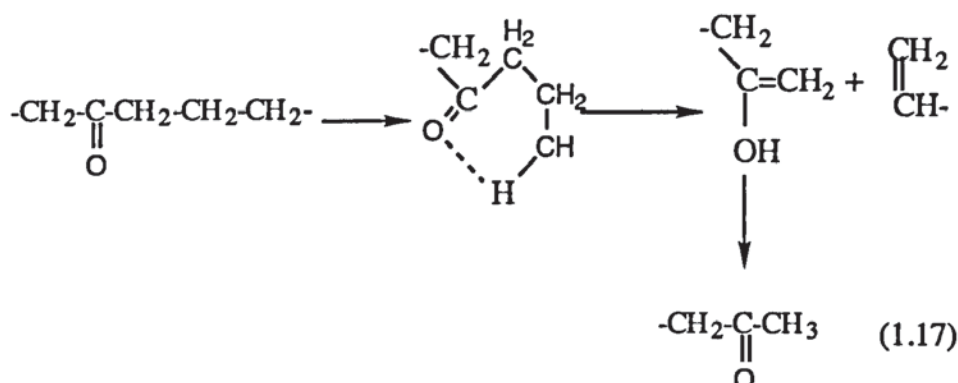
Carbonyl species formed as a result of melt degradation and photolysis of hydroperoxides can initiate further photochemical reactions [21,51]. However, carbonyl sensitisation is important only during the later stages of

photooxidation [47]. The two main primary photochemical processes which take place are [21,51]:

**Norrish I process:** which leads to the formation of free radicals which are precursors of further free radical reactions. The macroradicals  $-\text{CH}_2\cdot$  (in reaction 1.16) can then undergo further reactions with oxygen to give peroxy radicals. The peroxy radicals then abstract hydrogen atoms from the polymer substrate to form hydroperoxides and thus continue the autoxidation process, see reaction 1.16.



**Norrish II process:** occurs when there exists at least one hydrogen atom on the gamma carbon with respect to the carbonyl group. The reaction occurs via a six-membered cyclic intermediate involving intramolecular hydrogen atom abstraction and produces a ketone and a vinyl group in the polymer, see reaction 1.17.



Both mechanisms are responsible for the molecular breakdown of the polymer chain leading to degradation. As a result of Norrish I, which gives

rise to two free radicals, the main photooxidation species formed are carboxylic acids. However, Norrish II process gives rise predominantly to a vinyl and a ketone group as the main photooxidation species [51].

#### 1.4 INDUCED OXIDATION AND THE CONCEPT OF PHOTOBIODEGRADABLE PLASTICS.

The initiation and propagation stages of the free radical chain reactions can be further purposely accelerated during uv irradiation by incorporating either uv absorbing groups, which can initiate photolysis, or by incorporating groups which will generate free radicals which can then take part in the chain reactions. The result is to induce the rate of oxidation in the polymer by sensitisation [52-53]. Consequently, the purposely designed plastic will degrade much faster over the conventional stabilised plastic. This concept of induced degradation of plastics during uv irradiation has been viewed as an effective method to deal with the growing problems of plastics waste and litter [1-5,52-55]. However, before the plastic is induced to degrade it must fulfil certain criteria that enables it to be useful in its application, the most important of which are [1,56] :

- (i) if used in packaging, especially when in contact with food stuffs, it must not contribute to taste, odour, or toxicity [56]
- (ii) it must be stable and maintain its desirable physical properties for at least the life-time of the product [1].
- (iii) it must be resistant to attack by micro-organisms during its service life [56].
- (iv) it should (bio-) degrade when it has served its function [56].

Until recently the last two points were thought to be inconsistent with each other since it was believed if plastics were biologically degradable then they would no longer provide adequate protection against the attack of microorganisms on its contents. It has been found that the resistance of conventional plastics to microorganisms is primarily due to two factors [56]:

- (i) the low surface area and relative impermeability of plastic films and,
- (ii) the very high molar mass of plastics materials.

Induced degradable plastics are thus made from polymers designed to break down in the environment through various mechanisms often initiated by absorption of light.

#### **1.4.1 Biodegradable Plastics**

Biodegradable materials degrade through the action of enzymes produced by bacterial, fungus, yeast and moulds. Enzymatic degradation involves the catalysed hydrolysis of the backbone or side chains of the polymer [57]. In general, commodity plastics commonly used (for example polyolefins) are hydrophobic in nature which largely accounts for their success as barrier materials. To make plastics inherently biodegradable will make them less useful as packaging materials. The aim, therefore, is to induce biodegradability when required. Two main strategies have been used [58]:-

##### **1.4.1.1 Biodegradable Polymers in which the Macromolecular Backbone is Sensitive to Attack by Micro-organisms.**

Polymers containing ester groups in their repeat units open up the polymer backbone to hydrolytic attack by non-specific enzymes (esterases) which are secreted by soil micro-organisms [58]. The polymer chains are broken down into small molecules which are readily assimilated by soil micro-organisms (biodegraded).

Imperial Chemical Industries (ICI) have marketed a novel thermoplastic polyester under the trade name BIOPOL, that is prepared by a bacterial fermentation process [59-62]. This biologically produced plastic based on a copolymer linear polyester of 3-hydroxybutyric acid and hydrovaleric acid has been shown to be totally degradable by soil micro-organisms [62].

Amide and urethane groups are also susceptible to biodegradation which is a consequence of their chemical relationship to the naturally occurring polypeptides, the building blocks of proteins which like the synthetic polyamides contain hydrolysable amide groups [63]. Other polymers based on polylactic acid and poly epsilon-caprolactone have also been produced and are currently in use in biomedical applications [64].

#### 1.4.1.2 Polymers Containing Biodegradable Fillers.

Griffin [65] developed these types of biodegradable plastics in the 1970's. The rationale behind this type of degradable plastics is to incorporate natural biodegradable fillers such as starch and cellulose [66]. These natural fillers, for example starch, have been reported [57,67] to degrade readily in soil, sewage and marine environments where micro-organisms are active. However, the rate of this process depends not only on the structure of the polymer but also on the availability of the appropriate micro-organisms. The natural polymers offer the enzyme systems of the micro-organisms a foothold on the polymer surface - a prerequisite for enzymatic action. It is claimed [56] that this preferential attack on the natural filler leaves a mechanically weak plastic which leads to the breakdown of the synthetic polymer chains. The natural polymer serves as the nutrient carbon source for the micro-organisms resulting in the release of non-specific oxidant enzymes which can attack the synthetic polymer chains leading to biodegradation [67-68].

These starch-filled polyethylene systems have been further developed by the incorporation of small concentrations of photosensitisers based on transition metal ions to speed up the biodegradability process; for example, Ampacet who market many starch-filled polyethylene polymers often add iron stearate which acts as a photo pro-oxidant .

#### 1.4.2 Photodegradable Plastics

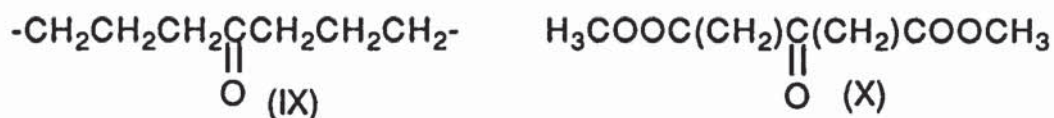
These types of degradable plastics rely on the absorption of uv light. There are two quite distinct processes which utilise sunlight as an initiator for inducing degradability. The first involves the photolysis of polymers containing uv sensitive groups and the second involves the use of photoinitiators for the oxidation of the polymer substrates [69], resulting in the breakdown of the polymer matrix into very small fragments. The ensuing self-accelerating reduction of the molar mass by chain scission and unzipping of the chain end causes the rapid and total breakdown of the polymer. Therefore, once the reaction has been triggered by the sunlight it will irreversibly continue even in the absence of light but in the presence of oxygen. It was shown [70] that the photo-oxidation products formed are subsequently removed continuously by certain micro-organisms leading to the ultimate biodegradation of the polymer.

It is known [69] that different oxygen containing impurities are formed in the polymer during processing and fabrication and these act subsequently as chromophores, thus contributing to the photosensitising effect of the polymer. In theory, therefore, omission of the conventional antioxidants and melt stabilisers could lead to fabricated products of reduced life-times. In practice, however, this does not provide a satisfactory solution to the problem since this leads to irreversible and uncontrollable changes in the melt viscosity of the polymer during processing.

#### 1.4.2.1 Carbonyl Modified Polymers.

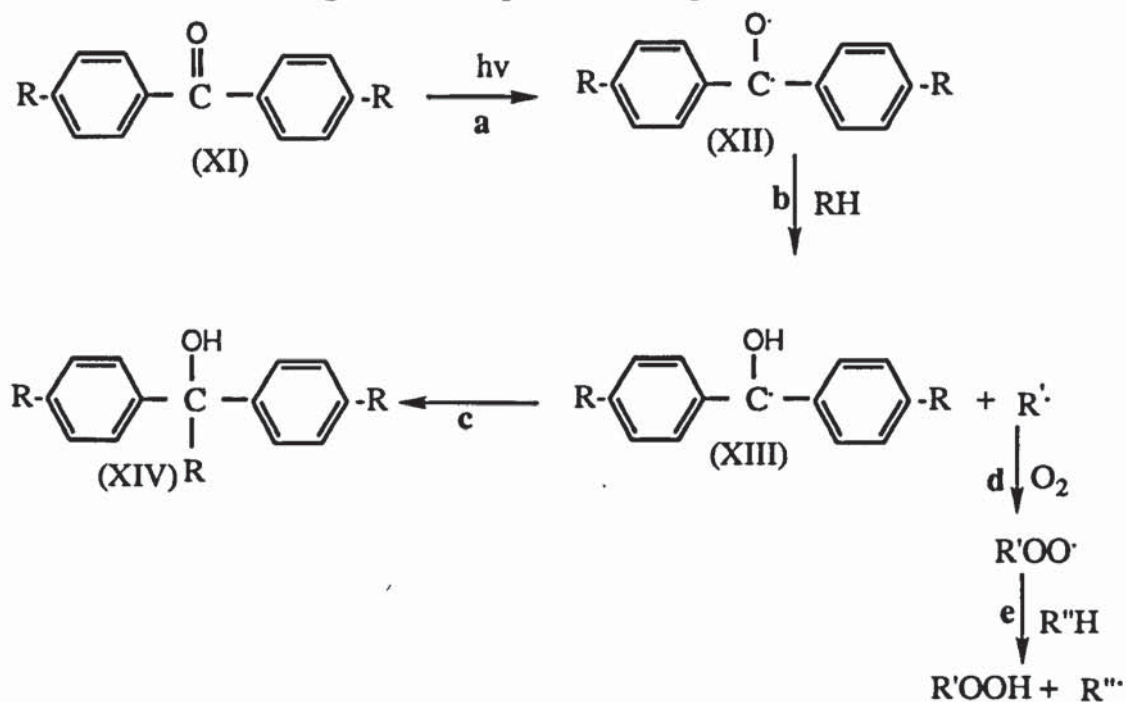
It has been shown (section 1.3) that carbonyl groups formed during melt oxidation can readily undergo photolysis on absorption of uv light by the well known Norrish reactions. By taking advantages of these fundamental studies Guillet and co-workers [6,71-72] were able to develop carbonyl containing polymers with enhanced sensitivity to uv irradiation (the 'Guillet' polymers are marketed as ECOLYTE). The basis of the process by which ECOLYTE plastics are made degradable is to introduce into the structure of the polymer a sensitising group which absorbs radiation in the 290-330 nm region of the solar spectrum. This was done by copolymerisation of vinyl ketones with olefins. Polymers of this type do not require oxygen to initiate photodegradation since this occurs rapidly on absorption of a photon by the carbonyl groups causing the chain to break at a point adjacent to the absorbing group (via Norrish-I: see reaction 1.16). The reaction involves the formation of free radicals which can initiate further degradation during the latter stages of the UV degradation of polyethylene. As the molecular chains are broken the molar mass is reduced, and the number of chain ends increases leading eventually to polymer embrittlement. This makes the plastic more susceptible to biodegradation by microorganisms. Degradation in the ECOLYTE systems commences without an induction period. However, these plastics are widely used for short term purposes, for example disposable cups and six pack beverage containers.

An alternative to the ecolyte polymers are the ethylene copolymers (ECO) which work on the same principle as the former. This plastic is made photosensitive by copolymerising PE with carbon monoxide. The photosensitive group is in-chain, see IX. There are many variations on the ecolyte and ECO polymers, such as the photodegradable polyesters (X) [73].



#### 1.4.2.2 Aromatic Ketones.

Most aromatic ketones absorb strongly above 300 nm; yet, unlike their aliphatic analogous, aromatic ketones (for example benzophenone, scheme 1.3, XI) cannot undergo Norrish photodecomposition reactions.



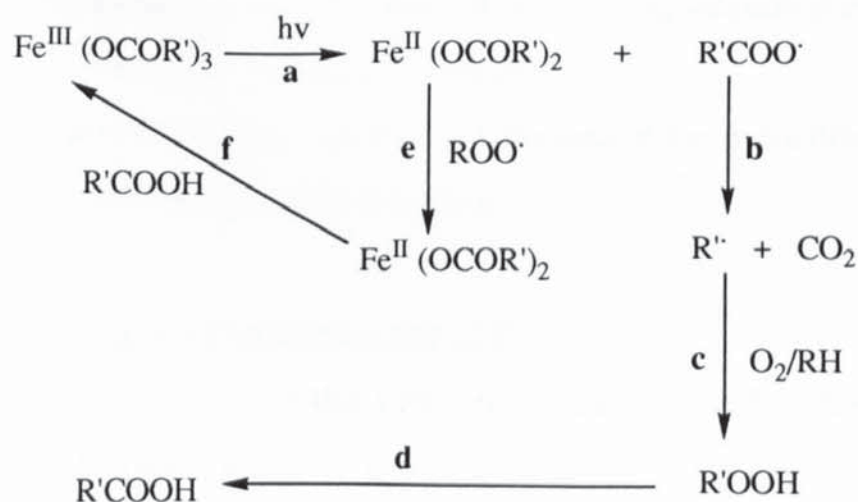
Scheme 1.3: Mechanism of action of aromatic ketones

The excited triplet states of aromatic ketones (XII) are highly reactive and are capable of abstracting a hydrogen atom from the polymer and initiating the homolytic reactions on the polymer backbone [69]. The macroradical generated,  $\text{R}\cdot$ , then initiates the oxidative chain processes. It has been reported [74-76] that aromatic ketones are effective photo pro-oxidants for the more oxidisable polymers such as polypropylene, polystyrene and polyisoprene but are less effective in polyethylene [48,77]. In the case of the latter the photodegradation is retarded due to the formation of the

relatively stable ketyl species (XIII), which lead to favourable competition between chain termination (reaction c) and chain initiation processes (reaction d,e) in scheme 1.3.

#### 1.4.2.3. Transition Metal Carboxylates and Related Metal Complexes.

The usefulness of such transition metal complexes as uv activators in initiating polymer photodegradation has been examined [48,77-80]. Metal carboxylates, for example, were shown to lead to highly accelerated oxidative degradation. The mechanism thought [69] to be involved, for example, ferric acetylacetonate see scheme 1.4, is photoreduction of the trivalent salt (reaction a) with the formation of an initiating free radical which starts a normal autoxidation chain resulting in the formation of carboxylic acids as the major end products of photo-oxidation (reaction b - d). The carboxylic acids in the presence of peroxy radicals can convert the divalent ion formed in the photoreduction reaction back to the ferric carboxylate (reactions e-f) which repeats the reaction again. Hence, the reaction is self-perpetuating and is extremely fast [69].



Scheme 1.4: Photoreduction of ferric Acetylacetonate

Although iron acetylacetonates (FeAcAc) and iron stearates are known to be highly active photoactivators for polyethylene, they suffer from a serious

practical deficiency in that they do not have any melt stabilising role [48,78-79]. The polymer therefore requires an additional melt stabiliser during processing.

Transition metal complexes thus cause a rapid and auto accelerating mode of photooxidation; however, they offer no delay time prior to the onset of degradation in addition to the fact that they require an additional melt stabiliser. There is, therefore, a new requirement for stabilisers which initially protects the polymer from photooxidation for a predetermined period depending on the use of the polymer, followed by a rapid and complete degradation at the end of the induction period. Such additives are termed 'ideal antioxidant photoactivators' (or delayed action photoactivators) and are the basis of time-controlled stabilisation of plastics which are used commercially in agricultural mulch films [69]. The ideal antioxidant-photoactivator must satisfy a number of requirements [59,78-79]:

- (i) it should be a good melt stabiliser during processing
- (ii) it should not sensitise the polymer to degradation during storage
- (iii) it must give an induction period
- (iv) the rate of photo-oxidation at the end of the induction period should be rapid and complete.

#### 1.4.2.4 Antioxidant Photoactivators (APA)

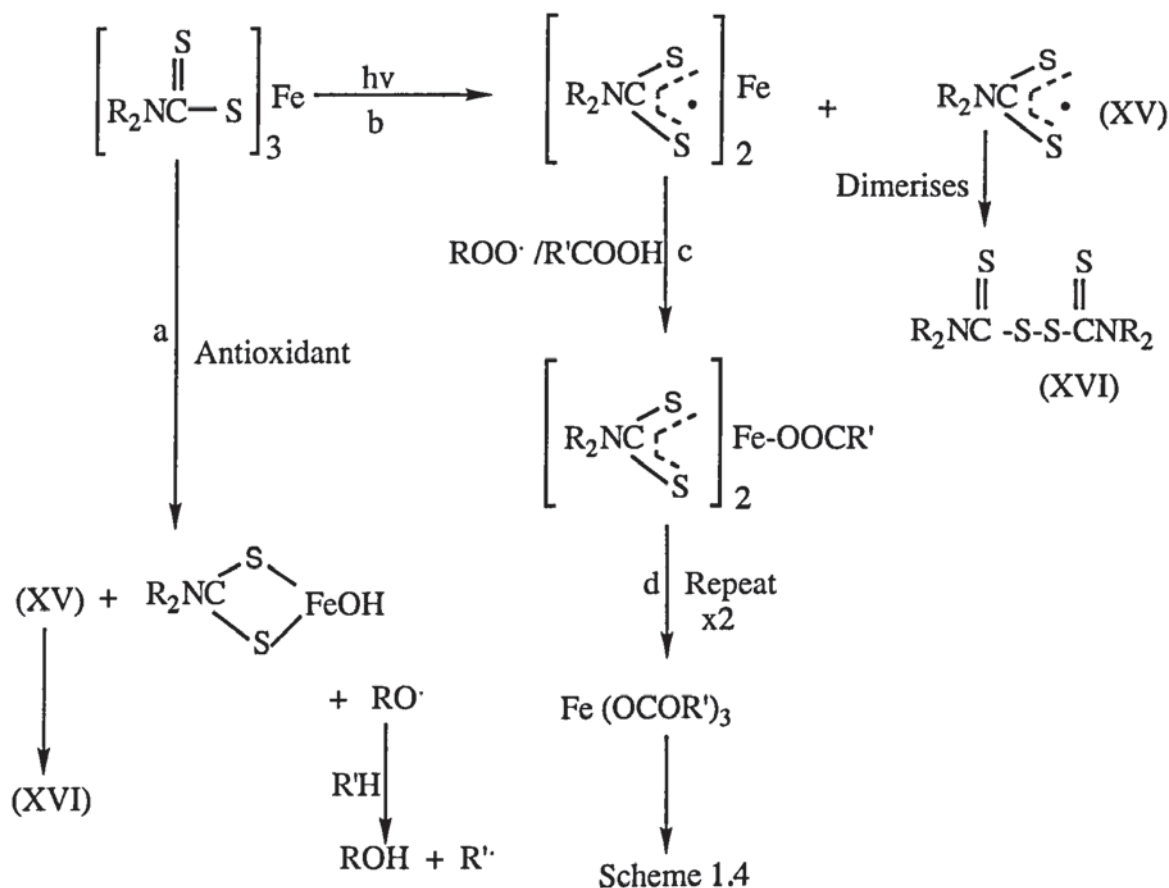
The practical solution to the problem of time-control stabilisation came from a fundamental study of antioxidant action. APA are photosensitising additives which act as antioxidants during processing but which on subsequent exposure to uv irradiation act as powerful photoactivators [67,72,79]. The antioxidants used are mainly metal dithiocarbamates. Iron dialkyl dithiocarbamates were shown [48,79-80] to behave in a similar

fashion to that of the iron stearates and acetylacetonates in that they are strong photosensitisers. The zinc complex is not a good light stabiliser since it is readily photolysed by uv light, while the nickel dithiocarbamates are by contrast excellent photostabilisers [44,79-80]. All the dithiocarbamates are effective melt stabilisers for polyolefins.

To achieve maximum flexibility in induction time control, two-component uv stabiliser/uv sensitiser combinations have been developed commercially [69] and are known as the 'Scott-Gilead' process. It has been found [78-79] that using combinations of iron and nickel dithiocarbamates gives the ideal behaviour required in time-controlled photodegradable films that are used extensively in agriculture. The nickel complex part of the system (photostabiliser) controls the induction period to photo-oxidation whilst the iron complex (photoactivator) is primarily responsible for the photodegradation of the polymer at the end of the induction period [78]. Most importantly, both the iron and nickel dithiocarbamates are effective thermal antioxidants by virtue of their ability to destroy hydroperoxides [80]. At low concentration, nickel dithiocarbamates sensitise iron dithiocarbamates leading to mutual photosensitisation whereas at high concentration they cause a pronounced but controllable induction period. The presence of a nickel complex does not modify the photoactivating effect of the ionic iron liberated from the iron dithiocarbamate so that long induction periods can be obtained followed by a very rapid photo-oxidation rate.

(i) Mechanism Of Action in APA systems.

The melt stabilisation of iron dithiocarbamates during processing has been reported by many authors [78,80] (see scheme 1.5 reaction a) due to the oxidation of the dithiocarbamate ligand to low molecular weight sulphur



Scheme 1.5: Mechanism of action of APA systems

acids ( $\text{SO}_2$  and  $\text{SO}_3$ ), which act as ionic catalysts for the destruction of hydroperoxides.

The photo-oxidation of polymers containing APA does not commence until the APA complex has been completely destroyed by uv light liberating free radicals and the ionic iron, (scheme 1.5 reaction b-d). The ionic iron reacts with the macrocarboxylic acid formed from the polymer oxidation and is converted to the corresponding polymer soluble carboxylate, thus causing a rapid oxidation at the end of the induction period (as shown in scheme 1.5).

By varying the concentration of the iron dithiocarbamate and by the addition of a small concentration of the nickel dithiocarbamate in the

polymer, both the induction period and the rate of photo-oxidation at the end of the induction period can be easily controlled.

During the induction period the nickel complexes behave as photo-antioxidants by catalytically destroying the hydroperoxides that are formed during photo-oxidation. The onset of photodegradation (due to the APA complex), which is usually complemented by the depletion of the nickel complex, results in the formation of low molecular weight carboxylic acids which are easily ingested by the micro-organisms, thus leading to the ultimate biodegradation of the polymer.

#### 1.5. CHARACTERISATION OF OXIDATION PRODUCTS IN POLYMERS.

Various techniques have been used to study the degradation of polymers and their degradation products [52]. These include size exclusion chromatography (or gel permeation chromatography) to measure the decrease in molecular weight [81-82], UV spectroscopy to follow changes in the oxidation products [83], NMR and ESR to study radical formation [84].

One of the most widely employed instrumental techniques is the use of Infrared spectroscopy and FT-IR [85-86]. Infrared analysis of oxidised polymers shows a broad, composite carbonyl peak consisting of several convoluted carbonyl peaks. To resolve the convoluted carbonyl peaks, several researchers have used derivatisation methods, using sulphur dioxide [87], nitric oxide [88] and sulphur tetrafluoride [89-91].

Many researchers have attempted to identify low molecular weight volatile oxidation products using gas chromatography [92-96]. Gas chromatography is very useful for studying thermal oxidation products, since the technique relies on heating the sample to atomise it. However, the effects of thermal

degradation on the photoproducts during GC analysis needs to be taken into account. This technique is, therefore, not ideal to identify photooxidation products.

### **1.6 OBJECTIVES.**

This research project is part of a large BRITE·EURAM programme which is a collaborative effort between the Polymer Processing and Performance Group at Aston University and the Photochemical and Microbiology laboratories of Clermont-Ferrand University, France. The overall objectives of the research programme are to "investigate the parameters involved in the degradation of representative examples of the present range of commercial polyethylene-based degradable plastics".

However, the objectives of this research (Environmental Degradation of PE Based Plastics) were:

- 1.6.1 To evaluate the initial chemical and physical properties of commercially available and laboratory extruded degradable polyethylenes.
- 1.6.2 To systematically study the affects of thermal and photooxidation on the degradable polymer samples.
- 1.6.3 To have a better understanding of the mechanisms of degradation of commercial degradable polyethylene-based polymers, with particular emphasis on their oxidation products. Further, to identify and characterise the photodegradation products which should lead to a better understanding of the mechanism of photooxidation.

1.6.4 To examine the recycling potential of degradable polymers mixed with other polyolefin materials. The area of recyclability of photo and biodegradable plastics has caused concern [11-12]. Industry and environmental groups have argued that degradable plastics will have a catastrophic effect on the recycling of conventional plastics waste, if these materials (degradables) end up in the mainstream recycling programmes [97].

## CHAPTER II

# EXPERIMENTAL AND ANALYTICAL TECHNIQUES

## CHAPTER II

### EXPERIMENTAL AND ANALYTICAL TECHNIQUES

#### 2.1 MATERIALS

Photobiodegradable polymer film samples were obtained from various industrial sources, these are summarised in table 2.1. Infra-red spectra of these films are shown in figures 2.1 - 2.7 (see pages 71-77). Unstabilised LDPE in pellet form and identified as "NOVEX LD5320AA" L-61 with a melt flow index of 2.3 g/10 mins was obtained from BP Chemicals (infra-red is shown in figure 2.8), unstabilised polypropylene powder identified as "Propathane HF-26" with a melt flow index of 0.53 g/10 mins was obtained from ICI Ltd (see figure 2.9 for infra-red spectrum) and EPDM (ethylene-propylene diene terpolymer), grade name "VISTALON 2504" was obtained from Exxon Co., (see figure 2.10). Polysulfone film (45  $\mu\text{m}$  thick) was supplied privately by A. Davies. Table 2.2 summarises the characteristics of all the 'control' polymer samples used in this work. Solvents employed for HPLC analysis were all HPLC grade supplied by Fisons. Iron and nickel diisononyl dithiocarbamate were kindly supplied by Robinson Bros., West Bromwich and used without further purification. Sodium hydroxide was obtained from BDH. Phosphoric and hydrochloric acid, both laboratory grade, were obtained from Aldrich chemicals. Diethyl ether, analar grade, was distilled at 33°C prior to use. Sulphur tetrafluoride gas was obtained from Fluorochem and Diethylaminosulphur trifluoride (DAST) was obtained from Aldrich chemicals.

#### 2.2 GENERAL EVALUATION TECHNIQUES

##### 2.2.1 Determination of Mechanical Properties.

Ultimate Tensile Strength, UTS and Elongation to Break, EB were determined using a Testometric Micro 500 tensometer connected to a

Table 2.1: Classification of photobiodegradable polymer samples and their source of origin.

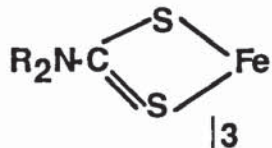
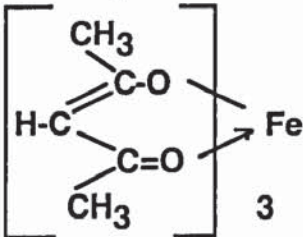
TYPE	COMPOSITION	ORIGIN	CODE	COLOUR & THICKNESS
Photolytic Copolymer	Ethylene-CO Copolymer/LDPE	ITW Hi-Cone PE	A3	transparent 151 $\mu\text{m}$
Metal complex	Fe Stearate / LDPE $(\text{C}_{17}\text{H}_{35}\text{COO})_3\text{Fe}$ ,	ATOCHEM	B1	transparent 25 $\mu\text{m}$
	FeDRC / LDPE 	PLASTOPIL	Bo1	transparent 35 $\mu\text{m}$
Photo Activators	FeDRC/NiDRC APA / LDPE	PLASTOPIL	B5	transparent 30 $\mu\text{m}$
Activators	FeAcAc/HDPE 	ENICHEM 221 HT	B7	transparent 13 $\mu\text{m}$
	FeDRC/HDPE	ENICHEM 2HT	B8	transparent 15 $\mu\text{m}$
Starch Filled	Starch + LDPE Fe stearate + $\text{TiO}_2$	AMPACET	C2	white 41 $\mu\text{m}$
PE	Starch + 8% Fe Stearate + 3% $\text{TiO}_2$ / LDPE	AMPACET	C3	white 45 $\mu\text{m}$
	Starch + organic dye / LDPE	AMPACET	C4	green 38 $\mu\text{m}$
	7% Fe Stearate + carbon black / LDPE	AMPACET	C5	black 31 $\mu\text{m}$

Table 2.2: Summary of 'control' polymers used, their origin and characteristics.

POLYMER	CODE	ORIGIN	STATE	MFI
unstabilised polyethylene (Novex LD5320AA)	PE (Bso)	BP Chemicals	pellets	2.3 g/mins
unstabilised polypropylene (Propathane HF-26)	PP	ICI Ltd	powder	0.53 g/mins
Ethylene-propylene-diene terpolymer (Vistalon 2504) * Mooney viscosity = 26 (at 125°C) Ethylene content = 50% Terpolymer component = ethylidene norbothene (4-7%)	EPDM	Exxon Co.	solid/ bulk	*

microprocessor, in accordance with ASTM D882 [98] under the following conditions:

Load cell = 100 N

Speed of testing = 499 mm

Separation between grips = 50 mm.

Sample size and dimensions (mm) of the test specimens used for the determination of mechanical properties are described in diagram 2.1. Five test specimens were used for every one measurement. The general stress-strain curve for PE film is shown in diagram 2.2.

Diagram 2.1: Diagram showing the shape and size of the test specimens for mechanical properties (not to scale). The dumbbell complies with the specifications of a M-II-type cutter of ASTM D882.

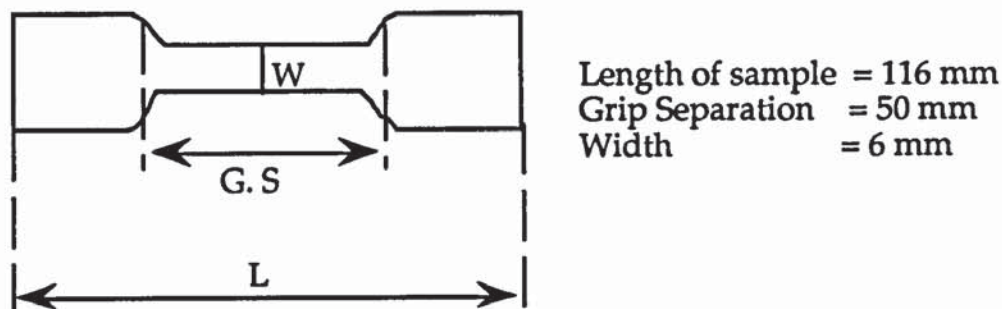
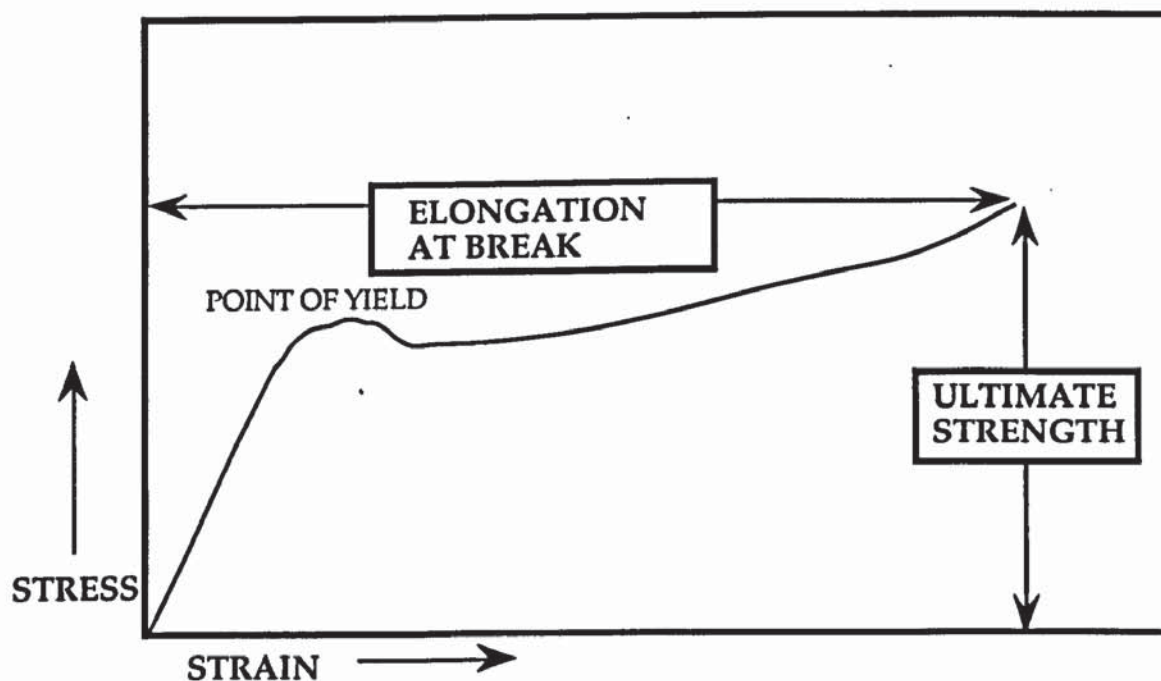


Diagram 2.2: Diagram showing the typical stress/strain curve for polyethylene.



### 2.2.2 Determination of Melt Flow Index

Oxidation of the polymer results in changes in molar mass either by chain scission in which case a decrease in molar mass is observed or by cross-linking whereby an increase in molar mass is observed. Molar mass of the polymer is inversely related to the melt flow index, MFI [99].

The MFI is defined as the amount of polymer extruded through a standard die in a given time under a known weight. All (including blends of PE:PP) MFI measurements were carried out on a Davenport Melt Flow Indexer at 190°C under a load of 2.16 kg through a standard die bore of 2.095 mm and expressed as weight (g) / 10 min.

The apparatus was brought to a steady temperature of 190°C ±0.5°C. The stopwatch was started and instantly the barrel was charged with 5g of polymer (cut into small pieces) under test. This charging was performed under one minute. The unloaded piston was inserted into the barrel and the polymer was allowed to reach an equilibrium temperature over four minutes. (The total time from start is now five minutes). The load was then placed on top of the piston and the polymer extruded through the die. The time interval for the cutoffs was thirty seconds, the first portion was discarded and further five samples were cut off at thirty second intervals. The MFI was calculated using the equation:

$$\text{MFI} = \frac{\text{average weight of cuts}}{\text{time interval of cut off in mins.}} \times 10$$

The experimental error was found to be ±0.02 g/mins , as shown in table 2.3 for unstabilised LDPE, sample Bso.

Table 2.3: Experimental error calculated for MFI using sample Bso.

No. of expt	MFI	
1	1.70	Average MFI value calculated is 1.71 ±0.02 g/mins
2	1.69	
3	1.73	

### 2.2.3 Determination of Molar Mass

Molar mass determinations of the polymer samples were carried out at Clermont Ferrand University, France, using Gel Permeation Chromatography as outlined below:

Sample solutions were prepared as 0.1% (w/v) by the addition of 1,2,4-trichlorobenzene to the polymer. The sample flasks containing the solvent were placed in an oven at 145°C for four hours. Part of each solution was filtered using a sample preparation filter assembly from Waters and Millipore consisting of a wood pulp based cellulose before injecting into the WATERS 150C-ALC/GPC. The estimated error of values quoted is  $\pm 10\%$ . The chromatographic conditions used are described below.

#### Chromatographic conditions.

Column:	Styragel HT length = 30cm particle size = 10 microns
Solvent:	1,2,4-Trichlorobenzene, with anti-oxidant (Santonox R at 250ppm)
Flow rate:	1.0 ml/min
Temperature:	145°C
Detector:	Refractometer
Calibration:	polystyrene standards

### 2.2.4 Natural Weathering of Polymer Samples

Photobiodegradable polymer samples (approximately 16 cm by 130 cm.) were exposed to direct weathering conditions outdoors according to ASTM G7 [100]. This involved mounting the plastic films on metal (aluminium) racks at an angle of 45° facing south. The polymer films were secured to the racks using screw nuts. Four corners of the test pieces were firmly screwed. The rack was located on top of the main building at Aston University,

Birmingham, for approximately ten months, between June 1993 and April 1994 . Three samples for every polymer were removed at intervals and changes in photooxidation products were monitored using infrared spectroscopy.

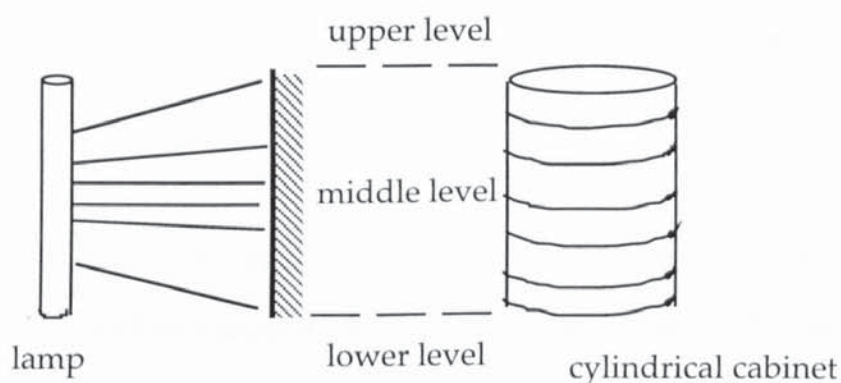
### 2.2.5 Determination Of Photo-Oxidative Behaviour On Exposure To UV Light.

#### *(i) S/B lamp UV cabinet*

Polymer samples were irradiated in two cylindrical rotating uv exposure cabinets labelled 'new' and 'old'. The light source comprised of 7 sunlamps and 21 actinic blue lamps (S/B) arranged in a symmetrical sequence (1 to 3 combination). The rotation of the cabinets ensures that an equal amount of radiation falls on all the samples. The cabinets were open to the atmosphere on both the lower and upper sides. The maximum in relative intensity in the cabinets occurs within the range 290-360 nm. The 'new' cabinet houses fresh new lamps with an average life-time of 1800 hours  $\pm 24$  (see figure 2.11A). This cabinet was used primarily for kinetic and rate studies. The light source of the 'old' uv cabinet had a lower intensity than the 'new' (300 hours old lamps were used) and the average life-time of the lamps was 2700 hours. This cabinet was used only to irradiate very large pieces of polymer (15g) for approximately 8 - 10 months to ensure complete photooxidation for degradation product analysis: consequently, the lower value for radiation intensity was considered not to be too important as extensive degradation was sought rather than a direct correlation of oxidation with time. When the polymer sample became brittle and started to fragment it was transferred to quartz test-tubes which were mounted towards the top end of the cabinet (see figure 2.11A). In both cabinets one sun lamp and three blue lamps were replaced every 300 hours to ensure that the intensity remained stable. The intensity of radiation output varied not only between the two cabinets but also within each

cabinet. The spectral output was greatest in the middle level of the cabinet, whilst the upper and lower levels of the cabinet received slightly less uv light. This is illustrated in diagram 2.3. Polymer samples were placed in the middle region of the 'new' cabinet when determining their photooxidative behaviour. Samples were removed at regular intervals for molecular weight and carbonyl area index measurements to compare the rate and extent of photo-oxidation.

Diagram 2.3: Distribution of the spectral intensity output of uv radiation from a lamp inside a uv cabinet.



### (ii) Sepap UV cabinet

Sepap 12.24 is an accelerated uv cabinet which was designed at Laboratoire de Photochimie in Clermont Ferrand, see figure 2.11B. The cabinet is fitted with four 400W medium-pressure mercury lamps located at the four corners of a square chamber. The samples were irradiated on a rotating support located at the centre of the chamber. The temperature in this cabinet is adjustable. In this work the temperature was set to the lowest value, 60°C. The intensity of this cabinet reads higher than the S/B new uv cabinet.

(iii) *Measurement of Light Intensity in Accelerated Weathering Cabinets*

The average relative radiation output in the cabinets was calculated (see table 2.4) using the polysulphone film method developed by Davies [101]. Polysulphone is sensitive to radiation below 320 nm and the principle of this method is to relate the degree of deterioration of this film to the dose of incident uv radiation. Polysulphone has an absorption band in the near uv which shifts towards the visible region on exposure to uv light. This shift can be quantified by determining the increase in absorbance of the film at 330nm before and after exposure, see figure 2.12. The increase in absorbance at 330nm can be expressed as equivalent amount of monochromatic radiation at 305nm, and intensity can then be calculated using the formula:

$$I \text{ (Wm}^{-2}\text{)} = \frac{60df}{t}$$

where d = equivalent dose of 305nm radiation from table [101]  
corresponding to the change in absorbance of film.

f = temperature factor [101]

t = time of exposure of film in mins.

Table 2.4: The average relative intensities calculated for the 'new', 'old' and sepap uv cabinets. The values calculated are an average of three readings. The values in brackets are the three readings measured.

Uv Cabinet	Intensity
'New': upper end	3.27
middle	4.10 (4.30, 4.28, 3.73)
lower end	3.12
'Old': middle	2.34
Sepap: middle	6

### **2.2.6 Determination of Thermal- Oxidative Behaviour**

Thermal-oxidation of the polymer samples was examined using a single-celled Wallace oven at a constant temperature of 70°C under a constant air flow of 0.07 m<sup>3</sup>/h. The lower temperature of 70°C (instead of the conventional 110°C) was used to assess the behaviour of photobiodegradable polymer samples in simulated composting and landfill environments. Three pieces of polymer for all samples were removed at timely intervals and their carbonyl absorption was measured using infra-red spectroscopy.

### **2.2.7 Thermal Oxidation in Aerated Water**

This experiment was carried out as an extension to the above experiment. The aim was to assess water as a factor for composting. Representative examples from the different classes of commercial degradable samples were placed in three-necked flasks containing HPLC grade water. The temperature was kept constant at 70°C. The flasks were flushed with air for several minutes at intervals everyday. At regular intervals triplicate samples were removed and changes in the carbonyl absorptions and molar mass were determined.

### **2.2.8 Soil Analysis**

Polymer film samples (rectangular specimens with dimensions of 5 cm x 2 cm) after oxidation (one month, 672 hours exposure to uv light in S/B 'new' cabinet, the samples were heavily oxidised) were buried in a back garden facing north in Coventry for a period of 10 months. All the samples were placed in one area of the soil at a depth of approximately 10 cm. Samples without any oxidation were also buried but in a different area close by under exactly the same conditions. The pH of the burial soil was measured to be 6.7 (pH measurement via a calibrated digital pH meter). All

the retrieved polymer samples appeared to be the same as before they were placed in the soil. The buried samples, at the end of the burial period of ten months (November 1992 to July 1993), were analysed using SEM. Prior to analysis the polymer samples were washed with HPLC grade water and air-dried.

## 2.3 POLYMER PROCESSING AND RECYCLING

### 2.3.1 Laboratory Extrusion of PE Degradable Samples.

#### 2.3.1.1 Extrusion of the Polymer

Extrusion of polyethylene samples was carried out using a single screw extruder fitted with a film die. A schematic diagram of this screw extruder is shown in figure 2.13 and table 2.5 shows the extruder specifications.

Table 2.5: Specifications of the Humboldt single screw extruder.

Machine	Humboldt single screw extruder model HE 45 - 20D
L/D ratio	20:1
Screw diameter	45 mm
Screw length	900 mm

The essential feature of the extruder is the extrusion screw which delivers material through the die and also heats the plastic by mechanically working it. The length of screw may be divided into three zones: feed, compression, and metering. The purpose of the feed zone is to pick up the pellets of thermoplastic from the feed hopper and to move them into the main length of the extruder. In the compression zone the loosely packed pellets are compacted and softened to produce a continuous stream of molten plastic. Finally the metering zone takes the molten plastic from the compression zone and feeds it at a controlled rate through the die. At this

point the polymer melt is brought to a correct consistency and the pressure required for extrusion. A high pressure is required to mix the melt to give it constant properties throughout and hence obtain smooth extrudates. At the end of the melt zone the Humboldt is fitted with a breaker plate, which is a thick plate drilled with holes. This has several functions [102]:

- helps to further increase the back pressure
- turns rotational flow of the melt into flow parallel to the screw axis
- holds back impurities.

The barrel holding the screw is hardened and lined since it must resist high pressures generated by the screw. Cold water or air is circulated around the barrel at the feed hopper to prevent the plastic granules from sintering together and thus blocking the feed opening. In order to optimise the efficiency of the barrel and the screw the temperature along the barrel was varied. There were five heating zones with a steady temperature gradient increasing from the feed to the die, see table 2.6, 2.8 and 2.9.

LDPE samples containing different formulations and concentrations of photo-antioxidant (NiDNC) and antioxidant photo-activator, APA, (FeDNC) were extruded into films (75  $\mu\text{m}$  thick) using the Humboldt single-screw extruder under carefully controlled conditions. Tables 2.6 and 2.7 show the extrusion conditions and the formulations of the different polyethylene samples extruded.

### 2.3.2 Recycling of Commercial and Laboratory Extruded PE Degradable Samples by Multiple Extrusion using a Single Screw Extruder

Multiple extrusion was carried out in a Humboldt single screw extruder fitted with a film die head and was based on a 10% blend of the photodegradable polymer film samples (as received) in virgin unstabilised

Table 2.6: Conditions used for the multiple extrusion of laboratory degradable samples using the Humboldt single screw extruder.

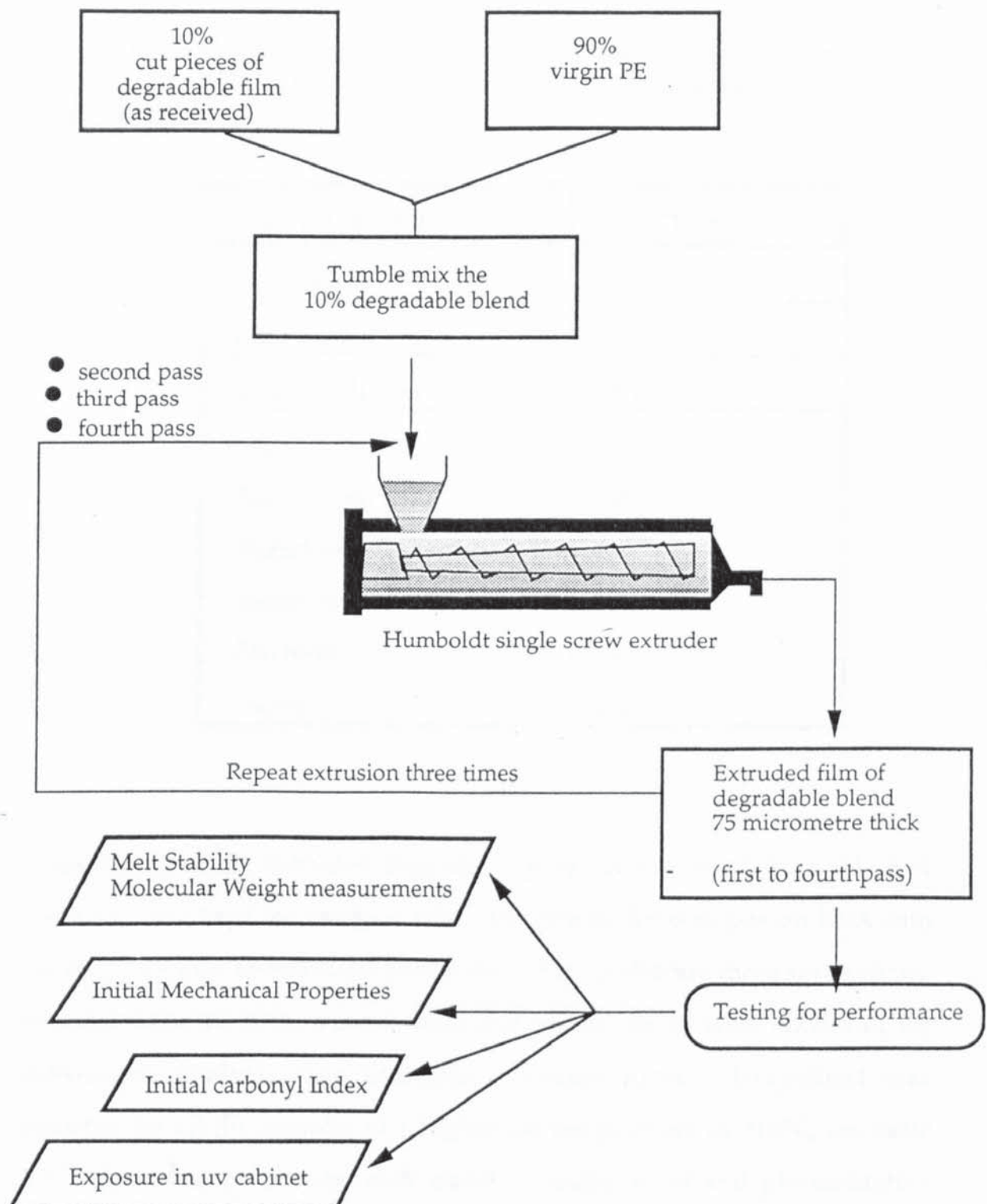
PARAMETER	SETTING
screw speed	high
motor power	5
screw revolution	45 RPM
temperature (°C):	
Barrel zone 1	160
Barrel zone 2	160
Barrel zone 3	160
Die head	180
Die tip	180

Table 2.7: Summary of samples extruded in the laboratory and their composition.

Sample code	Composition %		Appearance
	FeDNC	NiDNC	
Bso (control)	-	-	transparent
Bso1	0.01	-	light grey
Bso2	0.02	-	light grey
Bso3	0.03	-	light grey
Bso4	0.05	-	light grey
Bs1	0.01	0.01	light yellow
Bs2	0.02	0.01	light yellow
Bs3	0.03	0.01	light yellow
Bs4	0.05	0.01	light yellow

LDPE. Scheme 2.1 gives a schematic overview of the recycling process and tests used. Unstabilised LDPE was first extruded into a thin film at a die temperature of 160°C. The PE film was then cut into 1cm width strips and tumble-mixed (in a polyethylene bag) with the previously cut degradable film sample under examination at a ratio of 90:10, respectively. The 10% blend of degradable polymer films in virgin LDPE pellets was then fed into

Scheme 2.1: Schematic representation of the methodology adopted for recycling degradable blends using the single screw extruder.



the single screw extruder and was extruded into a thin film at die temperature of 180°C. Table 2.8 shows the extrusion conditions used indicating the temperature profile of the different zones of the screw.

Table 2.8: Conditions used for recycling of 10% blends of degradable polymers in virgin LDPE at die temperature of 180°C using the Humboldt single screw extruder.

PARAMETER	SETTING
screw speed	high
motor power	5
screw revolution	45 RPM
temperature (°C):	
Barrel zone 1	160
Barrel zone 2	160
Barrel zone 3	160
Die head	180
Die tip	180

A small part of the extruded degradable polymer produced from this first extrusion was kept for analysis while the remainder was passed back into the extruder and re-extruded under the same conditions three more times. Samples from the first, second, third and fourth passes were taken out for subsequent analysis. The multiple extrusion process (recycling) was repeated for all the samples at a higher die temperature of 210°C, see table 2.9. Mechanical properties, melt stability, molar mass and photooxidative behaviour of the multiple extruded samples were examined.

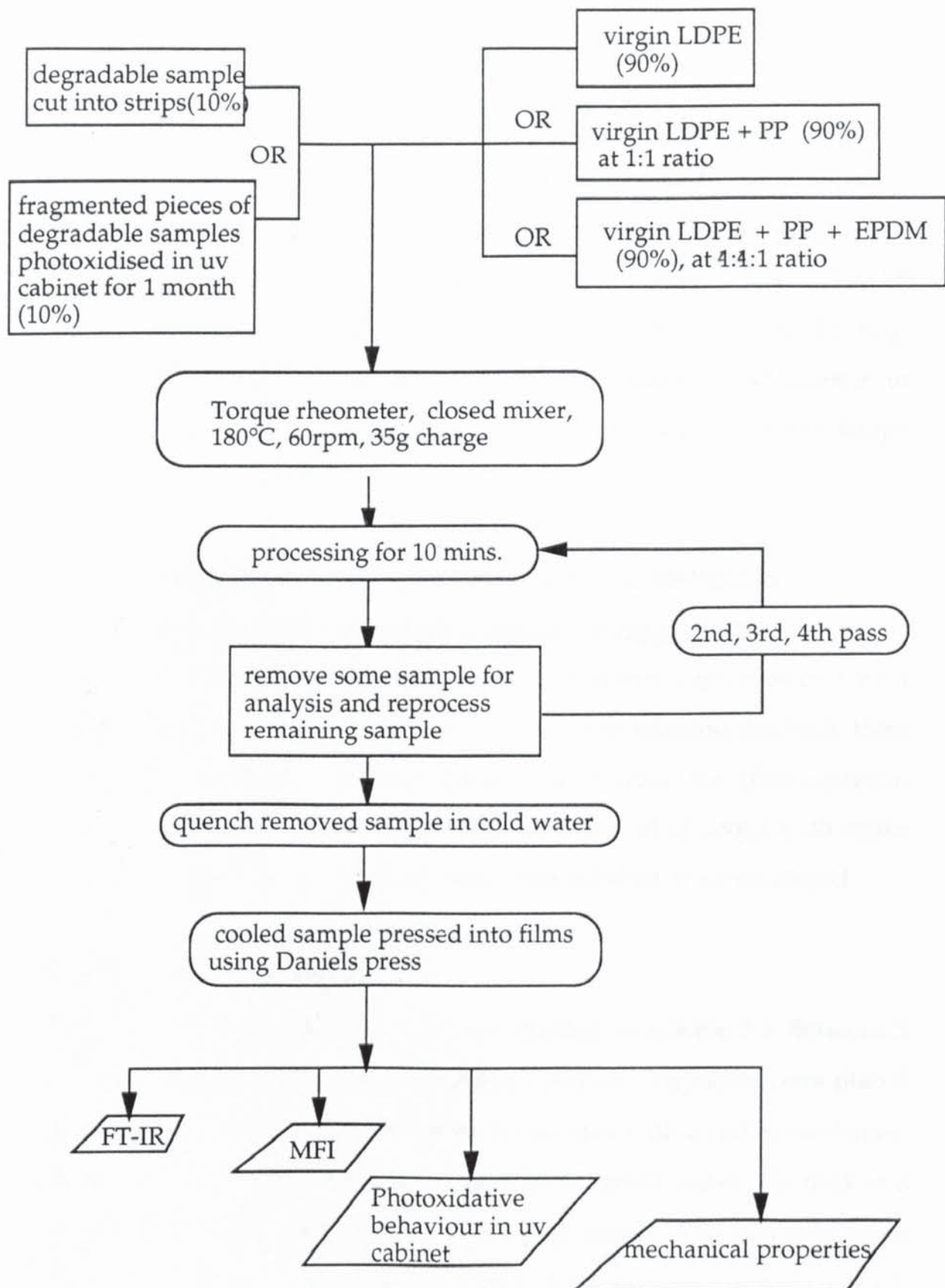
Table 2.9: Conditions used for recycling of 10% blends of degradable polymers in virgin LDPE at die temperature of 210°C using the Humboldt single screw extruder.

PARAMETER	SETTING
screw speed	high
motor power	5
screw revolution	45 RPM
temperature (°C):	
Barrel zone 1	180
Barrel zone 2	190
Barrel zone 3	190
Die head	210
Die tip	210

### 2.3.3 Recycling of PE-based Photobiodegradable Polymer Films Samples (Commercial and Laboratory Extruded) by Multistep Processing using an Internal Mixer

Multistep processing of the degradable polymer samples (as received and after photooxidation) as 10% blends (in LDPE, LDPE:PP 1:1 ratio and LDPE:PP:EPDM 4:4:1 ratio) of different degradable polymers was performed using a RAPRA HAMPDEN torque rheometer head fixed in a Brabender motor in a closed mixer with a full charge of 35g, see scheme 2.2. This is essentially a small mixing chamber containing mixing screws contra rotating at different speeds. The speed of the rotation was adjusted to 60 rpm. The degradable samples were cut into small strips (1cm x 2cm) prior to mixing with the other polymer components of the blends. The samples were reprocessed four times, representative sample being removed after

Scheme 2.2: Overview of the methodology adopted for reprocessing in an internal mixer.



each pass for analysis. The reprocessed samples were first pressed into thin films prior to analysis. Table 2.10 summarises the samples reprocessed.

### **2.3.4 Film Preparation**

Films were prepared by compression moulding at a temperature of 160°C using an electric Daniels press machine. The sample (1.5 to 2g) wrapped in cellophane was placed between two stainless steel metal plates. The samples were heated without any pressure for two minutes, after which 85 kg/cm<sup>2</sup> pressure was applied for a further three minutes. After heating, the compressed polymer samples were cooled by allowing cold water in to the press and polymer films were removed and stored in the fridge awaiting further analysis.

## **2.4 CHARACTERISATION AND ANALYTICAL TECHNIQUES**

### **2.4.1 Methodology for the extraction of photooxidation products**

The heavily photooxidised fragmented polymer pieces were extracted with different solutions in order to leach out the photooxidation products from the polymer backbone. Earlier attempts to extract the photooxidation products were made using water. After unsuccessful attempts with water different concentrations of sodium hydroxide solution were employed.

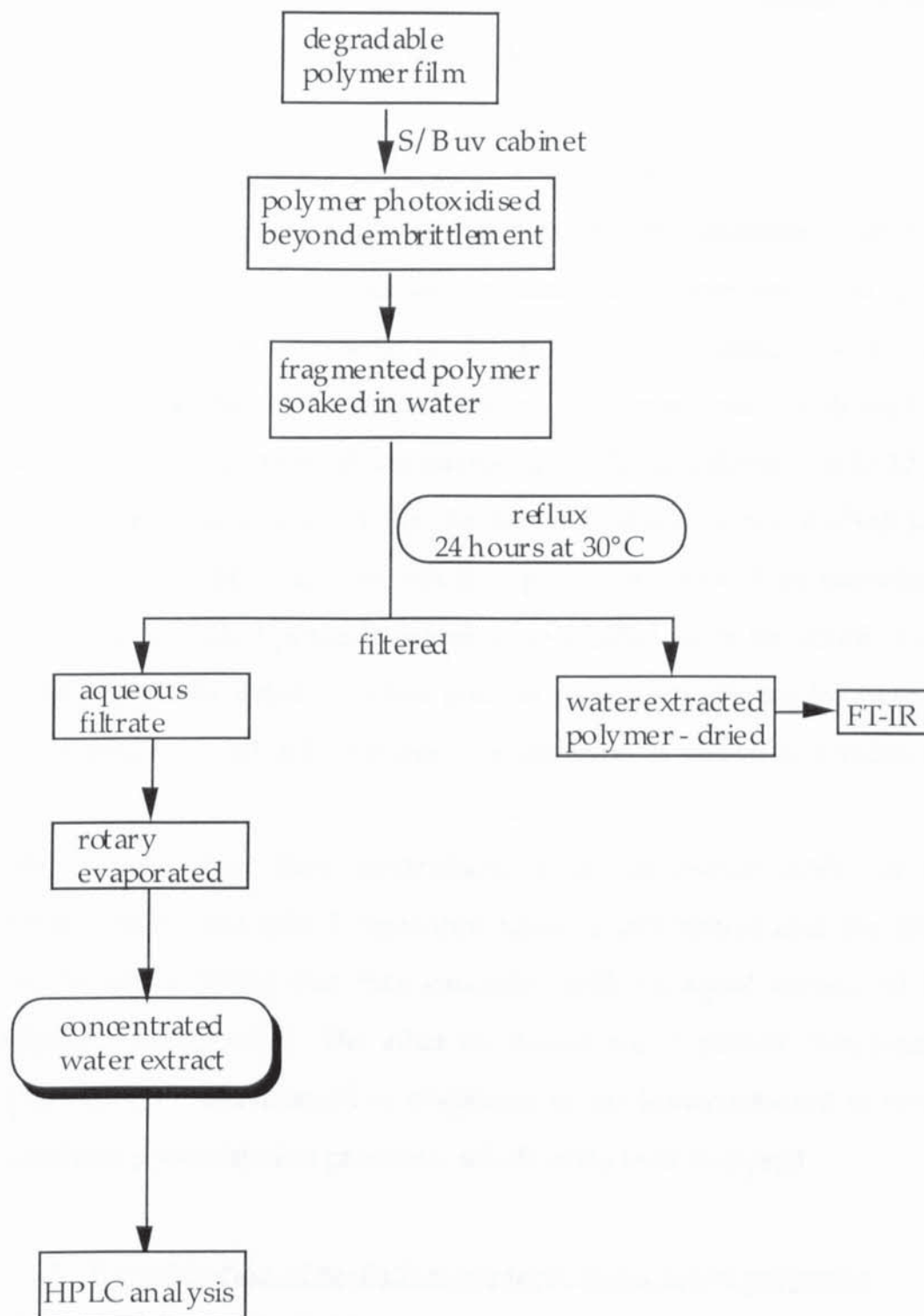
#### **2.4.1.1 Extraction using water**

The experimental procedure used is summarised in scheme 2.3. Between 3 to 5 grams of the extensively photooxidised polymer fragments were placed into a 250 ml capacity round-bottomed flask fitted with a reflux condenser. To this was added approximately 50 ml of HPLC grade water. The flask was then placed into a heating mantle and gently heated. The temperature of water in the flask was maintained at 30°C for a twenty-four hour period. The warm water was then filtered from the degraded polymer pieces using

Table 2.10: Samples reprocessed using the Torque Rheometer.

SERIES	SAMPLE COMPOSITION	SAMPLE CODE
I	LDPE + 10% Degradable samples as received	Bso (control 1) PE:Bo1 PE:B5 PE:A3 PE:C2 PE:C4
II	LDPE + 10% degradable samples photoxidised for a period of 672 hours (1 month), Bso was oxidised for 800 hours.	BsoD PE:Bo1D PE:C2D PE:A3D
III	LDPE : PP + 10% degradable samples as received	PE:PP (control 2) PE:PP:Bo1 PE:PP:B5 PE:PP:A3 PE:PP:C2 PE:PP:C4
IV	LDPE : PP + 10% degradable samples photoxidised	PP:PE:A3D PP:PE:C2D
V	LDPE: PP: EPDM + 10% degradable samples	PE:PP:EPDM (control 3) PE:PP:EPDM:Bo1 PE:PP:EPDM:B5 PE:PP:EPDM:A3 PE:PP:EPDM:C2 PE:PP:EPDM:C4

Scheme 2.3: Flow chart of the methodology adopted for extraction with water



Whatman filter paper, and the filtrate rotary evaporated. The water concentrates were then analysed by HPLC. The water extracted polymer was air-dried and infrared spectra obtained.

#### 2.4.1.2 Extraction using sodium hydroxide solutions

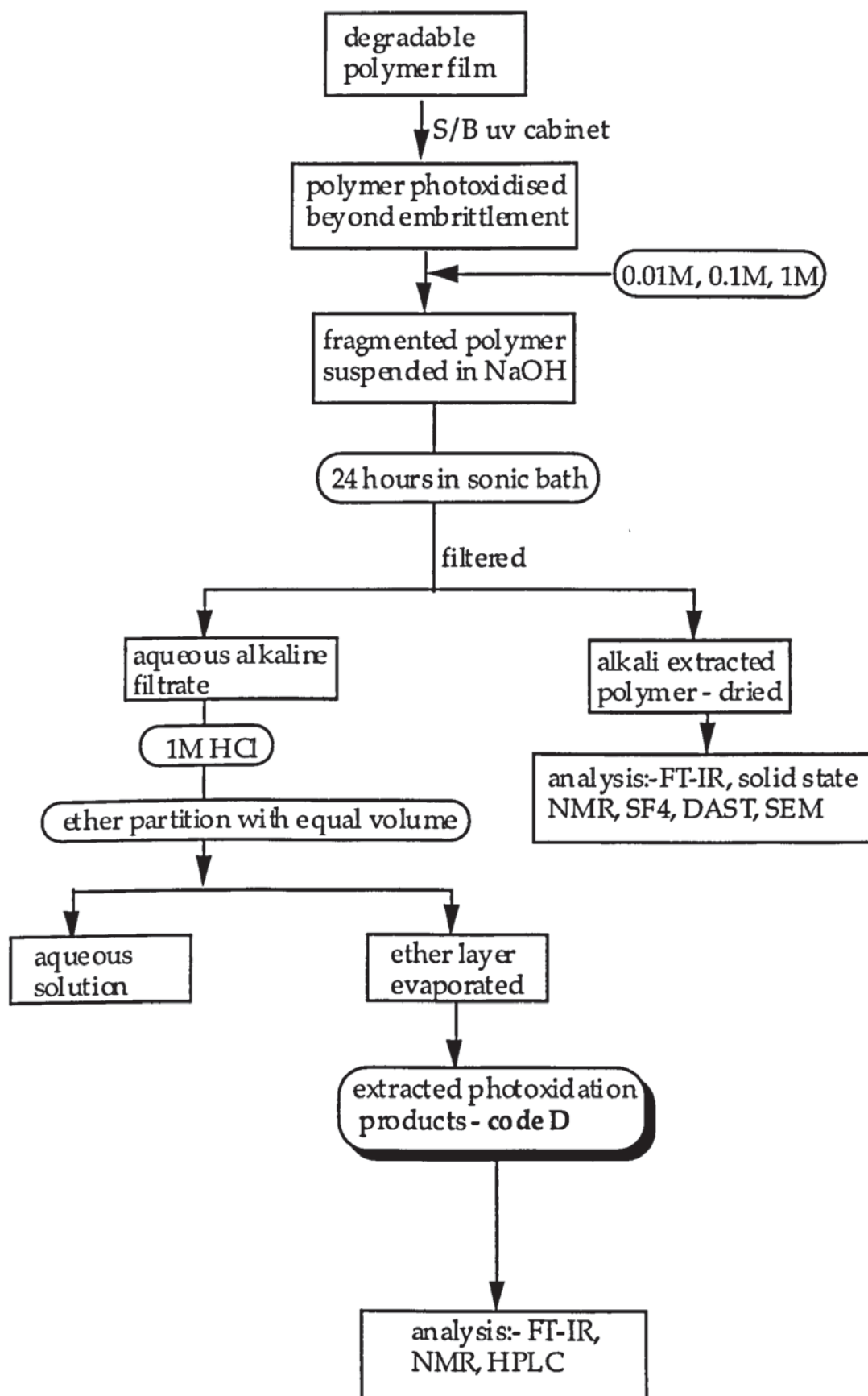
Initially, between 3 to 5 grams of the extensively degraded polymer was used; however, this amount was not enough to allow sufficient quantities of photooxidation products to be extracted. Scheme 2.4 shows the methodology used for the alkali extraction procedures mentioned in this study. Larger quantities of fragmented degradable polymers (6 to 12 grams) was placed into a conical flask. To this was added 250 ml of alkali solution (0.01M, 0.1M, 1M). The flask was then placed in a sonic bath overnight. The extracted degraded polymer pieces were filtered from the solution using a filter paper. The dried (vacuum oven at room temperature for twenty-four hours) alkali treated polymer was then analysed as shown in scheme 2.4.

The filtrate was then neutralised with drop-wise addition of 1M hydrochloric acid (pH 7 measured using a pH meter) and the resultant neutralised solution was then extracted with an equal volume of freshly distilled diethyl ether. The ether extraction was repeated. The ether layer was collected and allowed to evaporate in the fumecupboard to reveal the extracted photooxidation products, which were later analysed.

#### 2.4.2 Derivatisation of oxidation products in degraded polymers

The derivatisation (both SF<sub>4</sub> and DAST) was carried out by Dr. Coe and his team at Birmingham University as follows:

Scheme 2.4: Flow chart of the methodology adopted for alkali extraction



#### 2.4.2.1 Reaction with Sulphur tetrafluoride (SF<sub>4</sub>)

100 mg of the degraded polymer sample was placed into a 125 ml capacity stainless steel Parr mini reactor fitted with a teflon lid. To this was added 10 ml of dry dichloromethane. 5 ml of SF<sub>4</sub> (gas) was condensed into the reaction vessel. The content in the reaction vessel were stirred using a magnetic stirrer for 10, 24, 48 and 72 hours at room temperature. After the stirring the reaction vessel was vented and solvents allowed to boil off. The reacted polymer was recovered from the vessel, flushed with dichloromethane and dried. Infrared spectra were obtained of the derivitised degraded polymer.

#### 2.4.2.2 Reaction with DAST

100 mg of the degraded polymer sample and 3 ml of dry dichloromethane were placed into a 125 ml capacity stainless steel Parr mini reactor fitted with a teflon lid. To this was added 0.3g of DAST (liquid). The reaction vial was sealed and the mixture stirred at room temperature using a magnetic stirrer for 24, 48 and 72 hours. After the stirring the dichloromethane and the DAST were vacuumed off leaving the reacted polymer. Infrared analysis was then performed (at Aston University) on the reacted polymer.

#### 2.4.3 Infra-Red Spectroscopy

The instrument used was a Perkin Elmer 1710 Fourier Transform infra-red coupled to a M1700 data station which allows the spectra recorded to be displayed either in transmittance or absorbance and hence allows peak areas to be calculated from both transmittance and absorbance. Although all the spectra in this work were obtained and were shown in the transmission mode, the peak areas were calculated using the absorbance areas. The software enables the area to be determined in absorbance even though the spectrum may be displayed in transmittance. The measurement

of carbonyl area index ( $1710\text{ cm}^{-1}$ ) and vinyl area index ( $909\text{ cm}^{-1}$ ) was calculated using the equation

$$\frac{A_S}{A_R} \text{ (area of carbonyl peak at } 1710\text{ cm}^{-1}\text{, or vinyl (} 909\text{ cm}^{-1}\text{))}$$

$$A_R \text{ (area of reference peak of PE at } 1890\text{ cm}^{-1}\text{) [77]}$$

The areas of the specified peaks were calculated with the aid of the computer software using the baseline technique which involved drawing a tangent between points **A** and **B** taking the area under the curve with the base line of the peak i.e the area of **ABC** as illustrated in diagram 2.4.

**Sample preparation** : the FT-IR spectrum of the film polymer samples was obtained by placing the sample between magnetic holders. Neat liquid samples were smeared directly onto sodium chloride plates. Solid KBr discs were prepared of the degraded polymer.

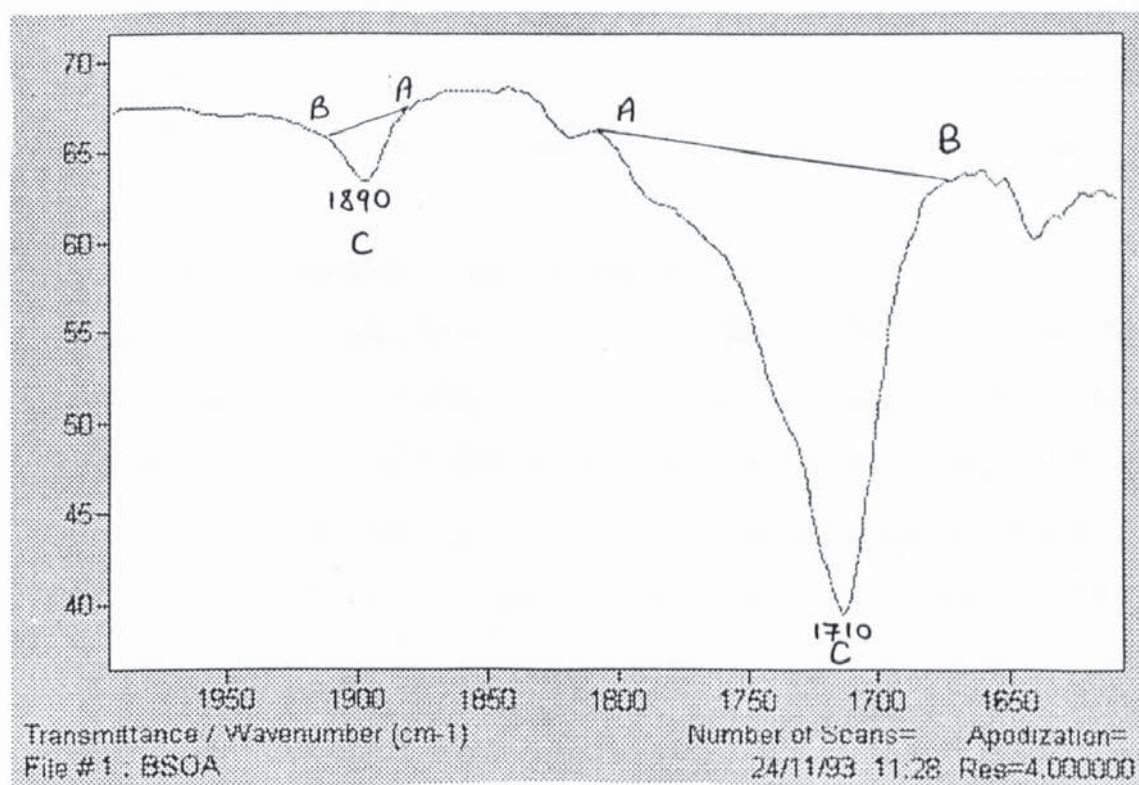


Diagram 2.4: Peak areas used for the calculation of carbonyl content.

#### 2.4.4 Analytical HPLC

The instrument used was a Philips analytical HPLC (Philips PU4021) equipped with a multichannel diode array detector which allows the chromatogram to be viewed at different wavelengths. The elution method was developed to give baseline resolution. The optimum conditions established are summarised in table 2.11.

Table 2.11: Conditions used for the HPLC analysis of the degradation products.

column-reverse phase	Hamilitons PRP-1 length = 63.5 cm inside diameter = 4.6 mm
mobile phase	85 % 1mM Phosphoric acid 15% Acetonitrile
flow rate	1.0 ml/min
temperature	19°C

#### 2.4.5 Nuclear Magnetic Resonance Spectroscopy

All spectra were obtained by using a BRUKER AC 300 high resolution FT-NMR spectrometer. Liquid samples were dissolved in deuterated chloroform ( $\text{CDCl}_3$ ) and spectra obtained at room temperature.  $^{13}\text{C}$  NMR was run using the JMOD method which shows positive (methyl and tertiary carbons) and negative resonances (methylene  $-\text{CH}_2-$  and quarternary carbons). Signal enhancement in the  $^{13}\text{C}$  NMR spectra was carried out using polarization transfer techniques[103]. Solid state spectra were obtained using the Magic Angle Spinning method. The polymer samples for solid state analysis were prepared by finely grinding the polymer. The extensively photoxidised polymer samples (which were very brittle) were easily ground using a mortar and pestle. However, the

received were first frozen by immersing in liquid nitrogen for several hours. The removed frozen polymer films were then placed in aluminium foil and crushed using a hammer.

#### **2.4.6 Scanning Electron Microscopy**

The instrument used was a STEREOSCAN 90B, made by Cambridge Instruments. 25 k electron volts were used to view the samples. The polymer samples prior to analysis were gold plated and mounted on individual stubs. The instrument was equipped with a 35 mm camera which enabled the samples to be photographed.

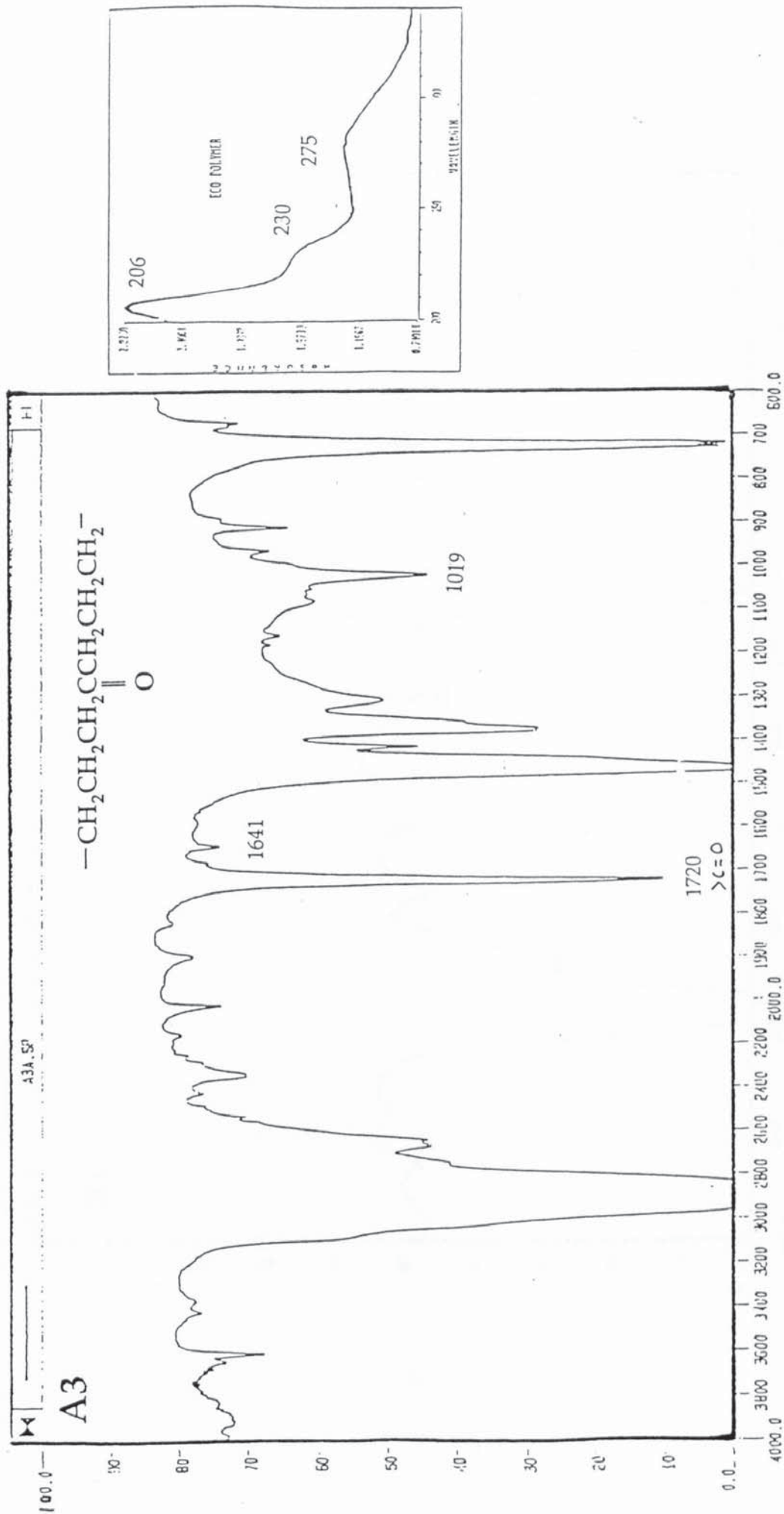


Figure 2.1: FT-IR and UV spectra of photodegradable PE based on ethylene copolymer class, 90 μm thick film, code A3.

01-1

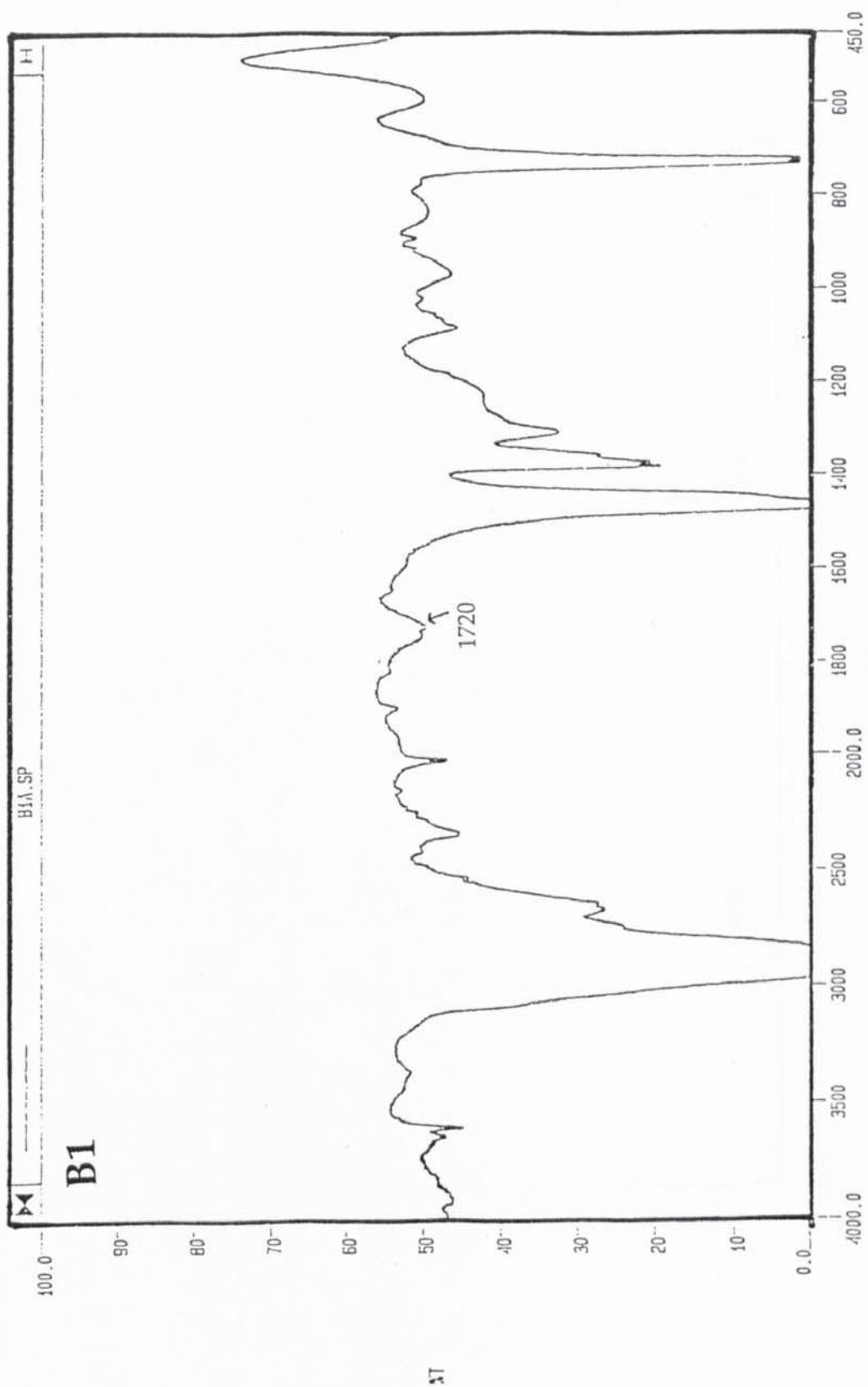
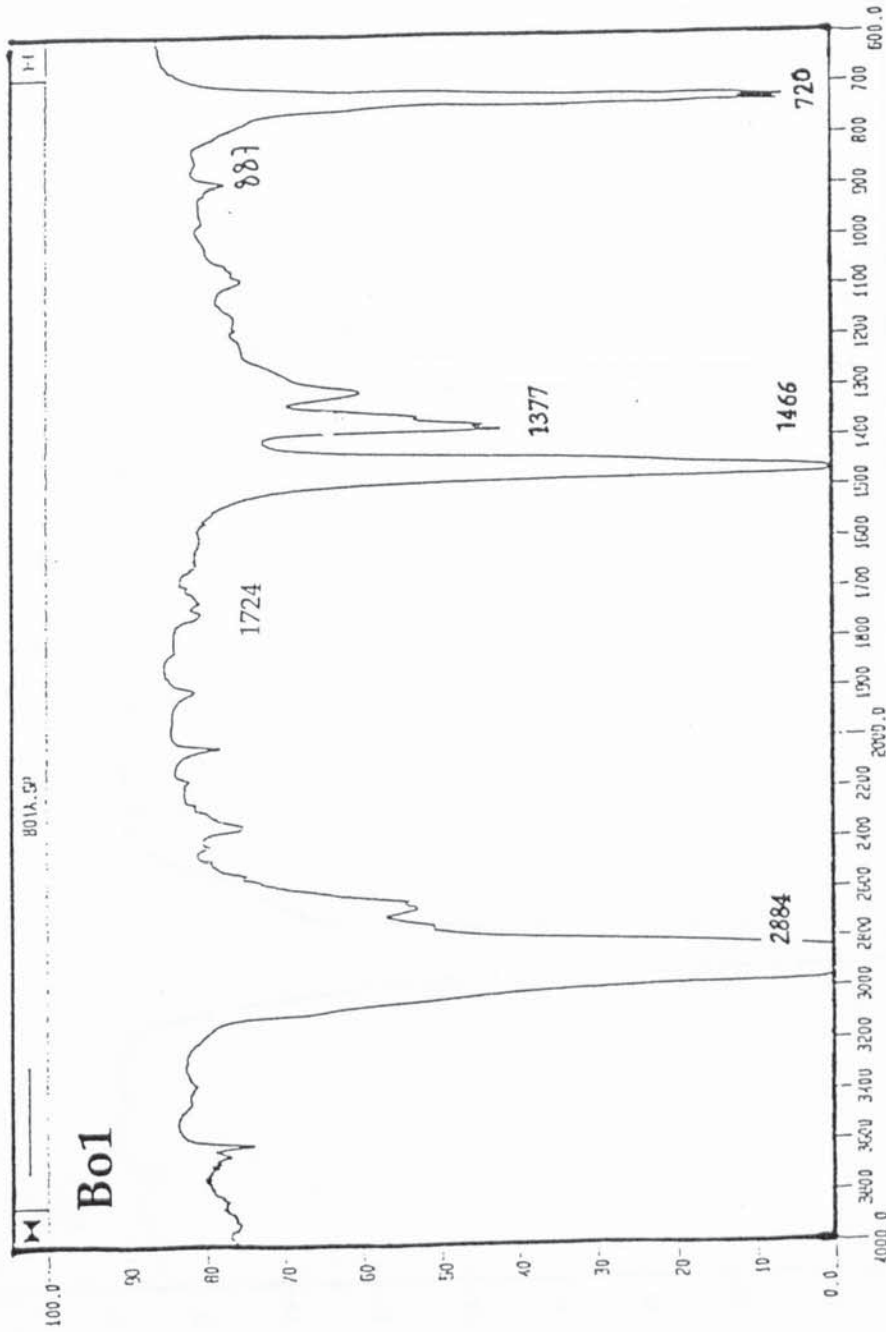


Figure 2.2: FT-IR spectrum of photodegradable PE system based on metal activator class containing iron stearate, code B 1. Spectrum is of 25  $\mu\text{m}$  thick film.



DX-1

Figure 2.3: FT-IR spectrum of photodegradable PE system based on metal photoactivator class containing iron dithiocarbamate, code Bo1. Spectrum is of 35  $\mu\text{m}$  thick film.

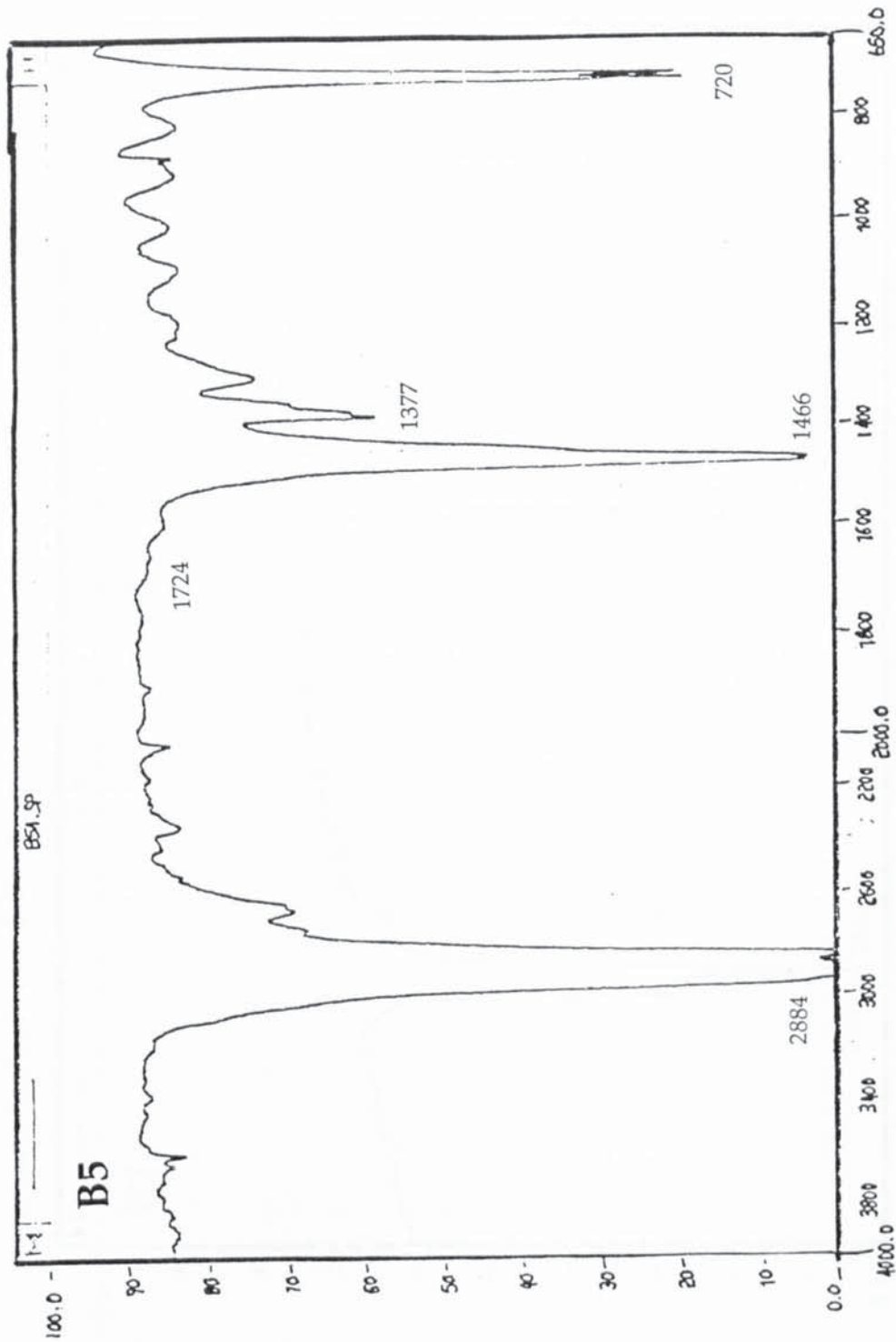


Figure 2.4: FT-IR spectrum of photodegradable PE system based on metal photoantioxidant-activator class containing iron and nickel dithiocarbamate, code B5. Spectrum is of 30  $\mu\text{m}$  thick film.

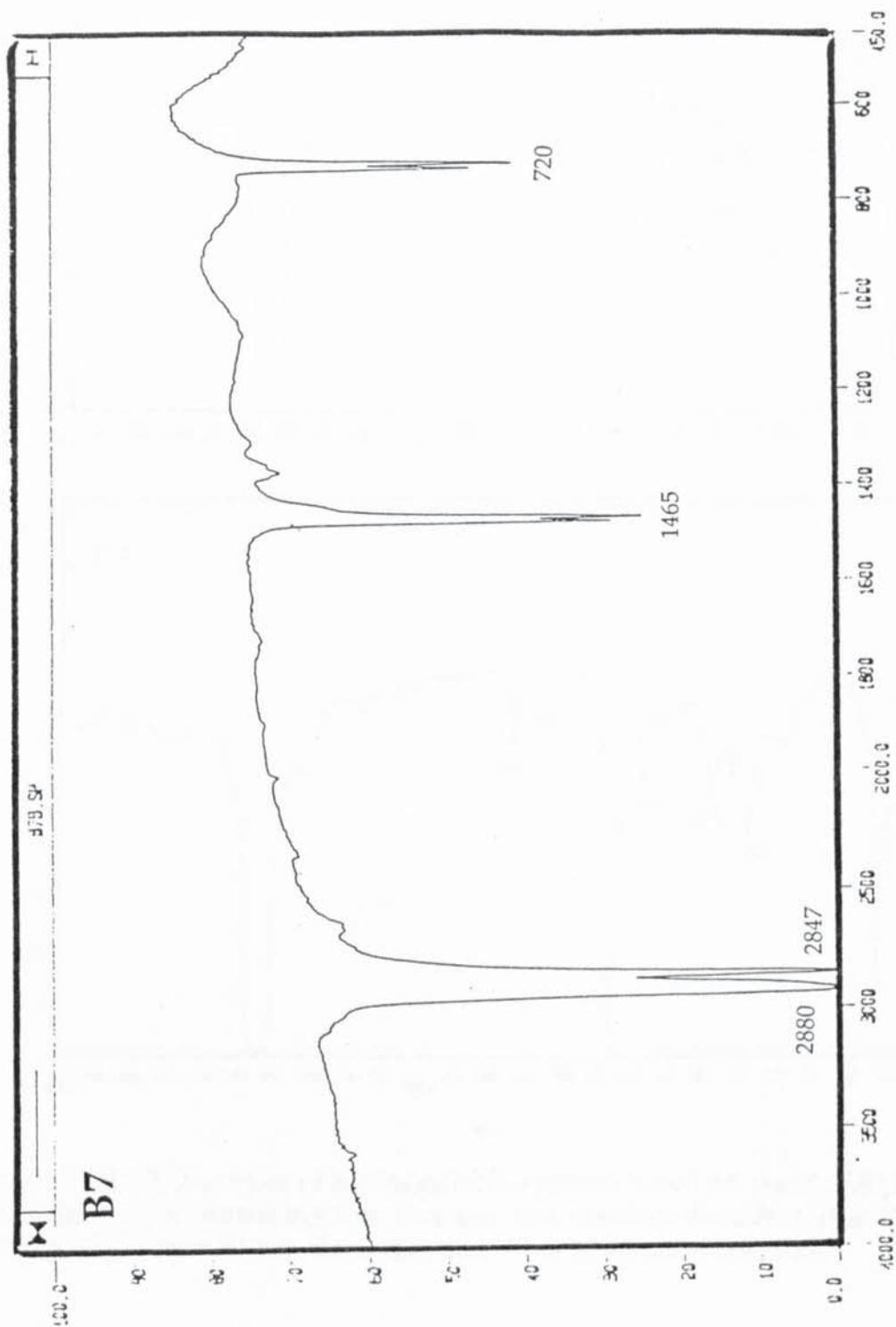


Figure 2.5: FT-IR spectrum of photodegradable HDPE system based on metal photoactivator class containing iron acetylacetonate, code B7. Spectrum is of 13  $\mu\text{m}$  thick film.

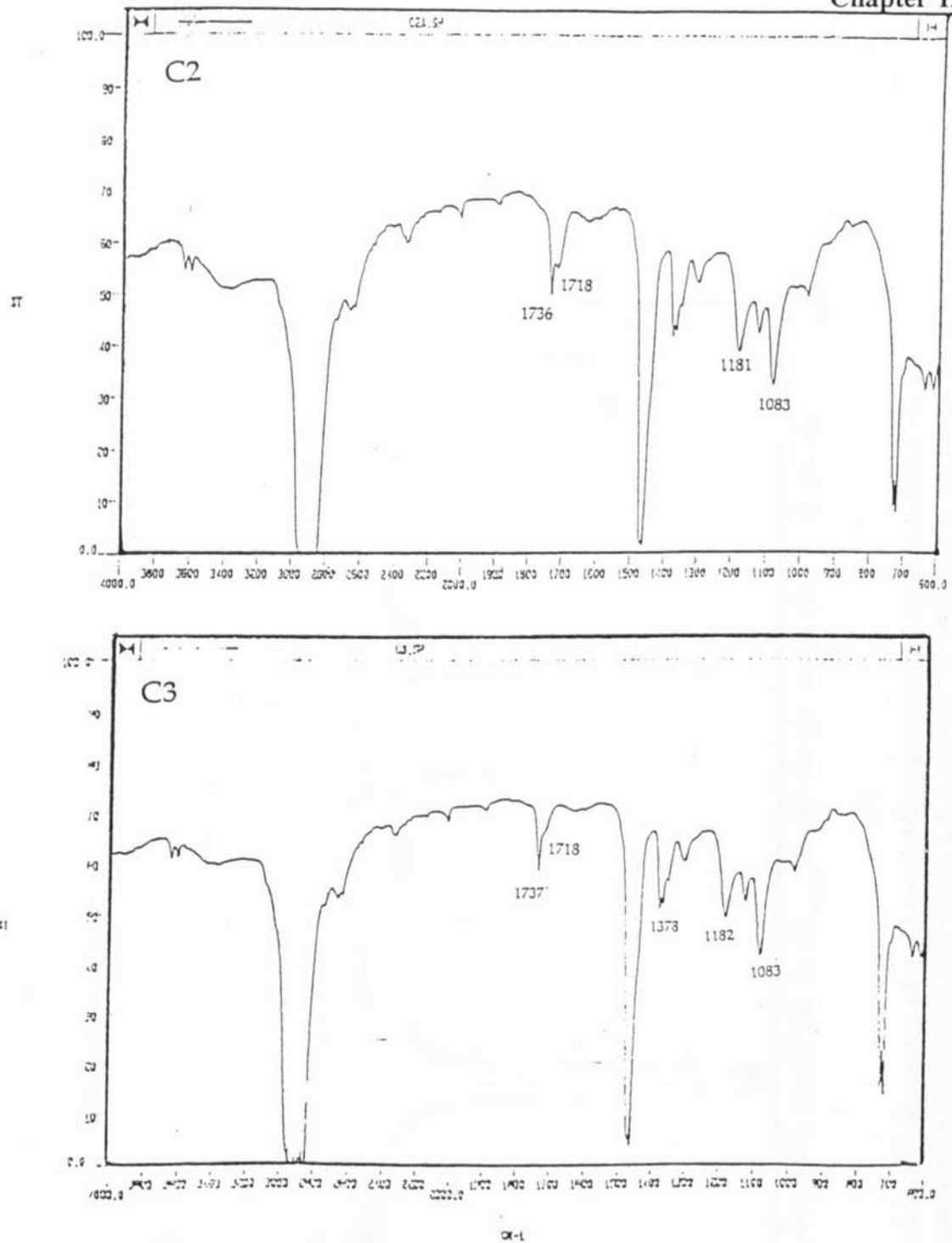


Figure 2.6: FT-IR spectrum of biodegradable systems based on starch-filled polyethylene class containing iron stearate and titanium dioxide codes C2 and C3. Spectrum of C2 is of 41 μm thick film and C3 is of 45 μm thick film.

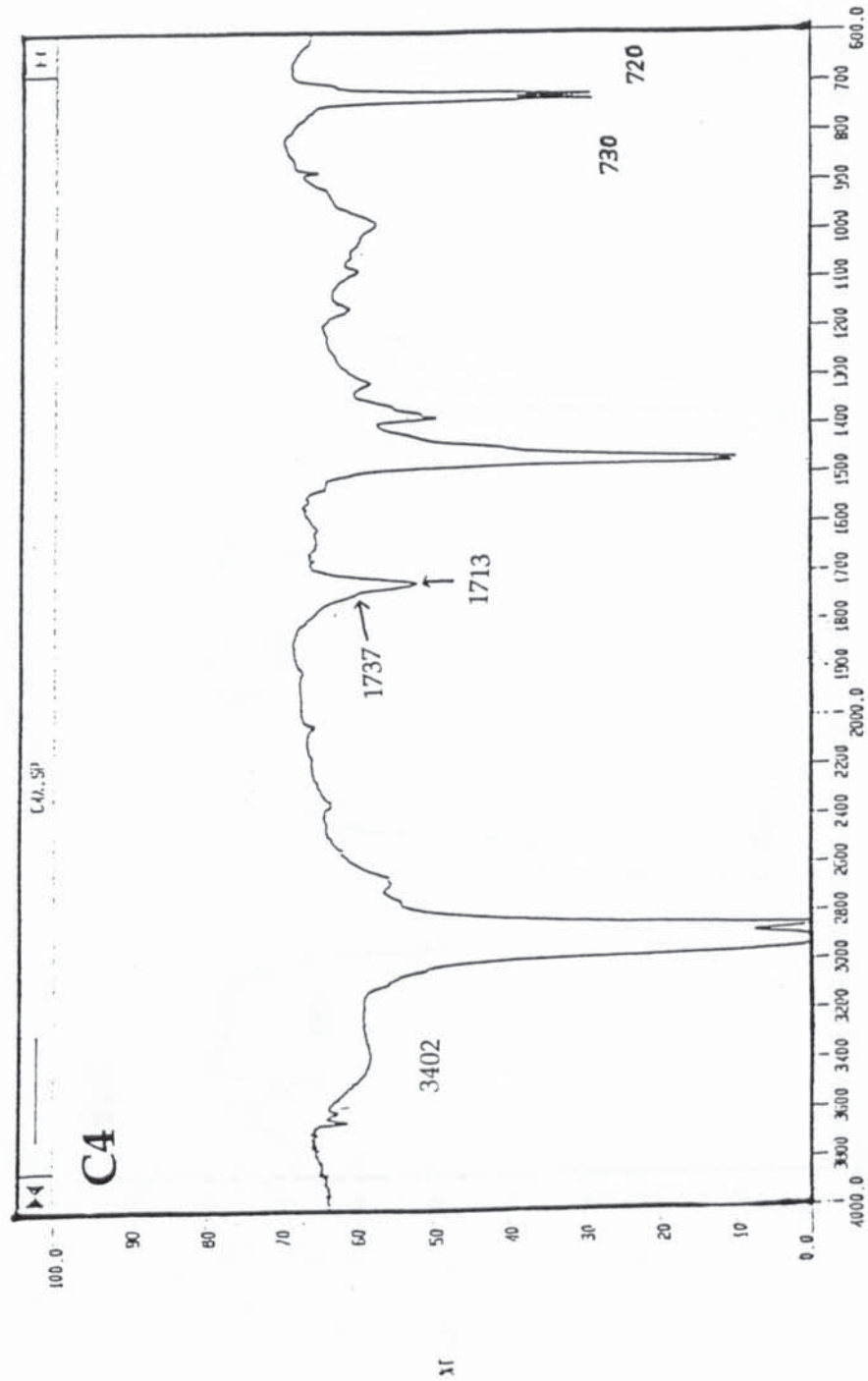


Figure 2.7: FT-IR spectra of biodegradable system based on starch-filled polyethylene class containing an organic dye, code C4. Spectrum is of 38  $\mu\text{m}$  thick film.

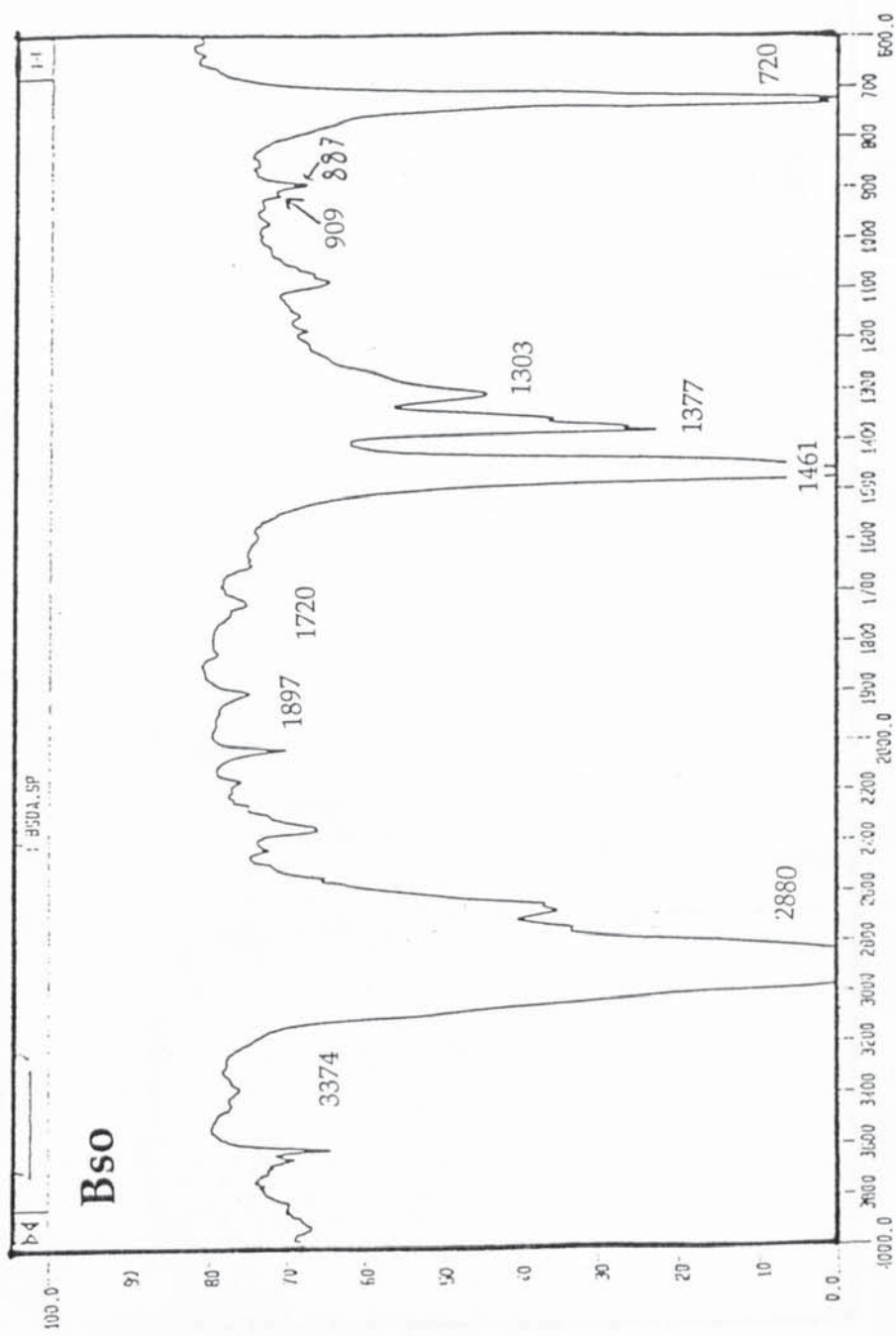


Figure 2.8: FT-IR spectrum of extruded film of unstabilised Low Density Polyethylene 75  $\mu\text{m}$  thick, grade "Novex LDPE" with a MFI of 2.3g/10 mins., ex. BP chemicals, code Bso.

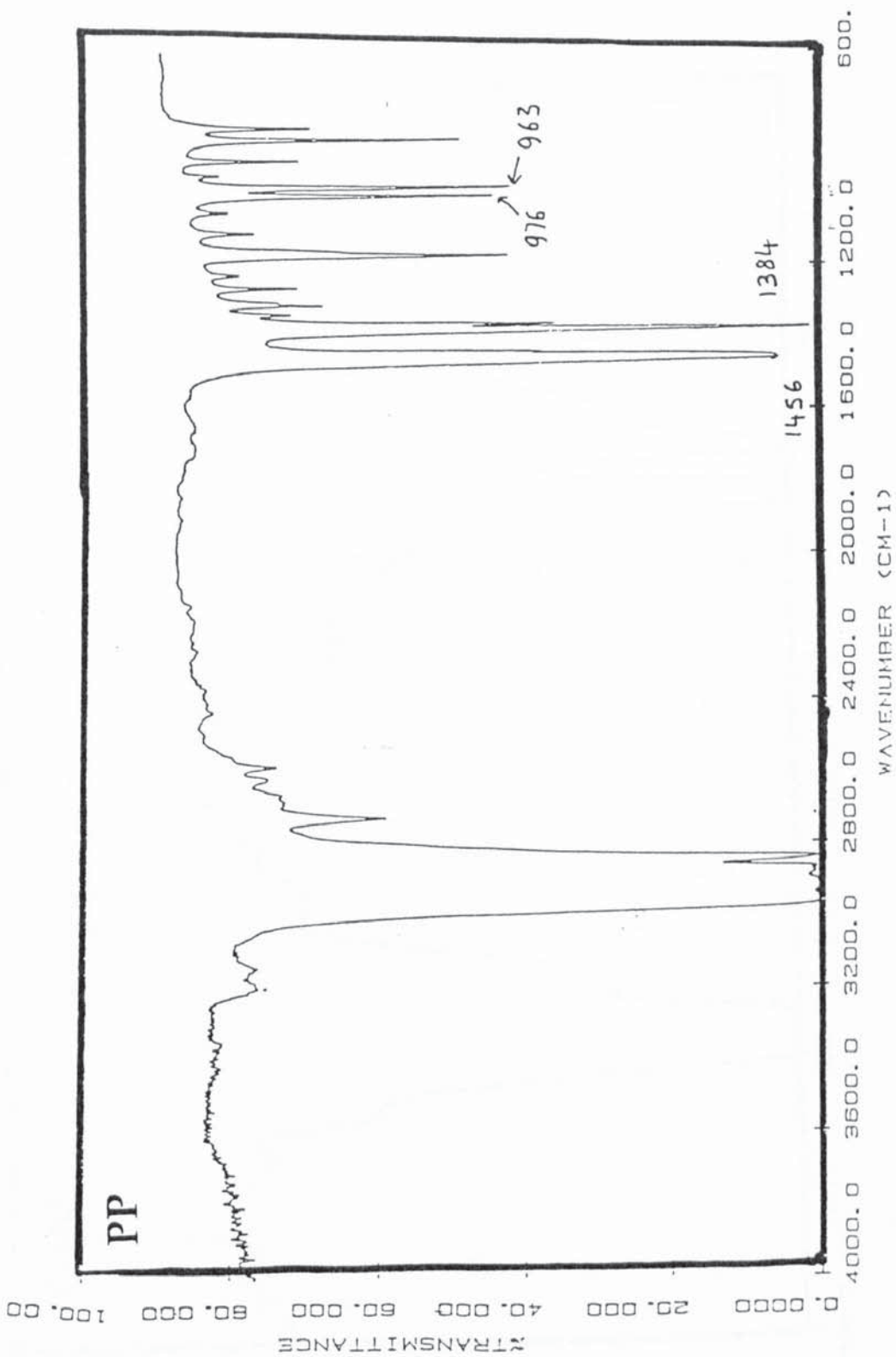


Figure 2.9 : FT-IR spectrum of compression moulded film of unstabilised Polypropylene 80 µm thick, grade Propathane HF-26 with a MFI of 0.53/10 mins, ex. ICI Ltd, code PP.

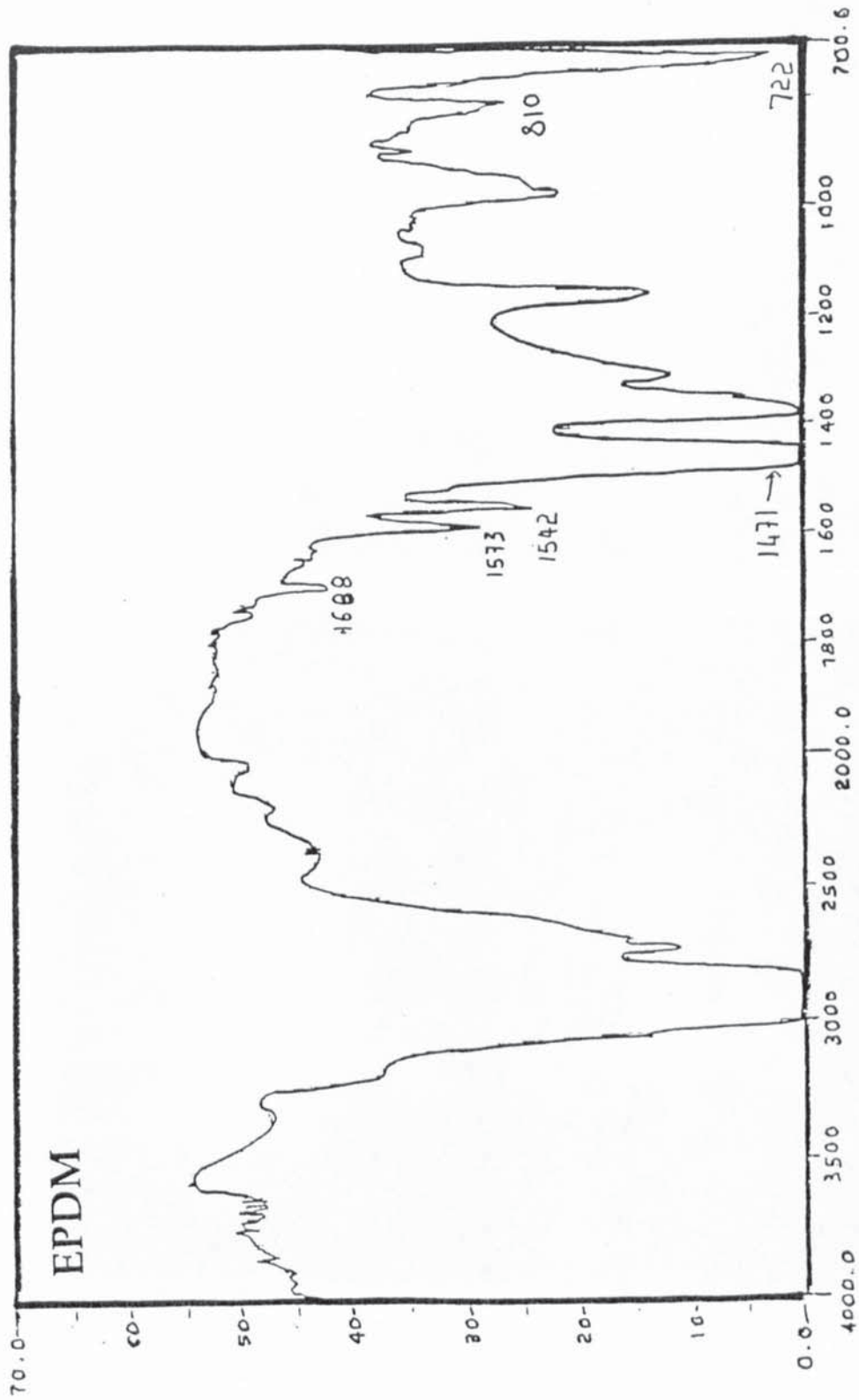


Figure 2.10: FT-IR spectrum of film of unstabilised Ethylene-propylene-diene terpolymer 150  $\mu\text{m}$  thick, grade Vistalon 2504, ex Exxon Co., code EPDM.

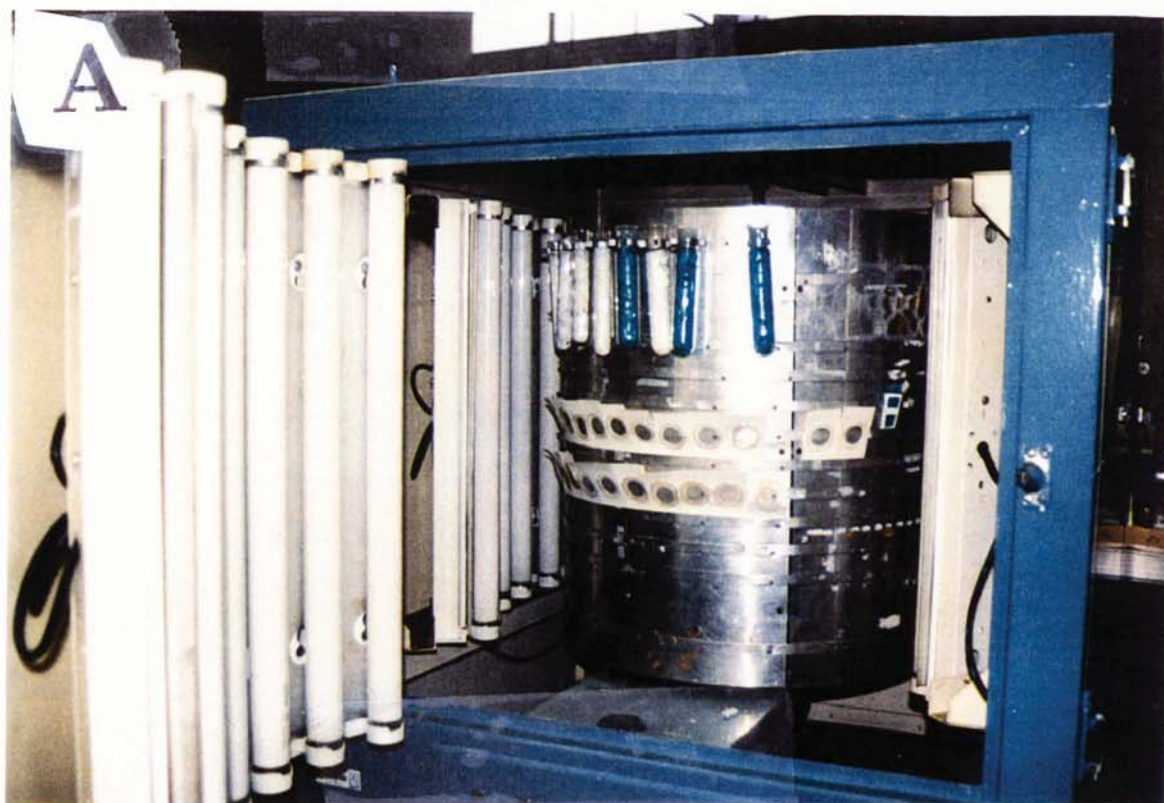
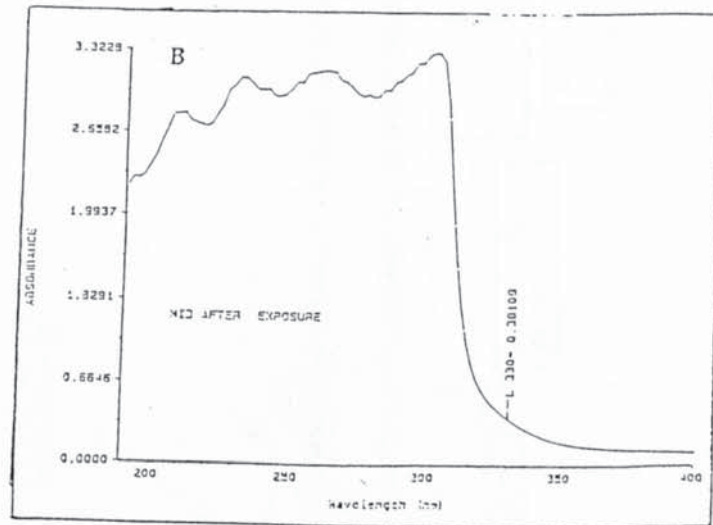
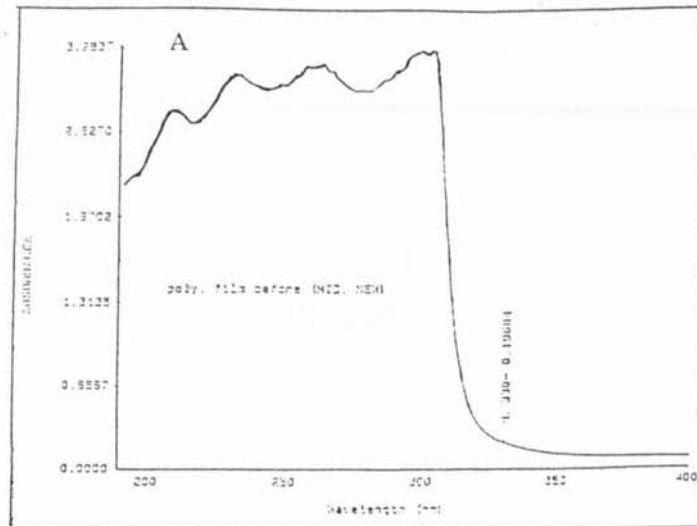


Figure 2.11: Accelerated UV cabinets, A = S/B uv cabinet; B = sepap 12.24



$$\Delta A = \text{change in absorbance} \\ 0.38109 - 0.19681$$

$$\Delta A = 0.1842; \text{which corresponds to } 1.31 \\ \text{equivalent dose of } 305 \text{ nm radiation (d)}$$

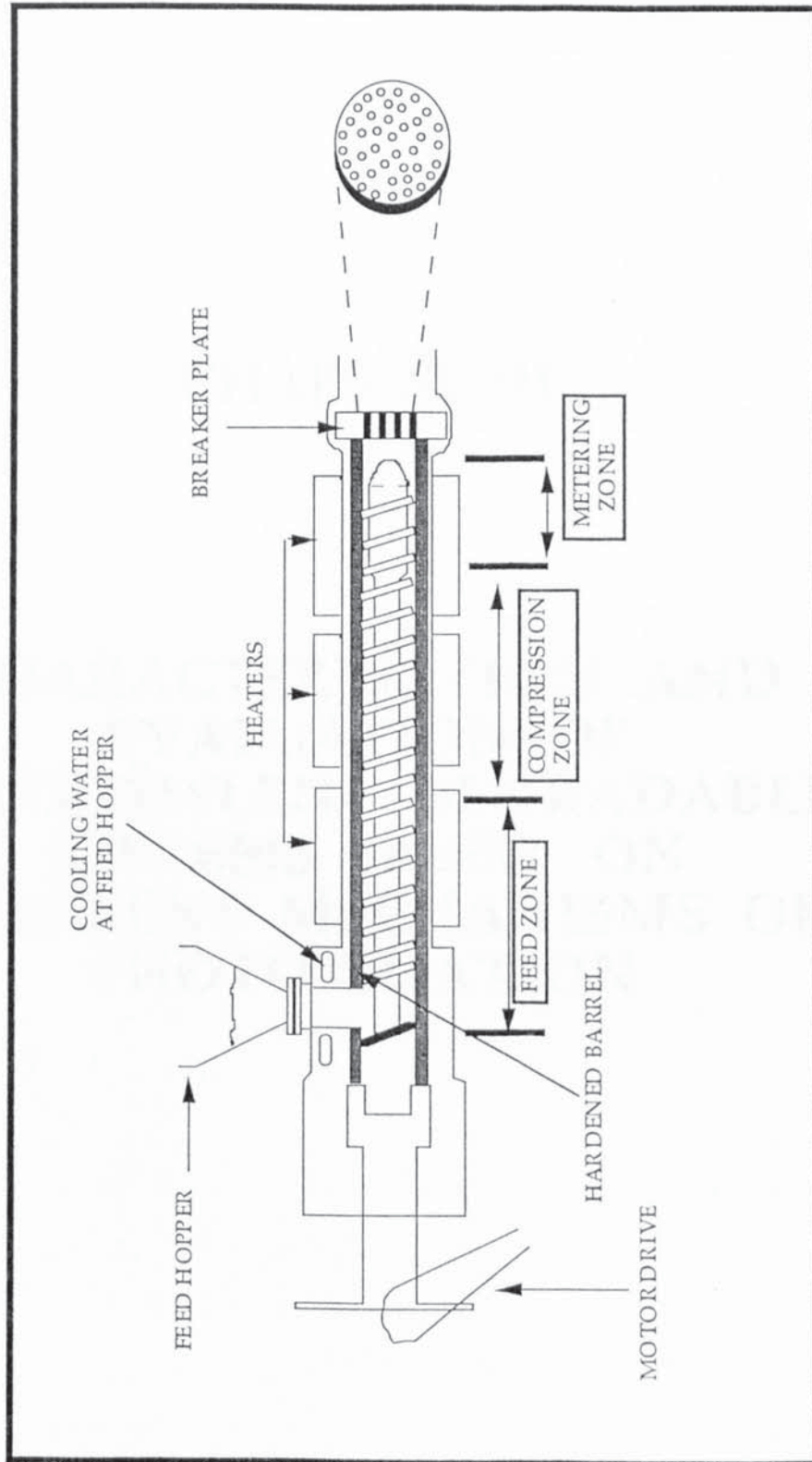
Intensity ( $I$ ) =  $\frac{60df}{t}$  where  $d$  is increase in absorbance expressed as equivalent dose of 305 nm radiation  
 $f$  = is the temperature factor if temperature of uv cabinet is greater than 25°C  
 $t$  = time of exposure of film in minutes.

$$I = \frac{60df}{t} = \frac{60 \times 1.31 \times 0.95}{20}$$

$$I = 3.73 \text{ Wh m}^{-2}$$

Figure 2.12: Uv absorption spectra of polysulphone film before (A) and after (B) uv irradiation in S/B new uv cabinet showing the change in absorbance at 330nm and its relationship to determining the intensity of radiation.

FIGURE 2.13: SCHEMATIC REPRESENTATION OF HUMBOLDT 40/20D SINGLE SCREW EXTRUDER



## CHAPTER III

# CHARACTERISATION AND EVALUATION OF POLYETHYLENE DEGRADABLE SYSTEMS BASED ON DIFFERENT MECHANISMS OF PHOTOXIDATION

## CHAPTER III

## CHARACTERISATION AND EVALUATION OF POLYETHYLENE DEGRADABLE SYSTEMS BASED ON DIFFERENT MECHANISMS OF PHOTOOXIDATION.

## 3.1. OBJECTIVES AND METHODOLOGY

The aim of the work described in this chapter was to characterise and evaluate the commercially available (table 3.1) and laboratory extruded (table 3.2) photobiodegradable polymer samples. The commercial samples were obtained from different sources. The laboratory extruded degradables which were based on a metal antioxidant photoactivator class (iron and nickel diisononyl dithiocarbamate) were processed in the laboratory using a single screw extruder, see scheme 3.1. In the case of the FeDNC based samples the concentration of the metal salt was increased from 0.01% to 0.05%, whilst in the Fe/NiDNC systems the concentration of NiDNC was kept constant at 0.01% and the concentration of FeDNC was varied from 0.01% to 0.05%, see table 3.2. The commercial degradable polymer samples were classified into the following three groups depending on the different modes of degradation which are initiated by the different additives used in these polymers ( see table 3.1):

- (1) Photolytic copolymer class containing a photosensitive group.
- (2) Metal activator class containing transition metal compounds or metal antioxidant photoactivator class based on dithiocarbamate ligand.
- (3) Starch-filled PE's containing transition metal salts.

The general experimental procedure used is outlined in scheme 3.1. Representative samples of each degradable category were oxidised under several conditions. Photooxidation was carried out under natural conditions

Table 3.1: Photobiodegradable polymer film samples.

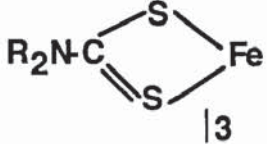
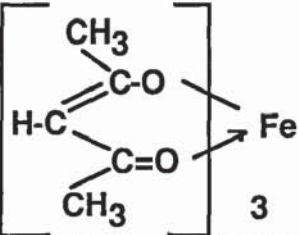
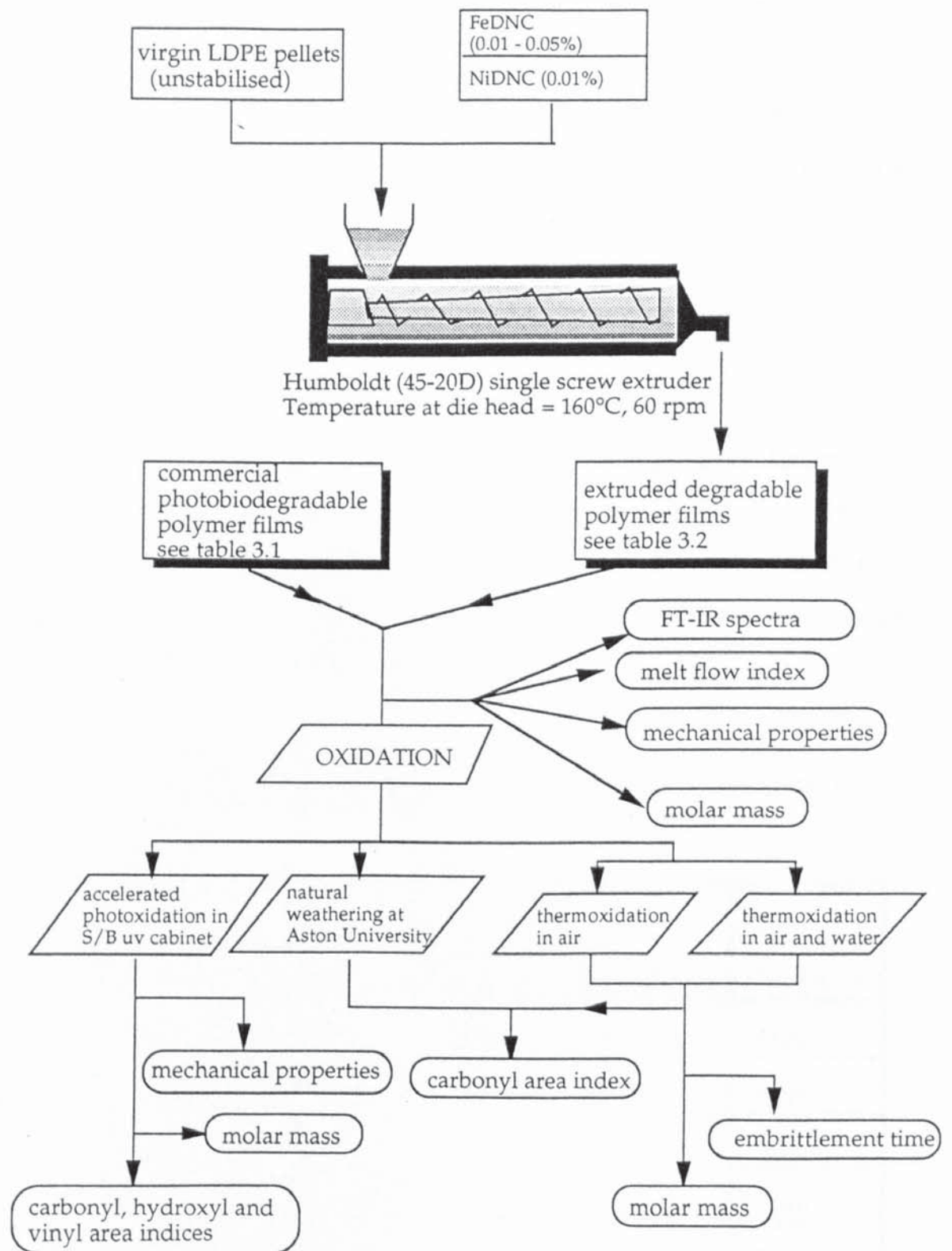
Type	Composition	Origin	Film Thickness as received ( $\mu\text{m}$ )	Group	Code
Photolytic Copolymer	Ethylene-CO Copolymer/LDPE	ITW Hi-Cone PE	151	A	A3
Metal complex	FeDRC/LDPE 	PLASTOPIL	35	B	Bo1
Photo	FeDRC/NiDRC/LDPE APA	PLASTOPIL	30		B5
Activators	FeAcAc/HDPE 	ENICHEM 221 HT	13		B7
	FeDRC/HDPE	ENICHEM 2HT	15		B8
Starch	Starch + Fe stearate ( $\text{C}_{17}\text{H}_{35}\text{COO}$ ) <sub>3</sub> Fe + TiO <sub>2</sub> /LDPE	AMPACET	41	C	C2
Filled	Starch + 8% Fe Stearate + 3% TiO <sub>2</sub> /LDPE	AMPACET	45		C3
PE	Starch + organic dye/LDPE	AMPACET	38		C4
	Starch + carbon black /LDPE	AMPACET	31		C5

Table 3.2: Laboratory extruded degradable polymer film samples based on metal antioxidant photoactivator class containing iron and nickel diisononyldithiocarbamate

Sample Code	Composition %		Thickness ( $\mu\text{m}$ )	Appearance
	FeDNC	NiDNC		
Bso (control)	-	-	75	transparent
Bso1	0.01	-	"	light grey
Bso2	0.02	-	"	light grey
Bso3	0.03	-	"	light grey
Bso4	0.05	-	"	light grey
Bs1	0.01	0.01	"	light yellow
Bs2	0.02	0.01	"	light yellow
Bs3	0.03	0.01	"	light yellow
Bs4	0.05	0.01	"	light yellow

in the outside environment and under accelerated laboratory conditions using a S/B UV cabinet, see sections 2.2.4 and 2.2.5. Thermoxidation was performed in the laboratory using a circulating Wallace air oven at 70°C to simulate the effects of composting (see section 2.2.6) and infrared spectra were obtained. The effect of water during thermoxidation was investigated by placing the sample films under test in flasks containing water (see section 2.2.7). The treated polymer films were then analysed for molar mass.

Scheme 3.1: Overview of the methodology adopted in chapter 3



Before and during oxidation, physical properties (mechanical properties, embrittlement time and melt stability) and chemical properties (determinations of the extent of change in carbonyl, hydroxyl and vinyl absorptions from peak area measurements using infrared spectroscopy and molar mass determination using GPC) were measured. Particular emphasis was given to the rates of the photooxidation curves to discuss whether the different modes of degradation gave rise to different oxidation products; these were further examined and are discussed in chapter 5.

## 3.2. RESULTS

### 3.2.1 Initial Physical Properties of Commercial Photodegradable Polymers.

Table 3.3 and figure 3.1 show the initial molar mass (MM, measured at Clermont-Ferrand, see section 2.2.3), mechanical properties and melt stability (expressed as melt flow index, MFI) of different commercial photobiodegradable polymer samples.

Table 3.3: Initial molar mass, mechanical properties and melt flow index of commercial photobiodegradable polymer samples, see table 3.1 for identity of samples

Sample	MM		Mech Props		MFI g/10 mins	Film Thickness
	Mn	Mw	UTS (MPa)	EB (%)		
A3	49,300	254,200	13.24	463	0.87	90 $\mu$ m
Bo1	46,000	266,000	24.10	141	0.74	35 $\mu$ m
B5	33,200	229,500	29.30	90	0.90	30 $\mu$ m
C2	55,000	271,000	26.40	130	1.00	41 $\mu$ m
B7	16,500	625,000	16.30	191	0.16	13 $\mu$ m
B8	15,900	594,200	48.81	392	0.16	15 $\mu$ m

The commercial samples listed in table 3.3 were all obtained from different sources and most likely are based on different grades of polyethylene. This fact must be borne in mind when comparing their different initial physical properties. All the samples have high molar mass, and showed relatively high tensile strength and large elongation to break values. They all exhibited melt flow index values of less than 1.00 (except the starch-filled PE system , C2, with a melt flow index of 1.00).

### 3.2.2. Initial Physical Properties of Laboratory Extruded Degradable Samples.

Table 3.4 and figure 3.2 show very similar initial values for molar mass, MFI and mechanical properties for LDPE samples extruded in the laboratory based on nickel and iron diisononyldithiocarbamate.

Table 3.4: Initial mechanical properties and melt flow index of laboratory extruded photodegradable polymer samples based on FeDNC and NiDNC, see table 3.2 for sample compositions.

Sample	Molar Mass		Mech Props		MFI g/10mins
	Mn	Mw	UTS (MPa)	EB (%)	
Bso (no antioxidant, control)	36,400	286,700	11.90	380	1.71
Bso1	35,000	268,500	13.9	354	1.78
Bso2	-	-	12.3	271	1.67
Bso3	-	-	13.80	419	1.79
Bso4	31,800	266,400	13.10	396	1.85
Bs1	-	-	11.50	364	1.76
Bs2	-	-	14.90	543	1.84
Bs3	-	-	13.40	439	1.57
Bs4	25,900	263,800	11.60	365	1.75

In all the samples, the same grade of unstabilised LDPE with a melt flow index of 2.3 g/10 mins was used; hence the physical properties of these samples are expected to be the same. The extruded samples showed molar mass values not too dissimilar from that of a control processed LDPE without any antioxidant, code Bso, see table 3.4. All processed samples exhibited lower MFI values than the virgin LDPE. With the exception of Bso2 and Bs3 all the extruded photodegradable samples displayed slightly higher values of MFI than the control (Bso) indicating that the extent of degradation in these samples is lower. These extruded samples were found to have comparable mechanical properties, (see figure 3.2 b and c) to that of the control sample. The addition of the antioxidants to these systems does not appear to have any significant contributions to the mechanical properties; see table 3.4 and figure 3.2.

### 3.2.3 Oxidation of Photodegradable Polymers

#### 3.2.3.1 Initial Calculation of Carbonyl Area Index of Samples as Received

Processed LDPE films always contain small traces of carbonyl species. These are the result of small levels of oxidation that usually take place during the processing and subsequent storage of the polymer. Other moieties that are also formed during the processing (due to melt oxidation) and storage stages of the polymer are small traces of hydroperoxides and vinylidene groups. The formation of these groups can be controlled by the addition of antioxidants and melt stabilisers during polymer processing (see section 1.2). The initial levels of carbonyl species present in the polymer backbone of commercial film samples (as received) and laboratory processed control (Bso) was determined using infra-red spectroscopy, see table 3.5. The different classes of photobiodegradable polymer samples displayed very different levels of initial carbonyl products. Figure 3.3 shows the infrared

Table 3.5: Determination of initial carbonyl area of degradable polymer film samples as received.

Sample	Initial Carbonyl Area *
Bso (Lab. extruded with no additives, control)	0.1
A3	19.4 $\neq$
C2	17.14
B1	8.89
Bo1	0.069
B5	0.054

\* value quoted is an average of three measurements of three different films.

$\neq$  the high value of initial carbonyl area index for this sample is a consequence of the in-built ketone functional group which is an inherent part of the polymer structure.

spectra in the carbonyl region of the different classes of degradable samples as received and illustrates graphically the initial carbonyl area index values obtained .

### 3.2.3.2 Photoxidation of Commercial Photodegradable Polymers Exposed in S/B UV Cabinet

The oxidation of the polymer can be monitored by infrared spectroscopy following the increase in absorbance of the chemical moieties formed; the most common is the carbonyl region, although, changes in the hydroxyl (around  $3400\text{ cm}^{-1}$ ) and the vinyl ( $909\text{ cm}^{-1}$ ) absorptions are also often monitored. Figure 3.4 shows the changes in carbonyl area index (calculated from absorption of carbonyl region, see section 2.4.3) during irradiation of unstabilised LDPE and commercial photobiodegradable polymer samples in the S/B UV cabinet. All the degradable samples which have been purposely designed to oxidise rapidly show much faster rates of oxidation compared

to the unstabilised extruded LDPE film sample, Bso. The "control sample" (Bso) displayed a slow but steady increase in the carbonyl curve. This was paralleled by a slow and steady build up of other functional groups such as hydroxyl, and vinyl, see figure 3.5.

The starch-filled PE system containing titanium dioxide pigment and iron stearate (e.g. C2) and the metal activator class containing iron stearate (e.g. B1) revealed the fastest rate of oxidation, (see figure 3.4). Figures 3.6 and 3.7 display the build up of oxidation products in films C2 and B1 during UV irradiation. Figure 3.8 shows the infrared spectra displaying the increase in oxidation products for the photolytic copolymer A3. This sample also gave a greater increase (compared to the other degradable samples) in the absorbance peak at  $1641\text{ cm}^{-1}$  which is assigned to a double bond. The photobiodegradable polymer sample B5 based on the antioxidant photoactivator class containing the sulphur based dithiocarbamate ligand, exhibited a slightly different shape of the carbonyl oxidation curve (figure 3.4). Until approximately 700 hours of UV irradiation very little changes in the oxidation curve were observed, after which time the carbonyl curve increased sharply. In polymers Bo1 (photoactivator) and B5 (antioxidant photo-activator), the oxidation products, based on the shape of the carbonyl envelope seen in the FT-IR spectra, seem to be identical, the only difference being the length of time taken for these products to appear, see figure 3.9. Figure 3.10 displays the oxidation curves for the various starch-filled PE samples when irradiated in the S/B UV cabinet.

### 3.2.3.3. Photooxidation of Laboratory extruded Photodegradable Polymers Exposed in the S/B UV Cabinet

Figure 3.11a shows the photooxidation rates of laboratory extruded samples, (codes Bso<sub>x</sub>, x = 1 to 4) containing iron diisononyldithiocarbamate

reflecting the antioxidant concentration of 0.01 - 0.05% irradiated in the S/B UV cabinet. Increasing the concentration of FeDNC leads to faster rates of polymer oxidation. Figure 3.11b shows the oxidation curves for the Bsx series ( $x = 1$  to 4) containing various concentrations of iron diisononyldithiocarbamate and a constant value of nickel diisononyldithiocarbamate (0.01%).

Table 3.6 and figure 3. 12 show the effect of UV irradiation on mechanical properties of samples Bso1-Bso4. Elongation to break was considered to be a more appropriate parameter than tensile strength for measuring physical degradation because it reflects the brittleness and consequent tendency of the plastic to fragment on exposure to UV light.

Table 3.6: Effect of photooxidation (exposure in new S/B UV cabinet) on mechanical properties (elongation to break (%)), see table 3.2 for identity of samples

Sample Irradiation Time, hours	Elongation To Break (%)			
	0	150	481	982
Bso1	354 (100)•	200 (56.50)	58 (16.38)	13 (3.67)
Bso2	271 (100)	141 (52.03)	48 (17.71)	16 (5.90)
Bso3	419 (100)	210 (50.48)	51 (12.17)	12 (2.86)
Bso4	396 (100)	205 (51.77)	39 (9.85)	9 (2.27)

- Values in brackets are calculated percentage retention of elongation to break

#### 3.2.3.4. Photooxidation of Photodegradable Polymers Exposed for Natural Weathering.

Figure 3.13 shows the results obtained when the commercial degradable polymer samples were exposed outside (at Aston University, Birmingham) under natural environmental conditions. The total exposure period was

ten months (June 1993 to April 1994). All degradables showed faster rates of oxidation than the unstabilised LDPE, control (Bso) sample.

### 3.2.3.5. Effect of Heat on Photodegradable Samples Exposed in a Wallace Oven

Table 3.7 reflected the effect of heat (70°C) on five photobiodegradable samples (starch-filled PE systems, C2 and C3, metal antioxidant photoactivator systems, Bso1 and Bs1 and unstabilised LDPE, Bso). The film samples were placed in a Wallace oven with circulating air; however, no light was allowed in. The carbonyl area index measurements are shown in figure 3.14. At this temperature only the starch-filled PE systems showed measurable thermal oxidation, both polymer samples becoming brittle after 40 days of exposure. The experiment was conducted for seven months. After a period of 190 days the other degradable samples still showed no signs of ageing at this temperature.

Table 3.7: Embrittlement time of samples exposed for thermal oxidation in a Wallace oven at 70°C with circulating airflow at 0.07 m<sup>3</sup>/h.

Sample	Embrittlement Time at 70°C, in air (0.07 m <sup>3</sup> /h) oven, Days
Bso, Bs1, Bso1,	>190 (6.7 months)
C2	43
C3	40

### 3.2.3.6. Effect of Heat and Water on Photodegradable Samples

Table 3.8 and figure 3.15 represent the effect of heat (70°C) and water and natural light on photodegradable samples. Under these modified conditions (compared to section 3.2.3.5) both unstabilised LDPE and starch-filled PE showed very accelerated rates of oxidation. Both samples exhibited considerable reduction in molar mass with a greater effect for the starch-

Table 3.8: Embrittlement time and molecular weight of samples exposed for thermal oxidation at 70°C with air and water.

SAMPLE	EMBRITTLEMENT TIME, Days	MOLAR MASS (Mw)	
		Initial	After embrittlement
Bs1, Bso1,		--	--
Bso	42	286 700	122 200
C2	15	271 000	49 000

filled sample. Surprisingly, under these conditions the photodegradable sample, Bso1 did not show any signs of ageing, even after four months of exposure.

### 3.3 DISCUSSION

#### 3.3.1 Evaluation of Initial Properties of Photodegradable Samples.

All commercial photobiodegradable polymers have high molar mass (Mw 250000 - 625000), see table 3.3 page 89. Molar mass and molar mass distribution of the polymer greatly influences physical properties such as tensile strength, elongation to break and melt flow index. It is possible to compare the different commercial samples by considering their molar mass distribution in terms of the heterogeneity index [102] ( $M_w/M_n$ ). Figure 3.16 shows that samples A3, Bo1, B5 and C2 have very similar ratios of the heterogeneity index, indicating similar molar mass distributions. This is further supported by figure 3.1 which reveals similarity in the physical properties, especially melt flow index (which is inversely proportional to molar mass) of these samples. Samples B7 and B8, which are based on HDPE, have very high heterogeneity indices of around 37 and are characterised by low melt flow index values, see table 3.3.



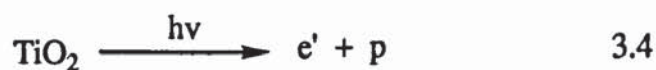
two samples is examined more closely (figure 3.3) it becomes evident that two absorption peaks are apparent in this region, a  $1736\text{ cm}^{-1}$  peak due to the stearate function and a  $1718\text{ cm}^{-1}$  most likely due to a ketone absorption formed as a result of the pro-oxidant behaviour of the iron stearate during processing [6,82,108]. The unstabilised LDPE, Bso, which has no in built mechanism of degradation shows the presence of small amounts of carbonyl oxidation products (initial carbonyl area index is 0.1), see figure 3.3. The carbonyl species absorbs at  $1720\text{ cm}^{-1}$  indicating that these products are ketones which are formed from hydroperoxides as primary products of oxidation [77]. The photobiodegradable polymer samples based on the metal antioxidant photoactivator and photoactivator classes, B5 and Bo1, respectively, showed the lowest content of initial carbonyl area index, much smaller than the unstabilised LDPE (figures 3.3a and b). This is due to the melt stabilising action of the DNC ligand which mops up any hydroperoxides that are produced during processing of the polymer and therefore prevents the formation of carbonyl containing oxidation products such as ketones [27,78-80].

### **3.3.2 Effect of UV Irradiation on Photodegradable Samples.**

Figure 3.4 shows that all degradable samples oxidise faster than the unstabilised control sample, and that all samples, except B5 (an antioxidant photoactivator) photooxidise without an induction period. A closer examination of the build up of the oxidation products in the carbonyl region of the infrared spectra of Bso, C2, B1, A3 and Bo1, B5 (figs. 3.5 -3.9) show that the carbonyl peak is a composite peak consisting of several different carbonyl products which are labelled in the expanded carbonyl region of the infrared spectrum, see figure 3.17.



reactions. Another factor that may be responsible for accelerated photooxidation rates of C2 and C3 is the inorganic pigment titanium dioxide [99] which is used to impart white colour to these samples. Allen [109] and Day [110] have examined the role of titanium dioxide pigments in polyolefins during photooxidation. It was found that although the pigment is able to scatter efficiently all wavelengths of visible radiation, it shows strong UV absorption. The absorbed UV radiation releases electrons and positive holes (p) in the crystal structure (see reaction 3.4) [111], which results in the production of free radicals such as the hydroxyl radical (see reaction 3.5) [111]. These radicals migrate to the surface of the polymer and cause the oxidation of the polymer substrate.



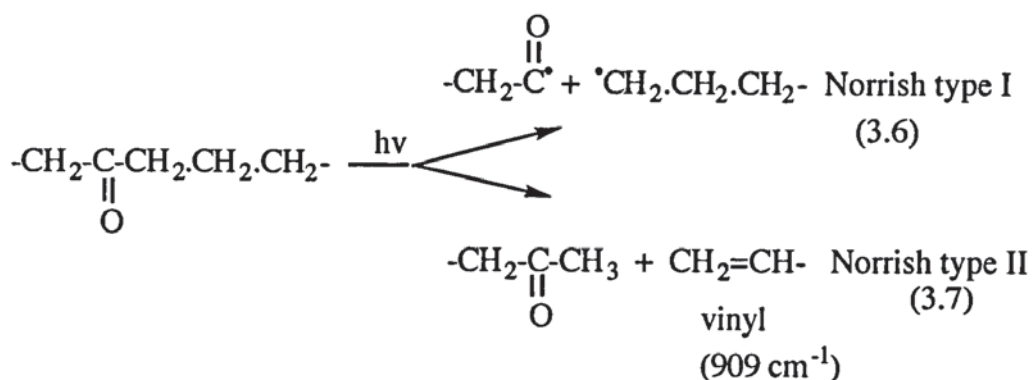
Polymer samples containing iron dithiocarbamate only, Bo1, showed a very fast rate of oxidation leading to a high content of oxidation products (figures 3.4 and 3.9). The onset of degradation in this sample occurred almost straight away without an induction period, see fig. 3.4. The system which is based on both iron and nickel dithiocarbamates (B5), on the other hand, showed an induction period (approximately 700 hours) during which very little oxidation took place, figure 3.4. This induction period is due to the high photostability of the NiDRC in the system [78-80,107]. The onset of degradation does not commence until the NiDRC has been consumed. However, after the end of the induction period at which point the concentration of NiDRC becomes very low, the photoreduction of the trivalent iron complex (FeDRC) comes into effect [78-80,107] and a very rapid rate of oxidation takes place. By varying the concentration of both iron and nickel DRC in these systems it is possible to accurately control the

rate of oxidation and the length of the induction period [42-44,80]. Higher concentrations of FeDRC are expected to give rise to faster rates of oxidation and higher quantities of oxidation products. This is supported by figure 3.11a which shows that increasing the concentration of the iron salt leads to faster rates of oxidation.

In the Bsx series, in which a low concentration of NiDNC was kept constant and the concentration of FeDNC was increased, the nickel complex is expected to act as a mild photosensitiser [42-44,107] leading to mutual photosensitisation between FeDNC and NiDNC. Figure 3.18 illustrates this affect clearly; at low concentration of iron, sample Bs1 (at 0.01%), the Fe/Ni system oxidises faster than the Fe system alone (Bso1), this effect being more pronounced at longer exposure times (fig. 3.18a). However, when the concentration of Fe is increased to 0.05% a reduction in the overall photosensitisation effect was observed and at this concentration there is a reversal in the activity i.e. the Fe system alone (Bso4) oxidises faster than the Fe/Ni (Bs4) system (fig.3.18b).

During the initial stages of UV irradiation of the photolytic copolymer (A3), the narrow ketone peak at  $1720\text{ cm}^{-1}$  decreases followed by an increase of a broad composite peak, see figure 3.8. Figure 3.19 shows a clearer picture of the changes in the carbonyl absorbance. The initial decrease of the absorbance at  $1720\text{ cm}^{-1}$  is due to the photolysis of the in-built ketone group [73] which can occur via reactions 3.6 and 3.7.

The favoured route is via Norrish-II, reaction 3.7, in the photooxidation of A3 compared to the other degradables, e.g. Bo1 and Bso, which accounts for the much larger increase of the vinyl content ( $909\text{ cm}^{-1}$ ) and the simultaneous decrease in the vinylidene content ( $887\text{ cm}^{-1}$ ) in regions of



the infrared spectra, seen in figs 3.5, 3.8 and 3.9. Figure 3.20 shows the area index measurements for vinyl ( $909\text{ cm}^{-1}$ ) and vinylidene groups ( $887\text{ cm}^{-1}$ ) for samples A3, Bo1 and unstabilised LDPE, Bso. It is clear that the amount of vinyl products formed in the photolytic copolymer, A3, is very much larger compared to the other two samples. Further, the shape of the curve in the case of sample A3 shows clearly that the vinyl content increases very rapidly, almost linearly, from the onset of degradation. Although, the metal photoactivator, Bo1, and the control, Bso, show increases in the vinyl content, the increase is more exponential.

Figure 3.21 compares the length of time taken during UV irradiation for the vinyl content to reach a value of 1.00 for these three samples and shows clearly the much shorter time required in the case of the photolytic sample (A3). Moreover, in the photolytic copolymer sample (A3), there is a much higher content of vinyl species and a lower content of a mixture of carbonyl products (see chapter 5). These findings clearly suggest that this sample photodegrades by a different mechanism to that of samples Bo1 and unstabilised LDPE. Figure 3.19 (FT-IR spectra of sample A3) shows major absorptions at  $1720\text{ cm}^{-1}$  in the carbonyl region, indicating that predominately ketones are formed confirming the predominance of a Norrish II pathway. However, figure 3.9 shows that the FT-IR spectra of Bo1 gives a major carbonyl absorption at  $1710\text{ cm}^{-1}$ , as a consequence of

Norrish I. Figure 3.22 illustrates that the rate of oxidation of sample Bo1 is not only faster than A3, but also the amount of oxidised carbonyl products formed (reproduced from figure 3.4) is greater. This provides further evidence that contribution of a Norrish II process for A3 is greater: oxidation via Norrish II gives rise only to an end-of-chain ketone and vinyl species, whereas via Norrish I photolysis, two free radicals are produced which can be further oxidised to carbonyls products, the net effect being greater quantities of carbonyls (particularly carboxylic acids) formed via Norrish I, see fig. 3.22. The difference in the nature of photooxidation products of samples A3 and Bo1 is fully expanded in chapter 5.

Regardless of whether photooxidation proceeds via Norrish I or Norrish II, the resultant effect is the same, this being the oxidative breakdown of the polymer backbone as demonstrated in figure 3.12, which shows an overall decrease in mechanical properties of the degradable laboratory extruded samples on exposure to UV light. After exposure of 481 hours, the mechanical properties for these samples has been reduced by 80%, suggesting catastrophic destruction of the molecular backbone of these polymers, see figure 3.12.

Natural weathering of degradable samples showed similar oxidation results to those obtained from accelerated weathering in the S/B (new) UV cabinet (despite the seasonal variable weathering conditions such as total hours of light, the average temperature, relative humidity ), see figure 3.13. This is to be expected since the UV radiation output of the S/B cabinet closely resembles the UV radiation output outdoors.

### 3.3.3 Effect of Heat on Photodegradable Samples at 70°C to Simulate Composting Environment

The products of thermal oxidation of LDPE, especially in the carbonyl region in the infrared spectra seem to be very similar to photooxidation, as shown in figure 3.14b. Again, a composite carbonyl peak is observed indicating a mixture of carbonyl products such as esters, ketones and carboxylic acids.

Starch-filled-PE based on transition metal salts and inorganic pigments showed the greatest rate of oxidation due to the pro-oxidant effect of iron stearate and titanium dioxide, see figures 3.14 and 3.15a. Thermal oxidation results in chain scission of the polymer backbone, which is reflected in figure 3.15b that shows the reduction in molar mass ( $M_w$ ) upto the point of embrittlement. The extent of reduction in the case of the starch sample is significantly greater (80%), whilst the reduction in  $M_w$  for the control sample was 60%. Figure 3.23 suggests clearly that water must be a major requirement for composting to occur. The embrittlement time has significantly reduced in the presence of water (figure 3.23b). For sample C2 at this temperature in the presence of water the starch may be hydrolysing, thereby creating weak links in the polymer backbone. The reasons for the dramatic reduction in strength of Bso control sample is not clear.

### 3.3.4 Overview of Results

All the purposely engineered degradable samples (both commercially obtained and laboratory extruded) photoxidised much more rapidly than the laboratory extruded unstabilised polyethylene sample, Bso, as shown by the rate of increase of the carbonyl content. Photoxidation of these samples proceeds mainly via Norrish I reactions, with the exception of the photolytic copolymer system (A3), which proceeds mainly via Norrish II

reactions. As a result of the greater contribution of Norrish II in sample A3, compared to the other systems, larger amounts of ketones are observed whereas for the rest of the degradable systems, in which Norrish II reactions predominated, carboxylic acids were the major photooxidation products. Furthermore, sample A3 gave much higher vinyl content which was produced at a higher rate during photooxidation compared to other systems, further confirming the importance of Norrish II processes in this sample.

Generally, the degradable samples underwent thermal oxidation much more rapidly than the control, Bso, particularly the starch-filled systems. Experiments conducted have shown that the major criteria for degradable samples to thermoxidise (other than heat itself) is the presence of water. Under these conditions, even polyethylene without additives thermoxidises very rapidly.

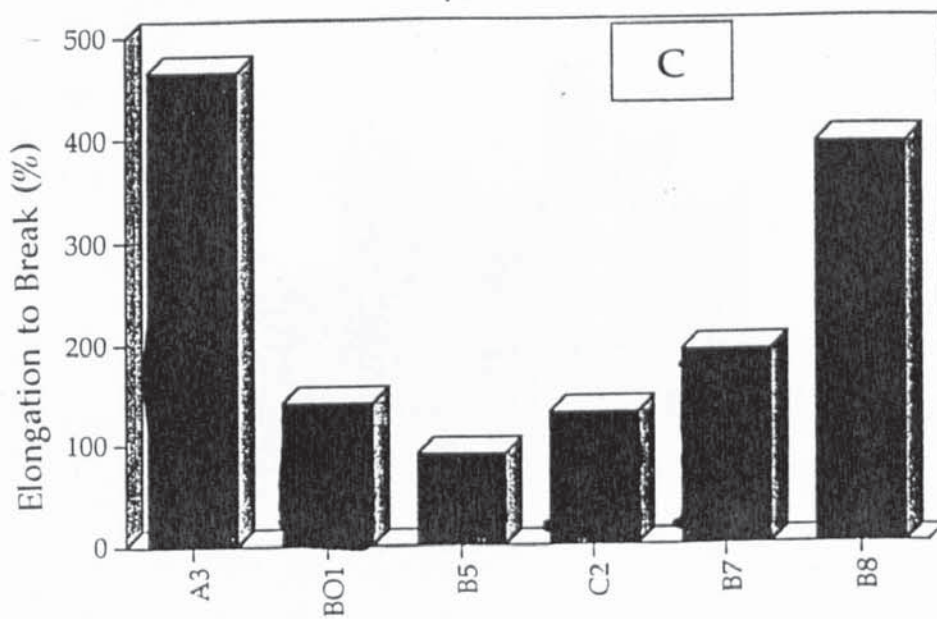
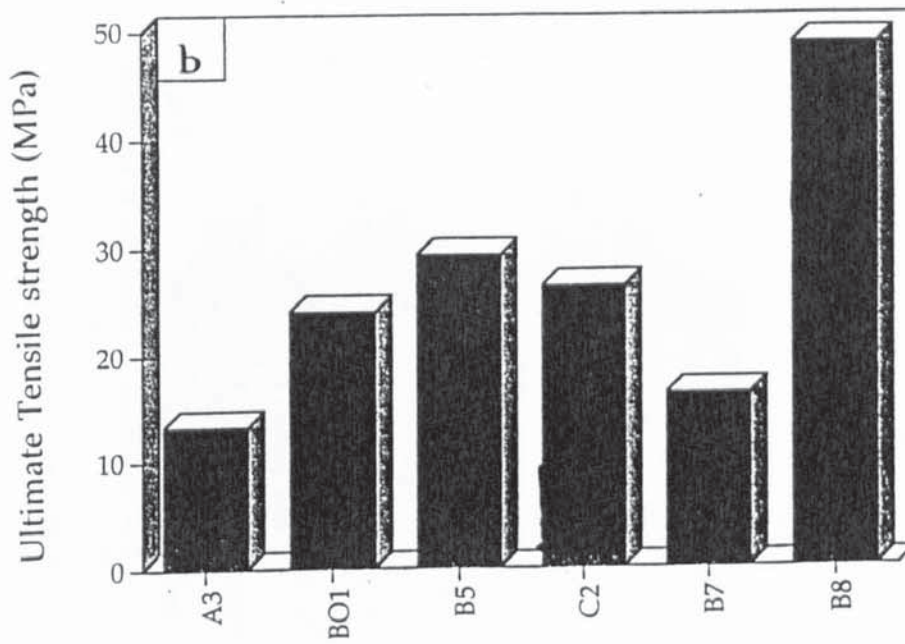
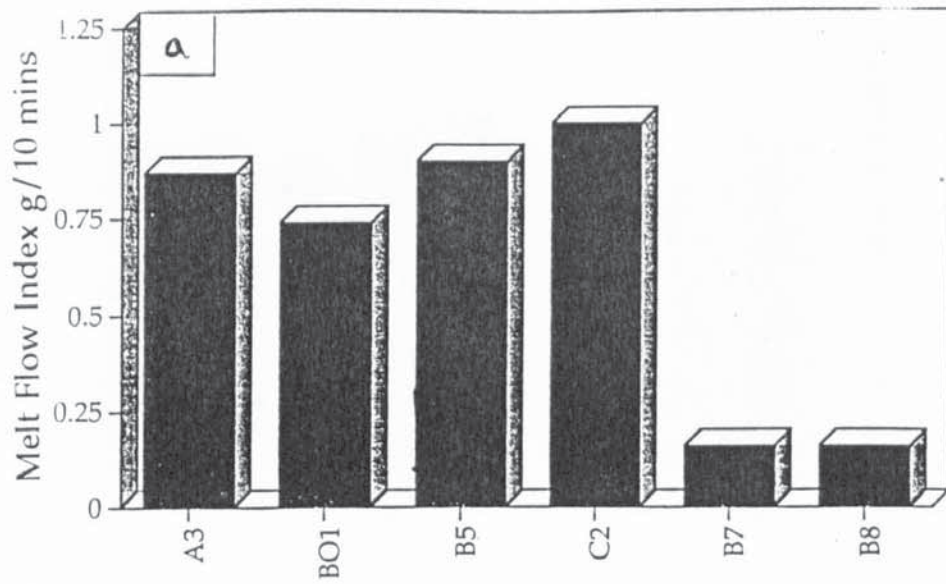


Figure 3.1: Melt flow index, MFI (a); ultimate tensile strength, UTS (b) and elongation to break, EB (c) of commercial photobiodegradable samples: For identity of samples see table 3.1.

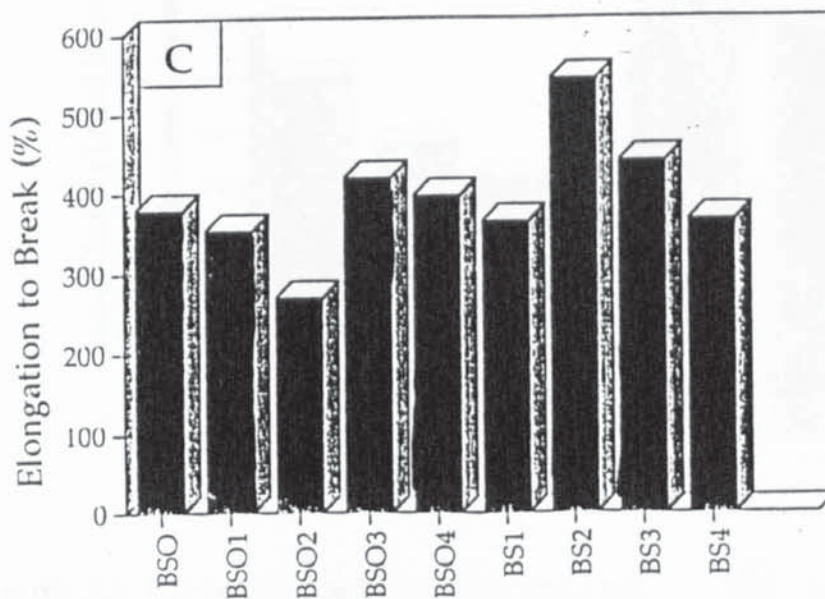
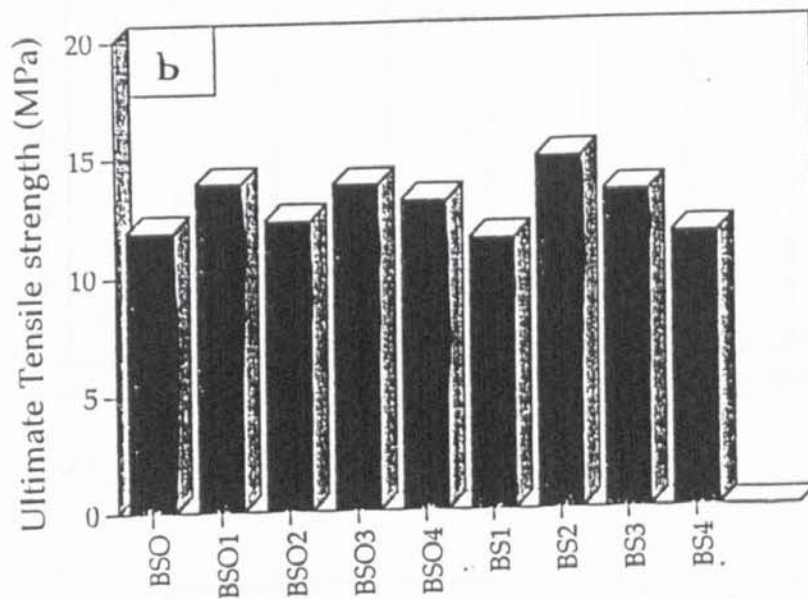
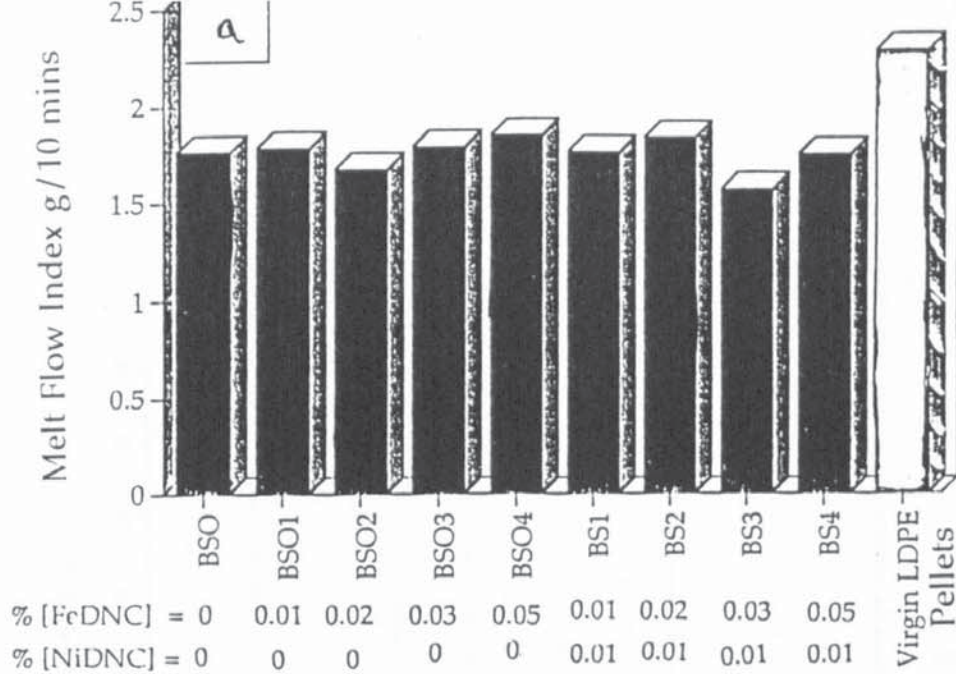


Figure 3.2: Melt Flow Index, MFI (a); ultimate tensile strength, (b) and elongation to break, (c) of laboratory extruded samples based on metal antioxidant photoactivator class using FeDNC and NiDNC.

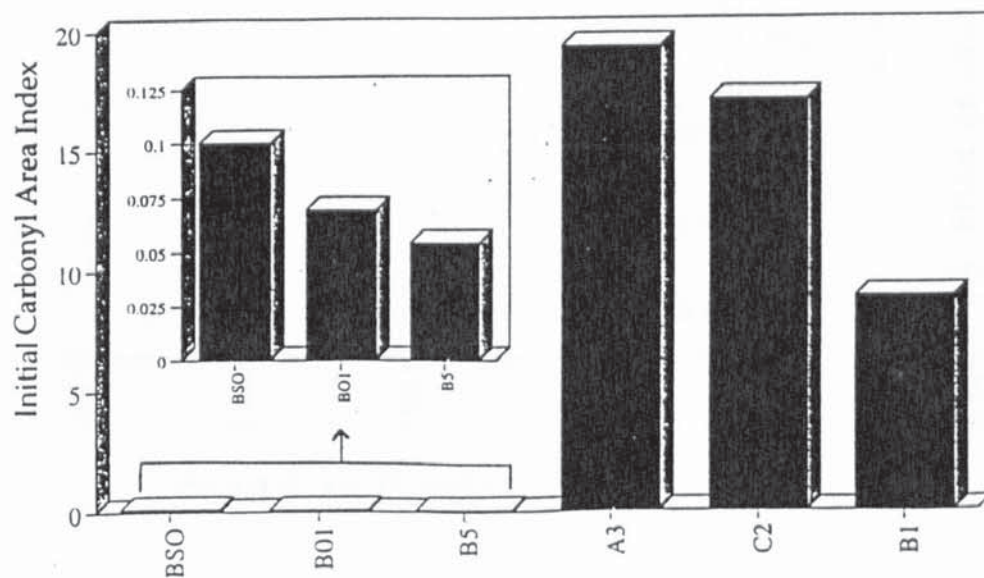
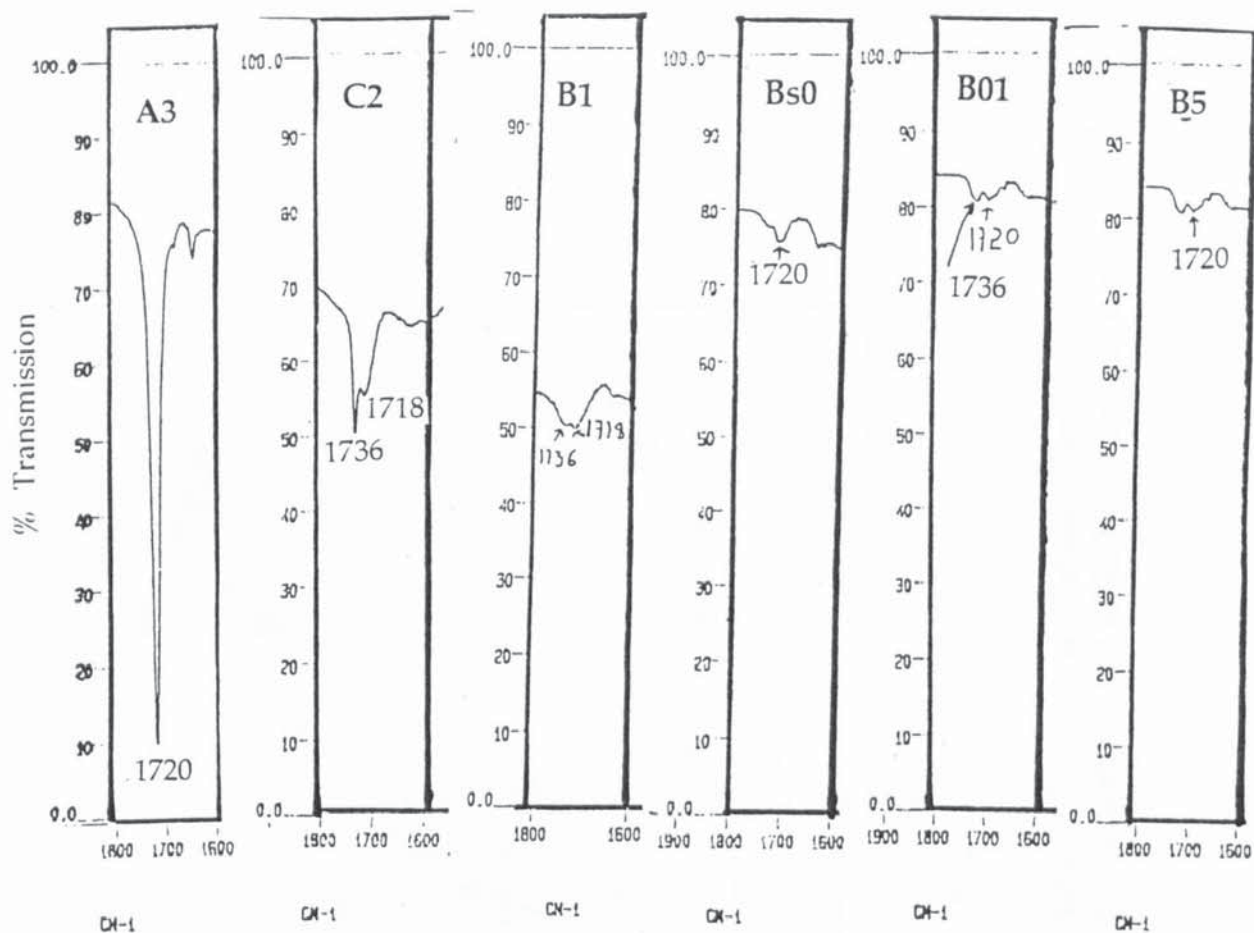


Figure 3.3: Carbonyl region from FT-IR spectra and graphical representation of the initial carbonyl area index of commercial degradable LDPE films (as received). See table 3.1 for codes of polymer samples.

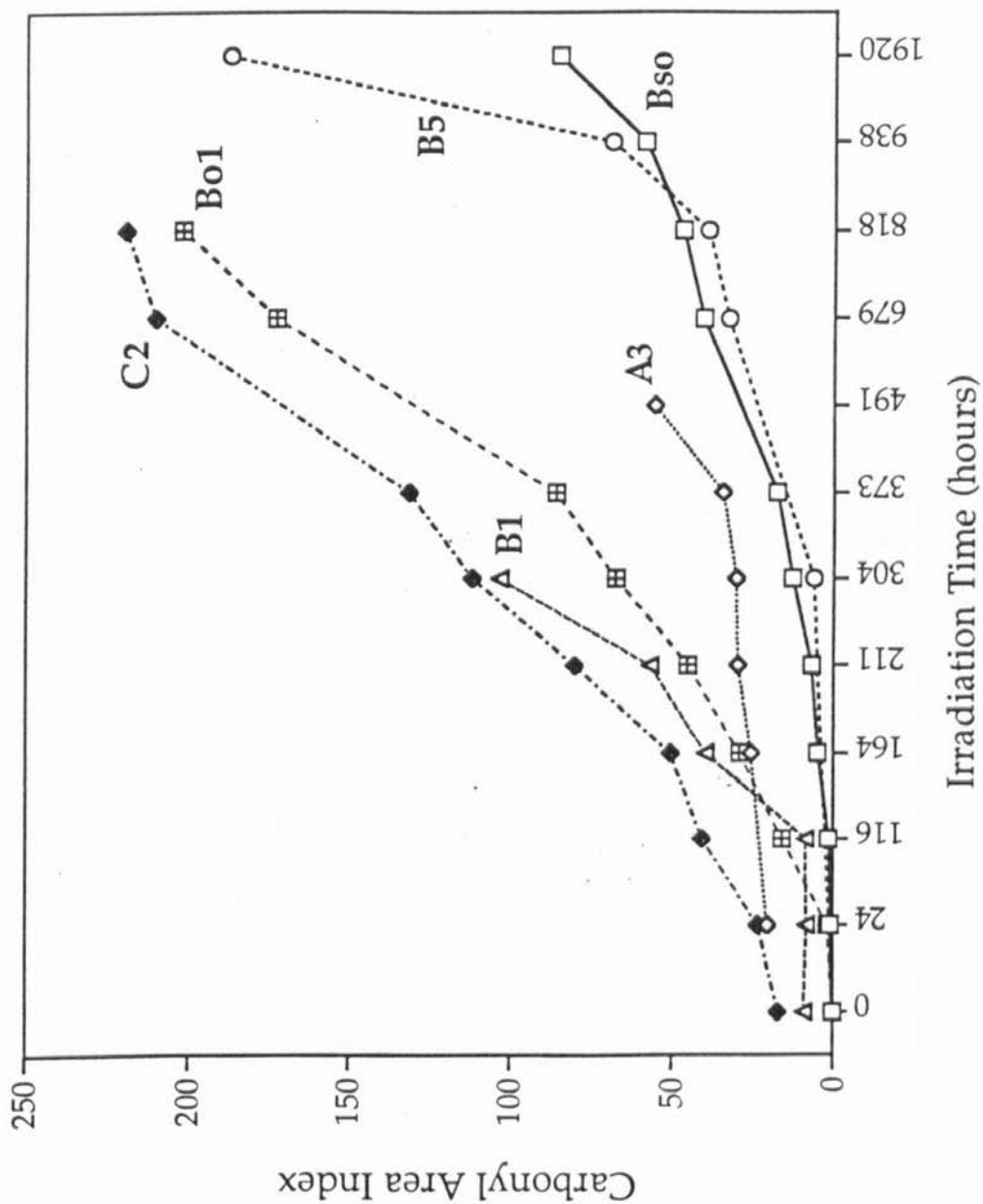


Figure 3.4: Effect of irradiation time (S/B new uv cabinet) on the rate of carbonyl group measured as carbonyl area index. See table 3.1 for sample codes.

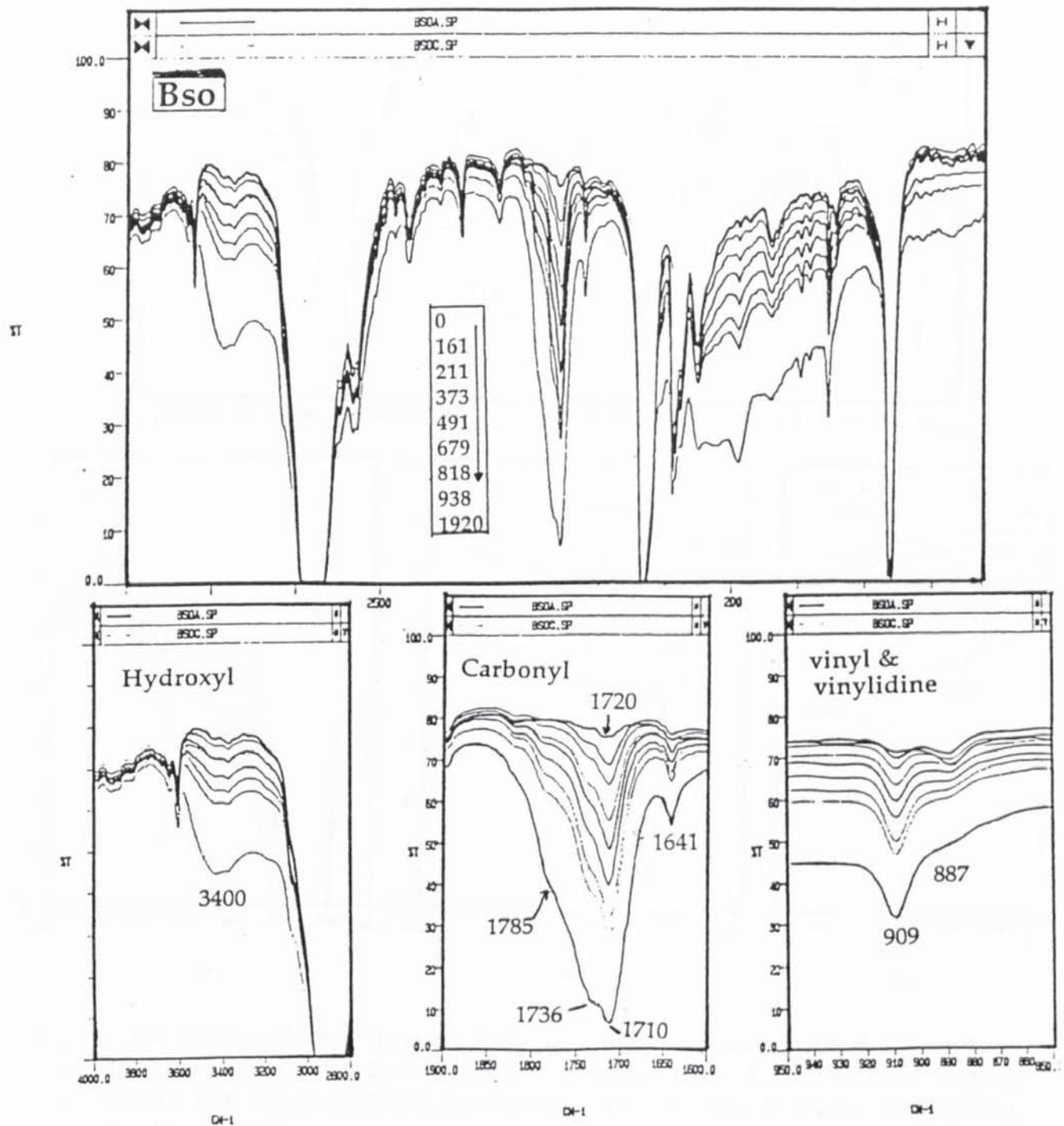


Figure 3.5: Changes in FT-IR spectra during exposure to uv light (S/B new uv cabinet) of processed unstabilised LDPE, thickness 75 $\mu$ m. Numbers in the box are irradiation times in hours and numbers on curves are absorption peak maxima (cm<sup>-1</sup>). %T (y axis) = Transmittance, cm<sup>-1</sup> (x axis) = wavenumber.

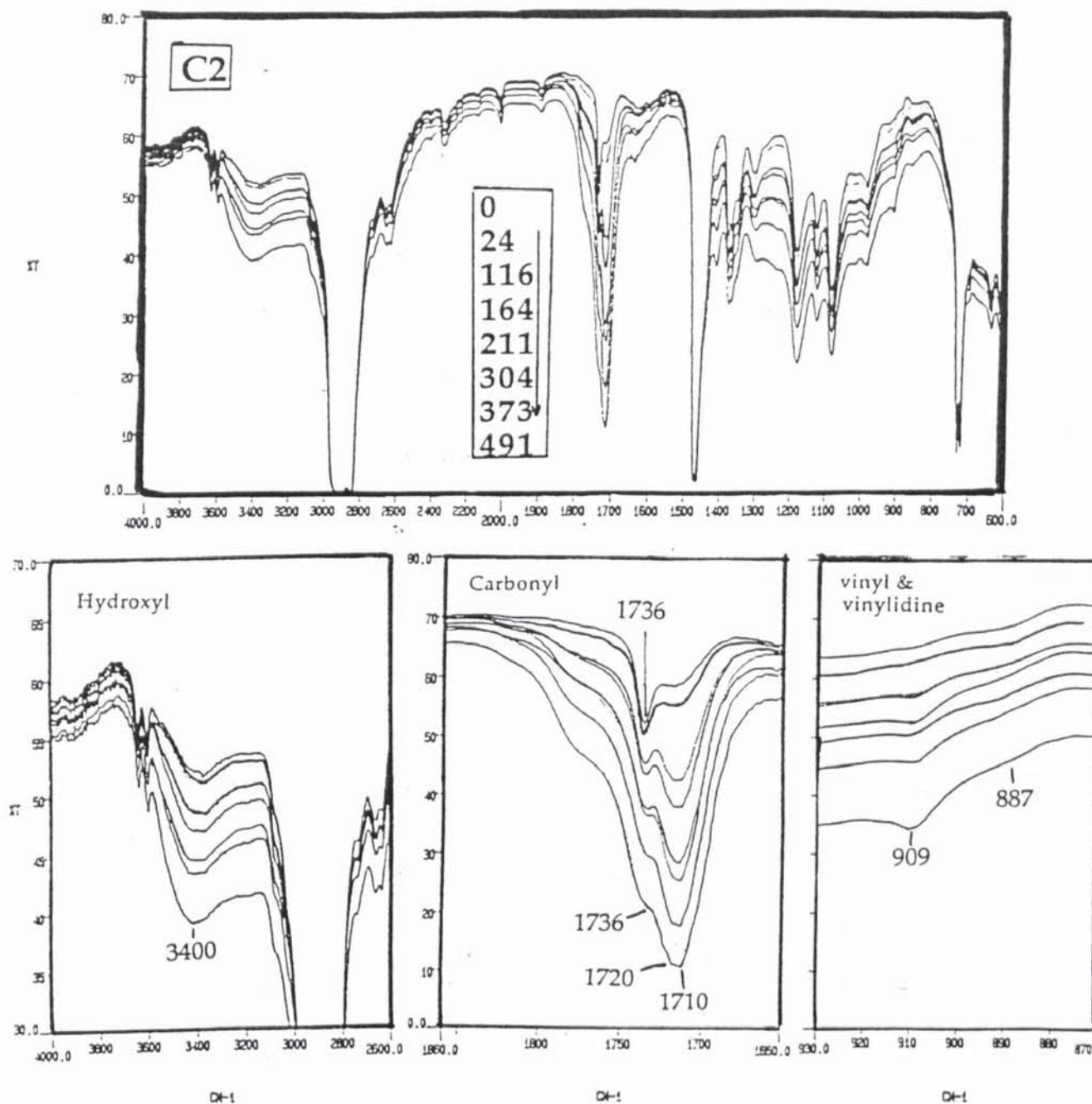
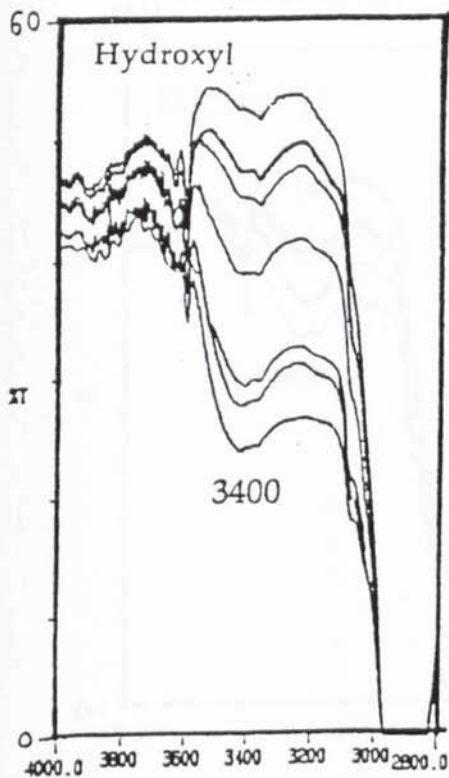
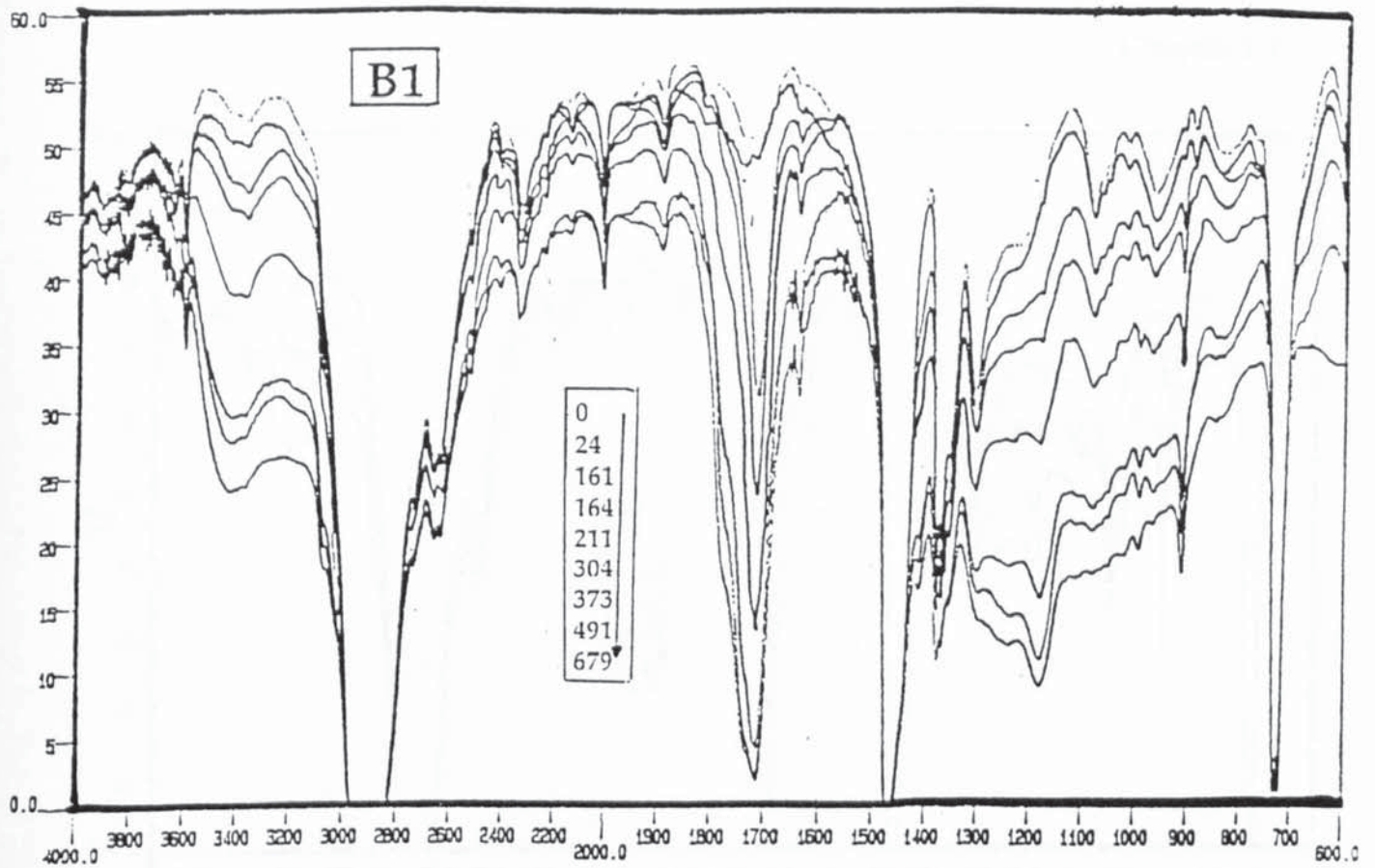
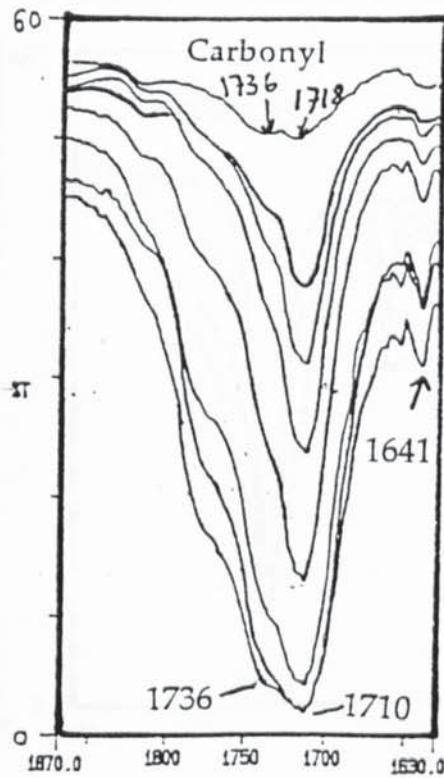


Figure 3.6: Photooxidation in new S/B uv cabinet of starch-filled PE system containing iron stearate and titanium dioxide, code C2, thickness  $41\mu\text{m}$ . Numbers in box are irradiation hours and numbers on curves are absorption peak maxima ( $\text{cm}^{-1}$ ).

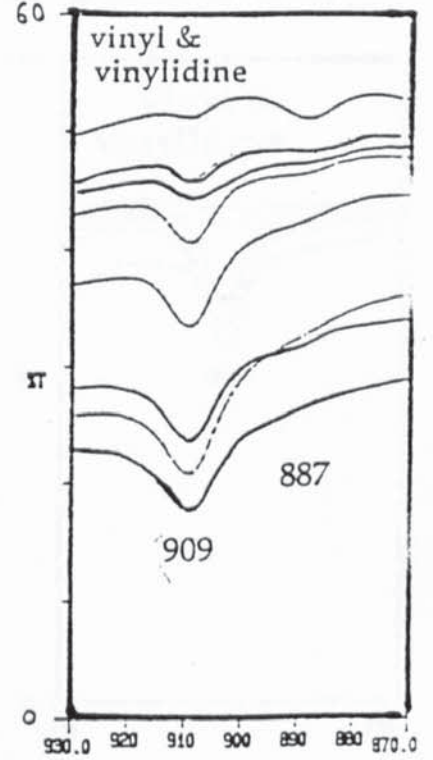
%T (y axis) = Transmittance,  $\text{cm}^{-1}$  (x axis) = wavenumber.



OH-1



OH-1



OH-1

Figure 3.7: FT-IR spectra showing the build up of oxidation products of metal activator class based on iron stearate, B1, during uv irradiation in S/B new uv cabinet, thickness 40  $\mu\text{m}$ . Numbers in box are irradiation hours. %T (y axis) = Transmittance,  $\text{cm}^{-1}$  (x axis) = wavenumber.

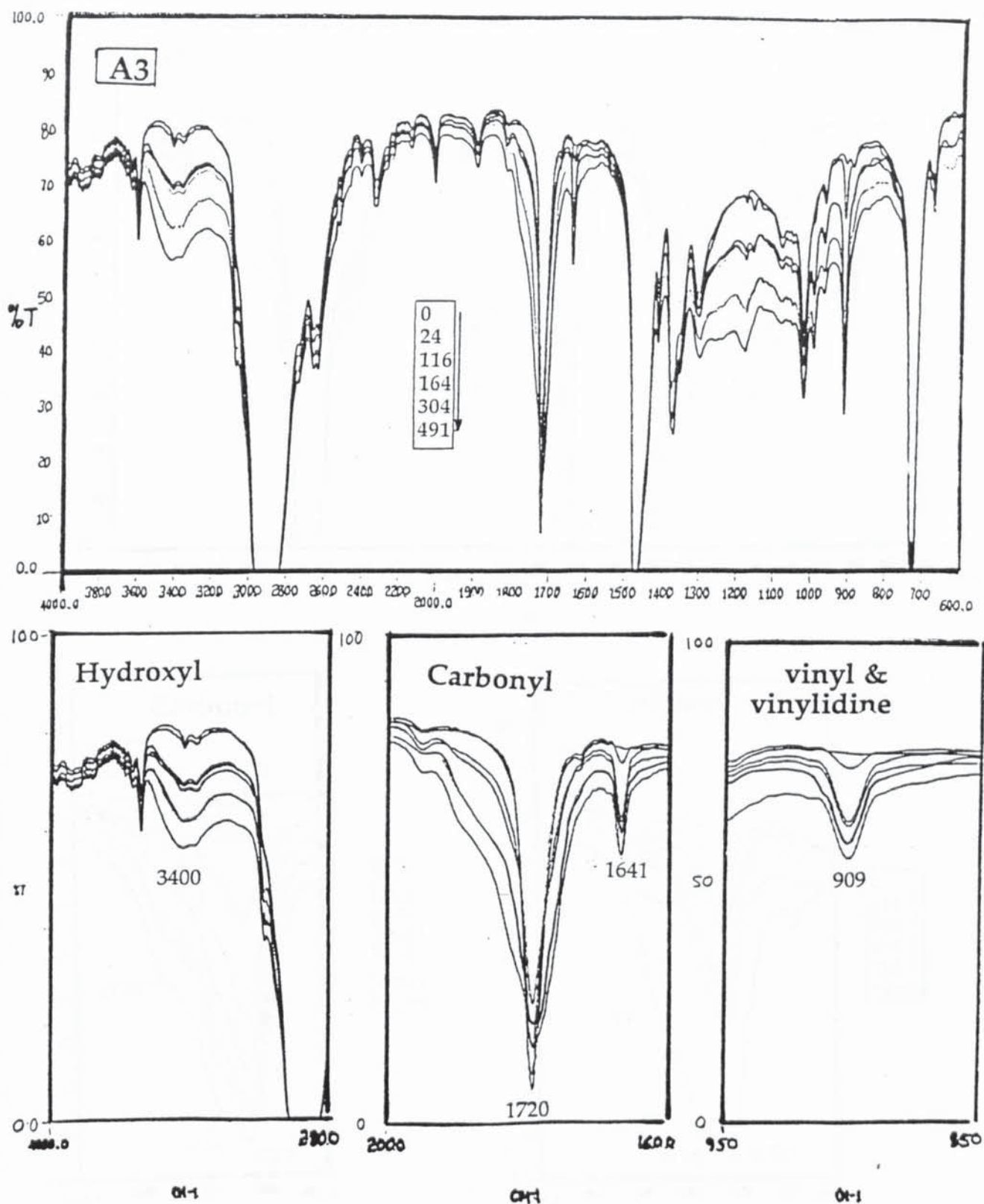


Figure 3.8: FT-IR spectra showing the build up of oxidation products of photolytic copolymer, A3, during uv irradiation in S/B new uv cabinet, thickness 90 $\mu$ m. Numbers in box are irradiation hours.

%T (y axis) = Transmittance, cm<sup>-1</sup> (x axis) = wavenumber.

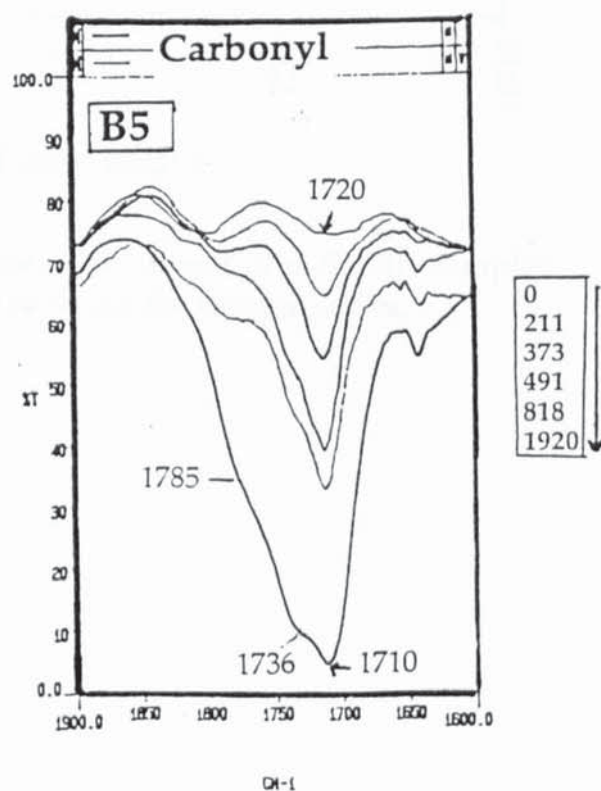
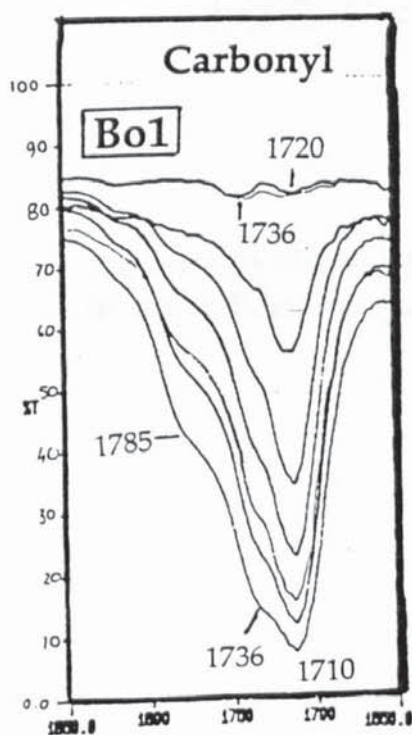
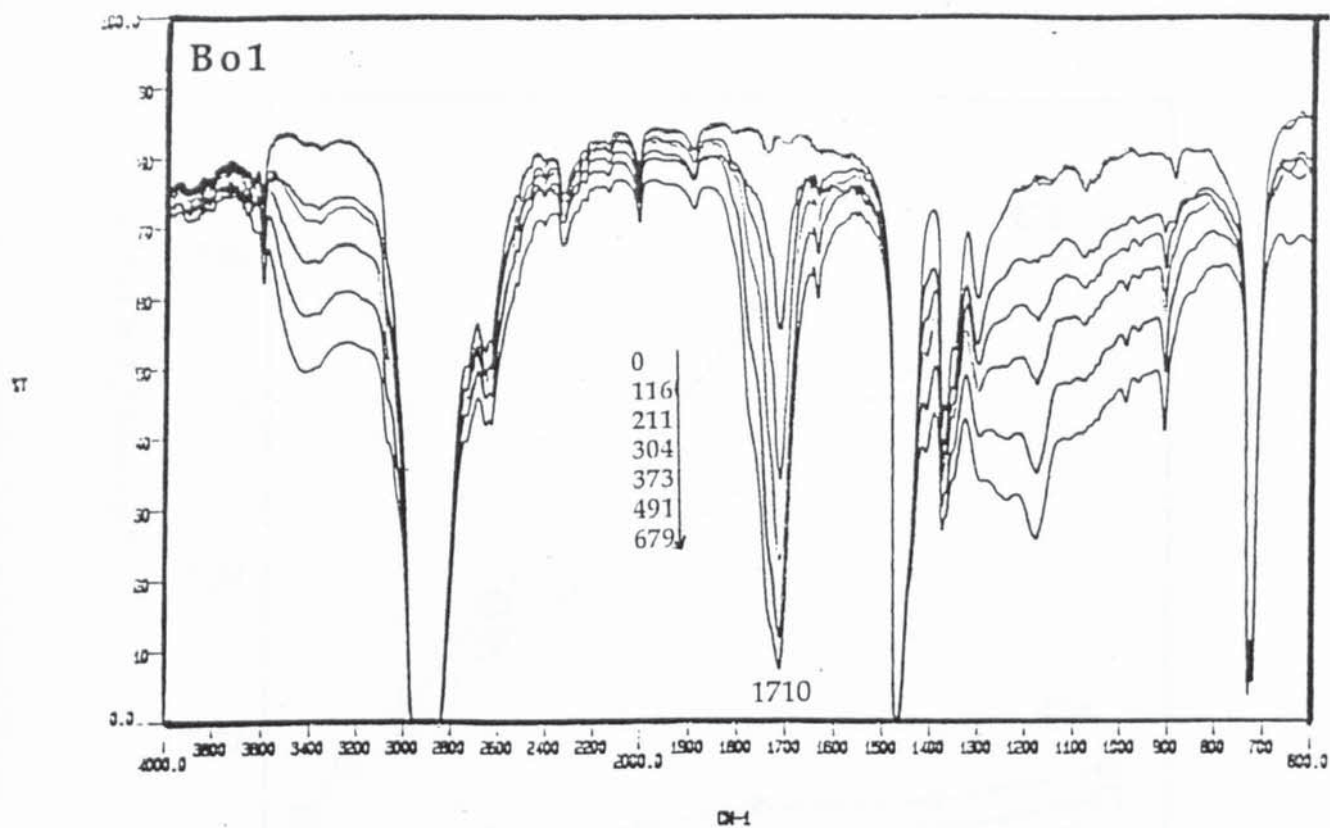


Figure 3.9: Comparison of photooxidation products formed during uv irradiation for metal photoactivator system, Bo1 (thickness  $35 \mu\text{m}$ ) and metal antioxidant photoactivator system, B5 (thickness  $30 \mu\text{m}$ ). Numbers in box are irradiation hours. %T (y axis) = Transmittance,  $\text{cm}^{-1}$  (x axis) = wavenumber.

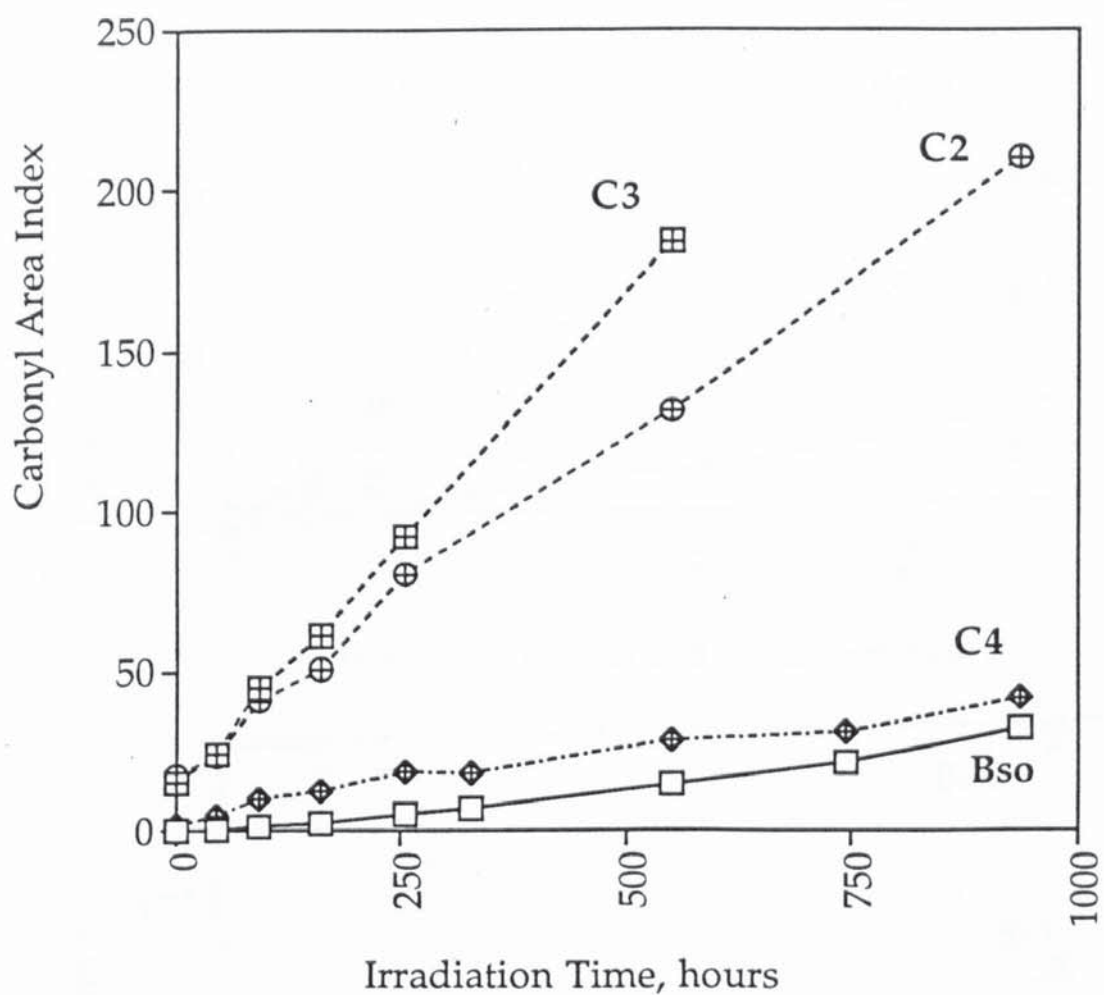


Figure 3.10: Photoxidation in S/B new uv cabinet of different samples of starch-filled PE systems; refer to table 3.1 for sample codes.

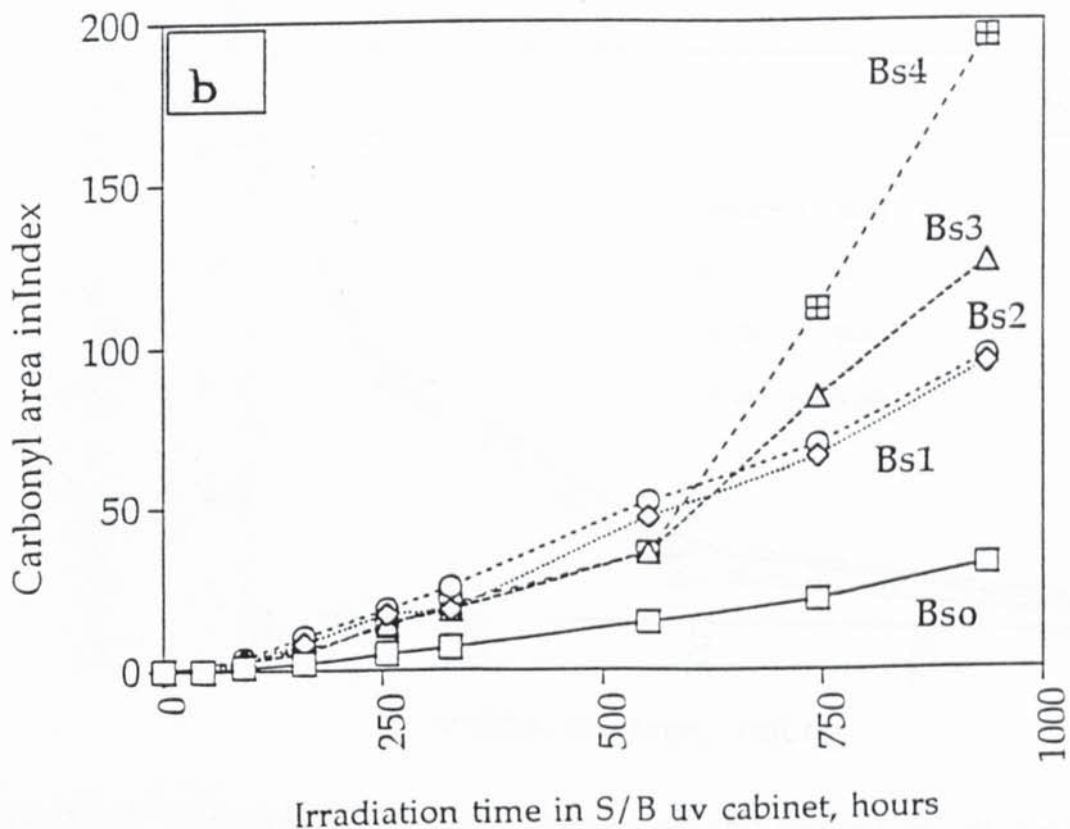
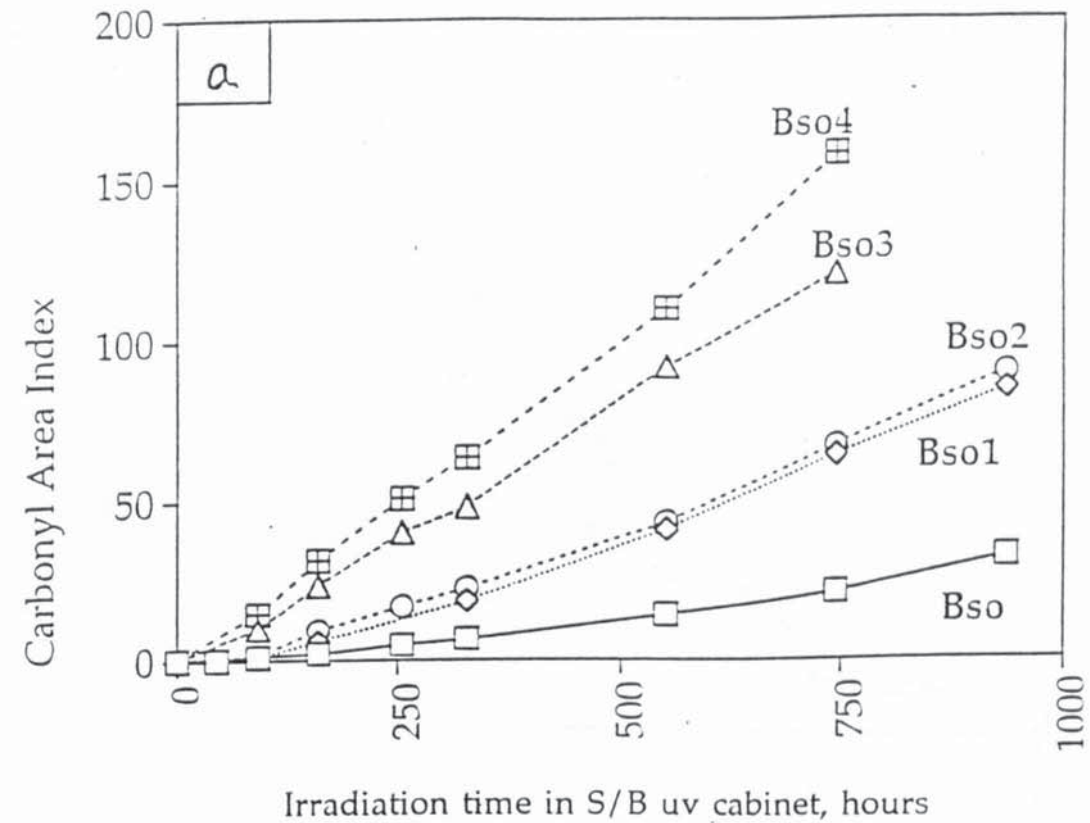


Figure 3.11: Photooxidation rate of laboratory extruded samples showing the increase in photooxidation with increasing concentration of FeDNC, (a) and the effect of using both Fe/Ni DNC, (b) on the rate of photooxidation. See table 3.2 p.87 for composition of samples.

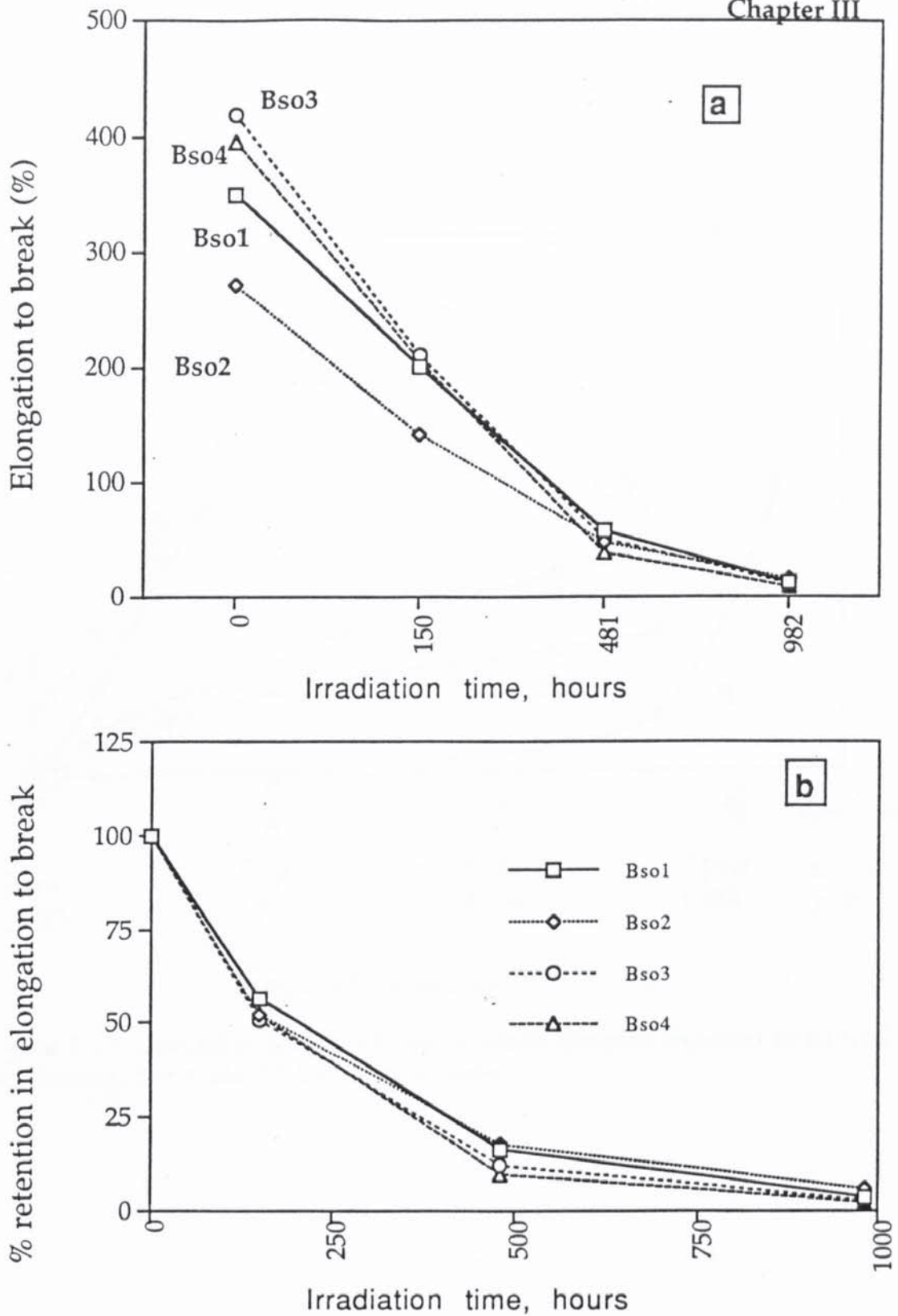


Figure 3.12: Decrease of elongation to break (a) and percent retention of elongation to break (b) of laboratory extruded PE films containing FeDNC on exposure to uv light in S/B cabinet. Each point is an average of five number of samples.

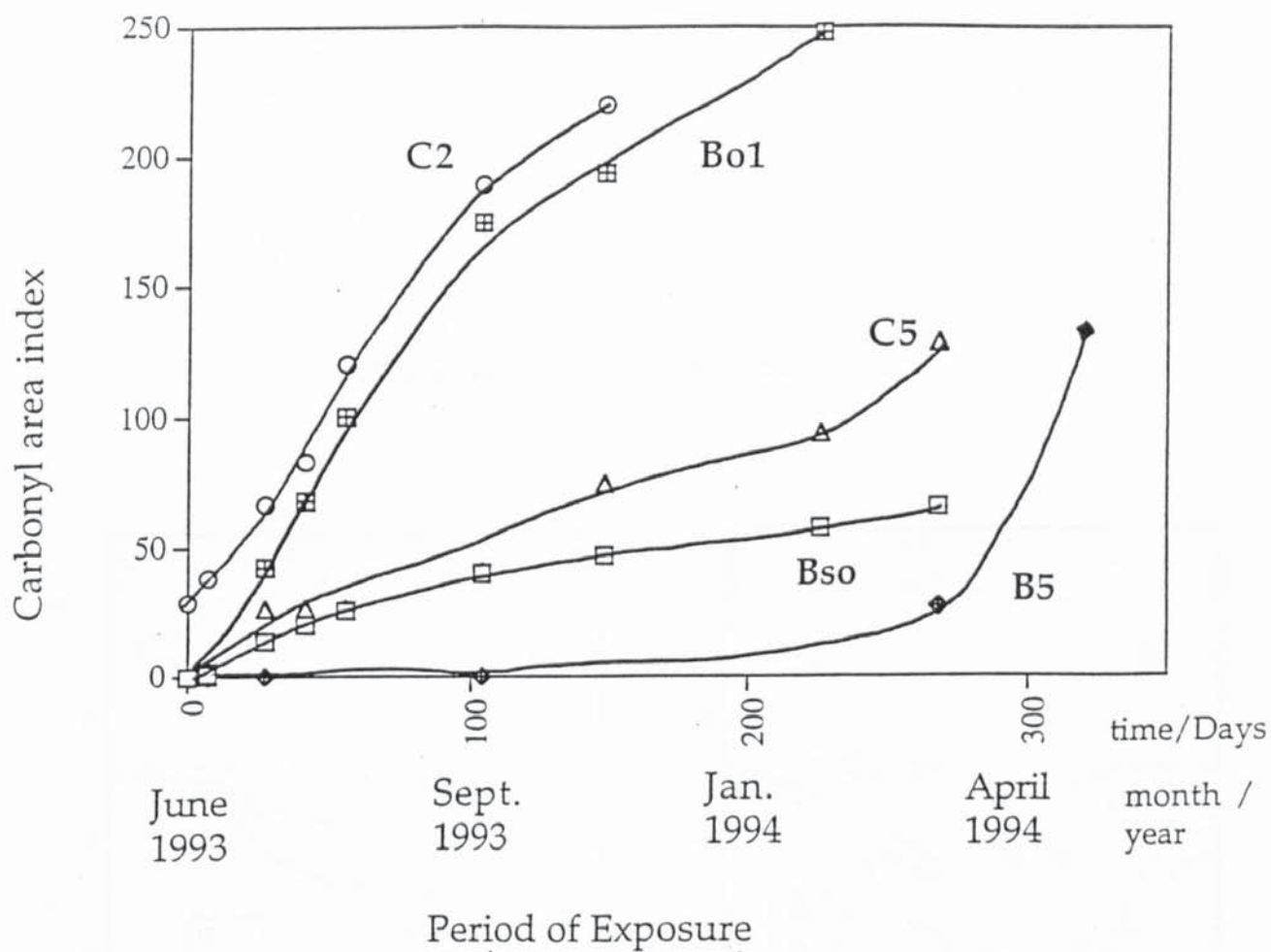


Figure 3.13: Oxidation of degradable polymer samples exposed to natural weathering. See table 3.1 for sample codes.

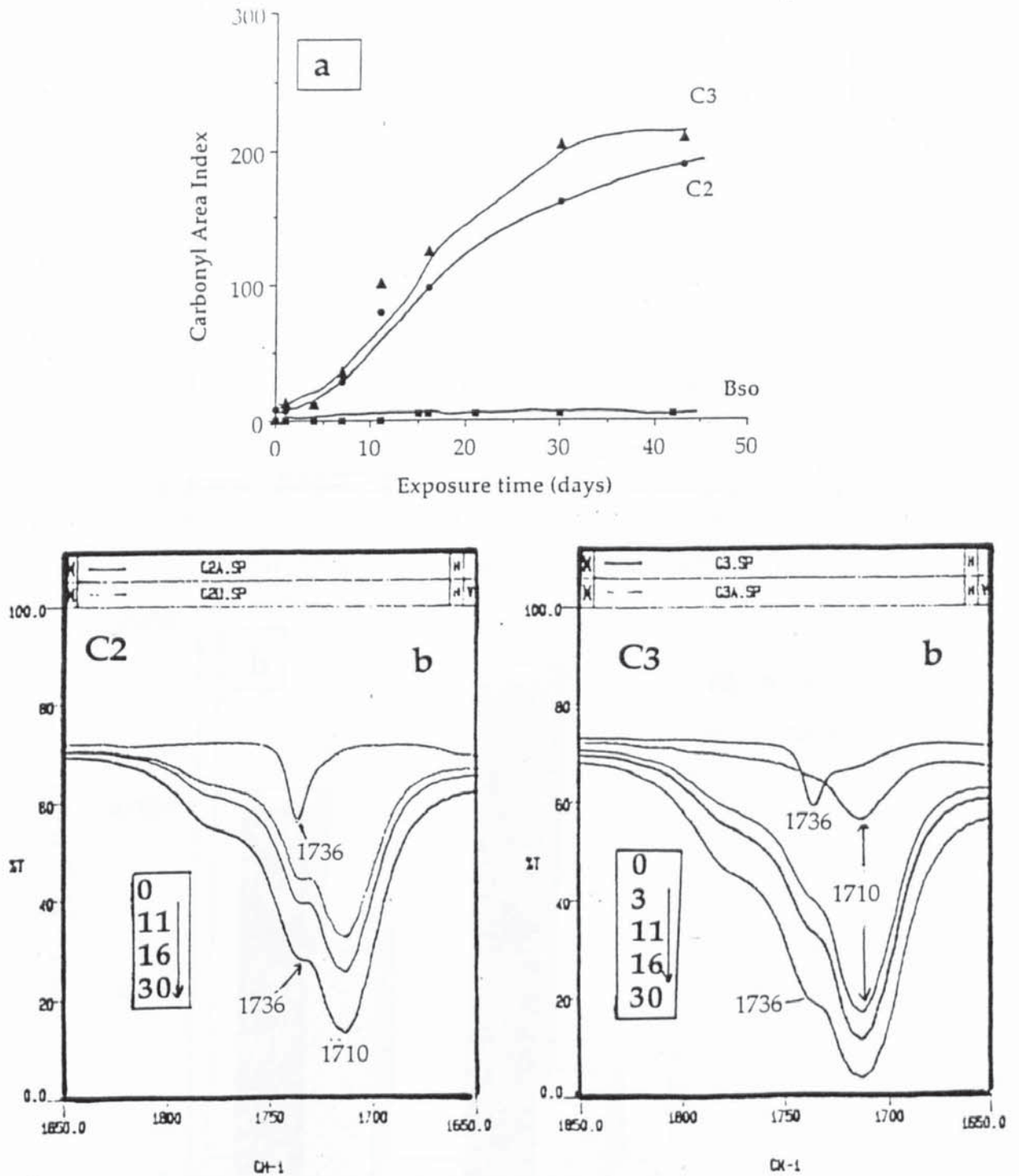


Figure 3.14-(a): Thermal oxidation rate of samples exposed in a Wallace oven at a temperature of 70°C with air (0.07 m<sup>3</sup>/h)  
 (b): FT-IR spectra of C2 and C3 showing the build up of thermoxidation products in the carbonyl region; see table 3.1 for codes. Numbers in boxes are heating times in days.  
 %T= Transmittance, cm-1 = wavenumber

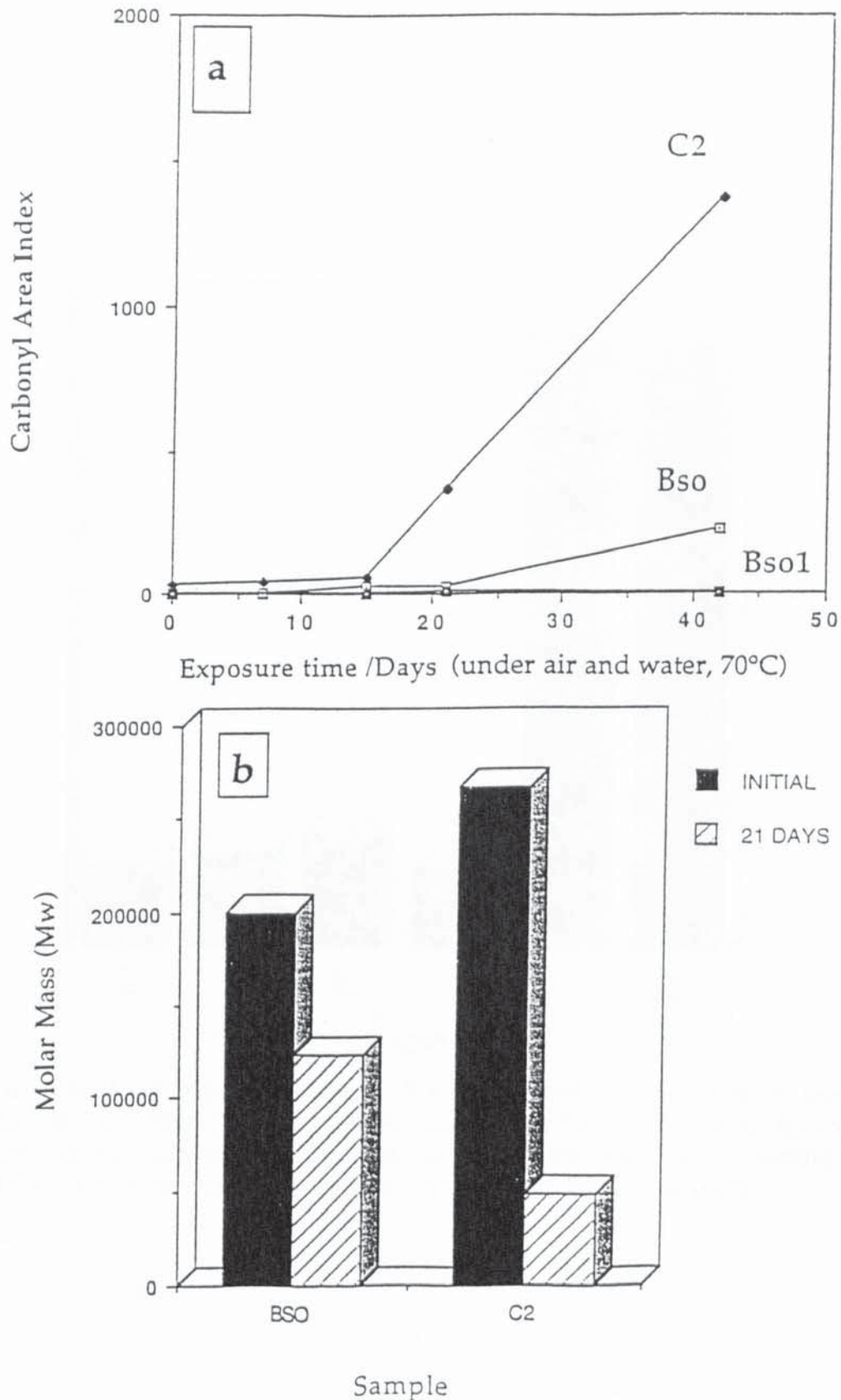


Figure 3.15: Thermal oxidation at a temperature of 70°C with air and water showing the rate of carbonyl formation (a) of starch filled PE system, C2; unstabilised LDPE, Bso and metal photoactivator, Bso1.

-b: Decrease in molar mass of samples C2 and Bso exposed for thermal oxidation in air and water after a period of 21 days.

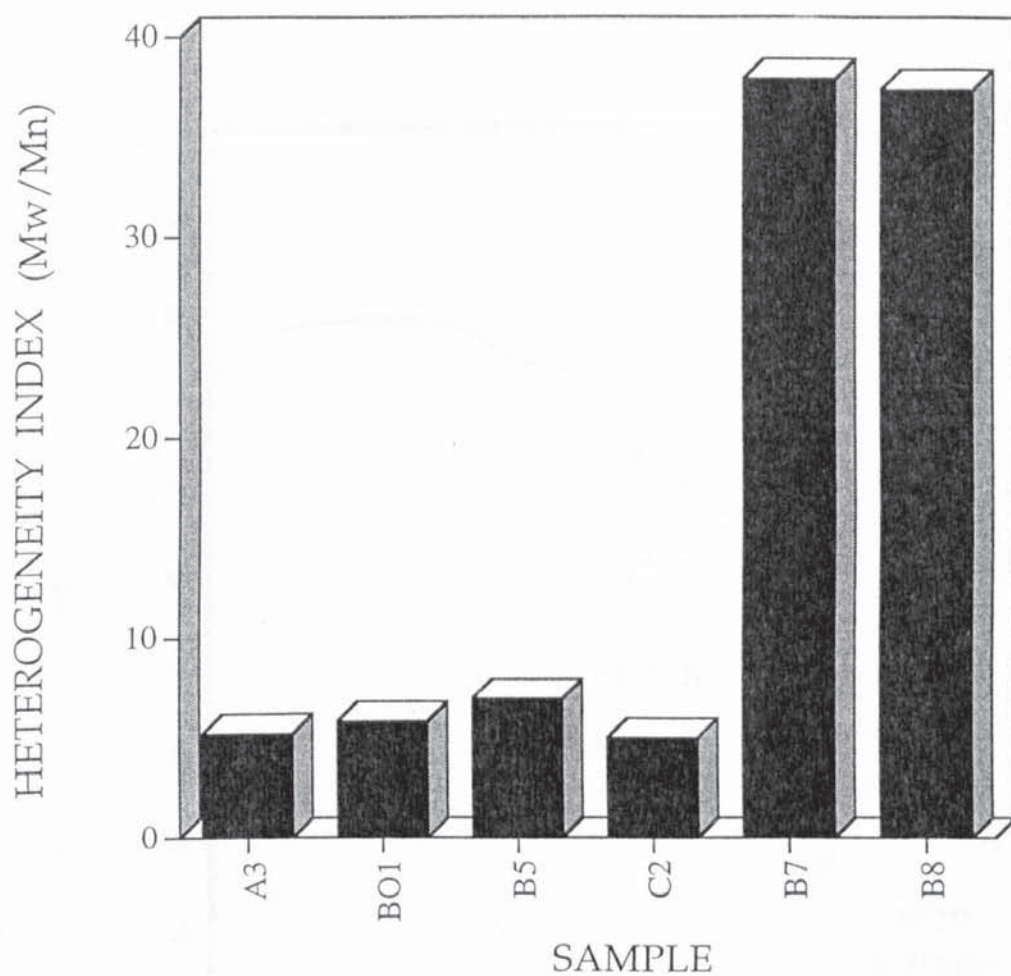


Figure 3.16: Heterogeneity index of degradable polymer samples (as received), photolytic copolymer, A3; metal antioxidant photoactivator class, B01 and B5; starch-filled PE containing iron stearate, C2; HDPE samples containing iron acetylacetonate and iron dithiocarbamate, B7 and B8 respectively.

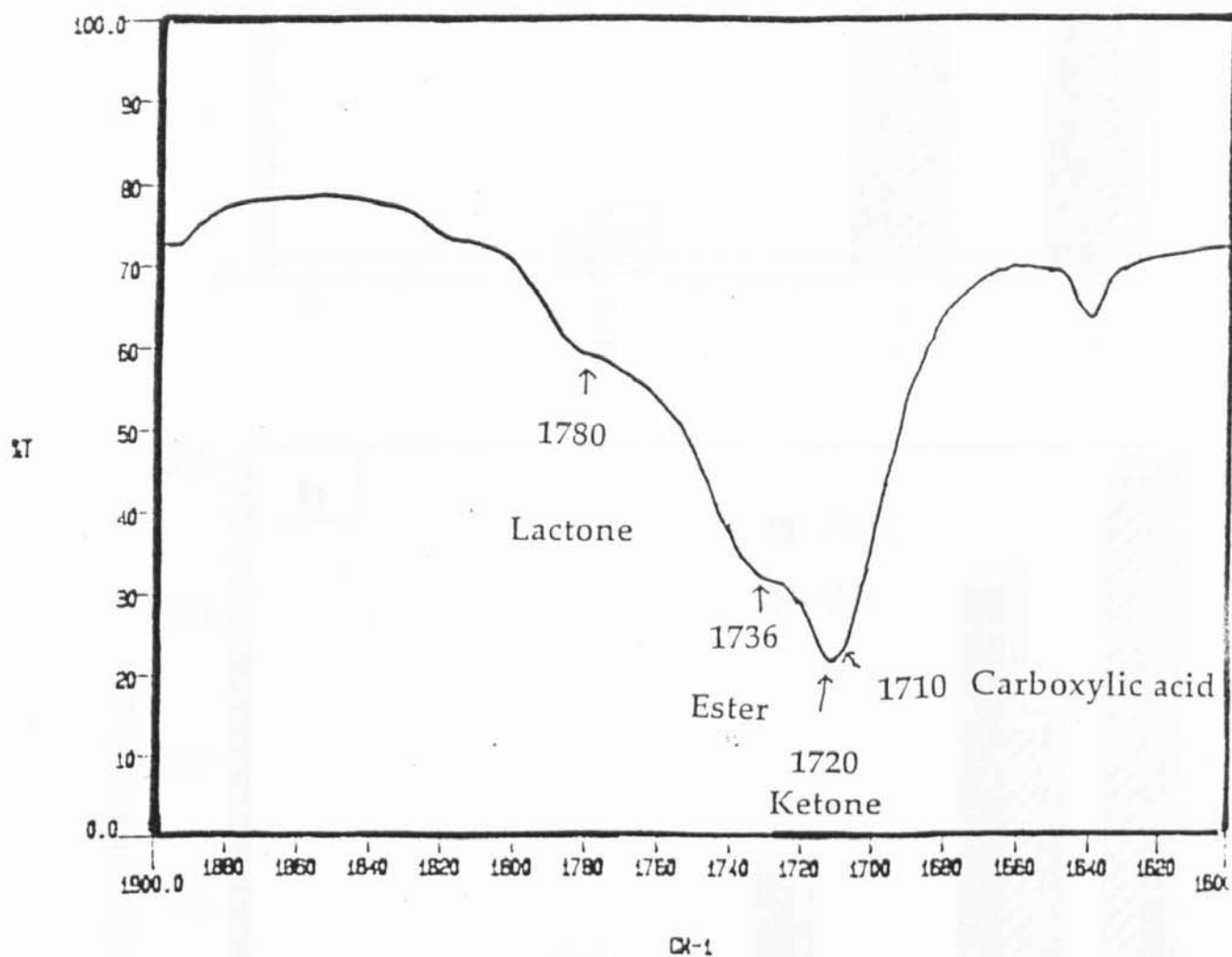


Figure 3.17: FT-IR spectrum of the expanded carbonyl region of unstabilised LDPE (sample Bso) showing the different photooxidation products observed after uv irradiation for approximately 1400 hours.

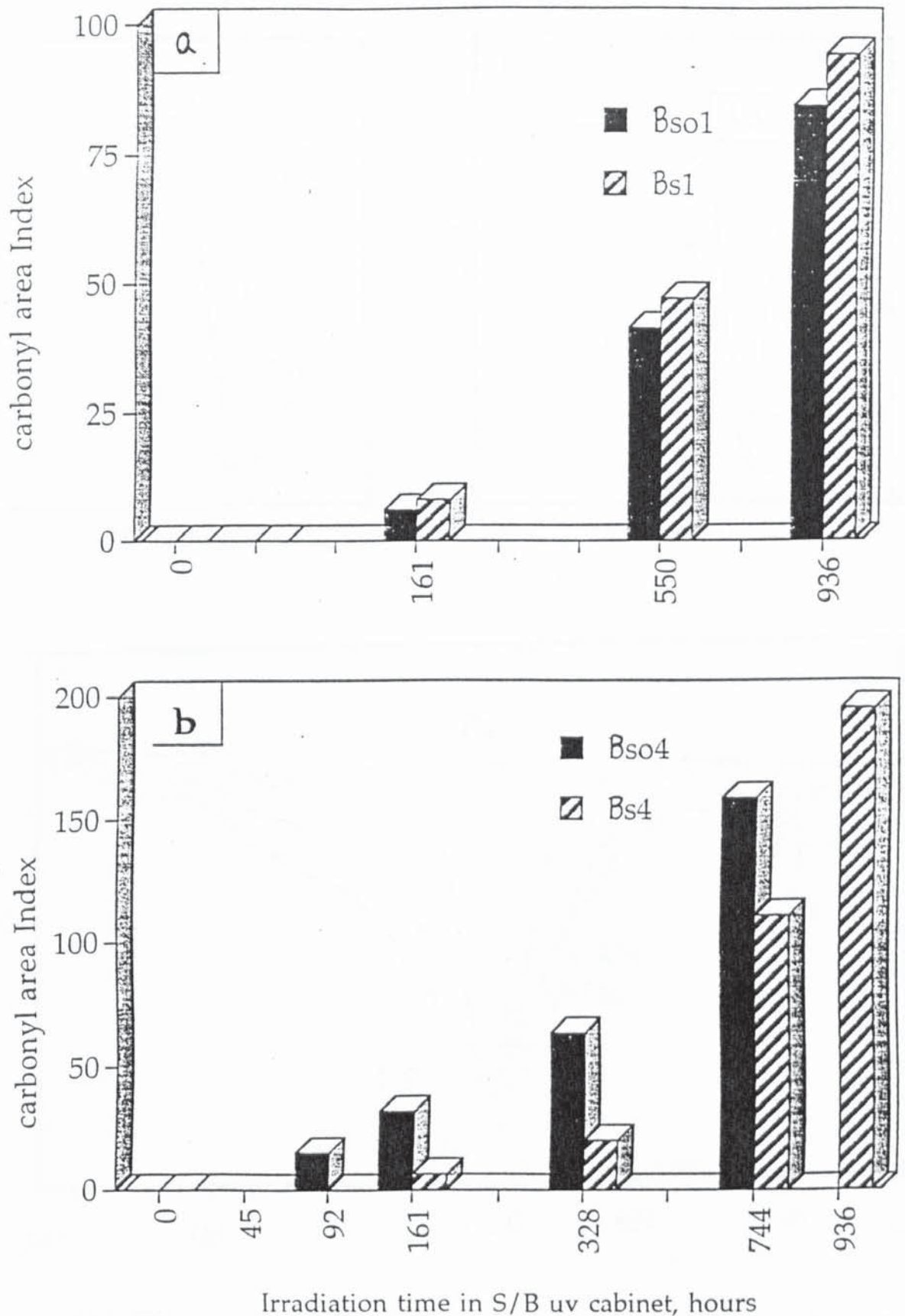


Figure 3.18: Photoxidation of laboratory extruded samples showing mutual photosensitisation of Fe/Ni DNC at low concentrations, **a** and the effect of increasing concentration of FeDNC, **b**.

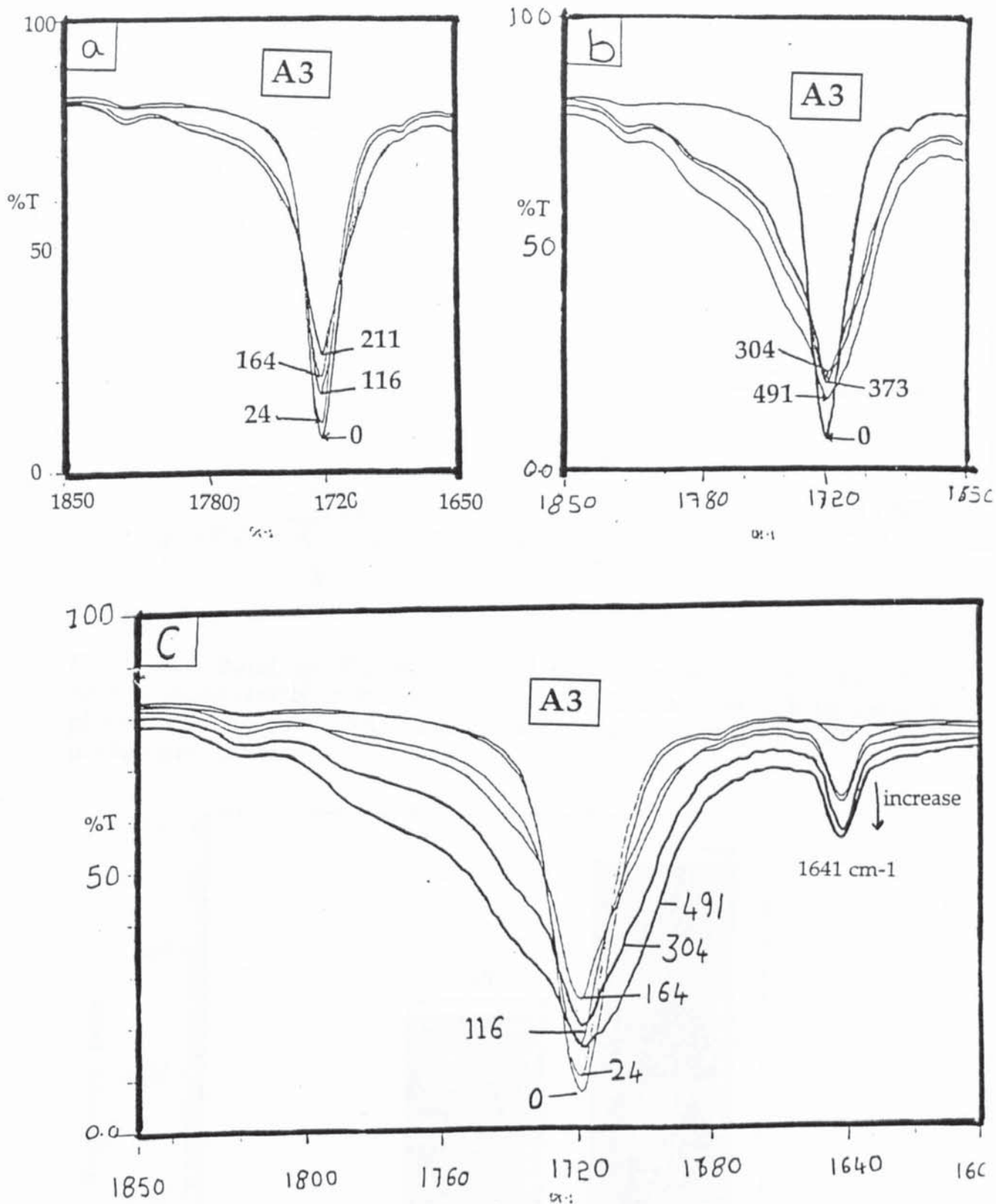


Figure 3.19: FT-IR spectra of photolytic copolymer, A3, showing the decrease in the ketone absorption, (a); the increase in other carbonyl products, (b) and the formation of unsaturation in the polymer at 1641 cm<sup>-1</sup> (c), during uv irradiation. Numbers in box are irradiation hours.

%T (y axis) = Transmittance, cm<sup>-1</sup> (x axis) = wavenumber.

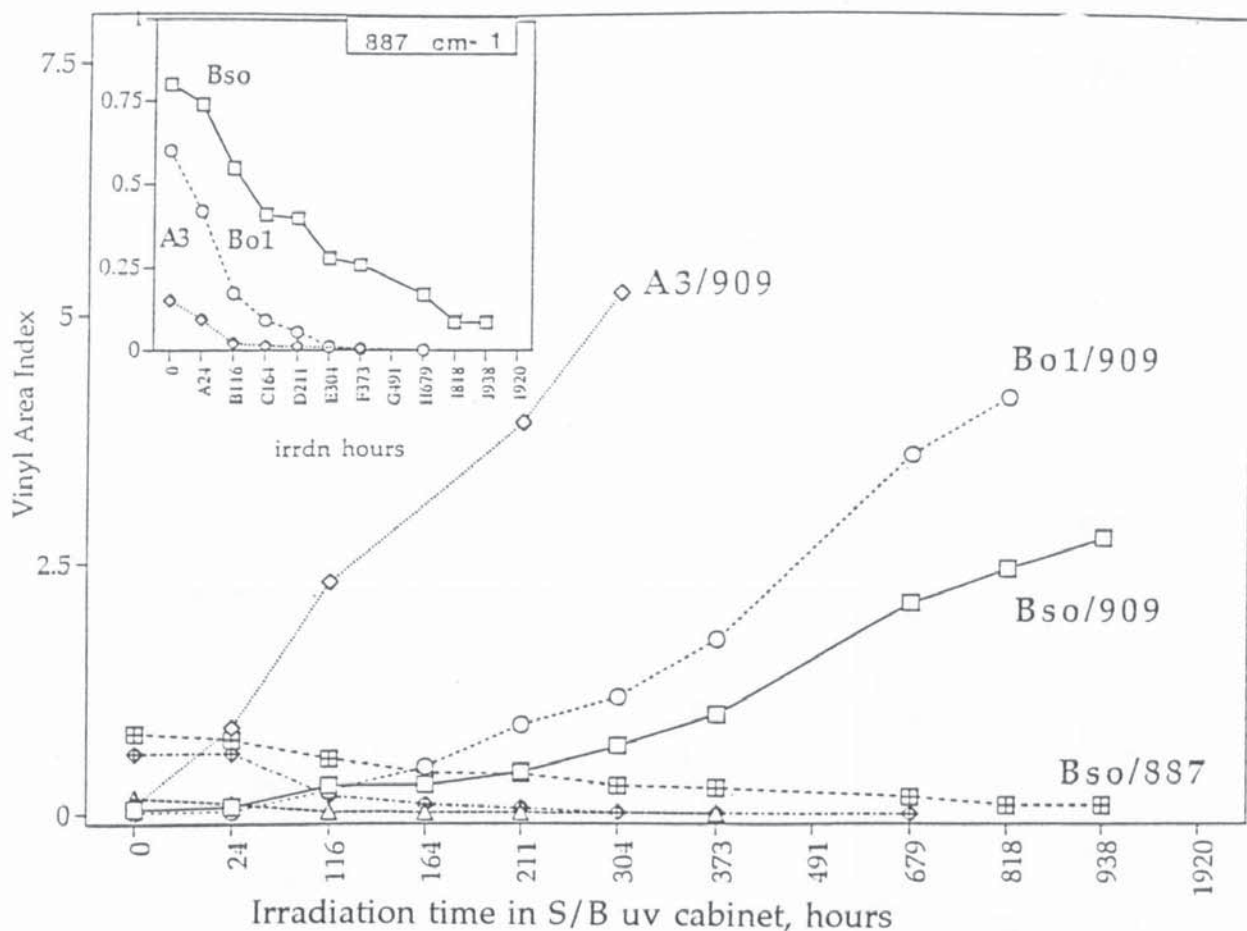


Figure 3.20: Build up of vinyl, 909  $\text{cm}^{-1}$  and decrease of vinylidene, 887  $\text{cm}^{-1}$  (shown more clearly in inset) during uv irradiation (new S/B uv cabinet) of photolytic copolymer, A3, metal photoactivator based on FeDRC, Bo1 and unstabilised LDPE, Bso.

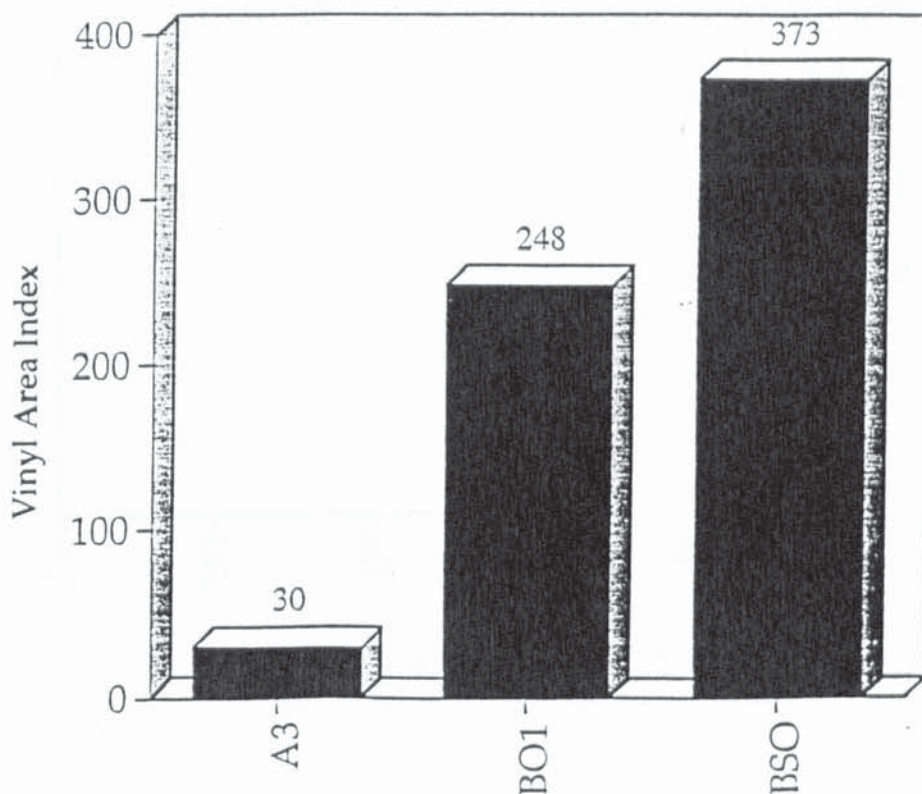


Figure 3.21: Comparison of time (numbers on histograms are in hours) taken for the vinyl content (909  $\text{cm}^{-1}$ ) to reach a value of 1.00 during uv irradiation for the photolytic copolymer, A3, metal photoactivator based on FeDRC, Bo1 and unstabilised LDPE, Bso.

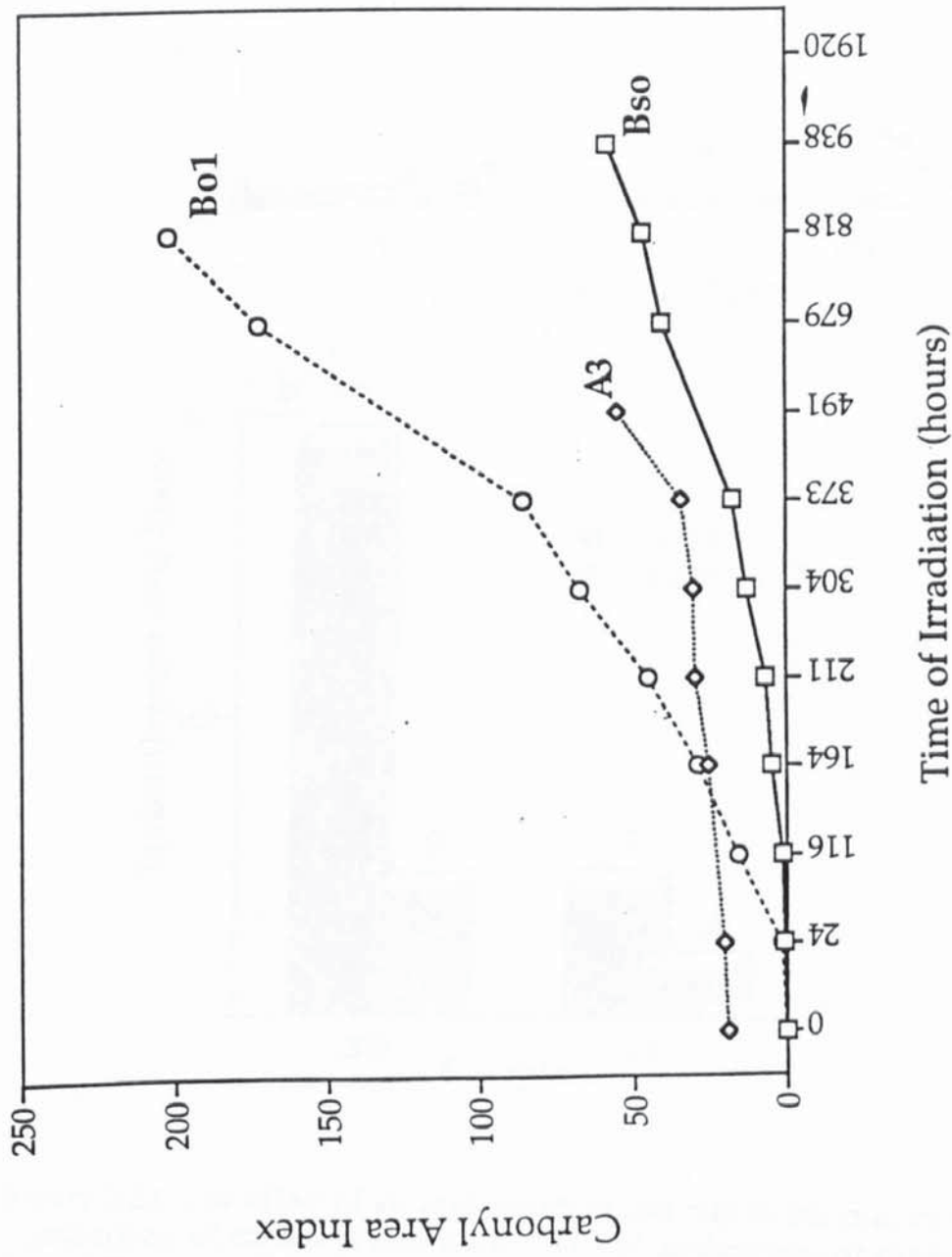


Figure 3.22: Comparison of rate and extent of photooxidation of samples irradiated in S/B new uv cabinet, unstabilised LDPE, Bso; photolytic copolymer system, A3; metal antioxidant photoactivator system, Bo1.

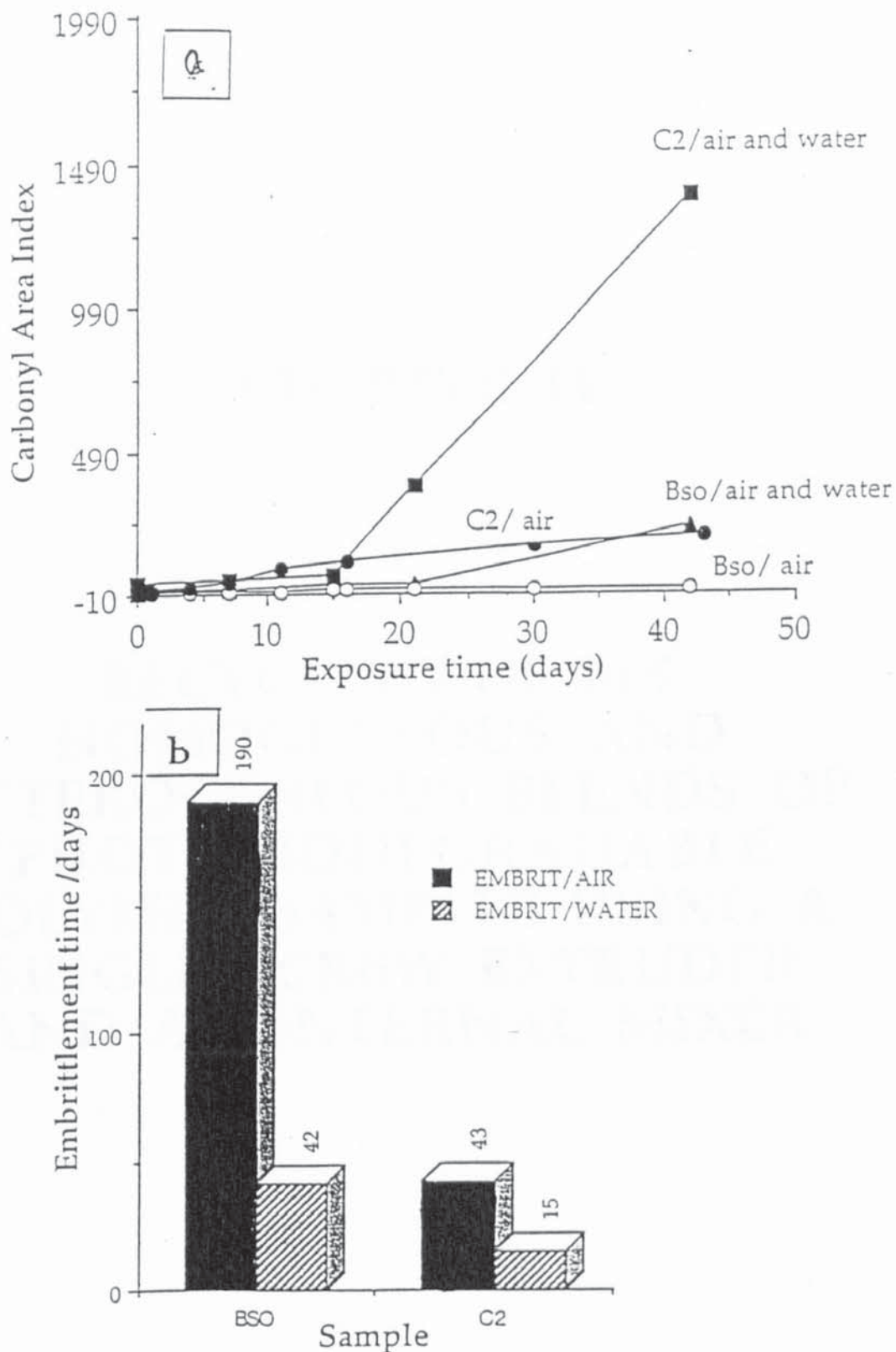


Figure 3.23: The effect of air and water on the rate of thermal oxidation at 70°C. Comparison of carbonyl area index, (a) and embrittlement time, (b) for starch-filled PE system (C2) and unstabilised LDPE (Bso) in the presence and absence of water.

## CHAPTER IV

# RECYCLING OF 10% HOMOGENEOUS AND HETEROGENEOUS BLENDS OF PHOTOBIODEGRADABLE POLYMER SAMPLES USING A SINGLE SCREW EXTRUDER AND AN INTERNAL MIXER

## CHAPTER IV

**RECYCLING OF 10% HOMOGENEOUS AND HETEROGENEOUS BLENDS OF PHOTOBIODEGRADABLE POLYMER SAMPLES USING A SINGLE SCREW EXTRUDER AND AN INTERNAL MIXER.****4.1 OBJECTIVES AND METHODOLOGY.**

The focus of the work described in this chapter was to assess the recycling potentialities of commercially available (table 4.1) and laboratory extruded (table 4.2) photobiodegradable polymer films as 10% homogeneous blends (in polyethylene) and heterogeneous blends (using a mixture of PE, PP and EPDM). The samples were recycled four times using multiple extrusion in a Humboldt 45-20D single screw extruder (homogeneous blends only, see scheme 4.1) and a multistep processing technique using an internal mixer (homogeneous and heterogeneous blends, see scheme 4.2). For the homogeneous blends which were recycled in the extruder the effect of temperature (180°C and 210°C) was investigated.

For the homogeneous and heterogeneous blends recycled in the internal mixer the temperature was kept constant by maintaining the oil temperature of the mixer at 190°C. Both non-photo-oxidised and photooxidised polymer samples were recycled as homogeneous and heterogeneous blends in the internal mixer. All the commercial polymer samples were irradiated in the 'new' S/B uv cabinet for a period of two to three weeks before being recycled. However, the unstabilised LDPE sample, Bso, and sample A3 were irradiated for a longer period, (see table 4.3 for the time of irradiation and the levels of carbonyl products formed in these irradiated samples). The recycling potential of photobiodegradable samples as homogeneous and heterogeneous blends was determined by mixing 10% degradable polymer samples with virgin PE alone (series I, see table 4.4); 1:1 ratio of PE and PP (series III and IV, see table 4.4) and 1:1:0.4 ratio of

Table 4.1: Commercial photobiodegradable polymer film samples used in the recycling experiments.

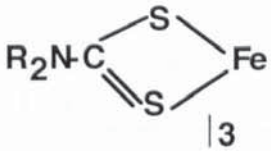
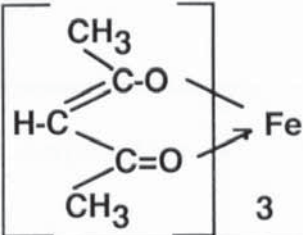
Type	Composition	Origin	Film Thickness	Code
Photolytic Copolymer	Ethylene-CO Copolymer/LDPE	ITW Hi-Cone PE	151 $\mu\text{m}$	A3
Metal complex	FeDRC/LDPE 	PLASTOPIL	35 $\mu\text{m}$	Bo1
Photo Activators	FeDRC/NiDRC/LDPE APA	PLASTOPIL	30 $\mu\text{m}$	B5
Activators	FeAcAc/HDPE 	ENICHEM 221 HT	13 $\mu\text{m}$	B7
	FeDRC/HDPE	ENICHEM 2HT	15 $\mu\text{m}$	B8
Starch	Starch + Fe stearate (C <sub>17</sub> H <sub>35</sub> COO) <sub>3</sub> Fe + TiO <sub>2</sub> /LDPE	AMPACET	41 $\mu\text{m}$	C2
PE	Starch + organic dye/LDPE	AMPACET	38 $\mu\text{m}$	C4
	Starch + carbon black /LDPE	AMPACET	31 $\mu\text{m}$	C5

Table 4.2: Laboratory extruded degradable polymer film samples based on metal antioxidant photoactivator class containing iron and nickel diisononyl dithiocarbamate used in the work described in this chapter.

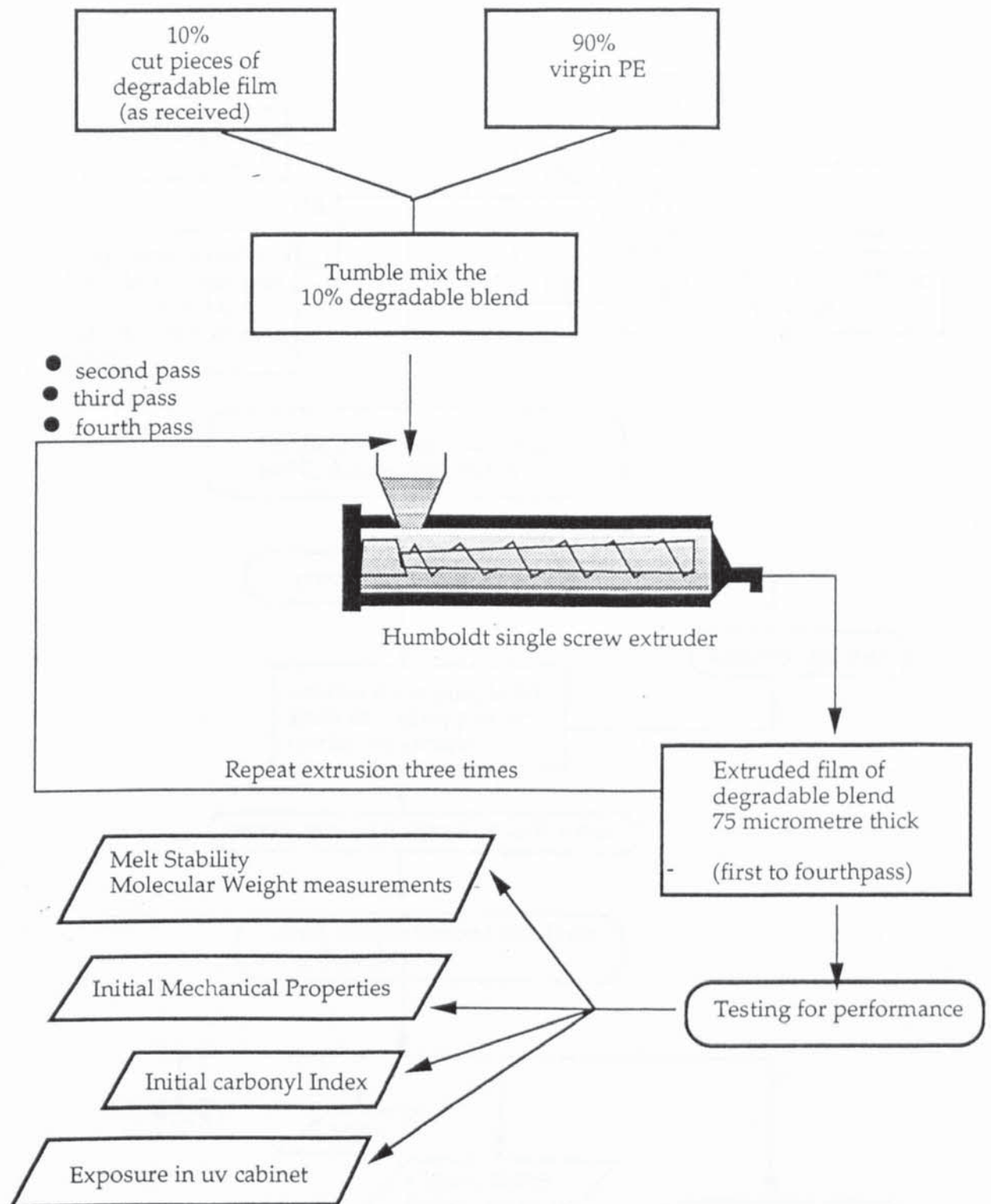
<i>Sample code</i>	<i>Composition %</i>		<i>Thickness</i> ( $\mu\text{m}$ )	<i>Appearance</i>
	FeDNC	NiDNC		
Bso (control)	-	-	75	transparent
Bso1	0.01	-	"	light grey
Bso3	0.03	-	"	light grey
Bs3	0.03	0.01	"	light yellow

Table 4.3: Summary of photoxidised film samples (in S/B uv cabinet) used as 10% homogeneous and heterogeneous blends in an internal mixer.

<i>Sample code</i>	<i>Composition</i>	<i>Time of Irradiation, Days</i>	<i>Amount of carbonyl Content (expressed as an area index)</i>	<i>Physical State of Degradation</i>
Bso (processed control)	no additives	140 $\neq$	>200	fragmented into small pieces
A3	Ethylene-Co	80 $\neq$	>155	fragmented into small pieces
Bo1	FeDRC	20	118	brittle and starting to fragment
B5	FeDRC + NiDRC	20	18	film still intact
C2	Starch+ Fe St.	12	105	brittle and starting to fragment
C4	Starch + organic dye	20	25	brittle

$\neq$  both these samples were extensively degraded since they had been exposed for irradiation for a longer period of time.

Scheme 4.1: Overview of the methodology adopted for recycling using a single screw extruder.



Scheme 4.2: Overview of the methodology adopted for reprocessing using an internal mixer.

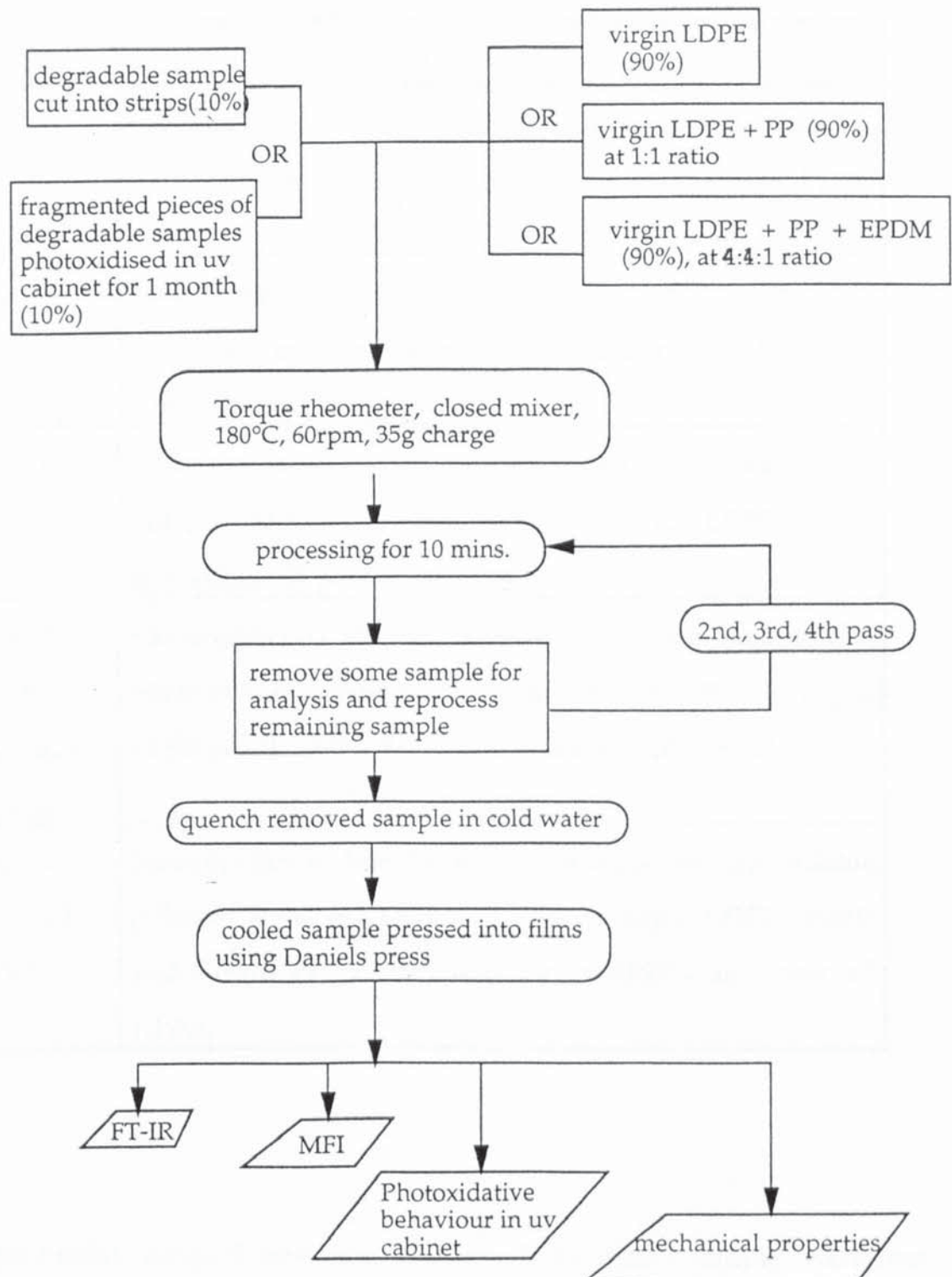


Table 4.4: Summary of homogeneous and heterogenous degradable blends recycled in an internal mixer. Processing conditions used are 190°C, 10 min and CM (closed mixer with restricted oxygen access).

SERIES	BLEND COMPOSITION
Series I PE	Homogeneous blends of 10% commercial degradable polymer film samples as received + 90% virgin LDPE pellets.
Series II PE (photoxidised degradable)	Homogeneous blends of 10% commercial degradable polymer films photoxidised in uv cabinet (as in table 4.3) + 90% virgin LDPE pellets.
Series III PE + PP	Heterogeneous blends of 10% commercial degradable polymer films as received + 90% of virgin LDPE pellets and Virgin PP powder at a ratio of 1:1.
Series IV PE + PP (photoxidised degradable)	Heterogeneous blends of 10% commercial degradable polymer films photoxidised in uv cabinet + 90% of virgin LDPE pellets and Virgin PP powder at a ratio of 1:1.
Series V PE + PP + EPDM	Heterogeneous blends of 10% commercial degradable polymer films as received + 90% of virgin LDPE pellets and Virgin PP powder and virgin EPDM at a ratio of 1:1:0.4.

PE:PP:EPDM (series V, table 4.4). The recycled polymer samples were then analysed for their chemical and physical properties. Changes in mechanical properties, melt viscosity, molar mass, oxidation products on exposure to uv light was examined (see chapter 2 for experimental details).

## 4.2 RESULTS

4.2.1 Recycling of 10% Homogeneous Blends (in Virgin LDPE) of Photobiodegradable Polymer Samples (as received) Using Single Screw Extruder; Series I.4.2.1.1 Melt Stability of Recycled Homogeneous Degradable-LDPE Blend Samples.

Table 4.5 shows the effect of extrusion temperature on the melt stability, expressed as melt flow index (MFI), of the recycled (upto four extrusion passes) degradable blend samples.

Table 4.5: Melt Flow Index of 10% Homogeneous Blends (in LDPE) of Photobiodegradable Polymer Samples (as received) recycled in a Single Screw Extruder at 180°C and 210°C.

SAMPLE	MFI, g/10 min							
	180°C				210°C			
	P1	P2	P3	P4	P1	P2	P3	P4
Bso	1.87	1.80	1.81	1.51	1.64	1.21	1.14	1.10
A3	1.73	1.66	1.41	1.42	1.62	1.36	1.24	1.42
B7	1.45	1.45	1.34	1.08	1.29	1.21	1.23	1.12
B8	1.39	1.40	1.37	1.32	1.47	1.46	1.15	1.14
B5	1.86	1.83	1.82	1.76	1.85	1.54	1.35	1.09
C2	1.62	1.58	1.44	-	1.45	1.35	1.32	0.87
C5	1.47	1.35	1.22	1.47	1.36	1.45	1.63	-
Bso1	1.79	1.75	1.64	1.59	1.48	1.43	1.43	2.04
Bso3	1.74	1.51	1.48	1.34	1.46	1.09	1.08	0.84
Bs3	1.71	1.61	1.59	1.57	1.38	1.75	1.18	-

Table 4.5 and figs 4.1 - 4.3 indicate that, in general, increasing the number of extrusion passes lead to a decrease in the MFI, and values obtained at 210°C

were lower than those at 180°C. At 210°C there was a much sharper decrease in MFI values. At 180°C, although all degradable PE blends showed lower MFI values compared to the PE control (Bso), the rate of change of MFI with the number of passes was relatively small and not very different from that of the control sample.

#### 4.2.1.2 Effect of Recycling on changes in Molar Mass.

Table 4.6 and figures 4.4 and 4.5 (180°C and 210°C, respectively) indicate that with the exception of starch-filled PE samples (C2 and C5) and Bso3 (which gave a decrease in the molar masses), all recycled degradable polymer samples showed an increase in molar mass with each pass.

Table 4.6: Changes in Molar mass of 10% Blends of Photobiodegradable Polymer Samples (as received) Recycled in a Single Screw Extruder at 180°C and 210°C with Extrusion Passes.

SAMPLE	MOLAR MASS ( $M_w$ ) $\times 10^2$							
	180°C				210°C			
	P1	P2	P3	P4	P1	P2	P3	P4
Bso	2278	2316	2320	2402	2316	2647	2716	2863
A3	2337	2318	2511	2510	2411	2471	2533	2531
B7	2316	2450	2449	2414	2769	2940	2778	2908
B8	2479	2568	2526	2657	2802	2698	2718	2749
C2	2354	2324	2573	-	2770	2767	2627	2713
C5	2502	2400	2488	2472	2724	2634	2469	-
Bso1	2396	2406	2474	-	2617	2682	2714	2376
Bso3	2298	2482	2548	2493	2746	2576	2437	2736
Bs3	2316	2422	2528	2463	-	-	-	-

At 180°C, the photobiodegradable samples exhibited higher molar mass values compared to the recycled control sample, Bso, see figure 4.4. At 210°C (figure 4.5) the incremental changes from pass 1 to pass 4 were smaller for the recycled blends of photobiodegradable samples compared to Bso. The irregular pattern for sample B7 (210°C) seemed to represent a genuine behaviour (see table 4.5 for MFI results which also showed the same irregularity). Figure 4.6 compares and illustrates more clearly the effects of the two recycling temperatures used on the changes in molar mass.

#### 4.2.1.3 Effect of recycling on mechanical properties.

Ultimate Tensile Strength (UTS) and Elongation to Break (EB) were determined after each pass of the recycled degradable blend samples. The results are shown in table 4.7 and figures 4.7 - 4.10 (dark filled box in these figures is the recycled control sample Bso and lined boxes are the degradable samples). The change in EB of these polymer samples after reprocessing was more informative than changes in UTS. PE control with no additives (Bso) showed a reduction in EB going from the first to the third pass followed by an increase for the fourth pass. In general all degradable blend samples did not give significant changes when compared to the PE control at 180°C. However, at 210°C more dramatic changes took place as reflected in the sharp reduction in EB with increasing number of extrusion passes.

#### 4.2.1.4. Effect of recycling on the subsequent photooxidative behaviour of degradable blends.

Figure 4.11 illustrates the build up of carbonyls for pass 1 and pass 3 at 180°C and 210°C for the recycled blend samples Bso and C2. The recycled degradable polymer sample, C2, showed a faster rate of photooxidation compared to the control sample, Bso in the case of each pass. The rate of

Table 4.7: Mechanical properties of samples recycled in an extruder at 180°C and 210°C.

SAMPLE CODE	MECHANICAL PROPERTIES			
	180°C		210°C	
	UTS (MPa)	EB (%)	UTS (MPa)	EB (%)
Bso.P1	30.8	434	19.1	582
P2	28.1	362	17.6	459
P3	27.0	342	16.1	534
P4	16.7	462	19.4	483
A3.P1	22.5	459	21.9	580
P2	25.2	329	17.6	551
P3	20.8	358	25.8	253
P4	25.2	271	27.9	180
B7.P1	16.1	436	12.2	341
P2	17.2	314	11.7	209
P3	16.6	305	14.2	246
P4	20.3	274	14.4	225
B8.P1	15.4	531	13.3	401
P2	14.2	501	14.7	481
P3	14.1	398	13.0	255
P4	12.8	274	12.7	260
C2.P1	23.7	331	15.9	446
P2	24.0	290	16.5	195
P3	17.1	450	15.7	267
			14.6	281
C5.P1	24.0	387	16.7	482
P2	30.5	292	15.0	316
P3	36.4	191	17.4	377
P4	19.9	371		
BSO1.P1	30.5	229	16.0	428
P2	33.5	229	18.5	333
P3	22.3	359	14.1	559
P4			16.4	763
BSO3.P1	23.3	423	17.3	607
P2	20.1	295	19.7	478
P3	20.0	273	21.9	571
P4	21.1	261	19.5	359
BS3.P1 180	31.3	516	22.1	431
P2	25.2	483	17.0	321
P3	22.3	410	15.2	275
P4	19.3	363	14.1	268

photoxidation for both samples was greater at the higher temperature of 210°C.

#### 4.2.2 Effect of Recycling on The Behaviour of 10% Homogeneous and Heterogeneous Degradable Blends (In LDPE) Reprocessed Using The Internal Mixer.

Table 4.4 (page 134) shows the five different categories of homogeneous and heterogeneous degradable blends which have been recycled in an internal mixer at 190°C. Five commercial degradable polymer samples were used for each series, A3, Bo1, B5, C2, C4. For each series, unstabilised LDPE processed at 180°C, Bso (see chapter 3, table 3.2, page 90) was also recycled in the internal mixer as 10% blend with other polymers as described in series I-V and the corresponding PE recyclates used as controls for the relevant series (controls I - V). Table 4.8 defines the meaning of each of the control samples used for recycling in an internal mixer.

##### 4.2.2.1. Melt stability of Reprocessed Samples.

Table 4.9 and figures 4.12 illustrates the effect of recycling using an internal mixer on the melt stability of degradable samples of series I, II and III. Series I (which is a homogeneous blend of 10% degradable as received in PE, see table 4.4) showed a decrease in the MFI with each concomitant pass in the internal mixer. For series II, Bso (control II), A3 and Bo1 displayed an increase, whereas C2, C4 and B5 displayed a decrease. In general the values obtained for series II were higher than those obtained for series I. Series III (heterogeneous blend of degradables as received in PE:PP) exhibited an increase in MFI with each pass which is most certainly due to the presence of PP in these samples. In series III, samples Bso (control III), C2 and C4, showed the largest incremental changes while sample Bo1 showed the lowest incremental change from pass 1 to pass 4.

Table 4.8: Control samples recycled in the internal mixer at 190°C.

SERIES/ CONTROL	CONTROL COMPOSITION
<b>Series I/Bso Control I</b>	Homogeneous blend of 10% Bso polymer sample as processed (180°C) + 90% virgin LDPE pellets.
<b>Series II/Bso Control II</b>	Homogeneous blend of 10% Bso polymer processed (180°C) and pre-photoxidised (see table 4.3) + 90% virgin LDPE pellets.
<b>Series III/Bso Control III</b>	Heterogeneous blend of 10% processed (180°C) Bso polymer + 90% of virgin LDPE pellets and Virgin PP powder at a ratio of 1:1.
<b>Series IV/Bso Control IV</b>	Heterogeneous blend of 10% Bso polymer processed (180°C) and pre-photoxidised (see table 4.3) + 90% of virgin LDPE pellets and Virgin PP powder at a ratio of 1:1.
<b>Series V/Bso Control V</b>	Heterogeneous blend of 10% processed (180°C) Bso polymer + 90% of virgin LDPE pellets and Virgin PP powder and virgin EPDM at a ratio of 1:1:0.4

#### 4.2.2.2. Effect of Reprocessing on Mechanical Properties.

Table 4.10 and figures 4.13-4.22 demonstrate the changes in ultimate tensile strength and elongation to break (for pass 1 and 3) of the recycled degradable blends. For all the samples the mechanical properties decreased from the first to the third pass. Series II (pre-photoxidised degradables in LDPE, see table 4.3 for extent of oxidation) showed a much sharper decrease in elongation to break compared to series I (the ultimate tensile strength is, however, comparable). The drastic reduction in elongation to break for

Table 4.9: Melt Flow Index of recycled (internal mixer) homogeneous and heterogeneous blends of photobiodegradable samples.

SERIES	SAMPLE	MFI g/ 10 mins			
		P1	P2	P3	P4
10% degradable as received in LDPE	<b>Series I /Bso</b>	2.73	2.09	1.85	1.67
	A3	2.84	2.65	2.67	2.34
	Bo1	1.98	2.74	2.14	1.70
	B5	1.88	1.96	1.99	1.77
	C2	2.06	1.88	1.68	1.44
	C4	2.37	3.22	2.58	2.12
10% pre- photoxidised degradable in LDPE	<b>Series II /Bso</b>	3.2	3.16	2.80	3.44
	A3	2.37	2.67	3.06	4.34
	Bo1	2.31	2.48	2.59	2.57
	B5	2.60	2.52	2.29	1.77
	C2	2.92	2.84	2.02	1.64
	C4	2.67	2.46	2.44	2.39
10% degradable as received in LDPE:PP (1:1)	<b>Series III /Bso</b>	3.53	3.80	5.28	8.39
	A3	2.37	2.67	3.06	4.34
	Bo1	2.63	3.15	3.76	3.77
	B5	1.87	3.31	5.71	5.62
	C2	2.26	2.55	3.90	8.39
	C4	2.52	3.27	5.02	8.18

series III and series V as compared to series I and II is solely due to the addition of PP in these samples. The addition of EPDM led to slightly better elongation to break values, especially for the control V (10% Bso as received recycled in LDPE:PP:EPDM).

Table 4.10: Mechanical properties (pass 1 and pass 3) of recycled degradable blends.

SERIES	SAMPLE	UTS (MPa)		EB (%)	
		P1	P3	P1	P3
10% degradable as received in LDPE	<b>Series I /Bso</b>	13.9	9.8	319	227
	A3	11.10	10.72	439	240
	Bo1	11.64	10.51	151	149
	B5	12.12	11.65	411	319
	C2	6.00	2.51	300	174
	C4	10.11	7.54	341	183
10% pre- photoxidised degradable in LDPE	<b>Series II /Bso</b>	11.99	10.88	154	86
	A3	10.99	7.12	54	38
	Bo1	11.61	11.88	98	60
	B5	10.12	8.56	101	75
	C2	11.58	11.55	87	115
	C4	7.34	5.23	89	53
10% degradable as received in LDPE:PP (1:1)	<b>Series III /Bso</b>	9.14	7.56	8.77	8.78
	A3	8.32	6.87	11.41	9.44
	Bo1	7.46	7.52	8.13	8.15
	B5	8.98	6.78	10.00	9.13
	C2	10.50	11.23	11.40	11.23
	C4	7.55	7.37	6.47	7.37
10% degradable as received in LDPE:PP:EPDM (1:1:0.4)	<b>Series V /Bso</b>	5.53	4.78	23.95	13.85
	A3	3.71	2.88	12.01	7.8
	Bo1	4.13	2.96	14.43	11.65
	B5	3.13	2.93	13.83	9.15
	C2	7.1	7.57	12.23	11.37
	C4	6.95	6.19	6.58	4.9

#### 4.2.2.3 Changes in Oxidation Products During Reprocessing

Table 4.11 shows the changes in oxidation products measured from the infrared spectra (carbonyl and vinylidene) of photobiodegradable samples after different recycling passes through the internal mixer. Figure 4.23 illustrates that the initial carbonyl index increased with each pass (for all

Table 4.11: Changes in Oxidation Products Produced after each Recycling Operation in an Internal Mixer (at 190°C).

Series/ Sample	Initial Carbonyl Index				Initial Vinylidene Index at 887 cm <sup>-1</sup>			
	P1	P2	P3	P4	P1	P2	P3	P4
<b>Series I /Bso</b>	1.11	1.47	2.04	3.98	0.95	0.90	0.84	0.79
A3	5.76	6.69	7.40	8.08	0.91	0.75	0.69	0.50
Bo1	1.64	2.52	1.87	1.94	0.73	0.74	0.72	0.79
B5	1.21	1.75	2.33	5.46	0.72	0.67	0.74	0.84
C2	2.12	2.41	2.71	4.92	0.70	0.86	0.61	0.62
C4	1.57	3.65	6.67	5.97	0.59	0.50	0.42	0.42
<b>Series II /Bso</b>	20.00	23.94	30.66	31.33	0.70	0.63	0.80	0.53
A3	16.58	19.89	20.8	41.50	0.65	0.64	0.58	0.63
Bo1	11.79	13.43	16.57	19.00	0.38	0.65	0.69	0.61
B5	2.7	4.1	4.96	5.83	0.53	0.54	0.52	0.44
C2	7.13	7.92	11.08	15.21	0.81	0.64	0.48	0.36
C4	4.65	5.38	6.98	10.12	0.67	0.58	0.57	0.41
<b>Series III /Bso</b>	1.03	1.31	1.83	3.14	-	-	-	-
A3	4.75	6.40	9.40	12.43	-	-	-	-
Bo1	0.47	1.13	2.68	3.06	-	-	-	-
B5	1.03	1.15	2.15	4.73	-	-	-	-
C2	1.62	1.65	3.54	3.70	-	-	-	-
C4	3.67	2.72	1.83	1.81	-	-	-	-
<b>Series V /Bso</b>	0.62	0.98	1.45	3.36	-	-	-	-
A3	-	-	-	-	-	-	-	-
Bo1	0.94	1.64	2.76	2.53	-	-	-	-
B5	1.02	0.98	1.44	1.53	-	-	-	-
C2	2.55	2.87	2.42	4.47	-	-	-	-
C4	2.02	2.31	2.53	2.88	-	-	-	-

series). The initial carbonyl index values were higher for series II since these samples were based on blends containing 10% pre-photoxidised samples, see table 4.3 (page 131). In all the series, the sulphur based dithiocarbamate samples Bo1, and to some extent, B5 exhibited the

smallest incremental changes between each pass. Generally, all commercial degradables in every series showed higher initial carbonyl index than the corresponding control samples (except Bo1). Figure 4.24 illustrates the decrease in vinylidene content during recycling in an internal mixer. For both series I and II the vinylidene decreased with each pass. However, the rate of change for sample Bo1 (series I) and B5 (series II) was smaller compared to that of the other degradable samples and the corresponding control samples.

#### 4.2.2.4 Photooxidative Behaviour After Reprocessing in an Internal Mixer.

Figures 4.25-4.33 show the FT-IR spectra of processed (first processing operation) and recycled (after three processing operations) of degradable blends obtained on subsequent uv irradiation in a sepap 12/24 uv cabinet. Figure 4.34 which demonstrates the effect of the recycling operations (after three processing operation) on the photooxidation stability homogeneous blends (series I) reveals that the commercial degradable samples A3 and Bo1 have oxidised far more rapidly than Bso (control I). The oxidation rates were higher for pass 3 than pass 1. B5-P1 (pass 1) exhibited higher oxidation (at later stages) than Bso-P1; however, B5 pass 3 (which oxidises more quickly than B5-P1) showed a lower oxidation rate compared to Bo1-P3, A3-P3 and Bso-P3. Insets in this figure show the increase in vinyl and decrease in vinylidene content (pass 1) of the same degradable samples.

Figure 4.35 displays the effect of recycled homogeneous (series I- degradable as received in LDPE, series II- pre-photooxidised degradables in LDPE) and heterogeneous blends (series III- degradables as received in LDPE:PP, series IV- pre-photooxidised degradables in LDPE:PP and series V- degradable as received in LDPE:PP:EPDM) when exposed to uv irradiation for samples C2 and A3 (pass 1). Both samples oxidised more quickly than the unstabilised

recycled control I sample, Bso. Heterogeneous blends oxidised faster than homogeneous blends. The addition of 10% pre-photooxidised degradable samples (see table 4.3) to the blends increased the oxidisability of these polymers.

### 4.3 DISCUSSION

#### 4.3.1 General Discussion

Photobiodegradable polymers have been heavily criticised [97] with regards to their recycling potentials, especially if they are to be recycled as part of the mainstream plastics waste. The aim of the experiments carried out in this chapter were to assess the recyclability of degradable polymers (both as received and after some extent of photooxidation) as 10% homogeneous and heterogeneous blends. Homogeneous blends were based on LDPE alone, and heterogeneous blends were based on a mixture of LDPE and PP because these polymers constitute the major components in mixed plastics waste. EPDM (series V) was added to the mixture of LDPE and PP to achieve better compatibility between the two polymers.

Processing and continued reprocessing (i.e. recycling) leads to structural and chemical changes in the polymer, which are brought about by oxidative processes [112], see scheme 1.1 page 22. The exact nature of the oxidation processes occurring depend on several factors:- the processing temperature, concentration of oxygen available, addition of melt stabilisers and the nature of the polymer itself.

#### 4.3.2 Effect of Recycling Temperature in a Single Screw Extruder on 10% Homogeneous Blends of Photobiodegradable Polymer films.

Multiple processing in the single screw extruder of photobiodegradable polymer samples at both die temperatures of 180°C and 210°C showed

similar trends in the change in properties. At 180°C unstabilised LDPE, Bso, and all the photobiodegradable samples examined showed signs of thermal oxidation, which became more prevalent with successive processing passes through the extruder, tables 4.5, 4.6 and 4.7 and figures 4.1, 4.4 and 4.7-4.8 illustrated this clearly. The decrease in MFI (which was followed by an increase in molar mass) from the first to the fourth pass clearly indicated that these samples were melt degrading via, mainly cross-linking reactions, see tables 4.5 and 4.6, figs. 4.1 and 4.4. Figure 4.36 demonstrates clearly that the decrease in MFI is accompanied by a simultaneous increase in the molar mass which is due to the molecular enlargement of the polymer [112]. The rate of change in the physical properties (MFI, molar mass, ultimate tensile strength) with the number of passes at 180°C of all photobiodegradable samples was relatively small and not very different from the unstabilised reprocessed LDPE control sample, Bso, as shown in figs. 4.1, 4.4, 4.7-4.8. However, samples B5, B7 and Bs3, which contain the dithiocarbonyl moiety exhibited the smallest rate of change in MFI and molar mass, indicating much lower melt degradation during the recycling process, see figures 4.1 and 4.4. This is due to the effective melt stabilisation of the dithiocarbamates used in these samples [41,80,107,113], which are known to act as efficient peroxide decomposers [41,113].

The rate of change in the physical properties of the photobiodegradable samples recycled in the single screw extruder at 210°C was much higher than at 180°C, suggesting greater melt degradation at the higher temperature, see figs 4.2, 4.5 and 4.9-4.10. Figures 4.3 and 4.6 showed clearly the effect of the processing temperature on the MFI and molar mass. Increasing the temperature led to a much sharper decrease in MFI (and an increase in molar mass) of the degradable samples, see figure 4.37. At this temperature, the unstabilised LDPE exhibited the greatest decrease in MFI

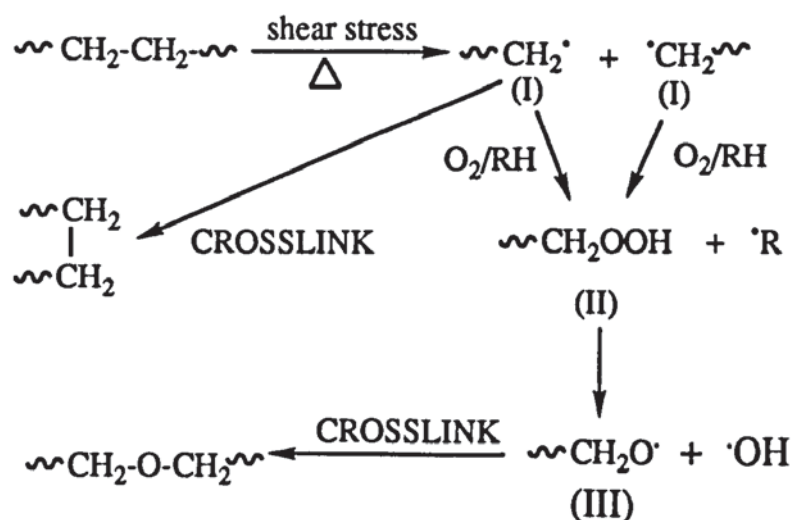
with each pass (see fig. 4.3) and the highest increase in molar mass (see fig 4.6), suggesting that the control sample is more extensively cross-linked compared to the photobiodegradable samples. Results shown in figures 4.2 and 4.6 suggest that at the higher temperature of 210°C, the starch-filled PE system containing carbon black, sample C5, (which shows an increase in MFI and simultaneous decrease in molar mass) undergoes predominantly chain scission during melt processing and reprocessing.

The measured mechanical properties at 210°C showed dramatic changes taking place during the recycling process, as reflected in the sharp reduction in the elongation to break values with increasing number of extrusion passes, see figure 4.10.

It is known that the thermal processing history of a polymer directly influences its photooxidative behaviour [114], because the greater the concentration of photosensitive impurities produced during processing, the faster is the rate of photooxidation. The photooxidative behaviour, determined as an increase in carbonyl content, of recycled unstabilised LDPE, Bso, and the starch-filled PE system, C2, is shown in figure 4.11. The high rates of photooxidation for the last extruder passes (pass 3, figure 4.11), suggested greater concentration of hydroperoxides, the initiators of oxidation, forming with increasing number of extruder passes. Increasing the temperature from 180°C to 210°C also causes much faster rates of oxidation for both the control sample and the starch-filled sample, as shown in figure 4.11. This is most likely due to the fact that at high temperature greater concentrations of hydroperoxides are formed; thus, the polymer samples undergo melt degradation more severely at 210°C compared to 180°C.

### 4.3.3 Recycling of Photobiodegradable Polymer samples as 10% Homogeneous and Heterogeneous Blends in an Internal Mixer.

It is well documented that melt degradation of PE occurs predominantly via crosslinking reactions which give rise to molecular enlargement [41,99,111-112], whereas PP degrades in the melt via chain scission leading to a reduction in molar mass [41,99,112-113]. This is reflected in results presented in table 4.9 and figure 4.12 which show the changes in the melt viscosity of the polymers. Series I (which is based on 10% photobiodegradable polymer samples as received in PE) and Series II (10% pre-photoxidised photobiodegradable samples in PE, see table 4.3) showed a decrease in the MFI with each concomitant processing operation through the internal mixer, see figure 4.12. The increase in the melt viscosity of the samples is a direct consequence of cross-linking reactions [41,99,112-113] that take place during the reprocessing of PE. Because of the high shear stress in the mixer, the PE backbone undergoes homolytic carbon-carbon bond fission [115] to give alkyl radicals (I) which react with oxygen to give alkyl peroxy radicals, see scheme 4.3.

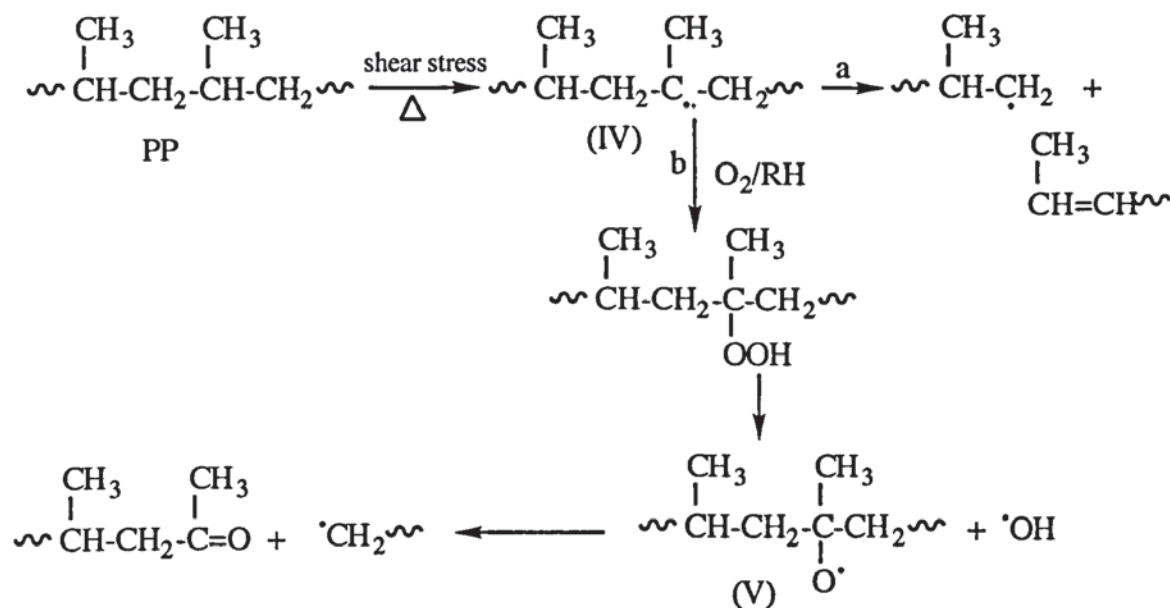


Scheme 4.3: Formation of radicals in PE during processing.

These alkyl peroxy radicals are very reactive and can abstract a hydrogen from another alkyl chain, thus forming hydroperoxides (II) and alkyl radicals [115]. The hydroperoxides formed undergo thermolysis to give

hydroxyl and alkoxy radicals (III), as shown in scheme 4.3. Under oxygen deficient conditions, the macroalkyl radicals (I) and the alkoxy radicals (III) cause cross-linking of PE [112,115]

Series II (based on 10% pre-photoxidised degradable in LDPE), which was used to simulate 'real life' situation of degradable plastics that have served part of their life before ending up in the recycling mainstream, exhibited higher MFI values than those for series I (10% degradable as received in LDPE), see figure 4.12. This is due to the oxidative chain scission breakdown of the polymer chains that has occurred during uv irradiation of the samples in series II (during uv irradiation the degradable samples undergo Norrish reactions, resulting in oxidative breakdown of the polymer backbone, see chapter 3). On the other hand all photobiodegradable samples in series III (based on 10% degradables as received in 1:1 ratio of LDPE:PP blend) showed an increase in the MFI values with each pass, confirming the dominance of the rapid chain scission of PP during processing, see figure 4.12. The mechanochemical scission in PP occurs very much the same as in PE to give alkyl radicals (IV), which in the presence of oxygen undergo oxidative chain scission [116], see scheme 4.4. Unlike in PE the alkyl (IV) and the alkoxy radicals (V) in PP are not stable enough to exist by themselves until they recombine to form crosslinked structures. Instead, both radical species undergo chain scission to give another alkyl radical and an olefin, see scheme 4.4 route a, and an alkyl radical and a ketone, see scheme 4.4 route b [116]. This oxidative chain scission eventually causes a decrease in molar mass in PP, as reflected in the increase in MFI, see figure 4.12.



Scheme 4.4: Degradation of PP during processing.

The melt degradation that occurs in the reprocessed homogeneous and heterogeneous blends is also reflected in the mechanical properties. All the control samples (control I, control II, control III and control V) showed a decrease in the mechanical properties from the first to third pass, see figures 4.13-4.22. The decrease between the passes was more clearly seen when measuring the elongation to break values. Series II revealed much lower values for elongation to break compared to series I, see figures 4.13-4.22. This is due to oxidative chain scission which occurs during photooxidation leading to the fragmentation of the polymer (see chapter 3). The incorporation of PP in series III (10% degradables as received in 1:1 ratio of PE:PP blend) and EPDM in series V (10% degradables as received in 1:1:0.4 ratio of PE:PP:EPDM blend) led to generally lower values of mechanical properties, as shown in figures 4.13-4.22. This effect was, again, most noticeable for elongation to break values (figs 4.14, 4.16, 4.18, 4.20, 4.22). Blends of PE and PP are immiscible and a phase boundary separates the two discrete polymer phases [117]. The low compatibility in the polymer

blends leads to a decrease in the mechanical properties [117]. This is clearly shown in the measured elongation to break for series III, see figures 4.13-4.22. The incorporation of EPDM into the mixture of PE and PP leads to slightly improved values for elongation to break (although this improved difference is largely for control V), see figure 4.14. 4.18 and 4.20 which showed the elongation to break for pass 1 and pass 3. This slight improvement is due to the ability of EPDM to act as a solid-phase dispersant in the PE:PP blend [112,117]. In doing so, EPDM increases the interphase adhesion and hence the mechanical properties.

Reprocessing of all the photobiodegradable blends (homogeneous and heterogeneous) in the internal mixer leads to an increase in the initial carbonyl content and a decrease in the vinylidene content ( $887\text{cm}^{-1}$ ) with each successive pass, see figures 4.23 and 4.24. This is due to the increasing concentration of hydroperoxides (precursors of oxidation) which are formed from the thermolysis of the vinylidene group (VI) which is present in PE as an impurity from the manufacturing stage, as shown in scheme 4.5 routes a-c [112-113,115]. Hence the formation of hydroperoxides and consequently the initial carbonyl content, is at least in part, directly parallel to the decomposition of the vinylidene groups during the high temperature thermal degradation [112,115], as demonstrated in figures 4.23, 4.24 and 4.38-4.39. Another important consequence of allylic hydroperoxides is the crosslinking reactions which are formed [112,115], as shown in scheme 4.5 routes d and e. This crosslinking during processing of PE (series I and II) is reflected in the decrease in the MFI of these samples, as shown in figures 4.12, 4.38 - 4.39.

Series II displayed much larger initial carbonyl content compared to series I, III and V, since this series is based on oxidised degradable samples.



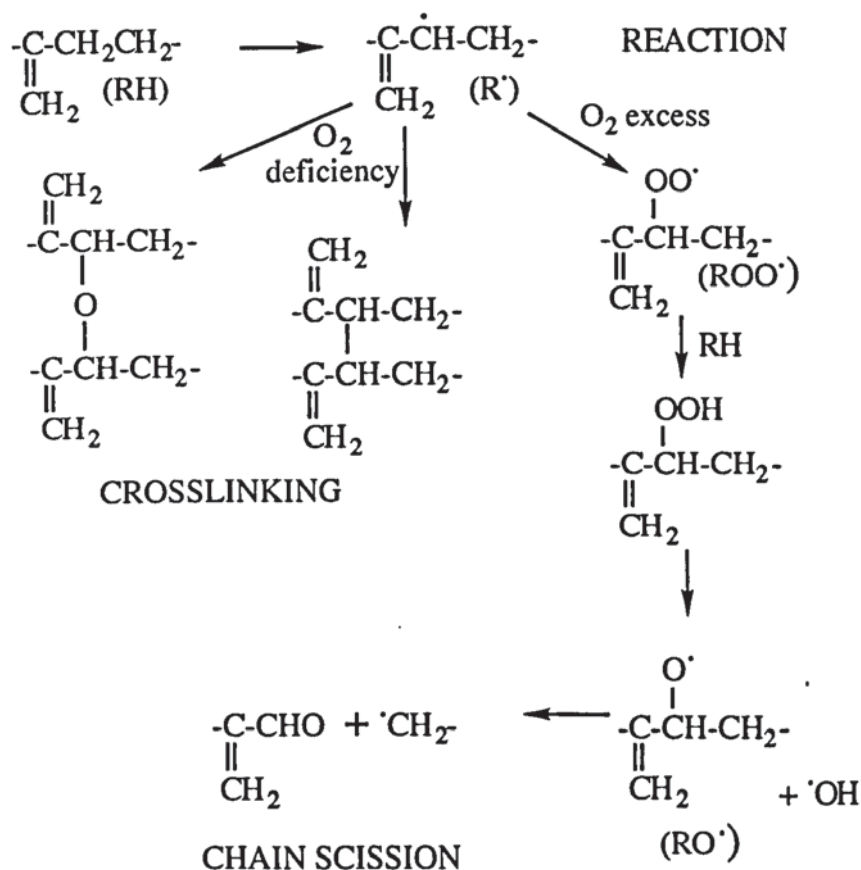
the increase in the hydroxyl, carbonyl, vinyl and vinylidene products. The greatest rates of oxidation were observed for the last extruder passes (pass 3 in figure 4.34). This is due to the larger concentrations of hydroperoxides and carbonyl products (formed in reaction 1.15) formed after three extrusion passes, as this is reflected by a decrease in vinylidene content and an increase in the initial carbonyl content (see figure 4.23 - 4.24). The net effect of the higher concentrations of these thermal oxidation products in pass 3 is to undergo accelerated photolysis during uv irradiation and thereby increase the rate of photooxidation (see figures 4.25-4.34).

The photooxidative behaviour of series I was very much the same as the photooxidative behaviour of degradables as received (chapter 3), see figure 4.34. During uv irradiation all the recycled photobiodegradables showed faster rates of oxidation compared to control I, recycled unstabilised LDPE. The increase in the carbonyl content was paralleled by an increase in the vinyl ( $909\text{ cm}^{-1}$ ) and a decrease in the vinylidene ( $887\text{cm}^{-1}$ ) contents, see figure 4.34. Figure 4.35 compares the photooxidation rates for the different blends (homogeneous and heterogeneous). Again, for all samples containing C2 and A3 blends (homogeneous and heterogeneous) the degradable polymer samples photooxidised much more rapidly than the reprocessed unstabilised LDPE, Bso (control I). However, the order of photooxidation between the different blends depended on the particular polymer used and on whether the degradables have been oxidised or not. Out of the three polymers used in the various blends, EPDM oxidised most rapidly, due to the presence of double bonds (ethylidene norbornene) in the side chain [117]. These unsaturated groups increase the photooxidation of EPDM. This is demonstrated in figures 4.33 and 4.35 for sample A3, which show that heterogeneous blend series V photooxidised more rapidly. It has been reported that during the processing stage of PP, higher concentrations

of hydroperoxides are generated compared to PE [113], which subsequently result in PP photoxidising more rapidly than PE, see figure 4.35. The addition of initially oxidised photobiodegradables polymer samples to blends series II and series IV leads to faster rates of oxidation, see figures 4.32 and 4.35.

#### 4.3.4 Comparison of Recycled Homogenous Blends using a Single Screw Extruder and an Internal Mixer.

During thermal processing at elevated temperatures LDPE degrades by two competing processes, which are crosslinking and chain scission [112,114,116], as shown in scheme 4.6.



Scheme 4.6: Competing reactions in PE during processing.

The extent to which of the two processes occurs is dependent on the concentration of oxygen present. In an extruder high pressures are generated which may prevent the diffusion of molecular oxygen, although

the feed hopper is open to the atmosphere. However, in the internal mixer, due to the lack of high pressures, molecular oxygen may enter the system and initiate the formation of hydroperoxides. Therefore, in a limited supply of oxygen (in an extruder) crosslinking will generally predominate for PE. This is supported by tables 4.5 and 4.9 and figure 4.41, which shows MFI of 10% blends of photobiodegradable samples as received in PE (series I). All degradables recycled in an extruder (at 180°C) show much lower values of MFI compared to degradables recycled in the internal mixer (at 190°C), see figure 4.41. So, although the MFI of samples recycled in the internal mixer decreased, indicating crosslinking, the extent of the crosslinking is lower than when the same samples are recycled in the extruder.

#### 4.3.5 Overview of Results

The experiments described in this chapter indicate that in general the degradable polymer samples can be recycled as blends with major polymers in waste, for example polyethylene and polypropylene, with a minimal loss in the properties of the blends [SC1]. However, the extent to which this loss in properties occurs is dependent on several factors:

##### 4.3.5.1 Number of Recycling Operations

Generally, the greater the number of recycling operations performed on the degradable polymer samples, the more inferior are the properties of the recyclates. Going from the first to the fourth pass there was a steady decrease in the physical and chemical properties.

##### 4.3.5.2 Temperature

The experiments have shown that recycling carried out at the higher temperature of 210°C leads to more severe degradation of the polymers (both during recycling and on subsequent exposure to uv light).

#### 4.3.5.3 Photoxidation

All the degradable blends that were based on pre-photoxidised polymer films gave inferior properties when compared to blends based on non-oxidised polymer films.

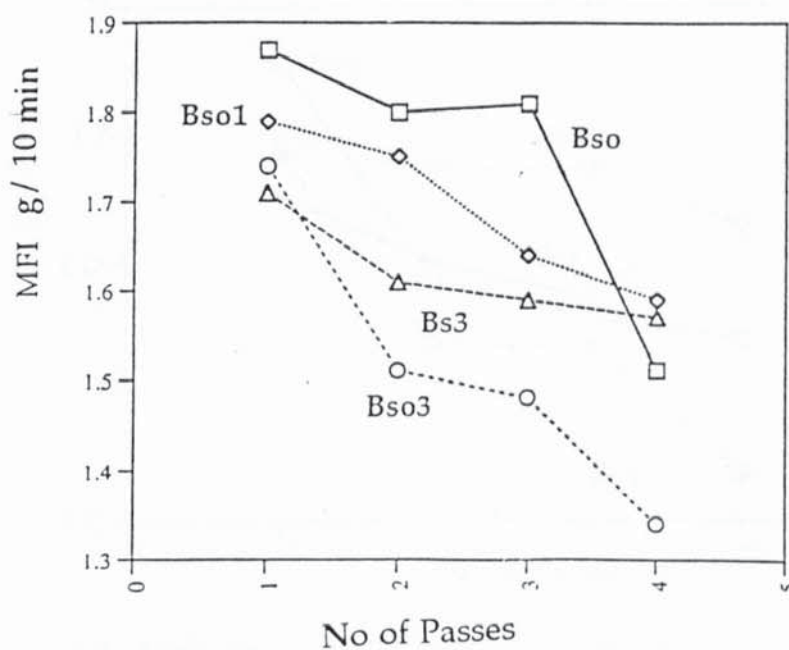
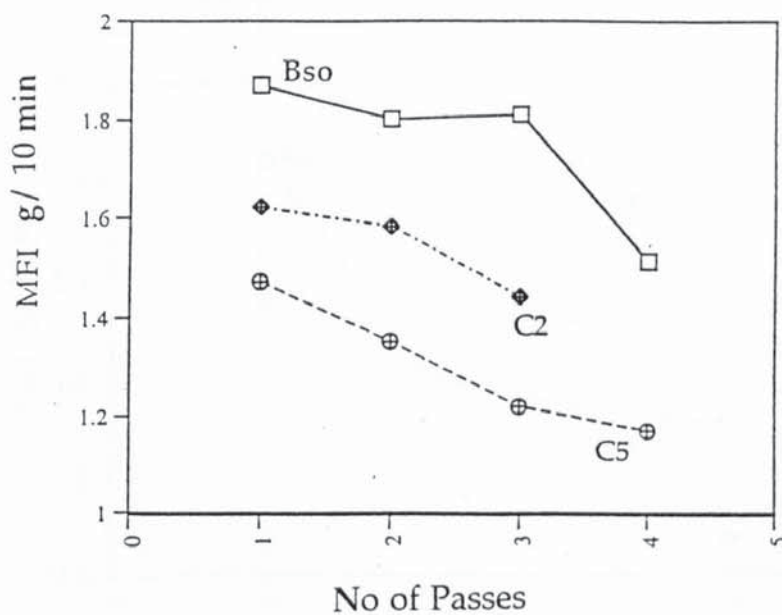
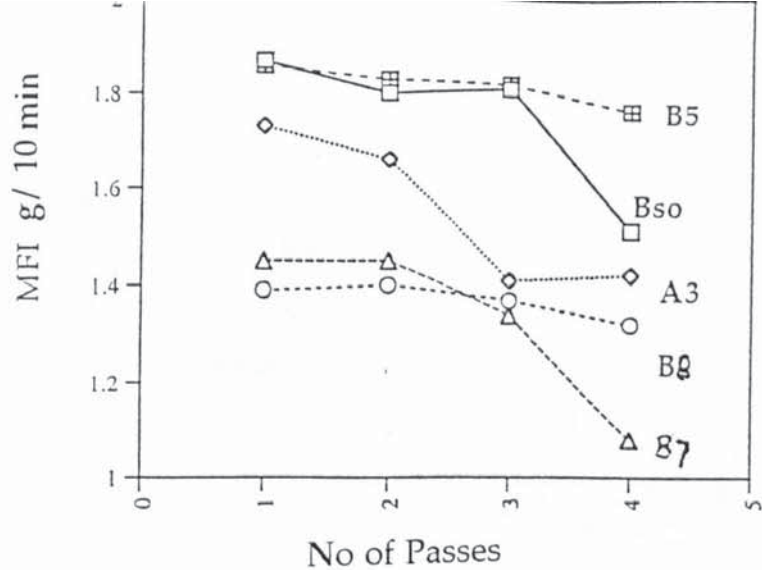


Figure 4.1: Melt flow index (MFI) of 10% homogeneous blends (in LDPE) of photobiodegradable polymer samples recycled at 180°C using a single screw extruder, SSE. See tables 4.1 and 4.2 for sample codes.

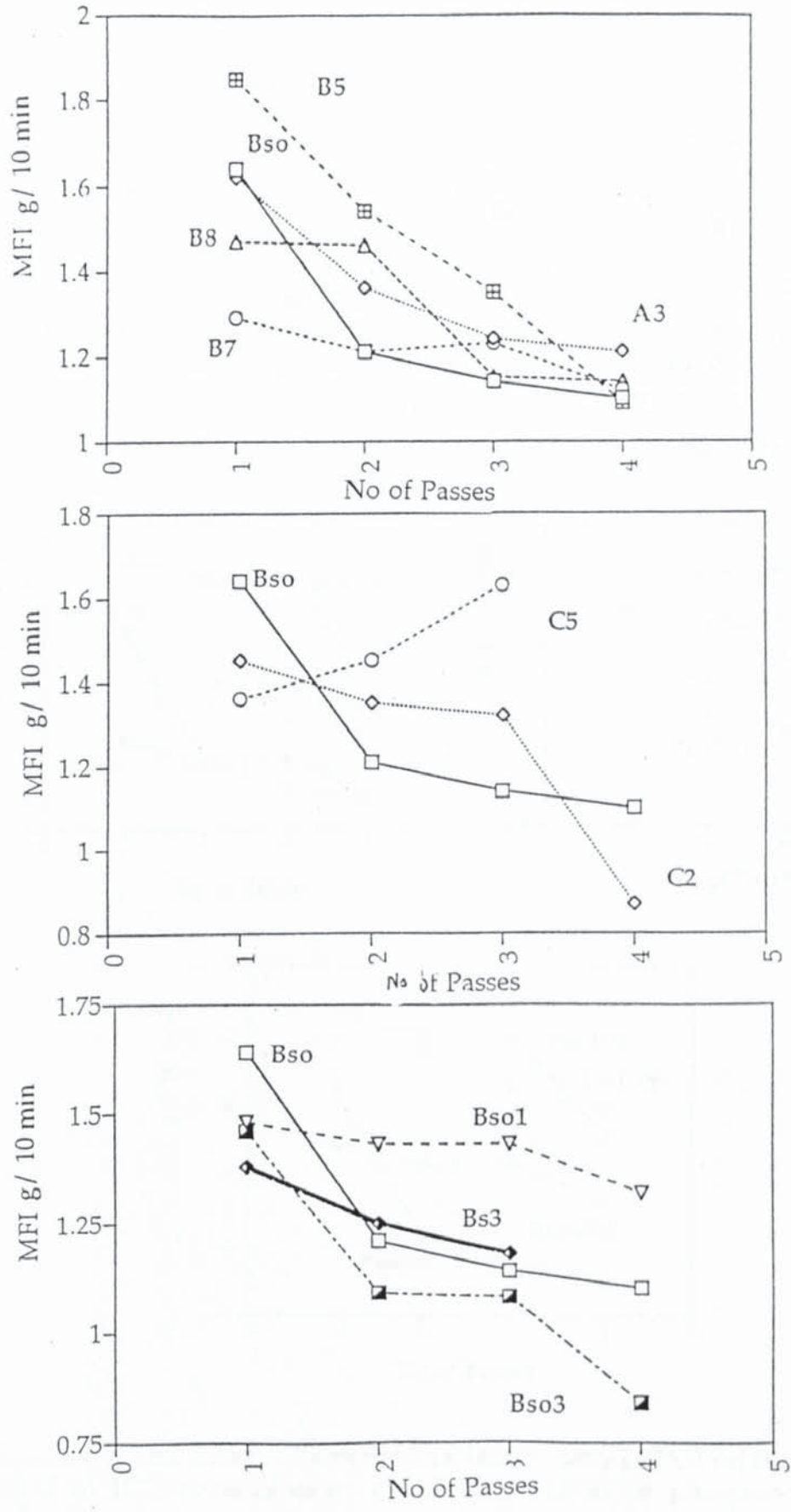


Figure 4.2: Melt flow index (MFI) of 10% homogeneous blends (in LPDE) of photobiodegradable polymer samples recycled at 210°C using a single screw extruder. See tables 4.1 and 4.2 for sample codes.

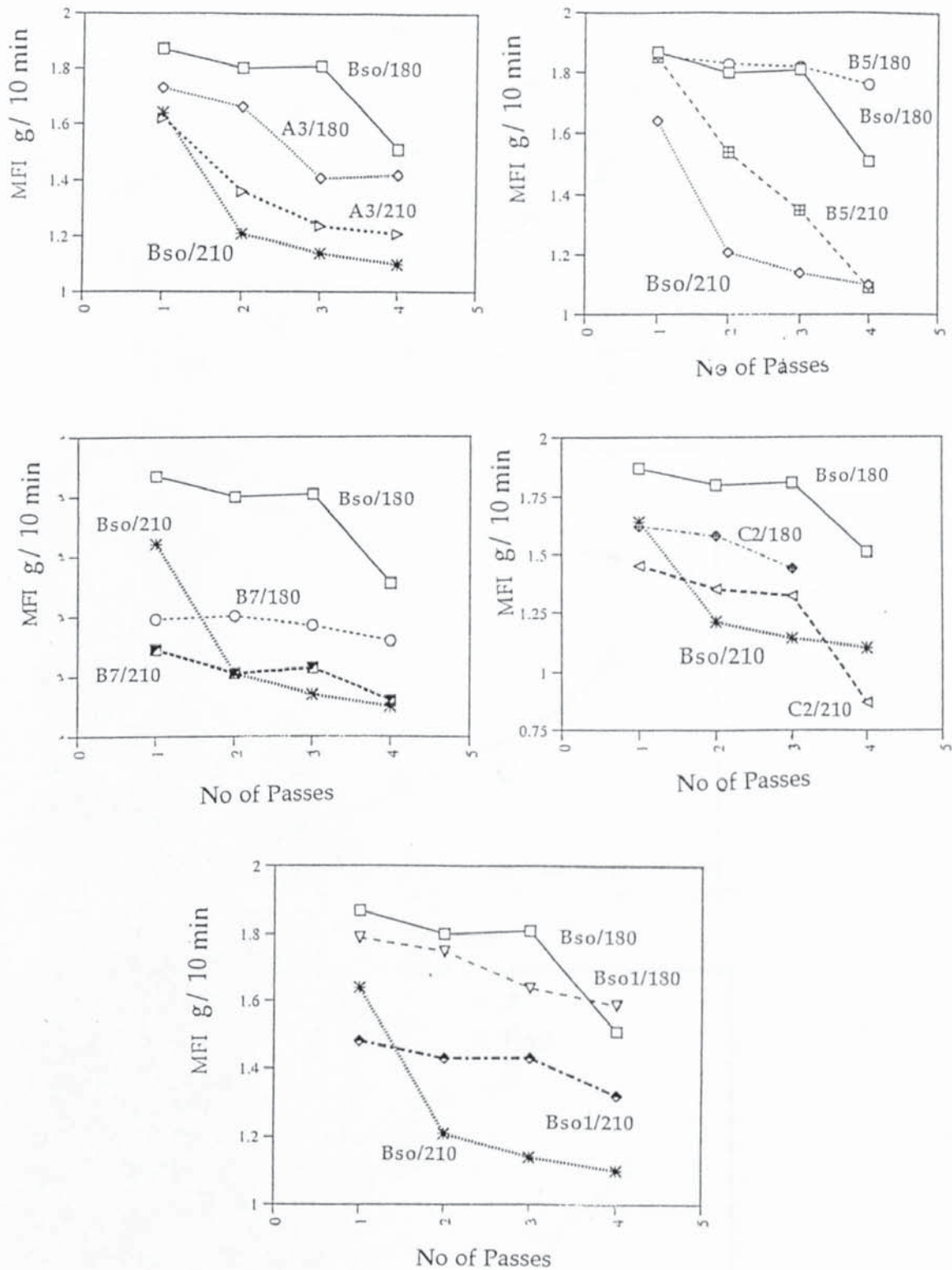


Figure 4.3: The effect of temperature (180°C and 210°C) on the melt flow index of 10% homogeneous blends (in LDPE) of photobiodegradable polymer samples recycled using a single screw extruder. See tables 4.1 and 4.2 for sample codes.

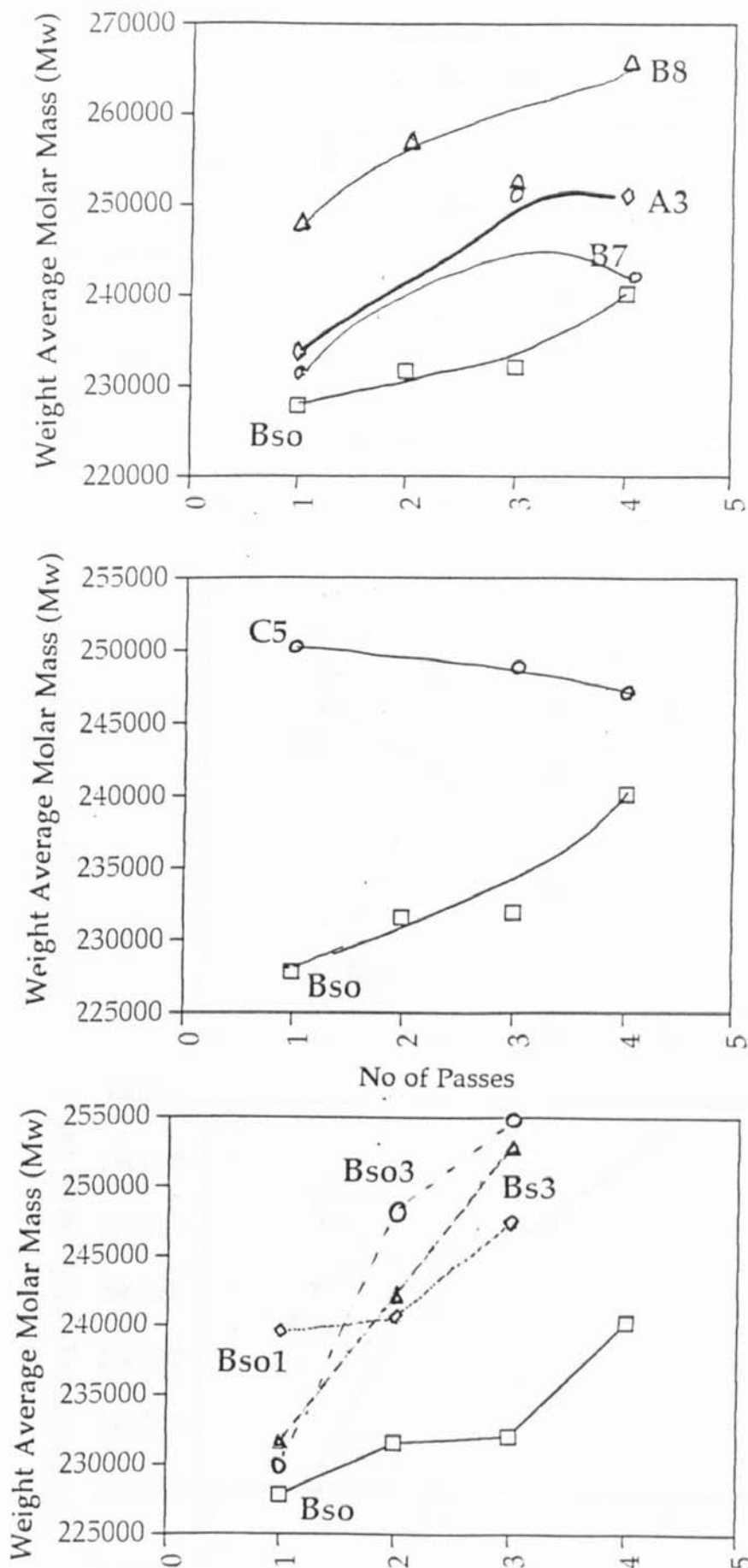


Figure 4.4: Changes in molar mass (Mw) of 10% homogeneous blends (in LDPE) of photobiodegradable polymer samples (as received) recycled at 180°C using a single screw extruder. See tables 4.1 and 4.2 for sample codes.

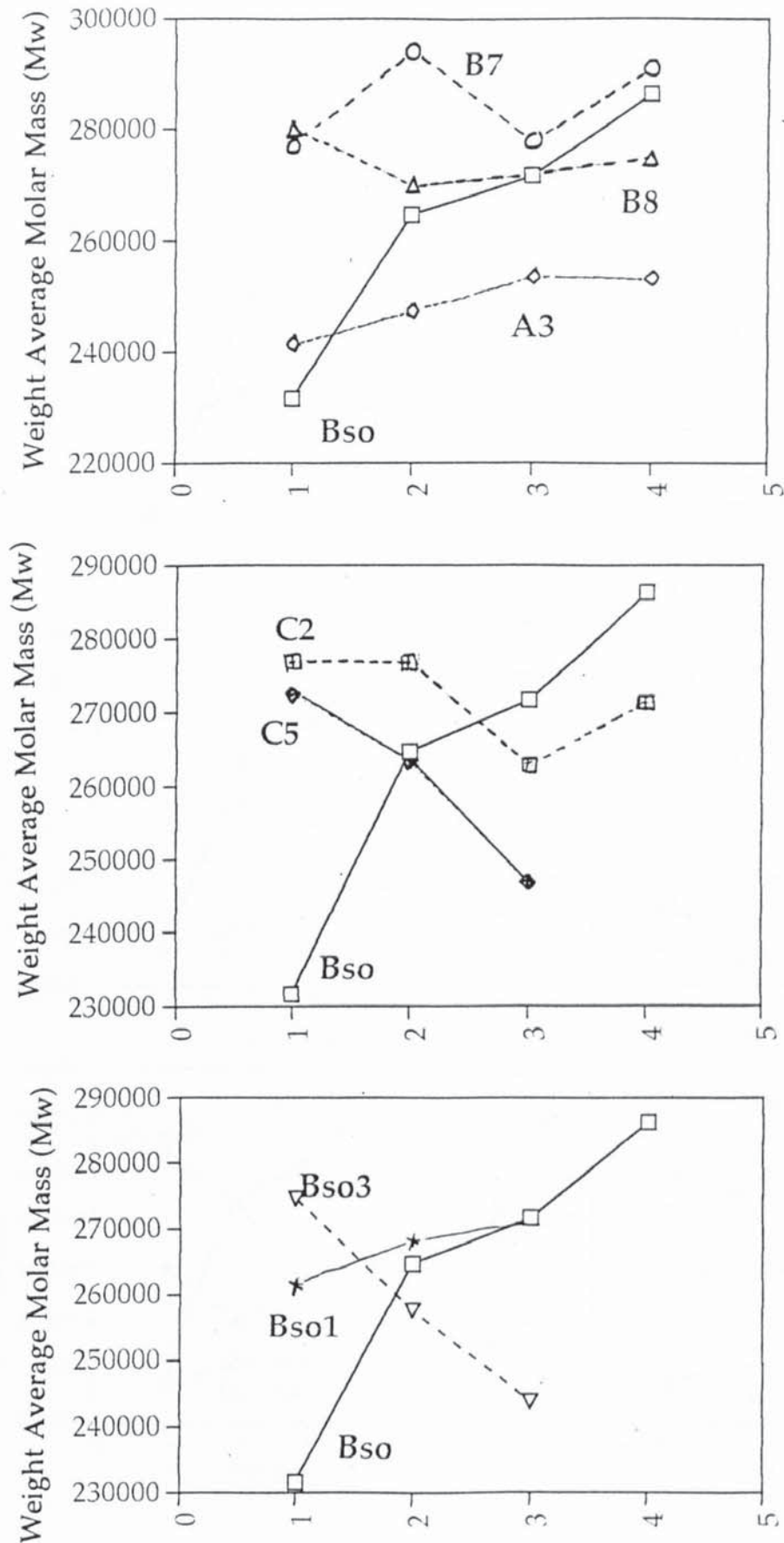


Figure 4.5: Changes in molar mass (Mw) of 10% homogeneous blends (in LDPE) of photobiodegradable polymer samples recycled at 210°C using a single screw extruder. See tables 4.1 and 4.2 for sample codes.

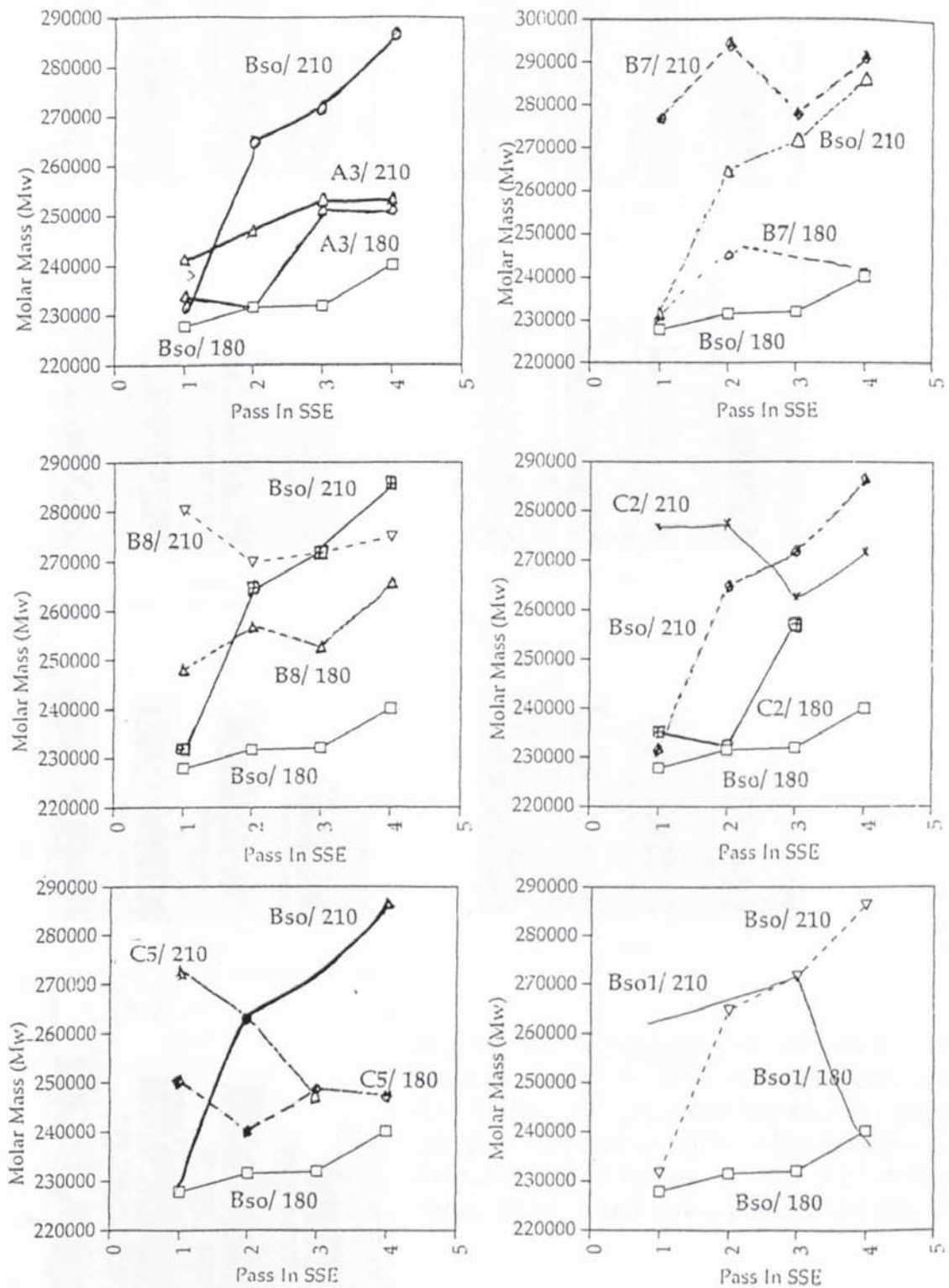


Figure 4.6: The effect of temperature (180°C and 210°C) on the molar mass of 10% homogeneous blends (in LDPE) of photobiodegradable polymer samples recycled using a single screw extruder. See tables 4.1 and 4.2 for sample codes.

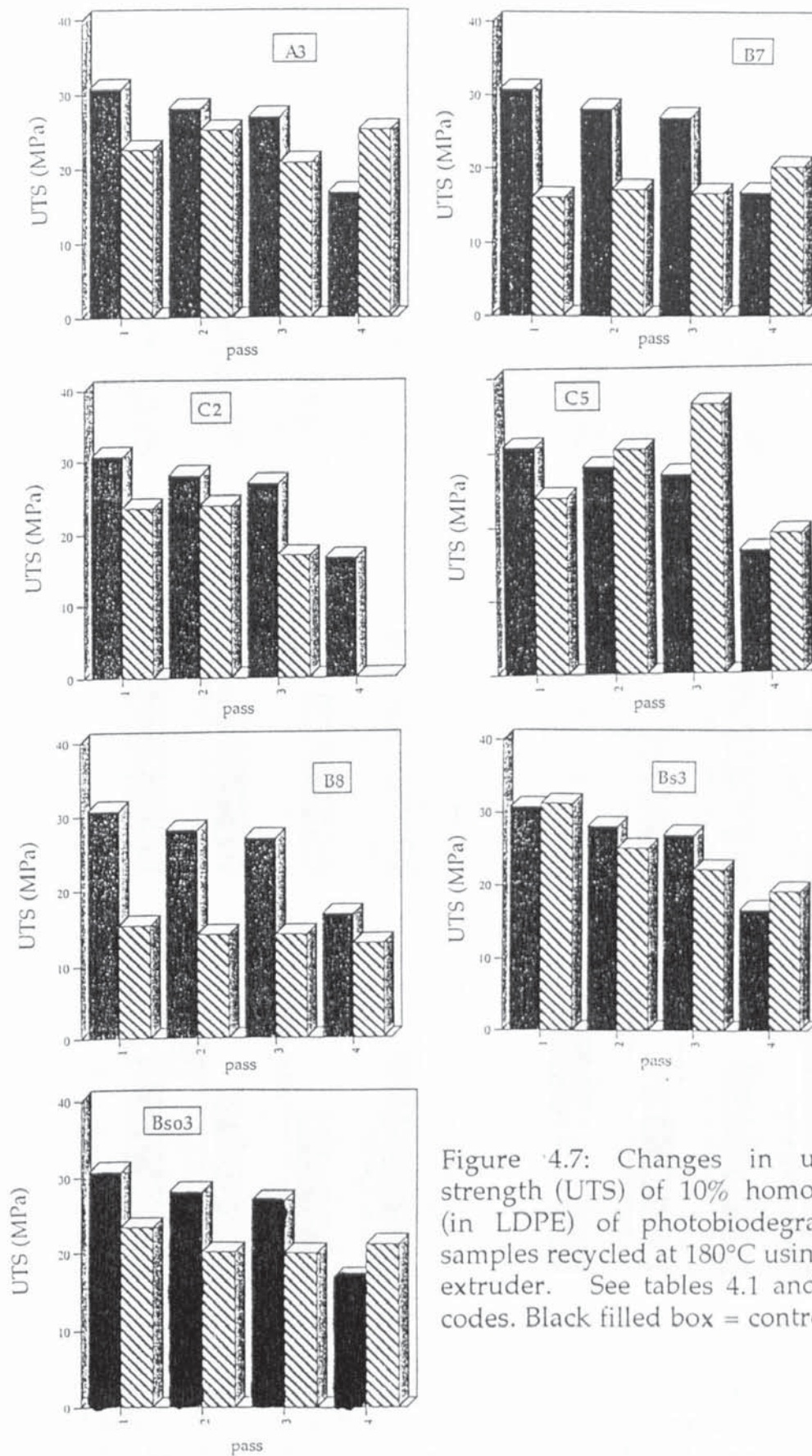


Figure 4.7: Changes in ultimate tensile strength (UTS) of 10% homogeneous blends (in LDPE) of photobiodegradable polymer samples recycled at 180°C using a single screw extruder. See tables 4.1 and 4.2 for sample codes. Black filled box = control sample, Bso.

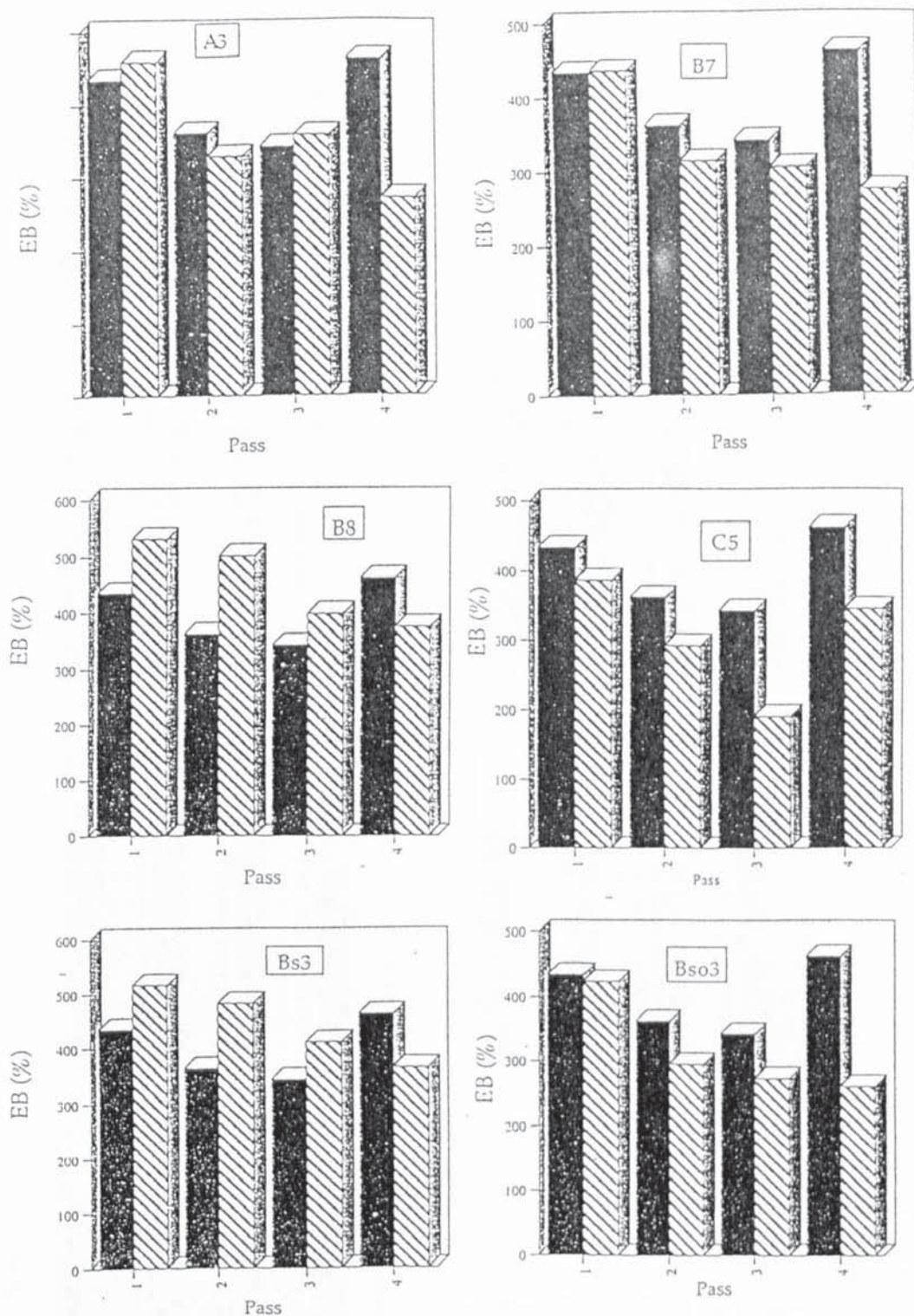


Figure 4.8: Changes in elongation to break (EB) of 10% homogeneous blends (in LDPE) of photobiodegradable polymer samples recycled at 180°C using a single screw extruder. See tables 4.1 and 4.2 for sample codes. Black filled box = control sample, Bso.

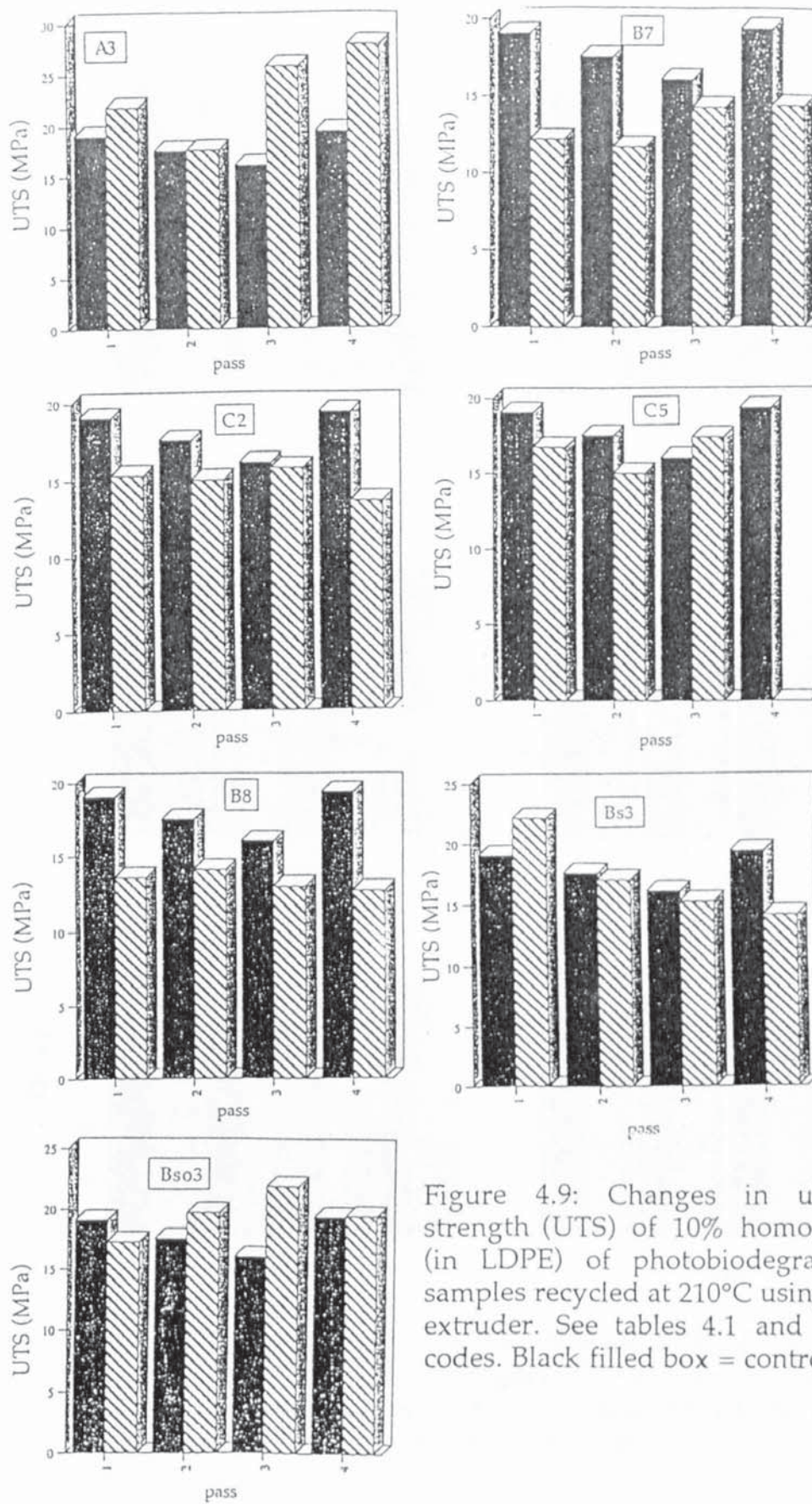


Figure 4.9: Changes in ultimate tensile strength (UTS) of 10% homogeneous blends (in LDPE) of photobiodegradable polymer samples recycled at 210°C using a single screw extruder. See tables 4.1 and 4.2 for sample codes. Black filled box = control sample, Bso.

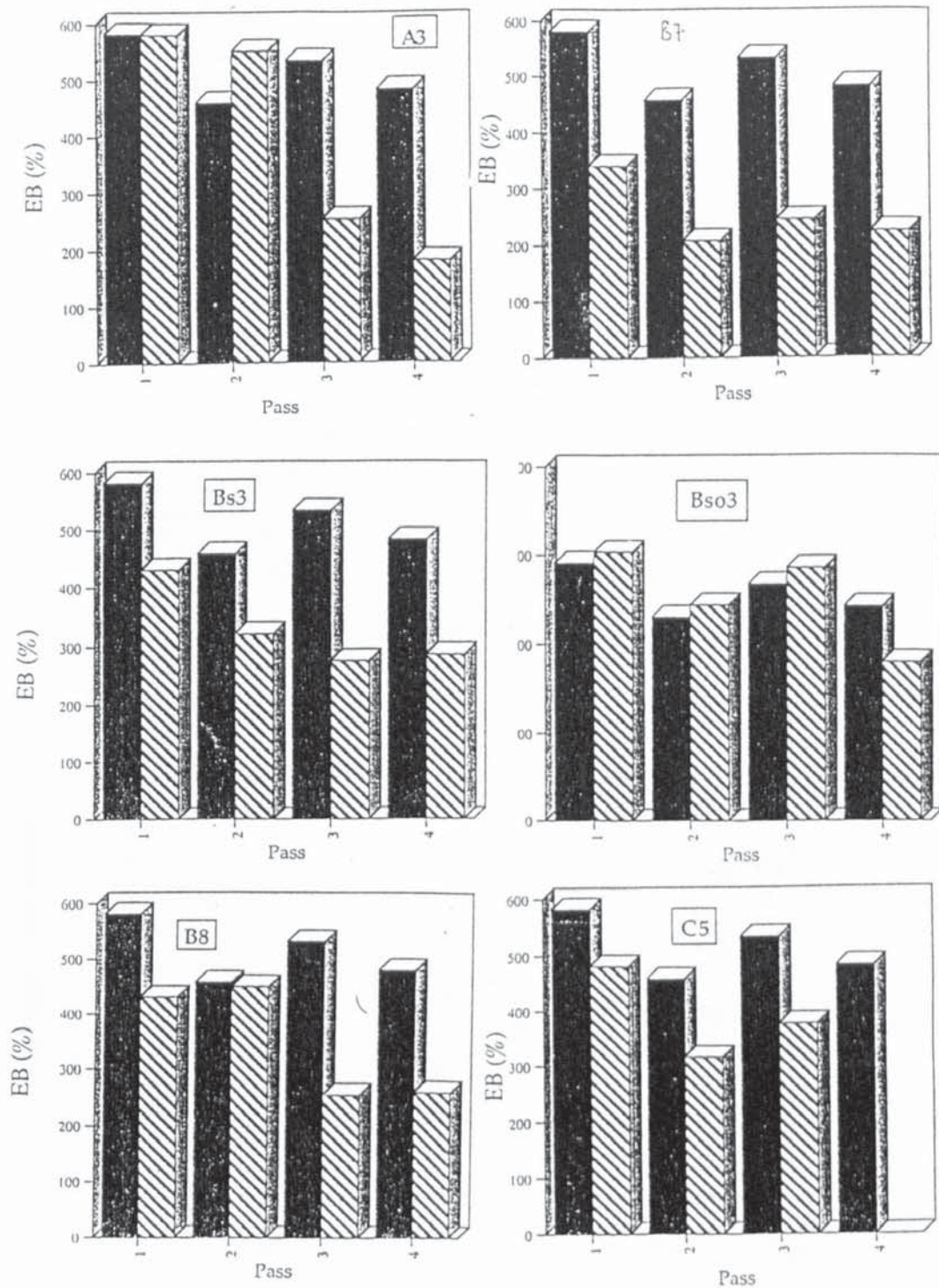


Figure 4.10: Changes in elongation to break (EB) of 10% homogeneous blends (in LDPE) of photobiodegradable polymer samples recycled at 210°C using a single screw extruder. See tables 4.1 and 4.2 for sample codes. Black filled box = control sample, Bso.

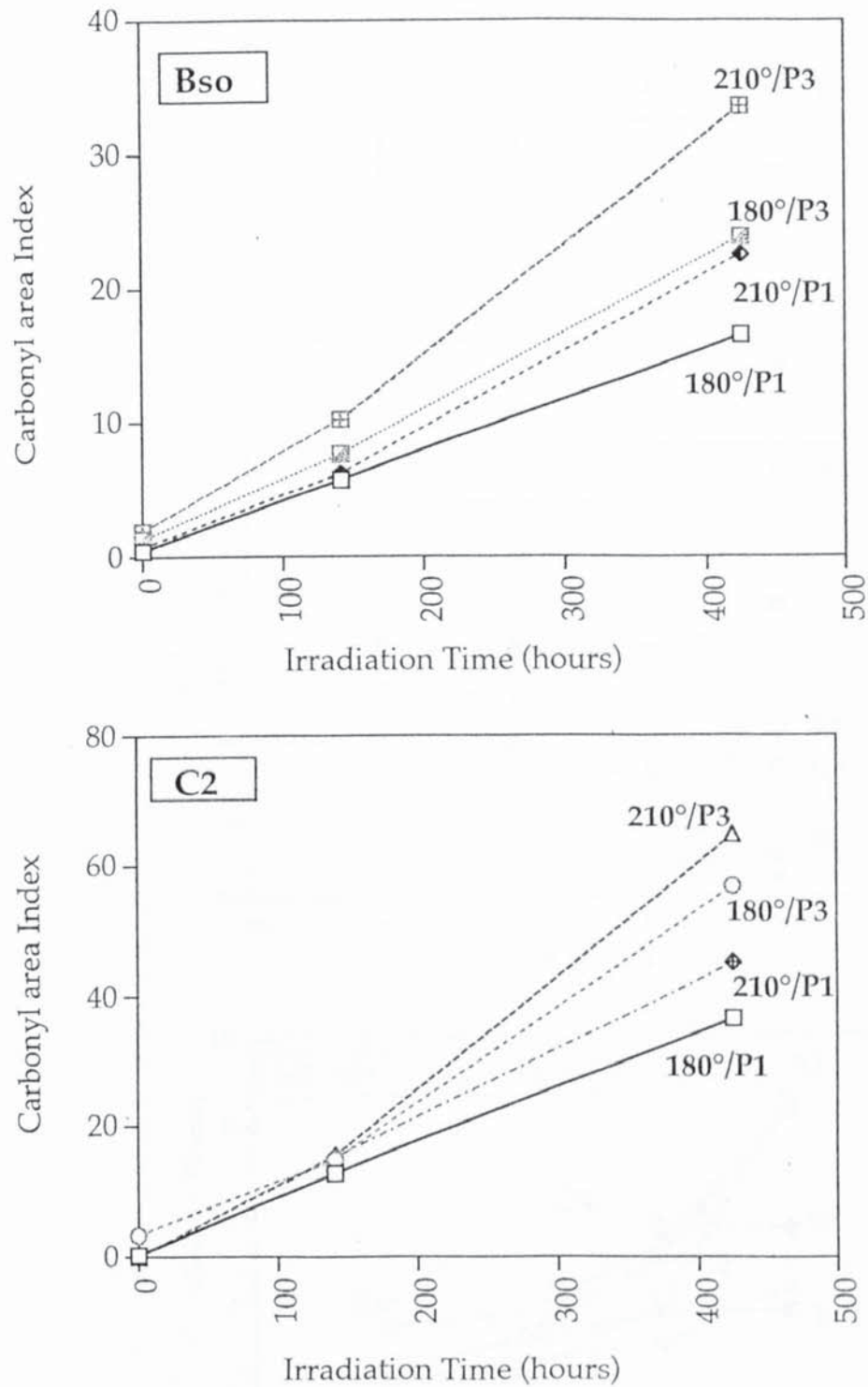


Figure 4.11: The effect of temperature on the recycling (single screw extruder) of 10% homogeneous blends (in LDPE) of samples Bso and C2 on the rate of photooxidation (new uv cabinet). See table 4.1 for sample codes.

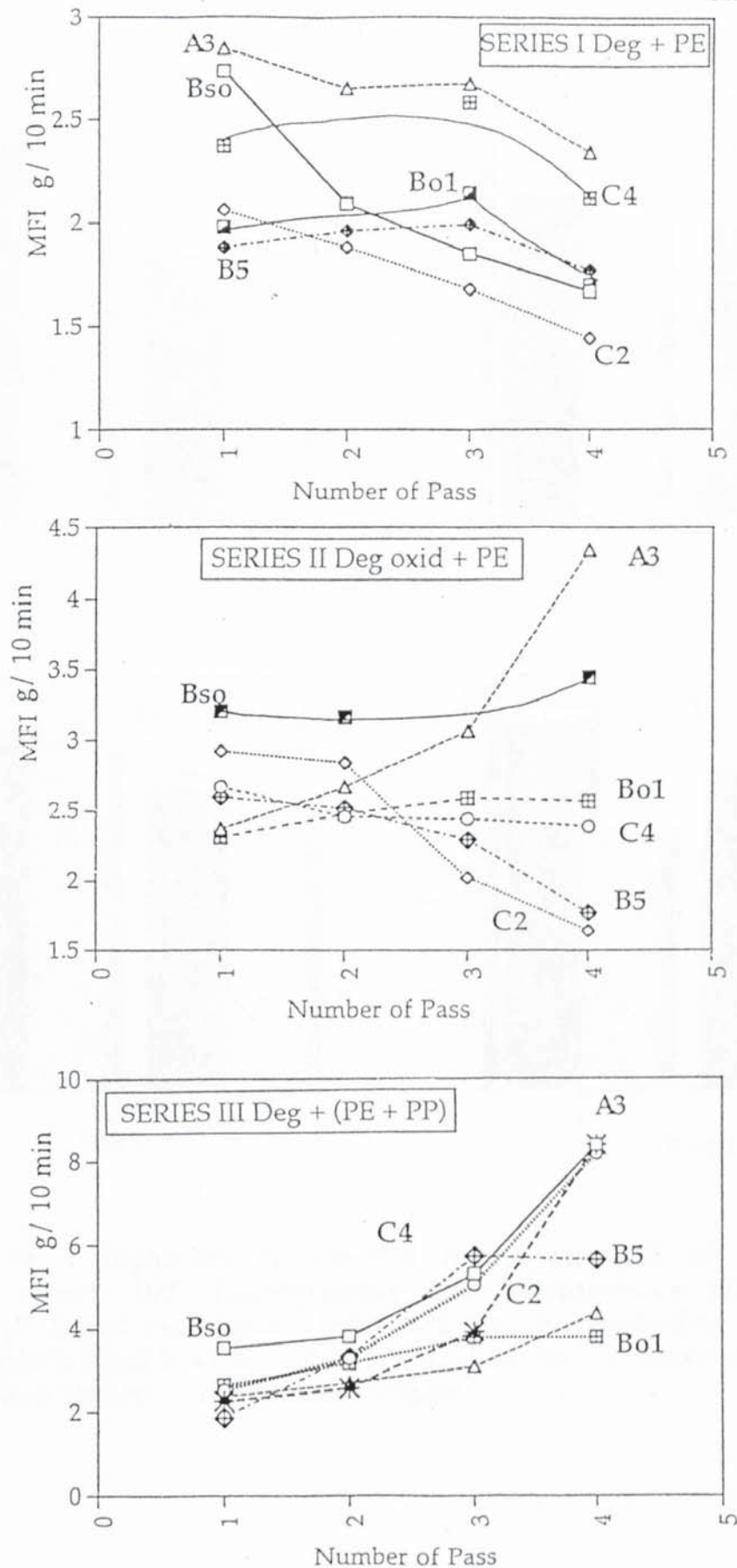


Figure 4.12: Melt stability of 10% homogeneous and heterogeneous degradable blends recycled at 190°C using an internal mixer. See tables 4.1 and 4.2 for sample codes, table 4.3 for conditions of pre-oxidation and table 4.4 for definition of series.

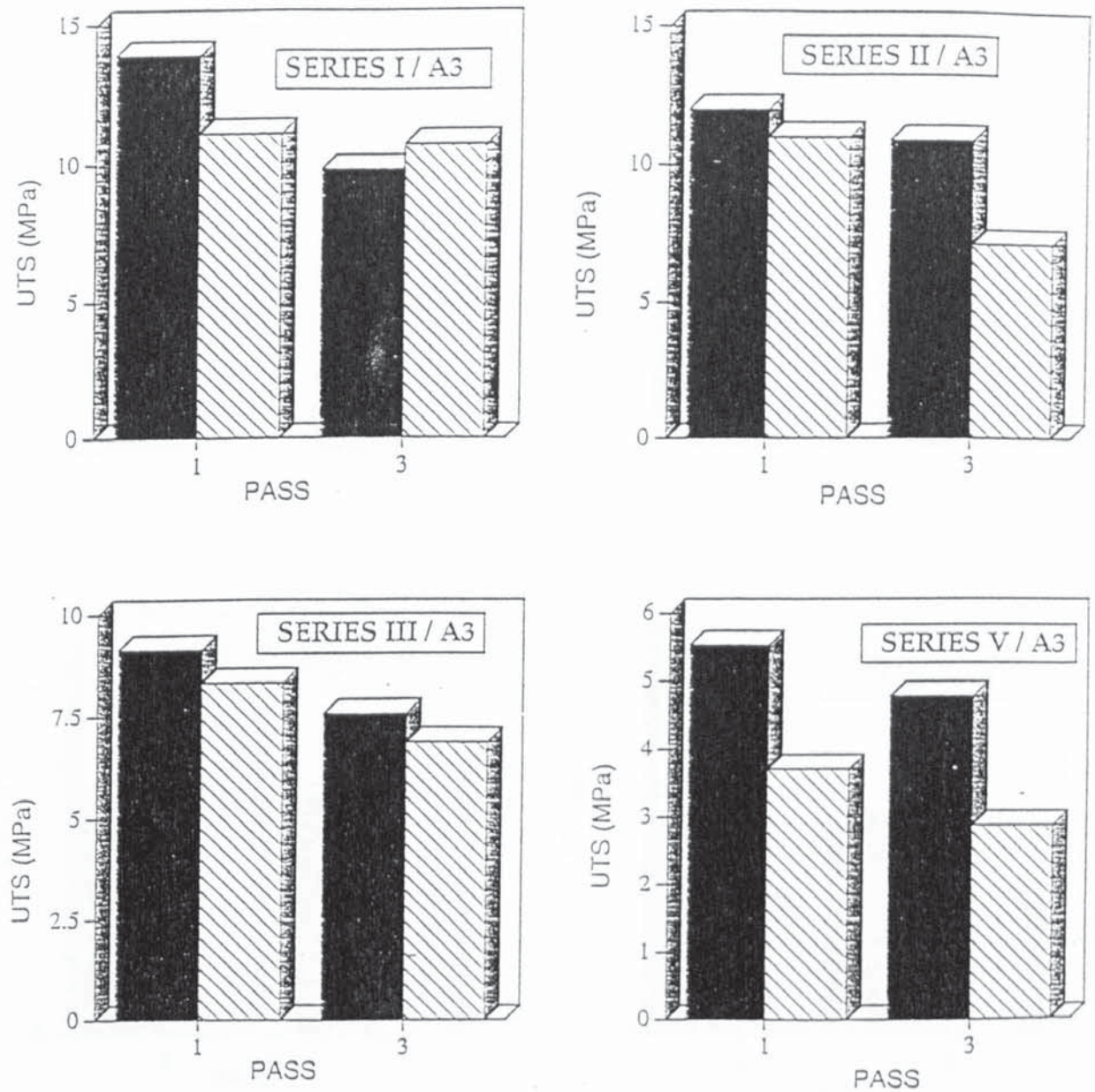


Figure 4.13: Comparison of ultimate tensile strength of recycled (internal mixer) 10% homogeneous and heterogenous blends of sample A3 (lined rectangular box) with the corresponding control samples (black filled box). See table 4.3 for definition of series and table 4.4 for identification of the control samples.

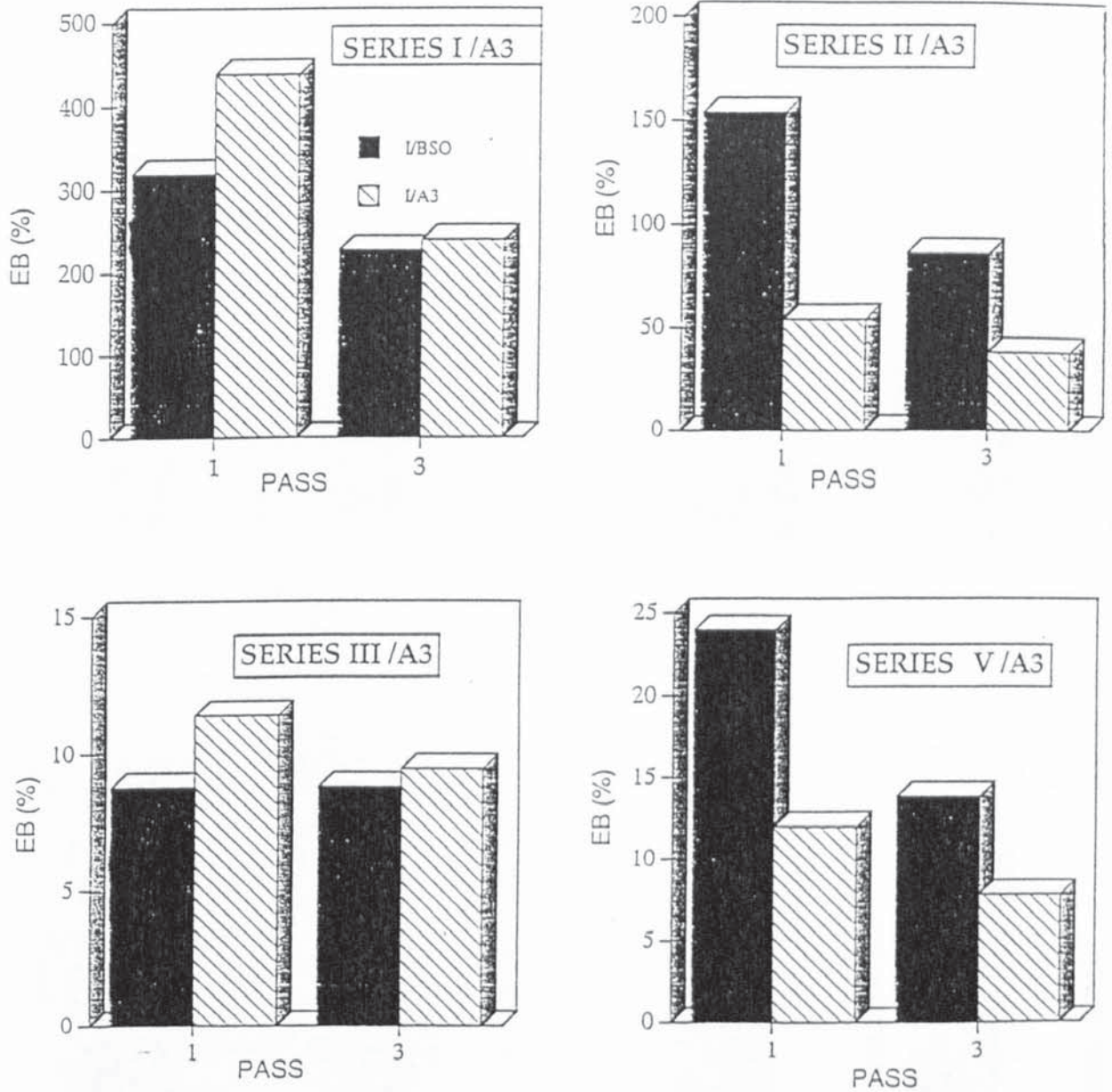


Figure 4.14: Comparison of elongation to break of recycled (internal mixer at 190°C) 10% homogeneous and heterogeneous blends of sample A3 (lined rectangular box) with the corresponding control samples (black filled box). See table 4.3 for definition of series and table 4.4 for identification of the control samples.

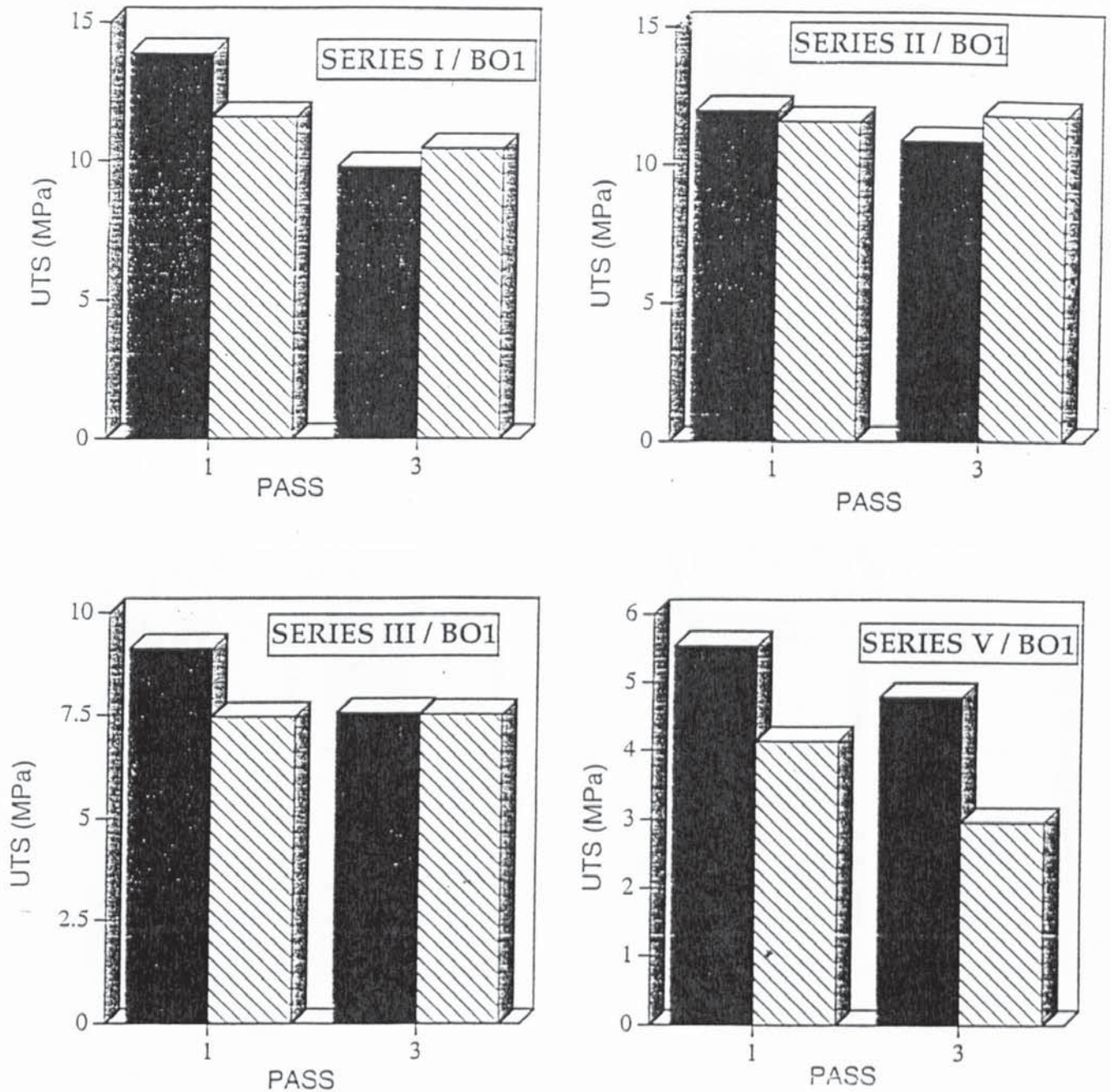


Figure 4.15: Comparison of ultimate tensile strength of recycled (internal mixer at 190°C) 10% homogeneous and heterogeneous blends of sample Bo1 (lined rectangular box) with the corresponding control samples (filled black box). See table 4.3 for definition of series and table 4.4 for identification of the control samples.

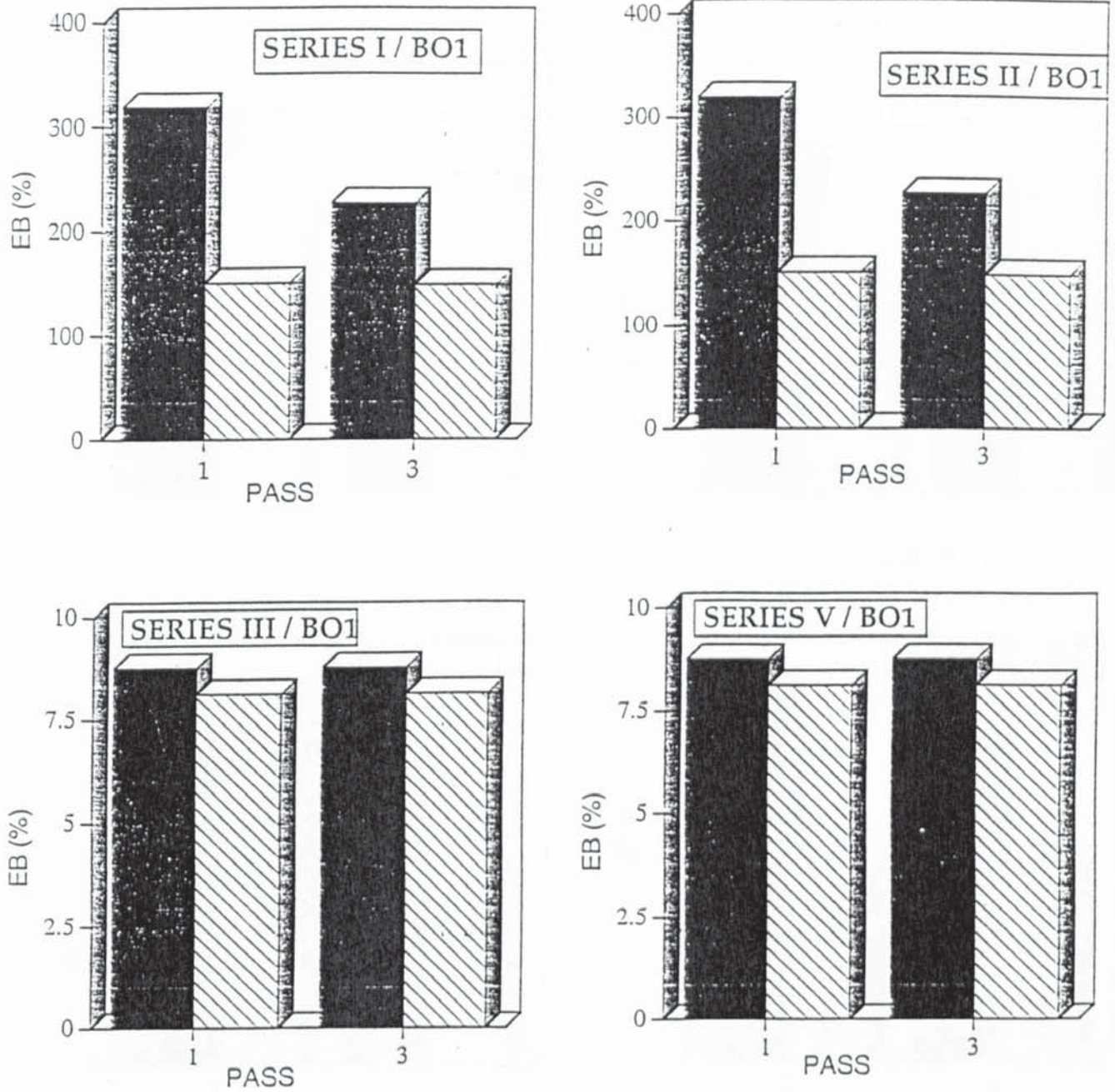


Figure 4.16: Comparison of elongation to break of recycled (internal mixer at 190°C) 10% homogeneous and heterogeneous blends of sample Bo1 (lined rectangular box) with the corresponding control samples (filled black box). See table 4.3 for definition of series and table 4.4 for identification of the control samples.

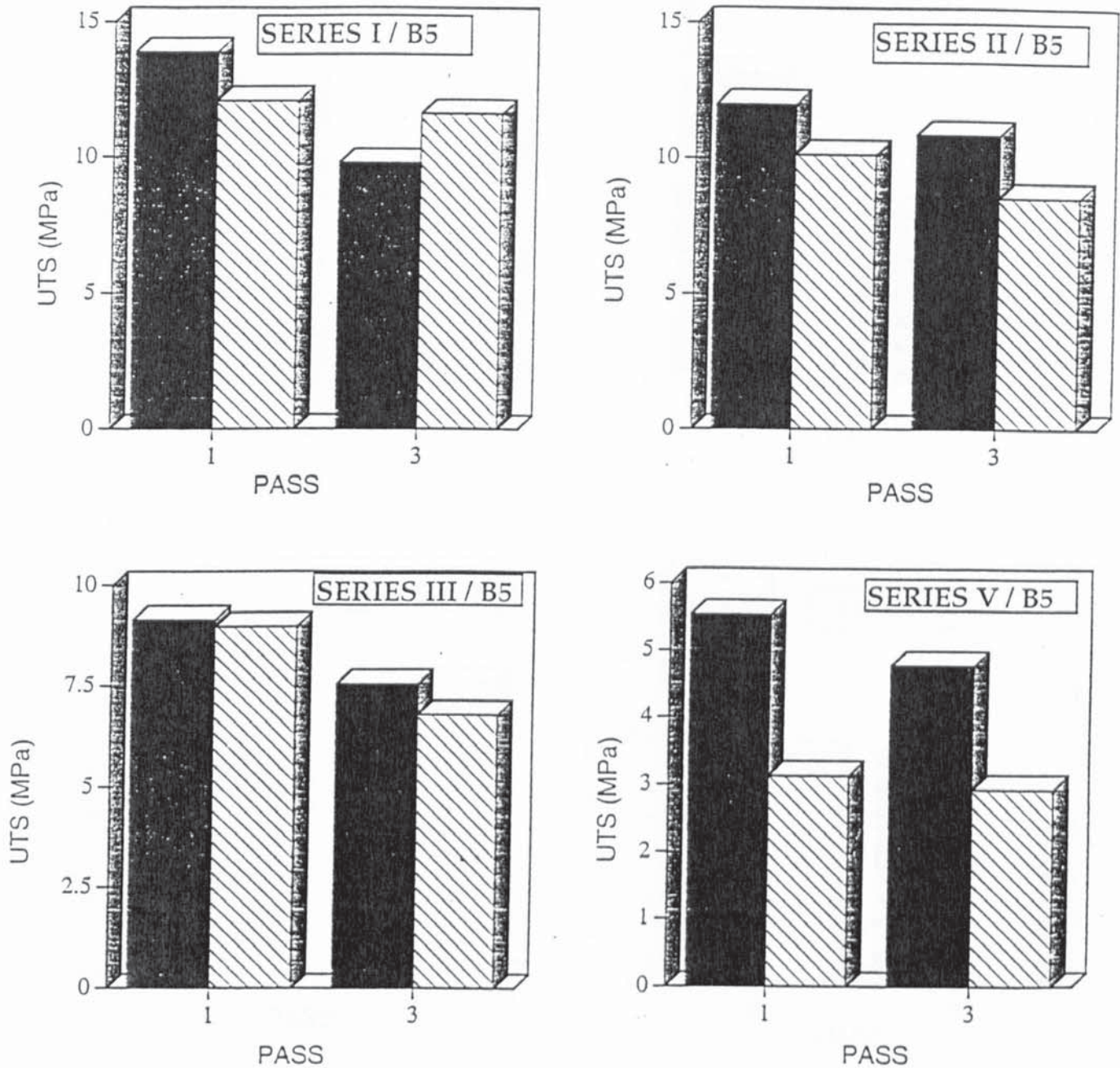


figure 4.17: Comparison of ultimate tensile strength of recycled (internal mixer at 190°C) 10% homogeneous and heterogeneous blends of sample B5 (lined rectangular box) with the corresponding control samples (filled black box). See table 4.3 for definition of series and table 4.4 for identification of the control samples.

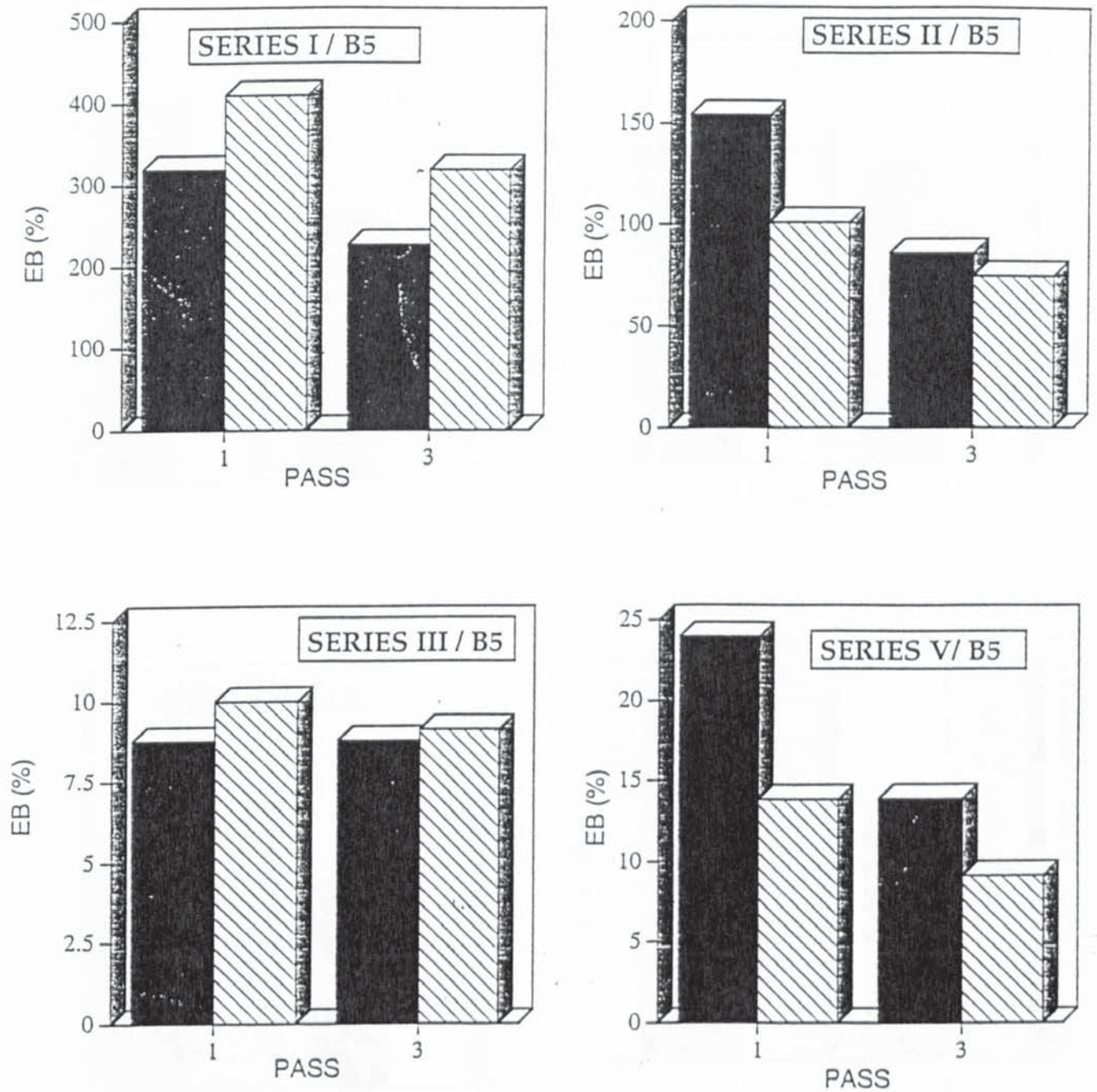


Figure 4.18: Comparison of elongation to break of recycled (internal mixer at 190°C) 10% homogeneous and heterogeneous blends of sample B5 (lined rectangular box) with the corresponding control samples (filled black box). See table 4.3 for definition of series and table 4.4 for identification of the control samples.

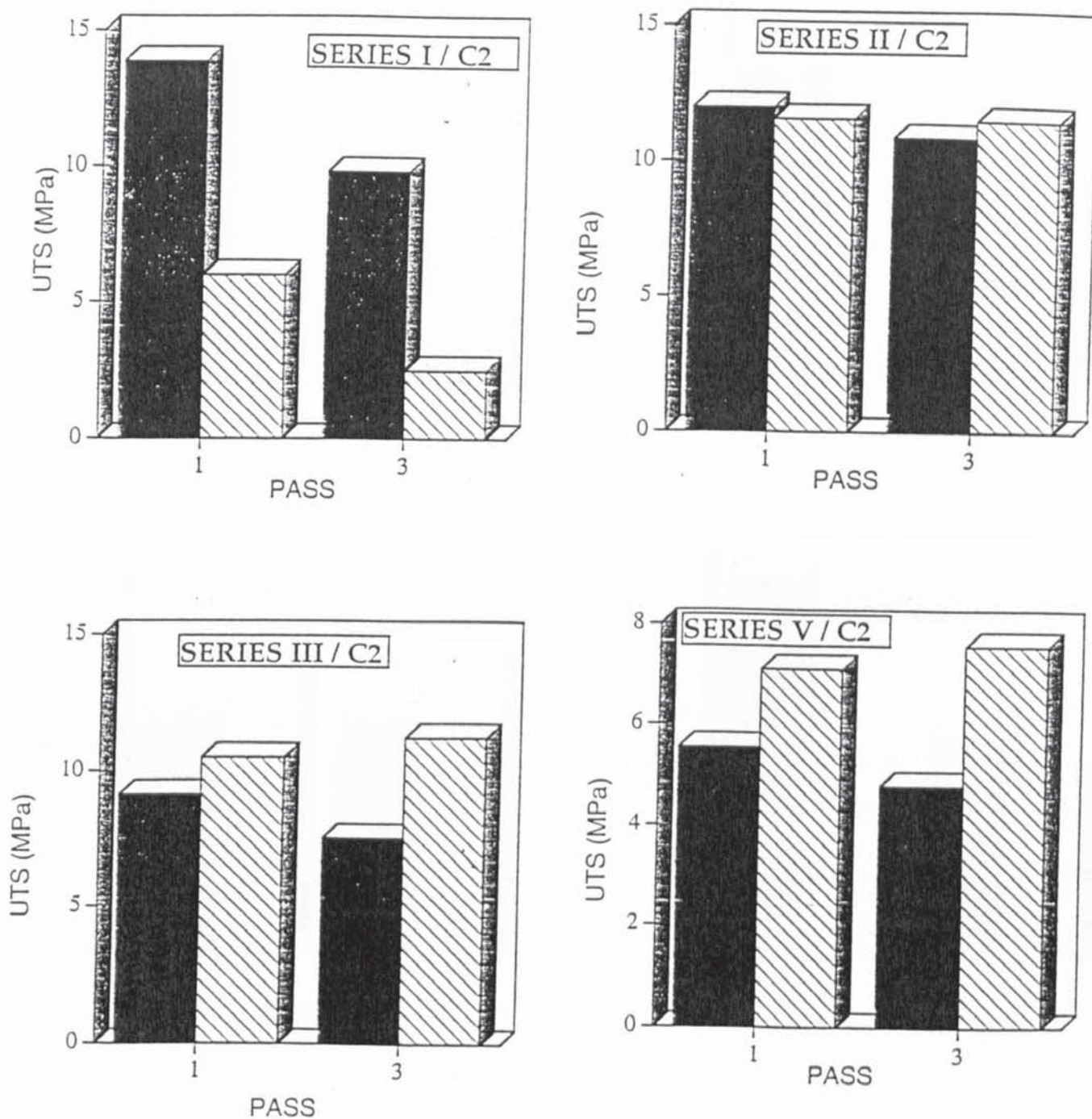


Figure 4.19: Comparison of ultimate tensile strength of recycled (internal mixer at 190°C) 10% homogeneous and heterogeneous blends of sample C2 (lined rectangular box) with the corresponding control samples (filled black box). See table 4.3 for definition of series and table 4.4 for identification of the control samples.

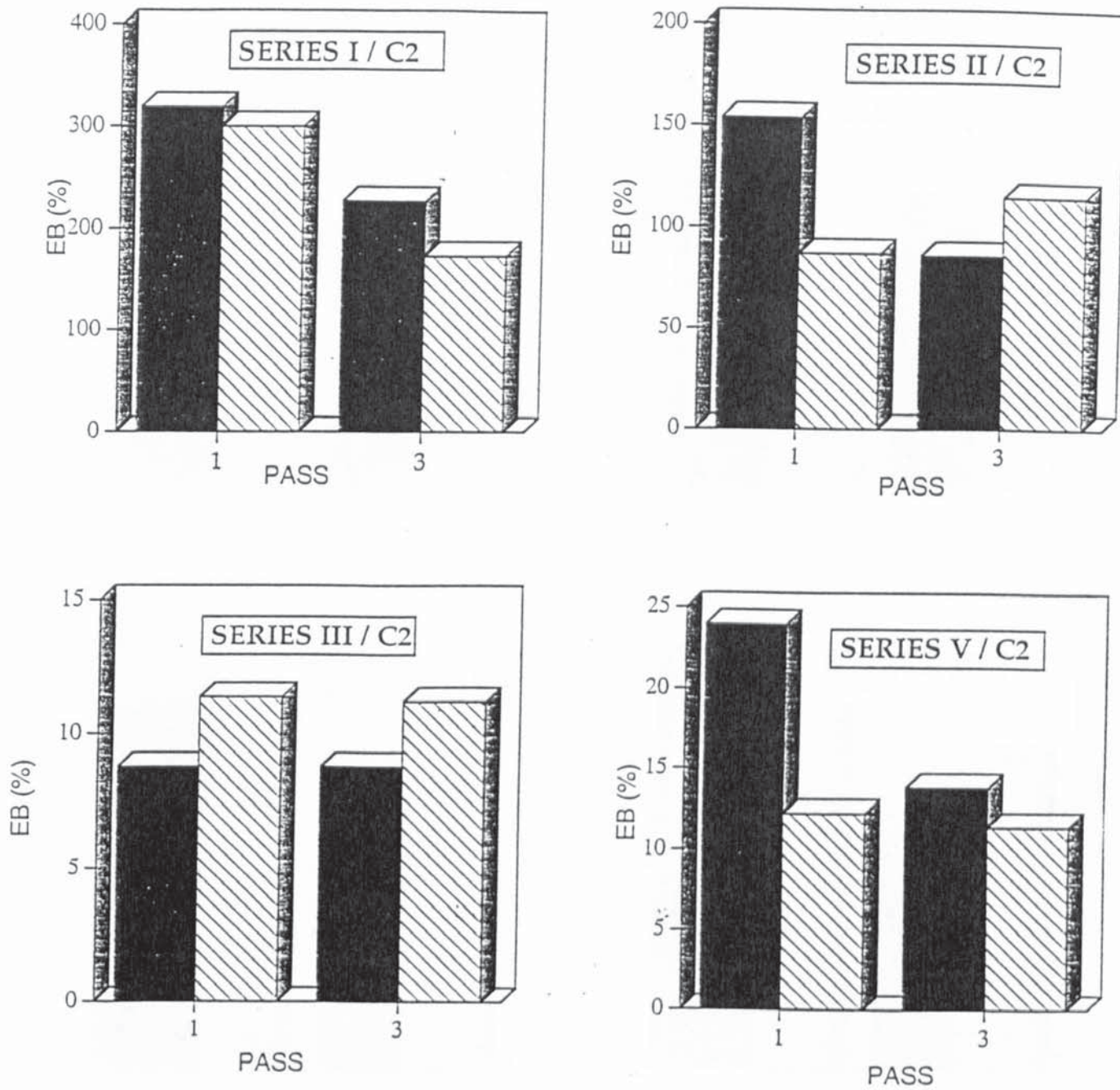


Figure 4.20: Comparison of elongation to break of recycled (internal mixer at 190°C) 10% homogeneous and heterogeneous blends of sample C2 (lined rectangular box) with the corresponding control samples (filled black box). See table 4.3 for definition of series and table 4.4 for identification of the control samples.

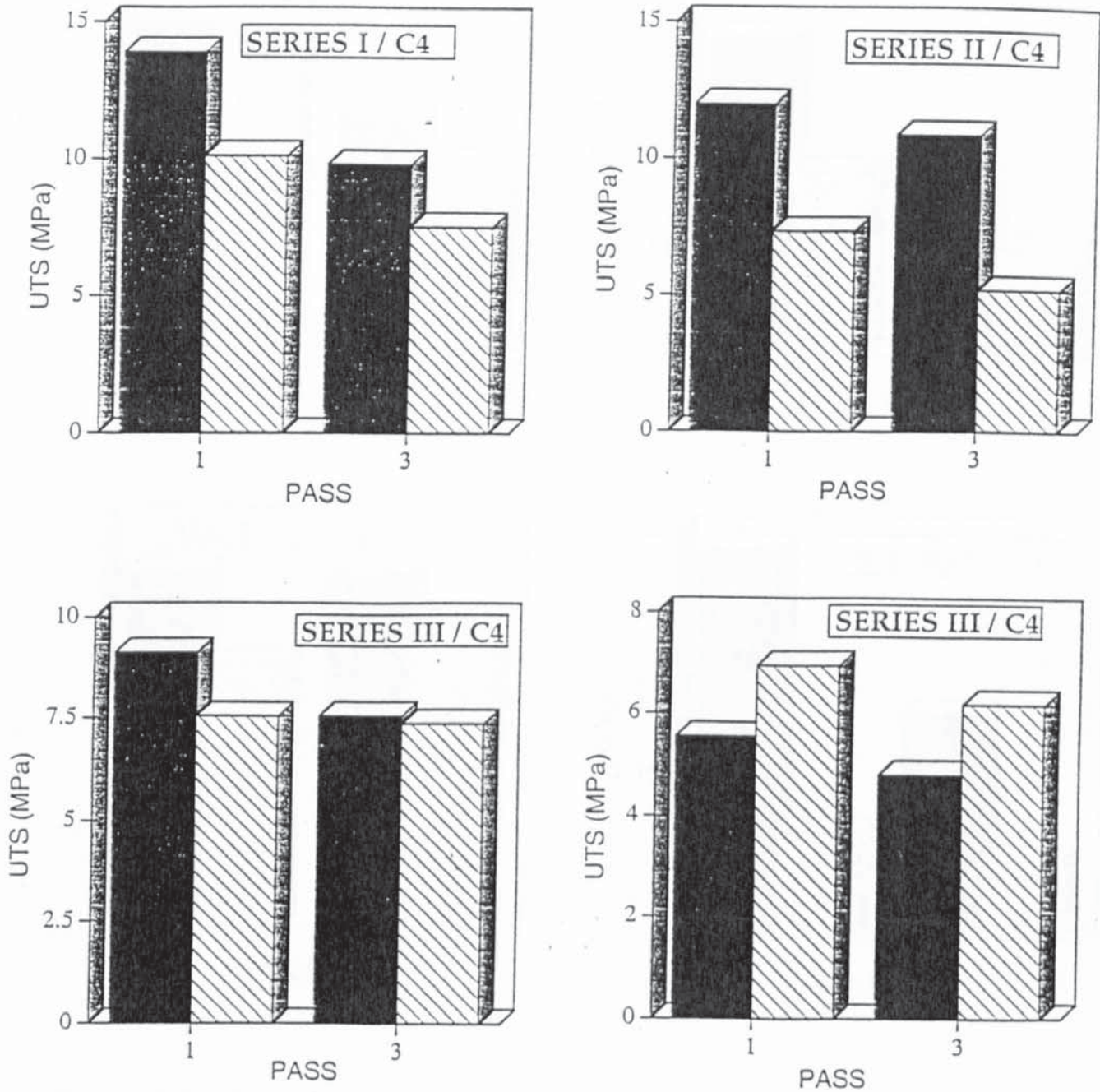


Figure 4.21: Comparison of ultimate tensile strength of recycled (internal mixer at 190°C) 10% homogeneous and heterogeneous blends of sample C4 (lined rectangular box) with the corresponding control samples (filled black box). See table 4.3 for definition of series and table 4.4 for identification of the control samples.

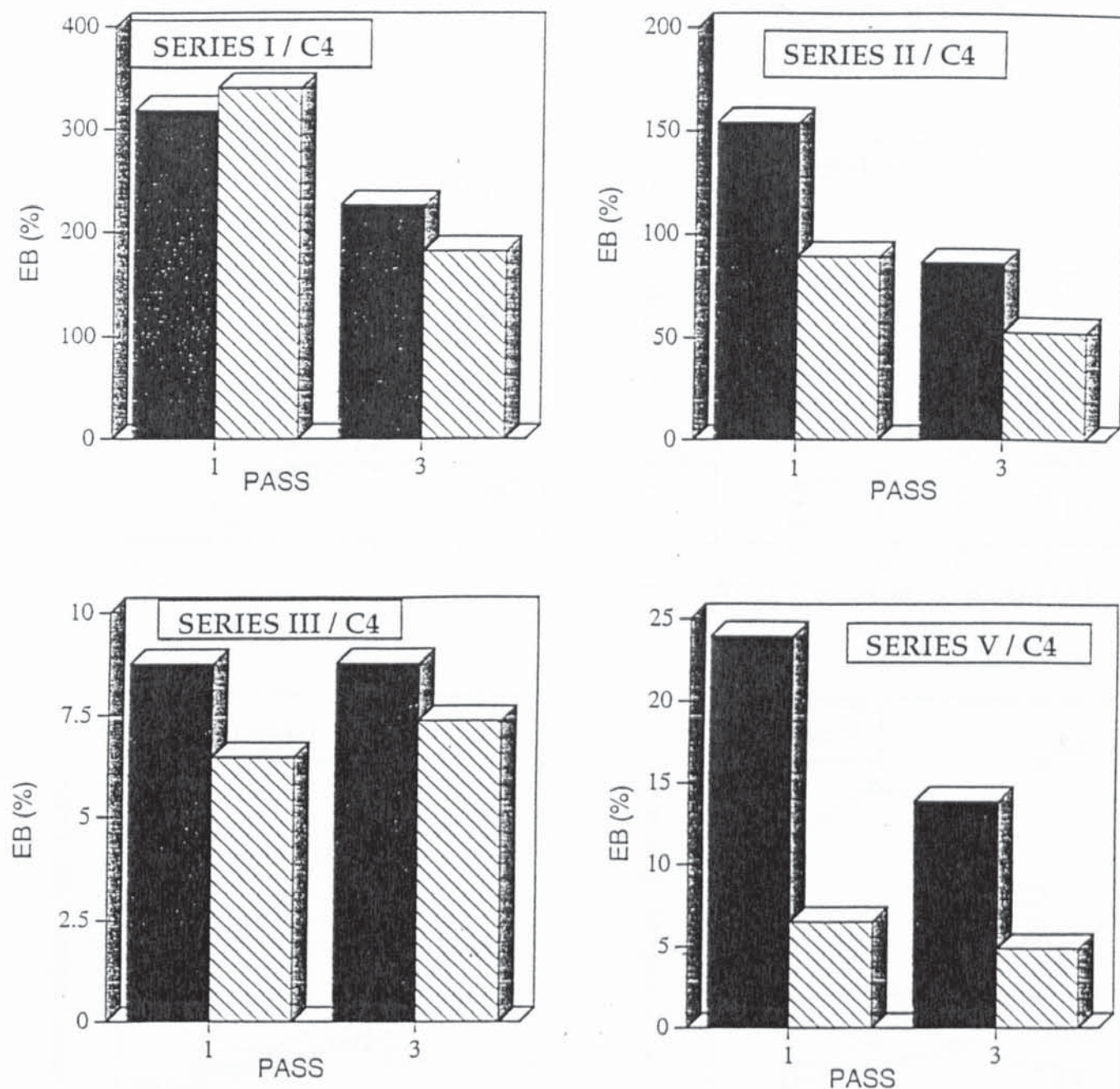


Figure 4.22: Comparison of elongation to break of recycled (internal mixer at 190°C) 10% homogeneous and heterogeneous blends of sample C4 (lined rectangular box) with the corresponding control samples (filled black box). See table 4.3 for definition of series and table 4.4 for identification of the control samples.

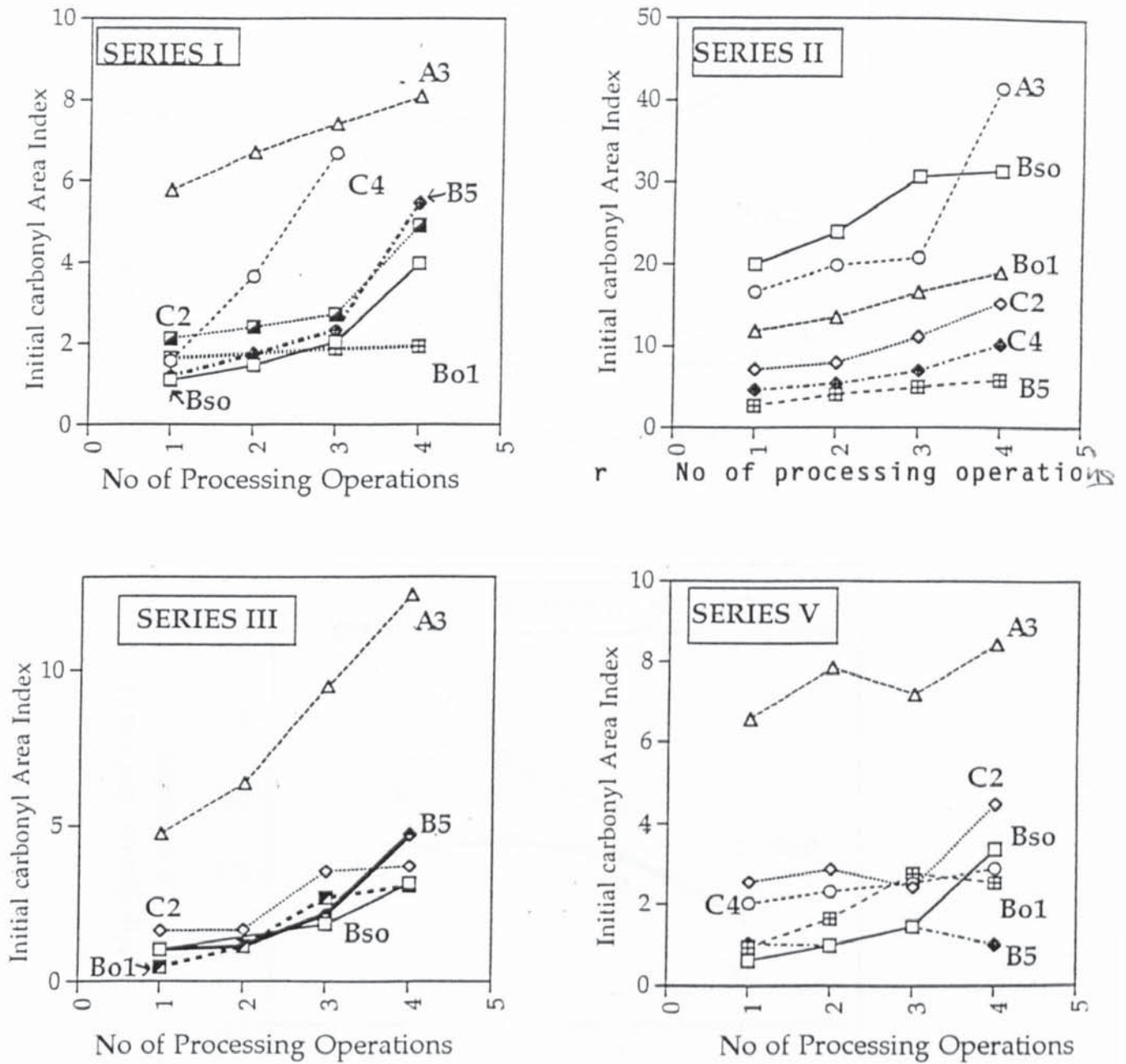
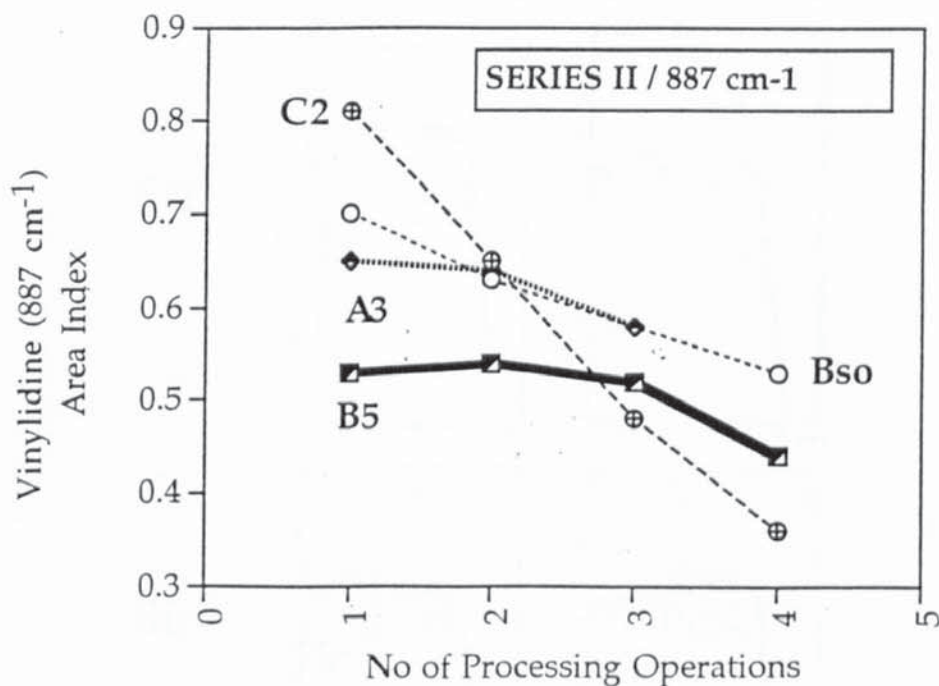
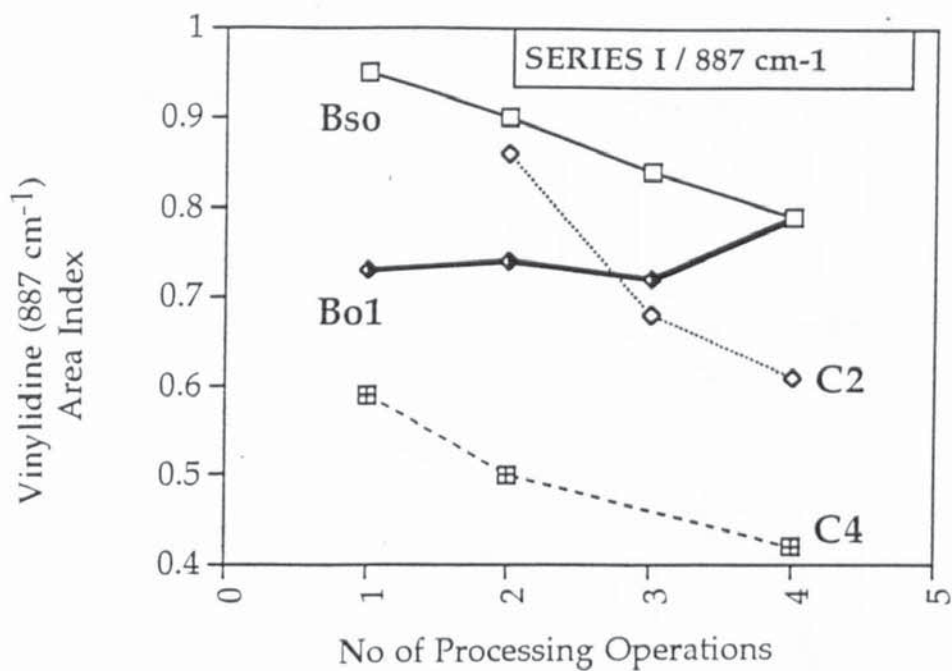


Figure 4.23: Increase in the initial carbonyl content after recycling (pass 1 to pass 4) of 10% homogeneous and heterogenous degradable blends recycled in an internal mixer at 190°C. See table 4.3 for definition of series.



**Figure 4.24:** Decrease in the vinylidene (887 cm<sup>-1</sup> from IR) content (pass 1 to pass 4) of 10% homogeneous and heterogenous degradable blends recycled in an internal mixer at 190°C. See table 4.4 for definition of series.

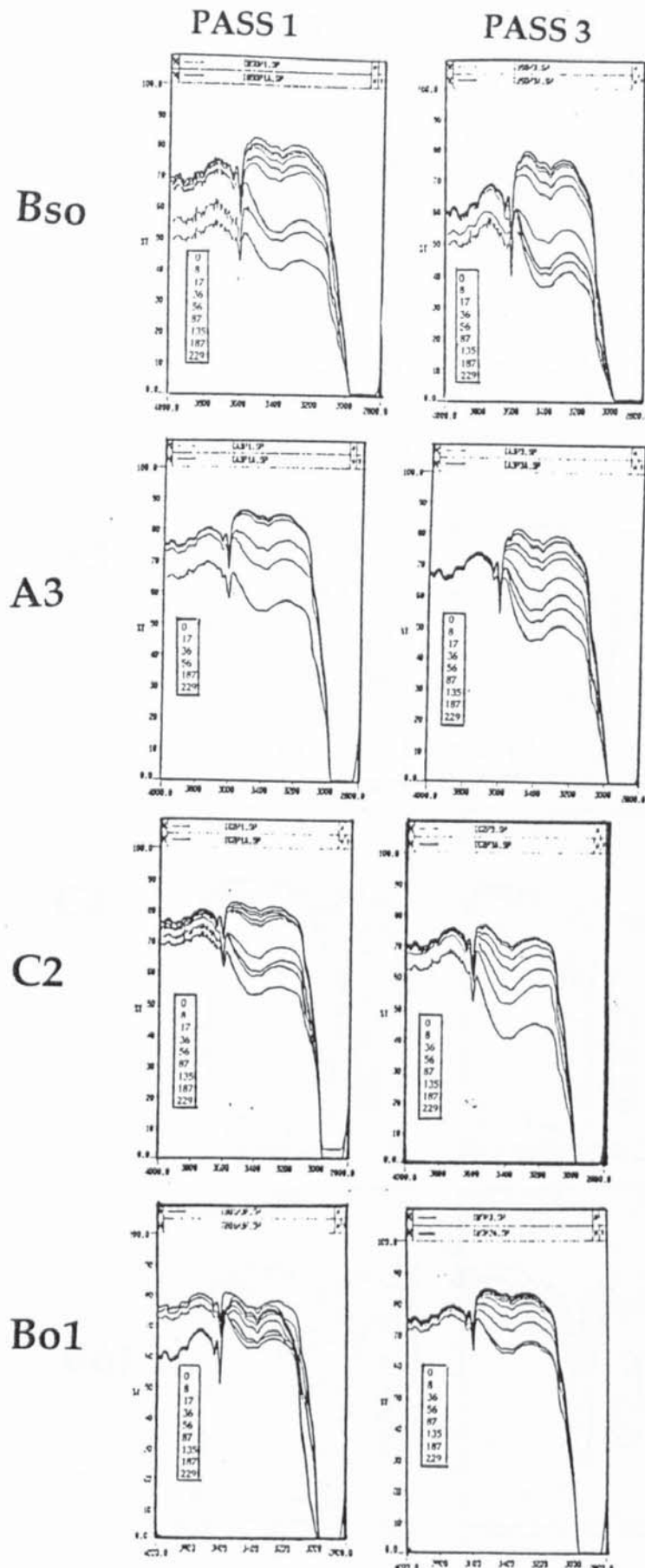


Figure 4.25: Overlay of FT-IR spectral region in the hydroxyl absorption area of recycled degradable samples of series I (10% degradables as received in LDPE) showing the increase in the hydroxyl content during uv irradiation (sepap uv cabinet), see table 4.1 for sample codes. Numbers in box are irradiation time, in hours.

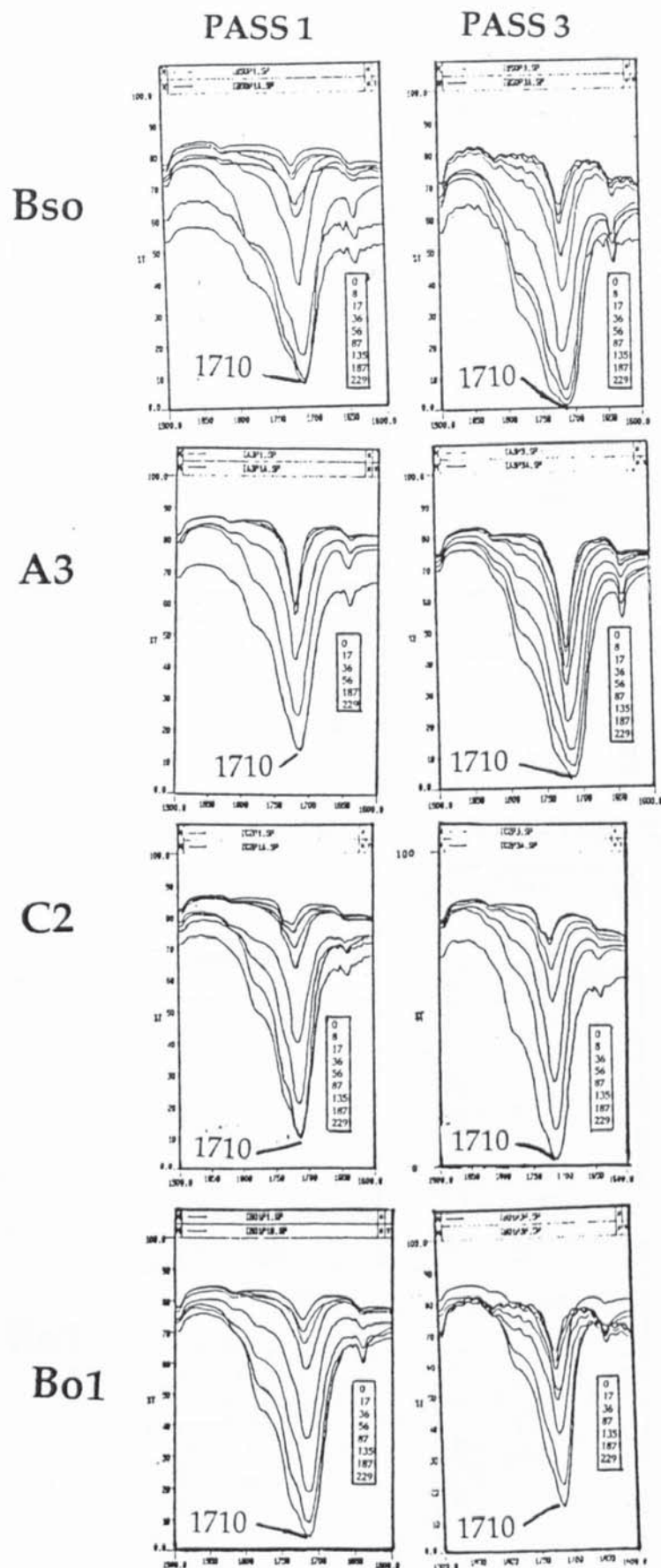


Figure 4.26: Overlay of FT-IR spectral region in the carbonyl absorption area of recycled degradable samples of series I (10% degradables as received in LDPE) showing the increase in the carbonyl content during uv irradiation (sepap uv cabinet), see table 4.1 for sample codes. Numbers in box are irradiation time, in hours.

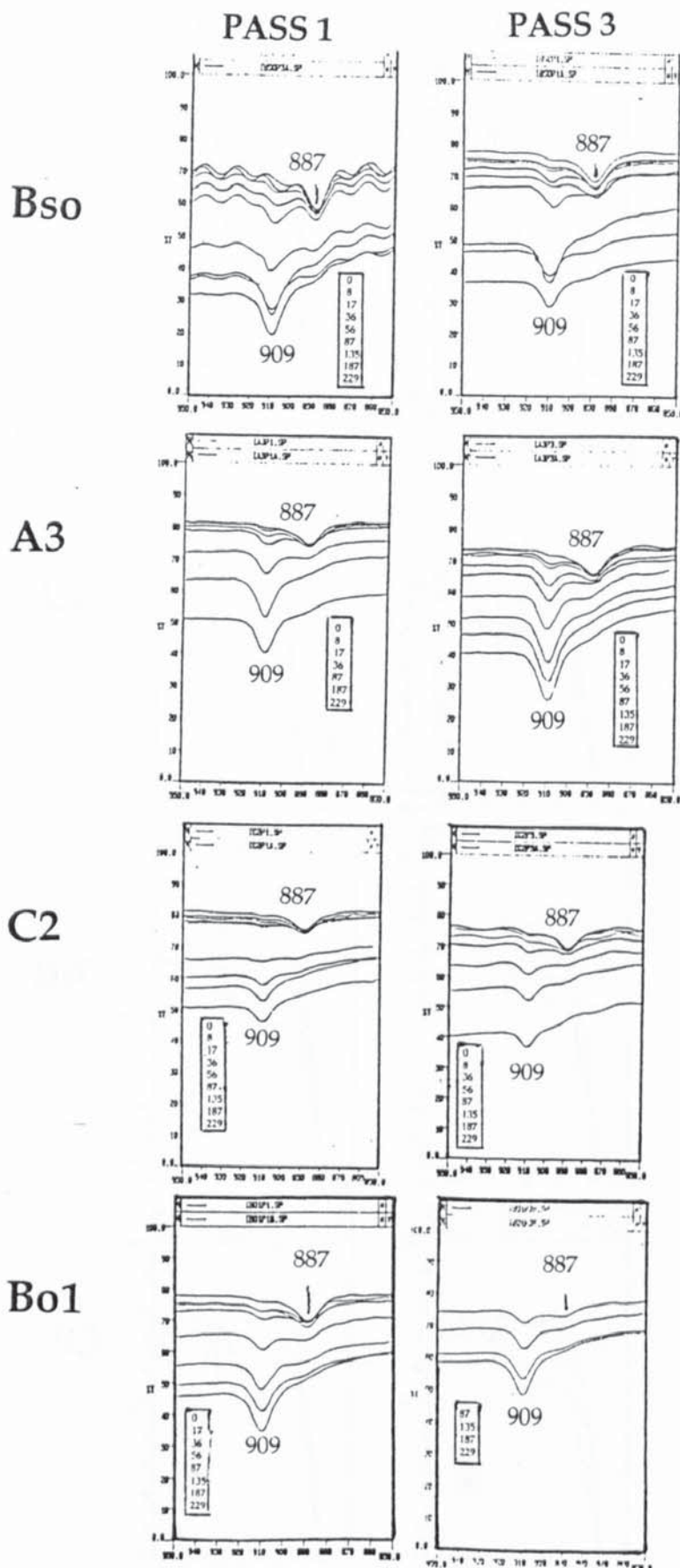


Figure 4.27: Overlay of FT-IR spectral region in the vinyl and vinylidene absorption areas of recycled degradable samples of series I (10% degradables as received in LDPE) showing the decrease in the vinylidene (887 cm<sup>-1</sup>) and increase in the vinyl (909 cm<sup>-1</sup>) contents during uv irradiation (sepap uv cabinet), see table 4.1 for sample codes. Numbers in box are irradiation time, in hours.

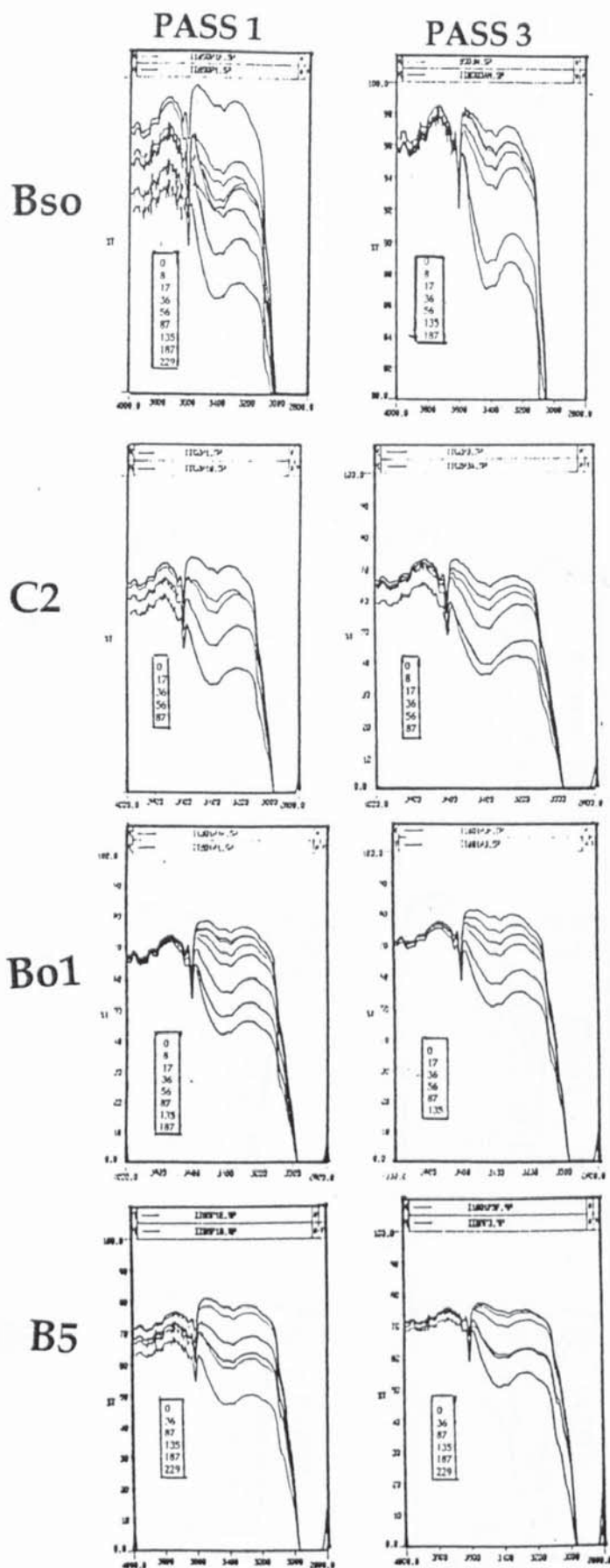


Figure 4.28: Overlay of FT-IR spectral region in the hydroxyl absorption area of recycled degradable samples of series II (10% pre-oxidised degradables in LDPE) showing the increase in the hydroxyl content during uv irradiation (sepap uv cabinet), see table 4.1 for sample codes. Numbers in box are irradiation time, in hours.

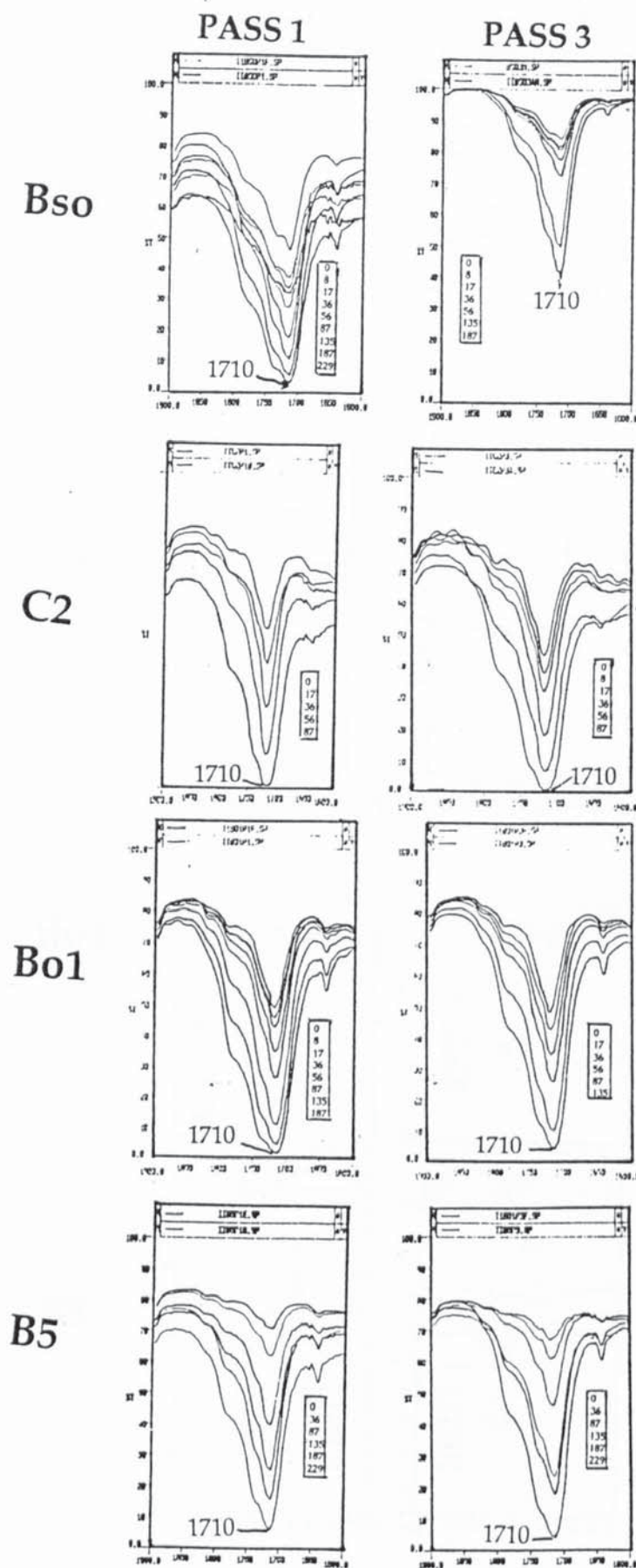


Figure 4.29: Overlay of FT-IR spectral region in the carbonyl absorption area of recycled degradable samples of series II (10% pre-oxidised degradable in LDPE) showing the increase in the carbonyl content during uv irradiation (sepap uv cabinet), see table 4.1 for sample codes. Numbers in box are irradiation time, in hours.

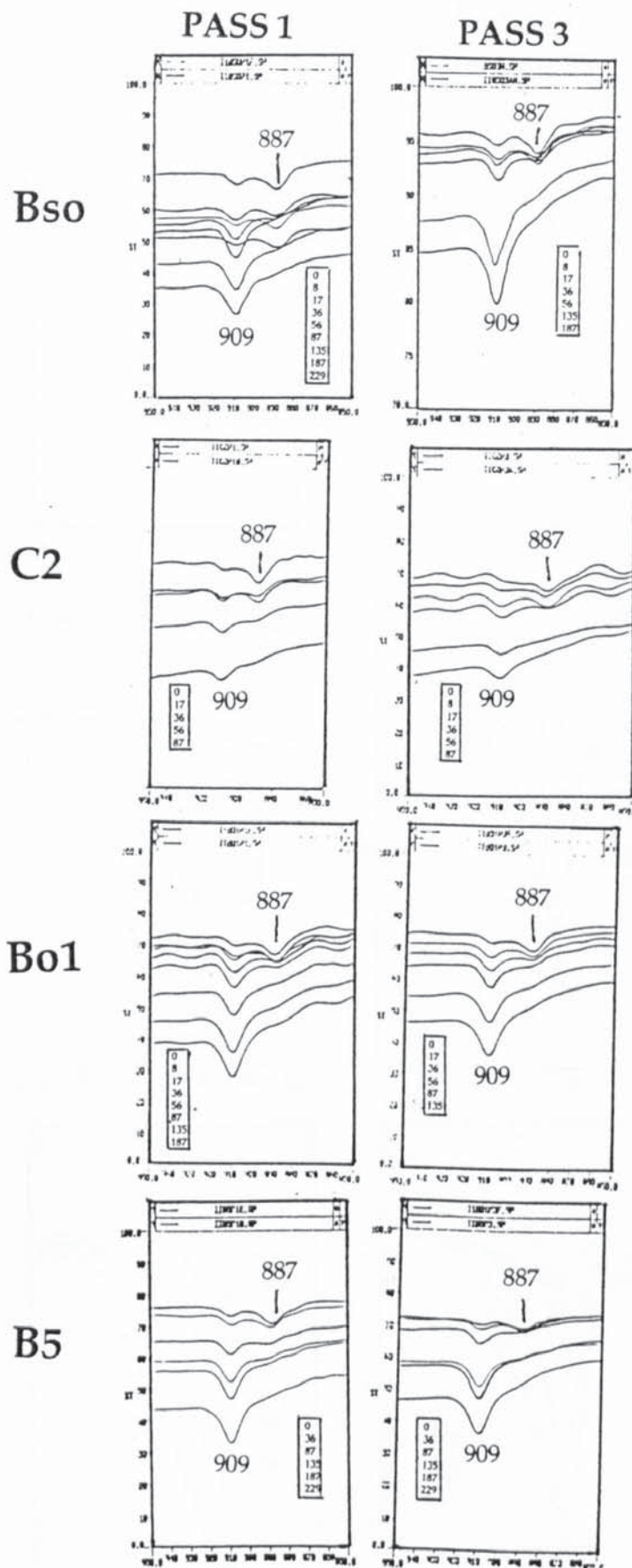
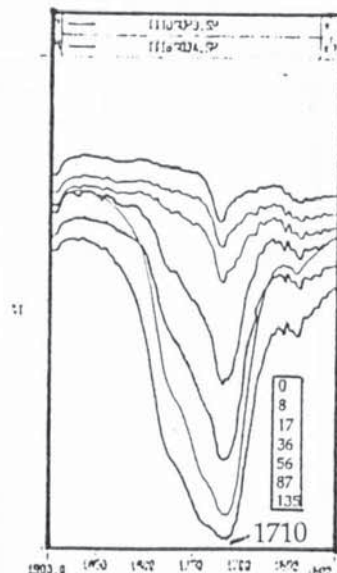
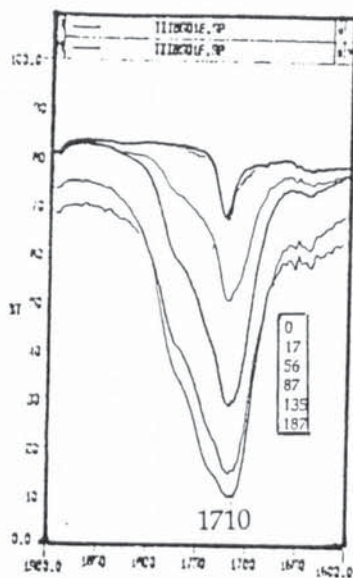
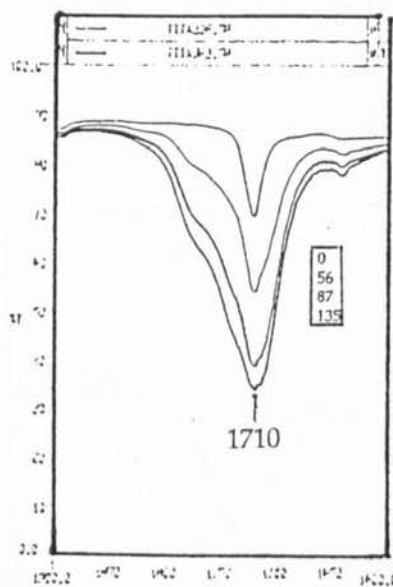
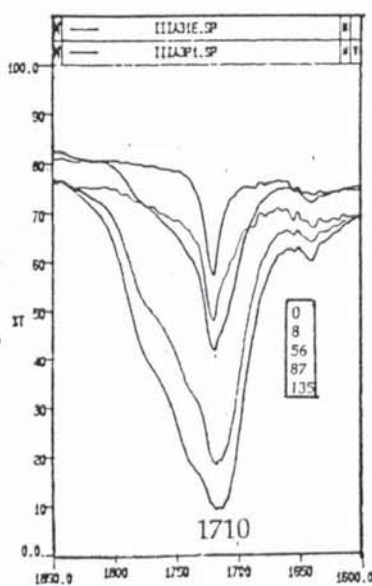


Figure 4.30: Overlay of FT-IR spectral region in the vinyl and vinylidene absorption areas of recycled degradable samples of series II (10% pre-oxidised degradables in LDPE) showing the decrease in the vinylidene ( $887\text{ cm}^{-1}$ ) and increase in the vinyl ( $909\text{ cm}^{-1}$ ) contents during uv irradiation (sepap uv cabinet), see table 4.1 for sample codes. Numbers in box are irradiation time, in hours.

Bso



A3



Bo1

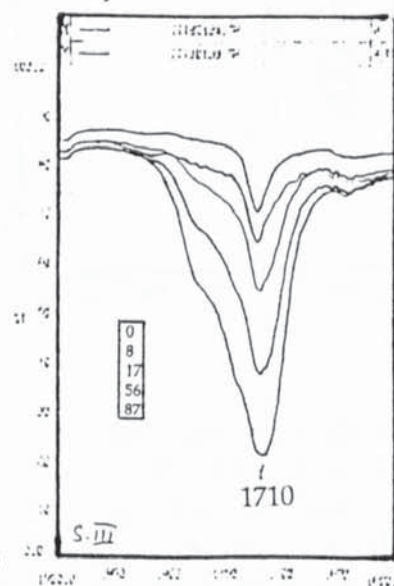
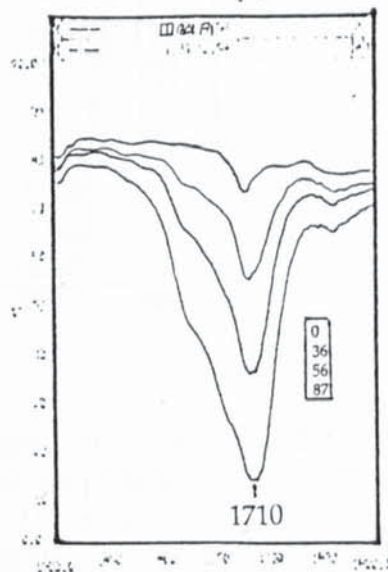


Figure 4.31: Overlay of FT-IR spectral region in the carbonyl absorption area of recycled degradable samples of series III (10% degradables as received in 1: ratio of LDPE:PP) showing the increase in the carbonyl content during uv irradiation (sepap uv cabinet), see table 4.1 for sample codes. Numbers in box are irradiation time, in hours.

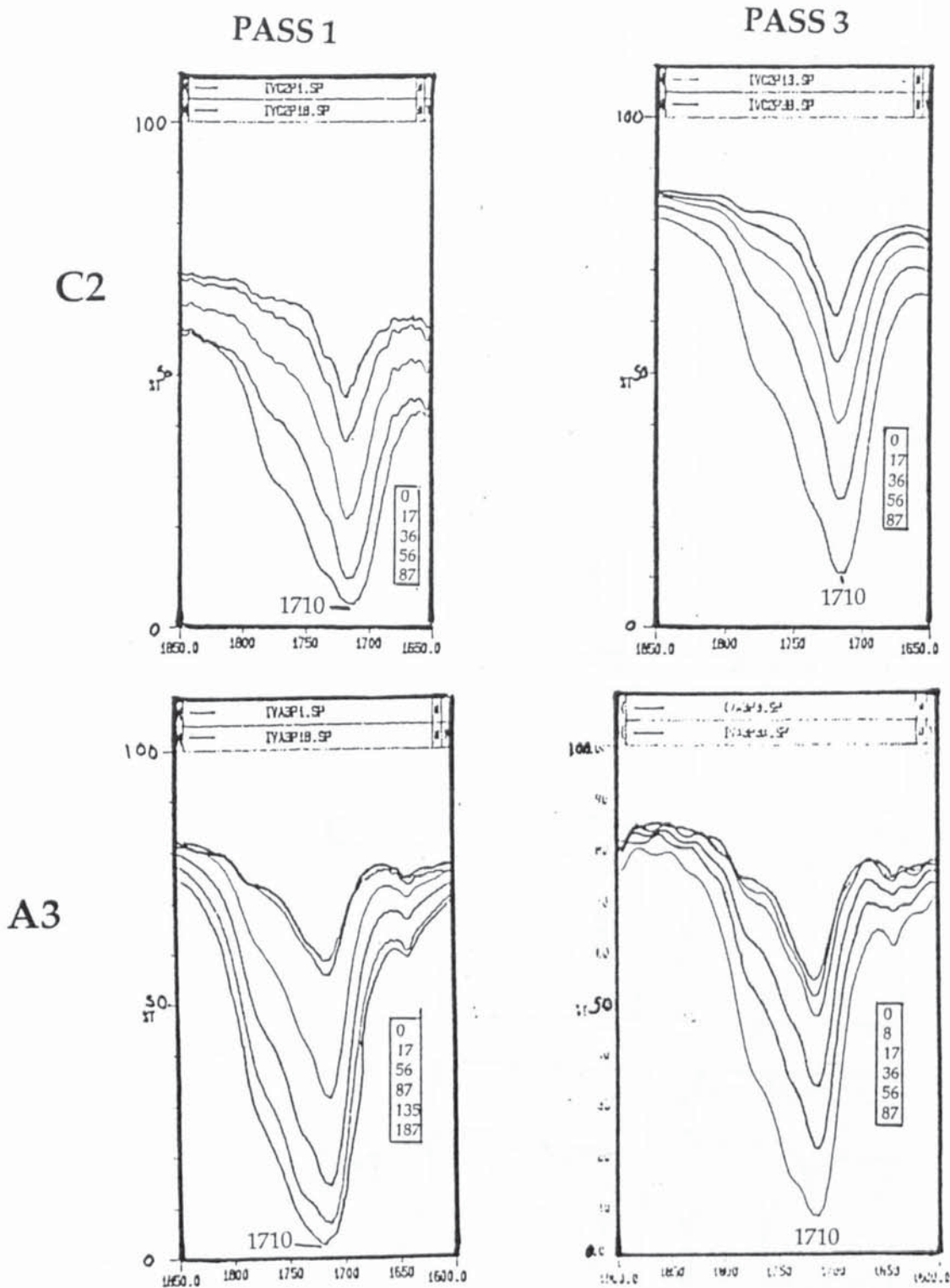
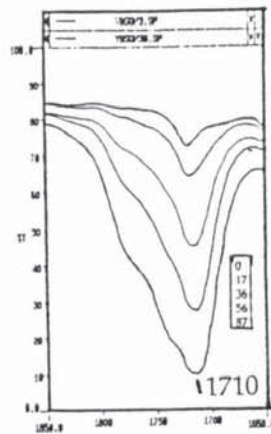
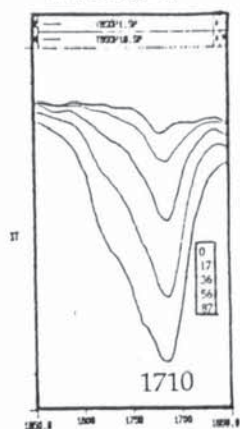
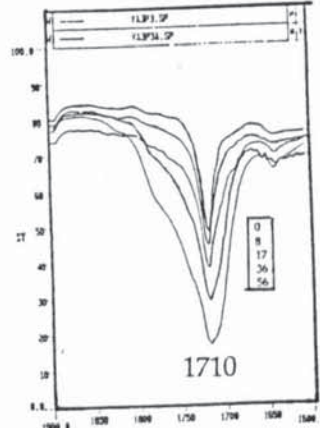
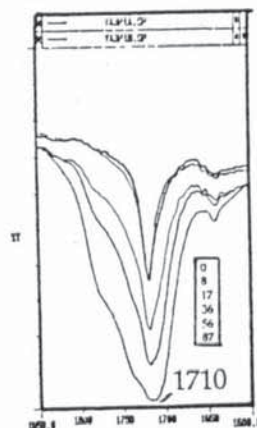


Figure 4.32: Overlay of FT-IR spectral region in the carbonyl absorption area of recycled degradable samples of series IV (10% pre-oxidised degradables in 1;1 ratio of LDPE:PP) showing the increase in the carbonyl content during uv irradiation (sepap uv cabinet), see table 4.1 for sample codes. Numbers in box are irradiation time, in hours.

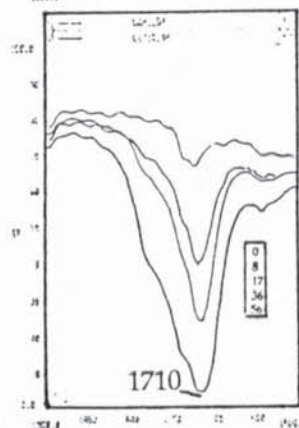
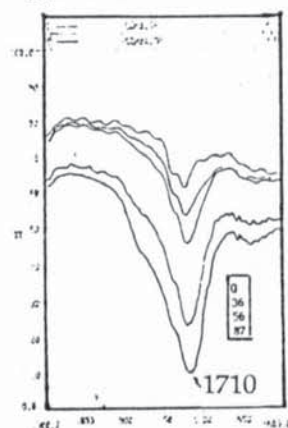
Bso



A3



C2



Bo1

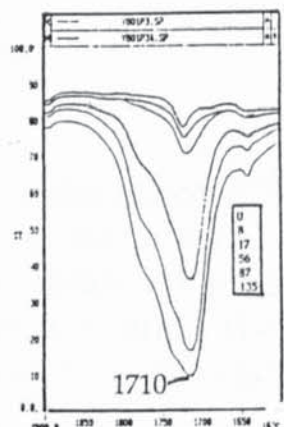
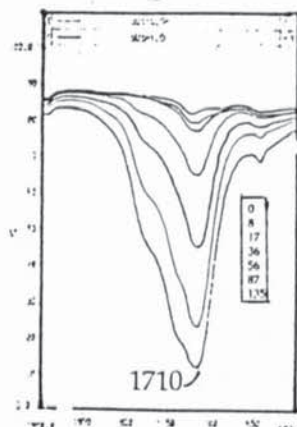


Figure 4.33: Overlay of FT-IR spectral region in the carbonyl absorption area of recycled degradable samples of series V (10% degradables as received in 4:4:1 ratio of LDPE:PP:EPDM) showing the increase in the carbonyl content during uv irradiation (sepap uv cabinet), see table 4.1 for sample codes. Numbers in box are irradiation time, in hours.

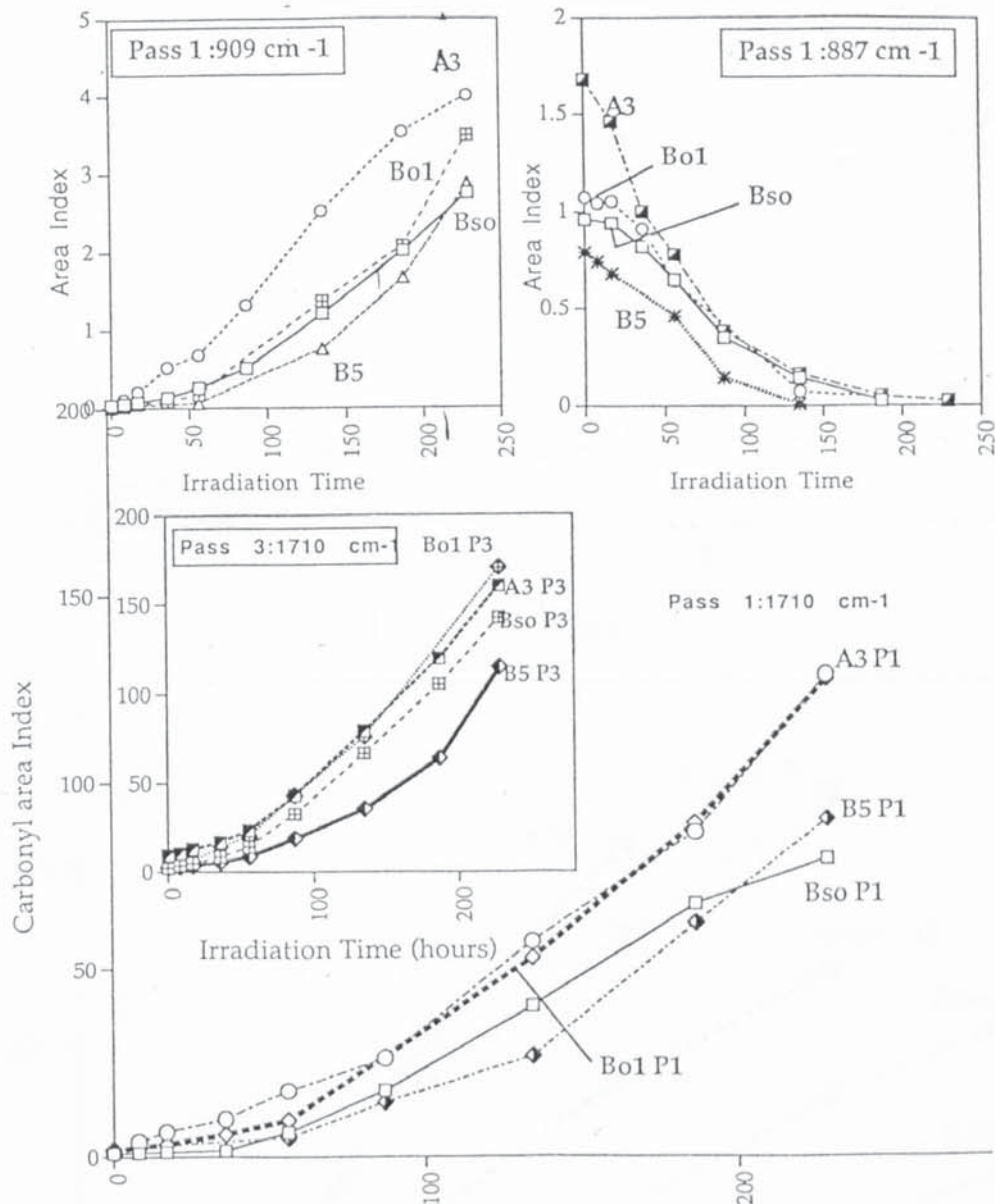


Figure 4.34: Photooxidation rates (sepap uv cabinet) of 10% homogeneous degradables as received in LDPE recycled in an internal mixer at 190°C. Main graph is the increase in carbonyl area index for pass 1, inset middle is the carbonyl area index for pass 3, inset top left is the increase in the vinyl content, inset top right is the decrease in the vinylidene content. See table 4.1 for sample codes.

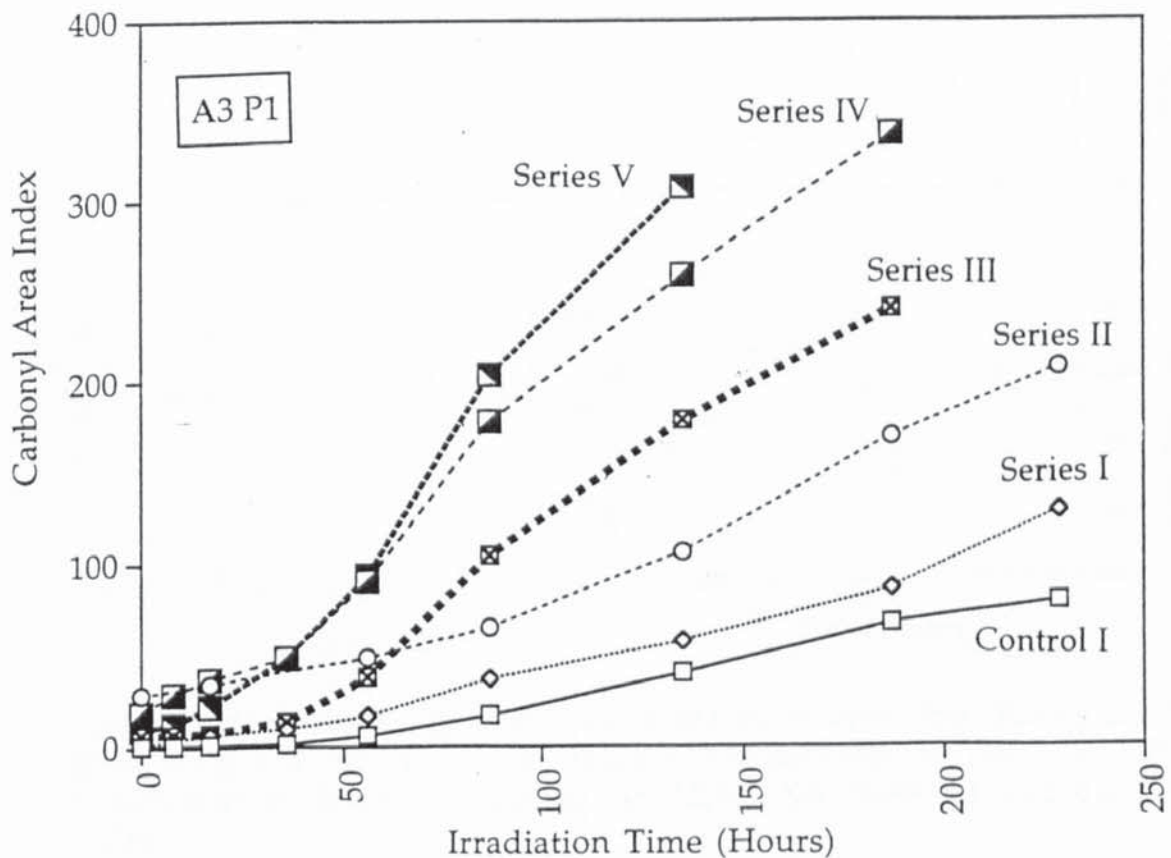
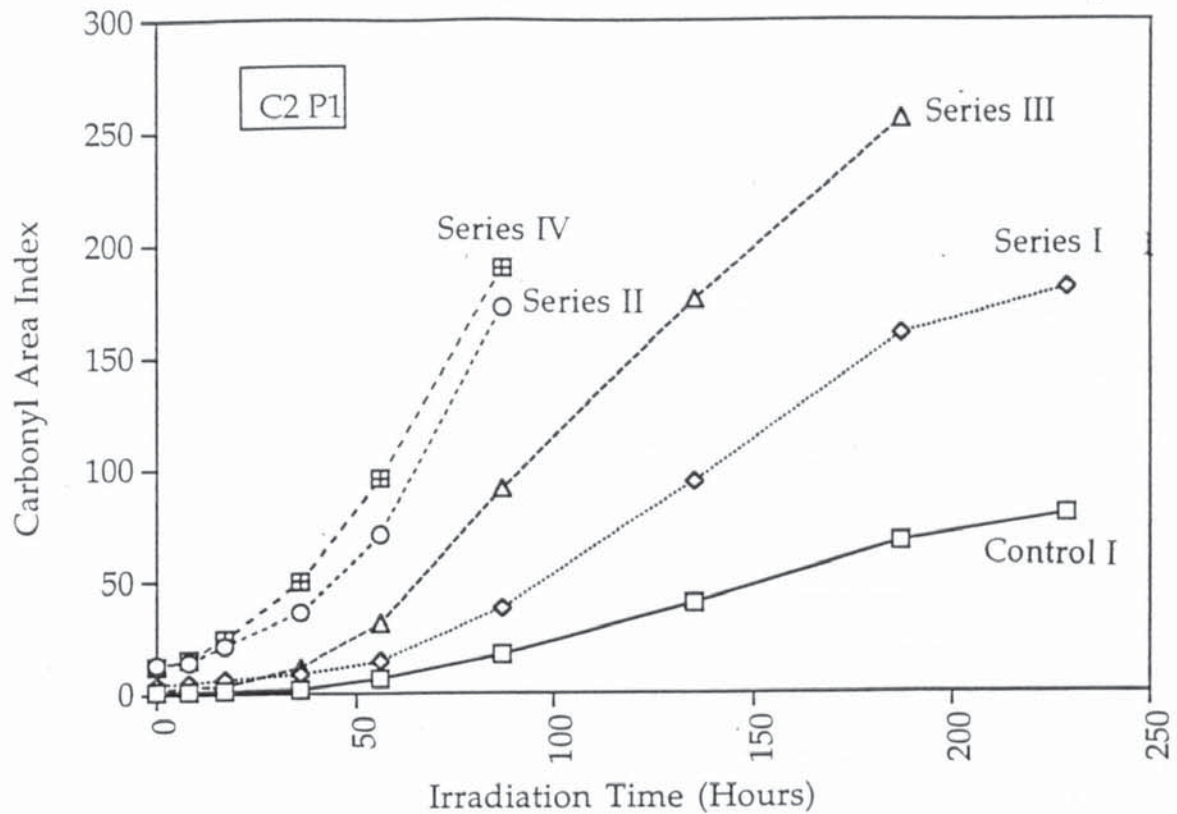


Figure 4.35: Comparison of the rates of photooxidation (sepap uv cabinet) of the different homogeneous and heterogeneous 10% degradable recycled blends after pass 1 (Series I-V, see table 4.3) for samples C2 and A3 (Pass 1) recycled in an internal mixer at 190°C. See table 4.1 for sample codes.

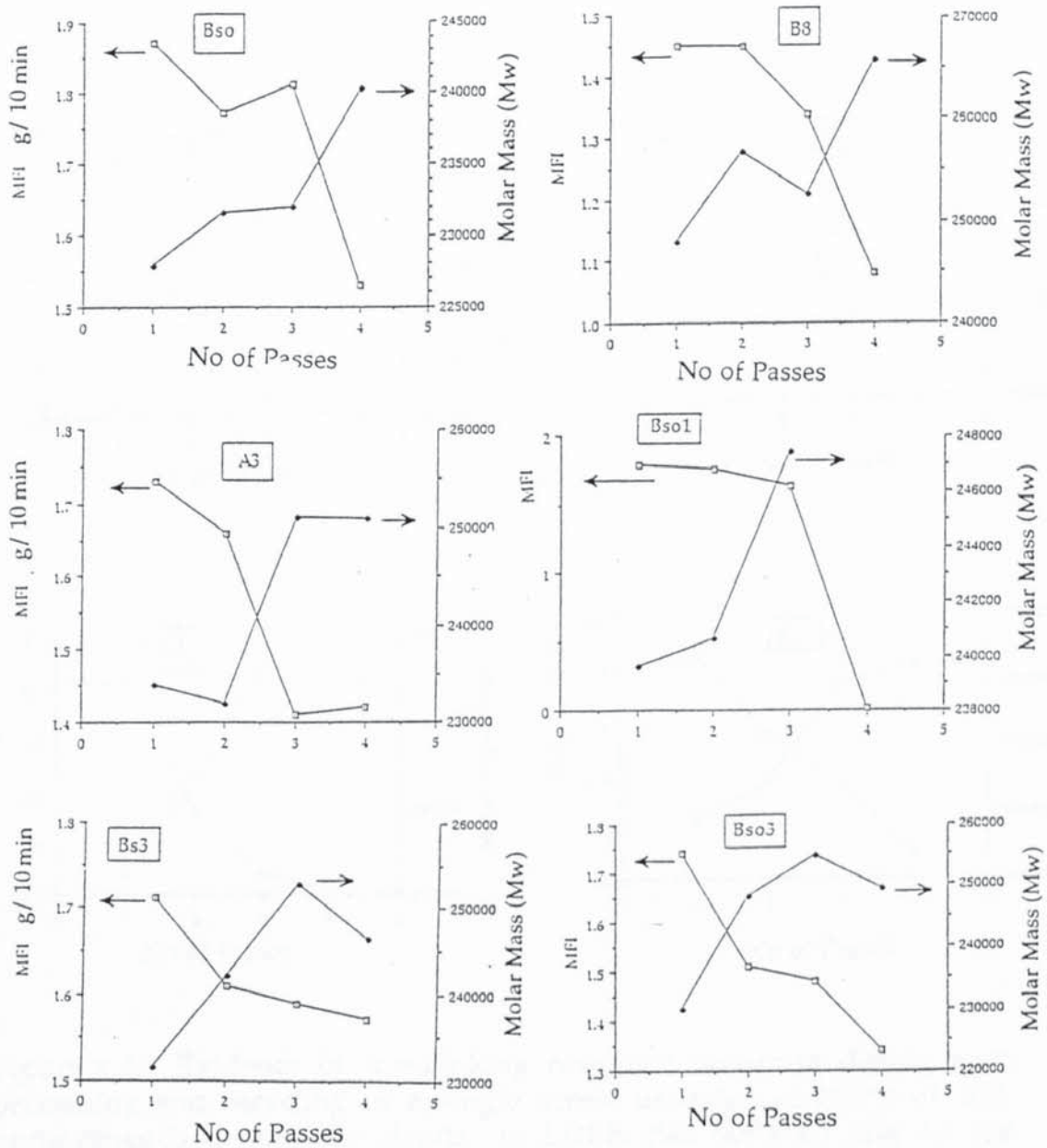


Figure 4.36: Evidence of crosslinking reactions occurring during melt processing and recycling in a single screw extruder at 180°C of 10% homogeneous degradable blends in LDPE. See table 4.1 and 4.2 for codes.

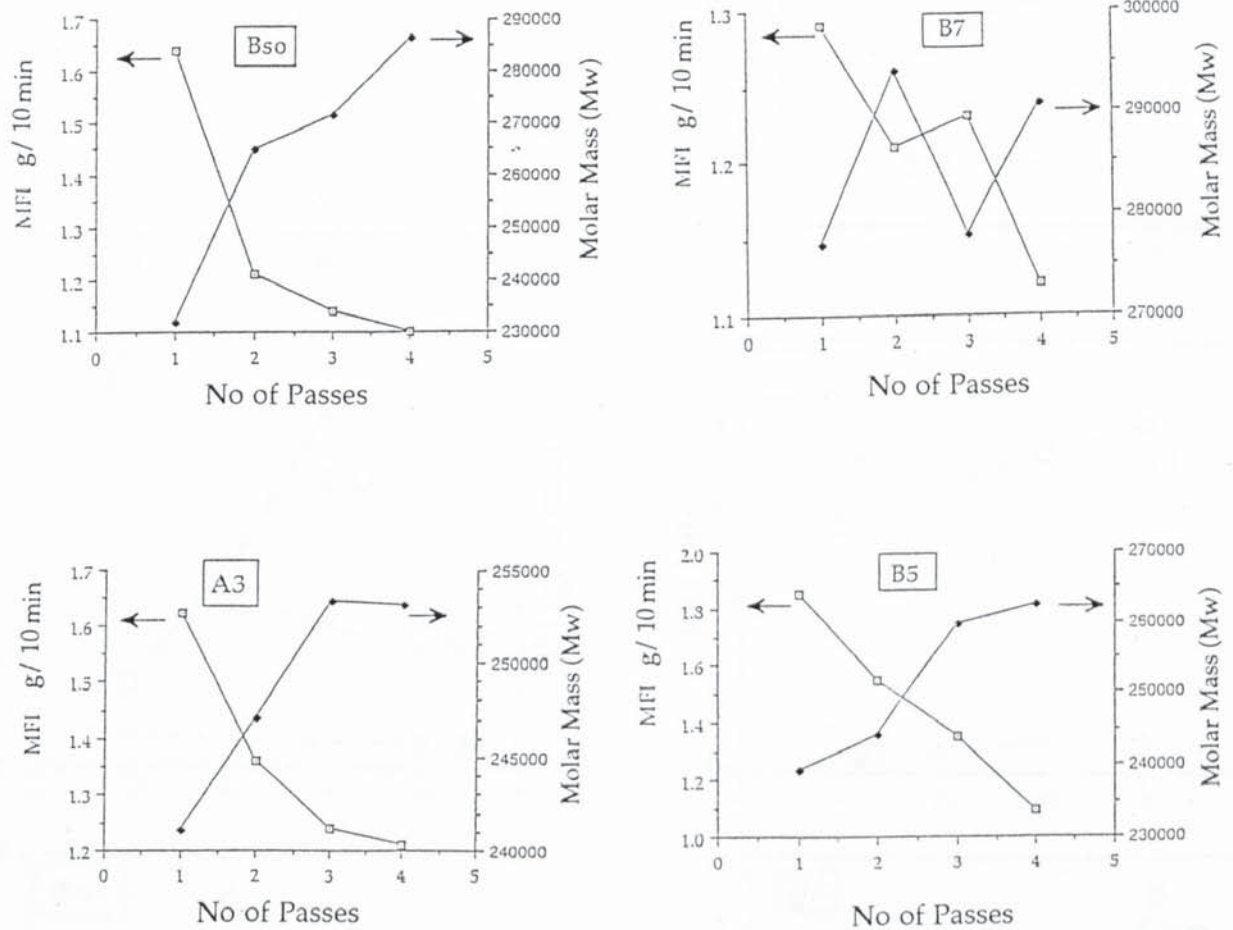


Figure 4.37: Evidence of crosslinking reactions occurring during melt processing and recycling in a single screw extruder at 210°C of 10% homogeneous degradable blends in LDPE. See table 4.1 and 4.2 for codes.

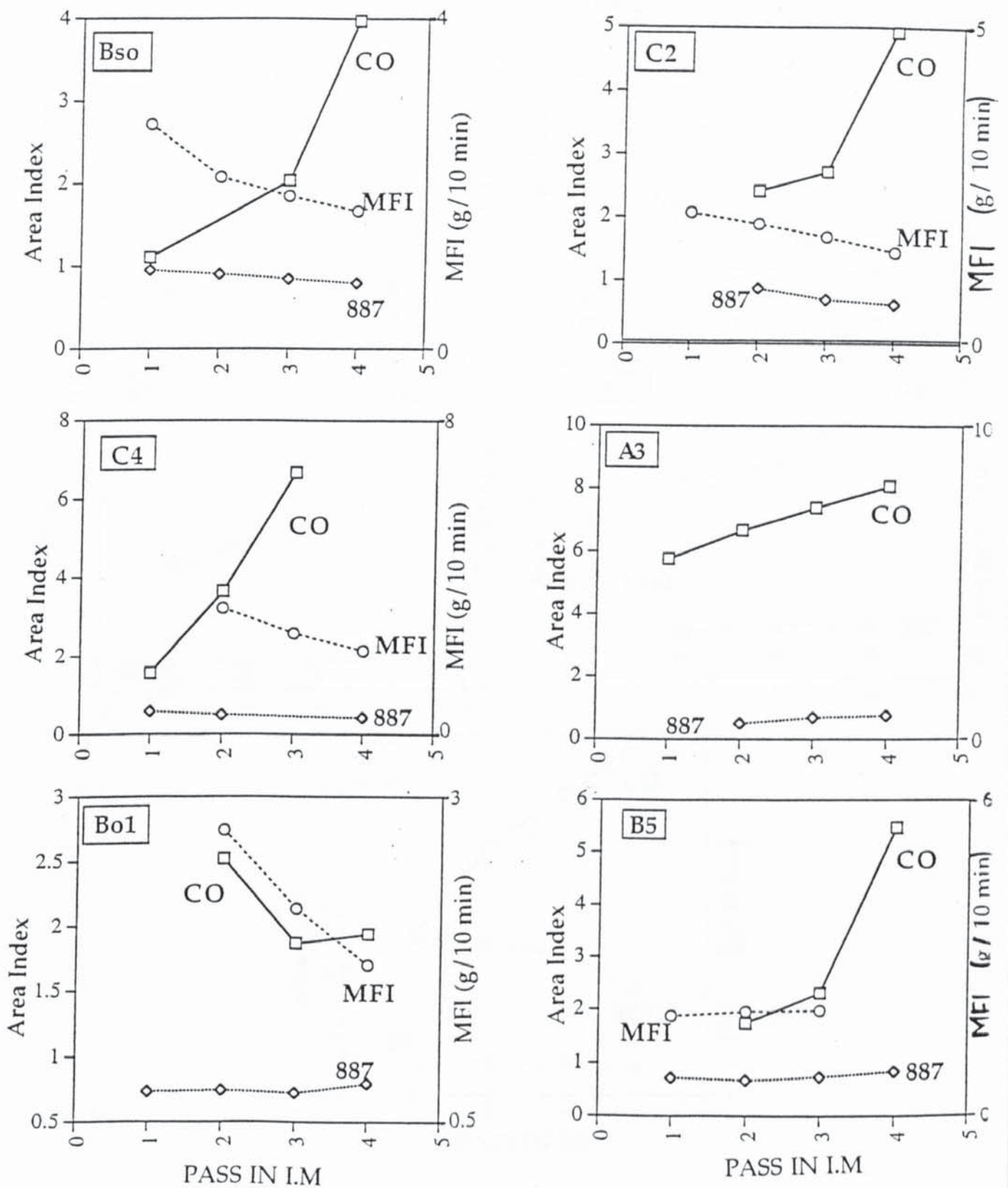


Figure 4.38: Changes in oxidation products for Series I (10% degradable as received in LDPE) during recycling in an internal mixer. See table 4.1 for sample codes. CO = carbonyl area index, 887 = vinyl area index, MFI (g/10 min) = change in melt flow index.

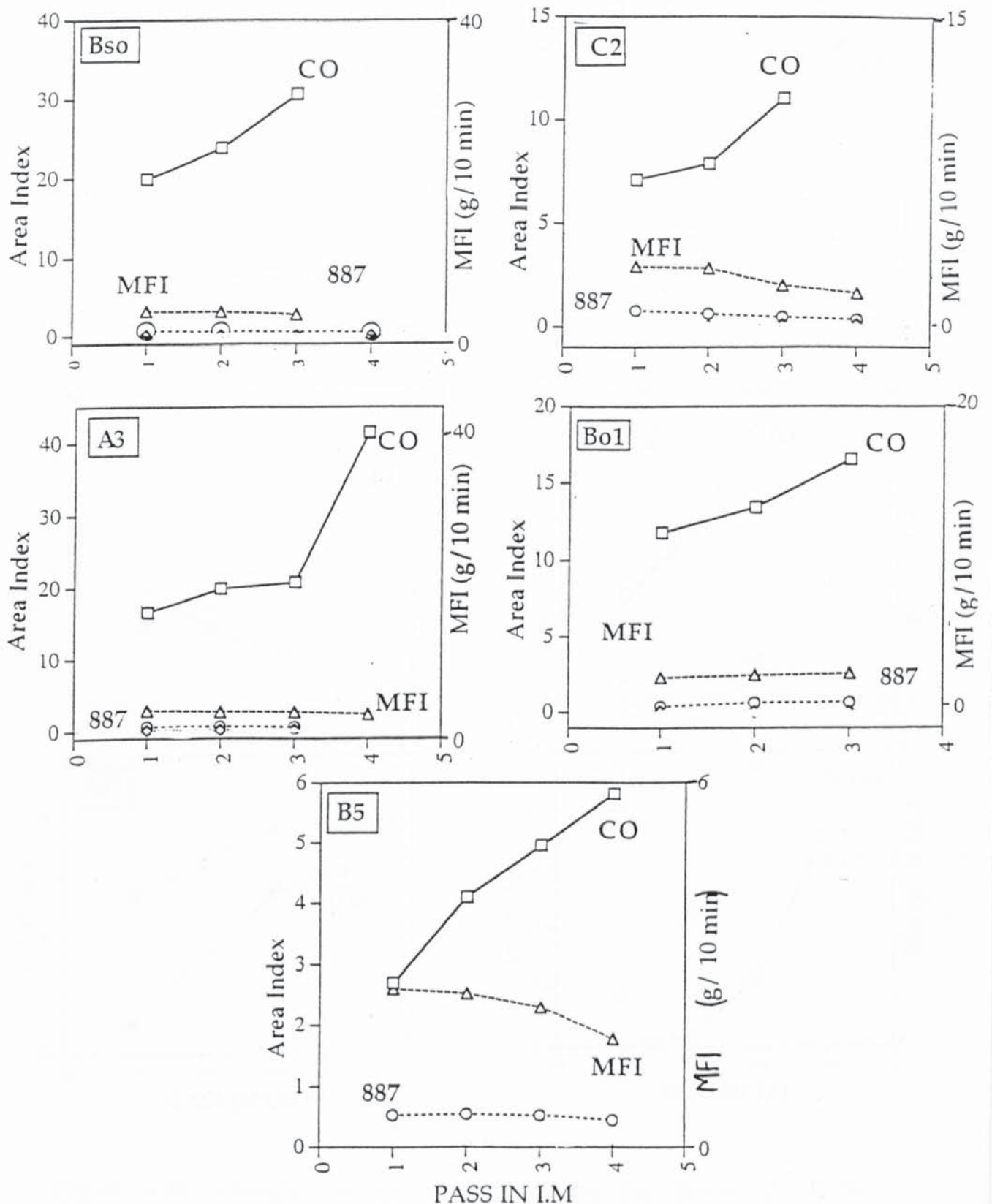


Figure 4.39: Changes in oxidation products for Series II (10% pre-oxidised degradables in LDPE) during recycling in an internal mixer. See table 4.1 for sample codes. CO = carbonyl area index, 887 = vinyl area index, MFI (g/10 min) = change in melt flow index.

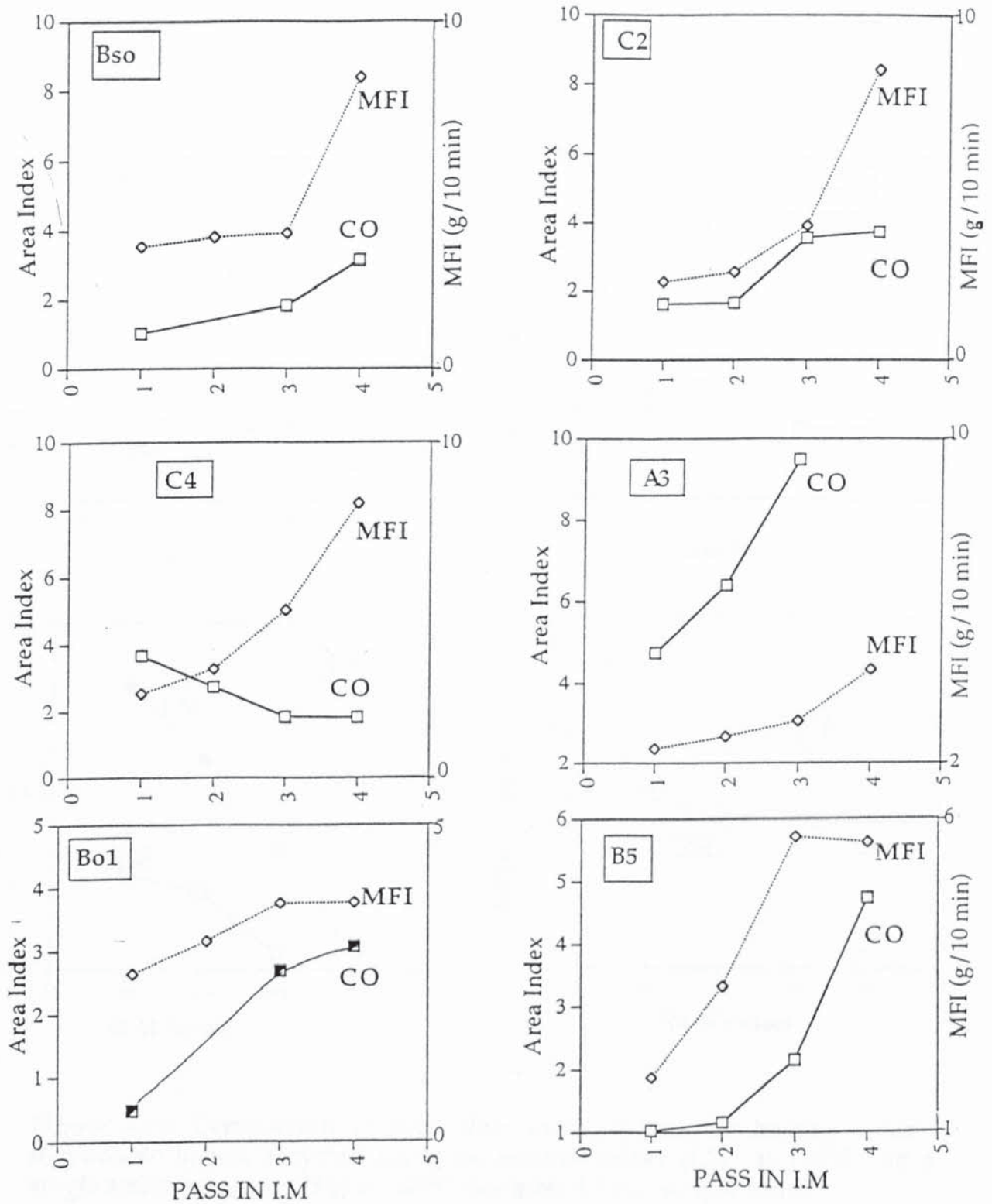


Figure 4.40: Changes in oxidation products for Series III (10% degradable) as received in 1:1 ratio of LDPE:PP during recycling in an internal mixer. See table 4.1 for sample codes. CO = carbonyl area index, 887 = vinyl area index.

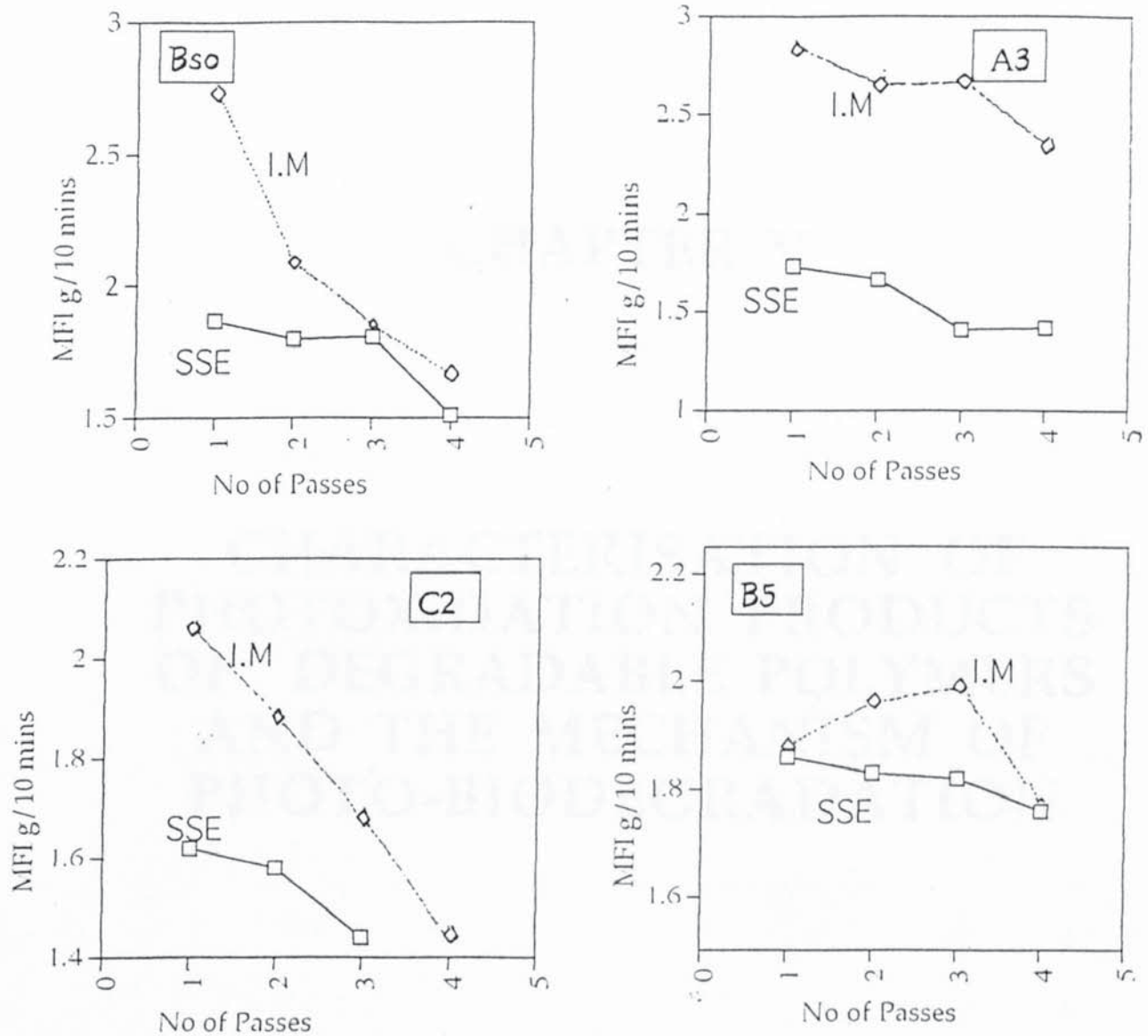


Figure 4.41: Comparison of melt flow index values for homogeneous degradable blends recycled using an internal mixer (I.M.) at 190°C and a single screw extruder (SSE) at 180°C. See table 4.1 for sample codes

## CHAPTER V

# CHARACTERISATION OF PHOTOXIDATION PRODUCTS OF DEGRADABLE POLYMERS AND THE MECHANISM OF PHOTO-BIODEGRADATION

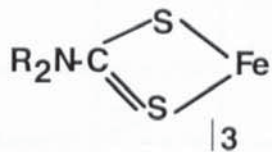
## CHAPTER V

**CHARACTERISATION OF PHOTOOXIDATION PRODUCTS OF  
DEGRADABLE POLYMERS AND THE MECHANISM OF PHOTO-  
BIODEGRADATION**

## 5.1 OBJECTIVES AND METHODOLOGY

The identification of the photooxidation products is paramount to understanding the exact mechanism of photooxidation. Hence, this part of the research focused on the identification and characterisation of the photooxidised products of degradable polymers. The degradable systems examined and presented in this chapter are shown in table 5.1.

Table 5.1: Photobiodegradable polymer film samples.

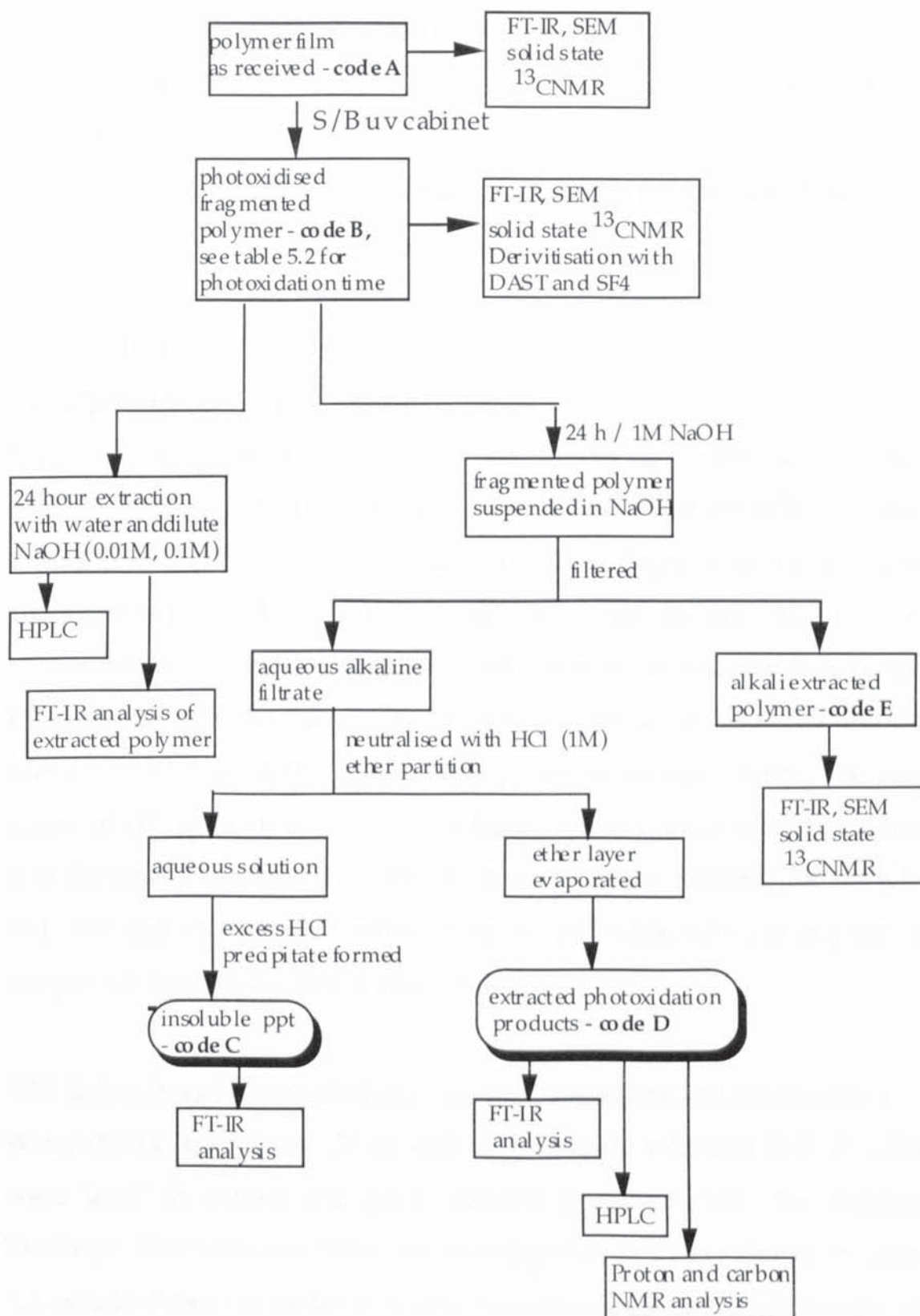
Type	Composition	Origin	Film Thickness as received (m)	Group	Code
Photolytic Copolymer	Ethylene-CO Copolymer/LDPE	ITW Hi-Cone PE	151	<b>A</b>	A3
Metal complex Photo Activators	FeDRC/LDPE 	PLASTOPIL	35	<b>B</b>	Bo1
Starch Filled PE	Starch + Fe stearate (C <sub>17</sub> H <sub>35</sub> COO) <sub>3</sub> Fe + TiO <sub>2</sub> /LDPE	AMPACET	41	<b>C</b>	C2
control	Unstabilised LDPE	processed in lab	75	-	Bso

Degradable polymer samples were photoxidised in the S/B UV cabinet well beyond their embrittlement time. This was made possible by transferring the brittle fragmented polymer into quartz test-tubes. The heavily photoxidised polymer pieces were extracted with warm water (30°C) and various concentrations of sodium hydroxide (0.01M, 0.1M, 1M) to leach out the photoxidation products (see chapter 2 for full experimental details). Table 5.2 displays the duration of exposure time (in S/B UV cabinet) for the degradable samples. The water extracts were analysed directly by HPLC; however, the sodium alkali extracts were first neutralised and then partitioned using ether which was distilled just before use. The ether was then evaporated and the extracted products collected. The major limitation encountered with this part of the work was the very small quantities of product extracted. Analytical techniques such as FT-IR, HPLC and proton and carbon NMR were utilised to elucidate the structure of the extracted photoxidation products, see scheme 5.1.

Table 5.2: Time of exposure (in 'old' S/B UV cabinet) of photobiodegradable polymer film samples.

Type	Code	Film Thickness as received ( $\mu\text{m}$ )	Exposure Time/ months
control	Bso	75	11
Photolytic Copolymer	A3	151	8
Metal complex Photo Activator	Bo1	35	8
Starch Filled PE	C2	41	5

Scheme 5.1: Flow chart of the methodology adopted for analysis of degradable samples.



The photoxidised polymer itself was examined after treatment with the various extracting media by analytical techniques such as FT-IR, solid state  $^{13}\text{C}$ -NMR and scanning electron microscopy (SEM). Derivatisation of the photoxidised polymer, using diethylaminosulphur trifluoride (DAST) and sulphur tetrafluoride ( $\text{SF}_4$ ), was also undertaken to help unravel the nature of photoxidation products still bound to the polymer backbone.

## 5.2 RESULTS

### 5.2.1 Photoxidation of Degradable Polymers

Figure 5.1 shows the FT-IR spectra of unstabilised LDPE (Bso), ECO sample (A3), metal carboxylate sample (Bo1) and starch-filled PE (C2), obtained during photoxidation in S/B UV cabinet. All the degradable systems show an increase in the hydroxyl, carbonyl and vinyl regions. The rates of photoxidation of these samples has been described in chapter 3. A typical FT-IR spectrum in the carbonyl region for samples A3 and Bo1 (C2 and Bso showed the same FT-IR in the carbonyl region as Bo1) during the later stages of UV irradiation is shown in figure 5.2. It is clear from this figure that the final photoxidation products formed in the polymer for samples Bo1 (Bso and C2) are predominately carboxylic acids, whereas in polymer sample A3 ketones are predominantly formed.

### 5.2.2 Extraction of Photoxidation Products using Water and dilute Alkali

Water (HPLC grade) and dilute sodium hydroxide solutions (0.01M, 0.1M) were used to extract the photoxidation products from the polymer backbone. The results of the water extraction (at 30°C) are shown in figure 5.3, which shows the carbonyl region of unstabilised LDPE polymer before and after water treatments. No visual differences are observed in the carbonyl region, indicating that the carbonyl based photoxidation products

are unaffected by water treatment. HPLC analysis of the water extract did not show any chromatographic peaks. Extraction using dilute alkali solutions (0.01M and 0.1M) was also attempted. Even under these conditions the extraction of the oxidation products was not successful, see figure 5.4. The photoxidised polymers swelled in both water and dilute alkali solutions, although extraction of the degradation products was not possible.

### 5.2.3 Extraction of Photoxidation Products using 1M Sodium hydroxide

The concentration of the alkali solution was increased from 0.1 molar to 1 molar and the extraction of the photoxidation products was attempted. Increasing the concentration of the alkali solution did lead to some successful extraction of the degradation products.

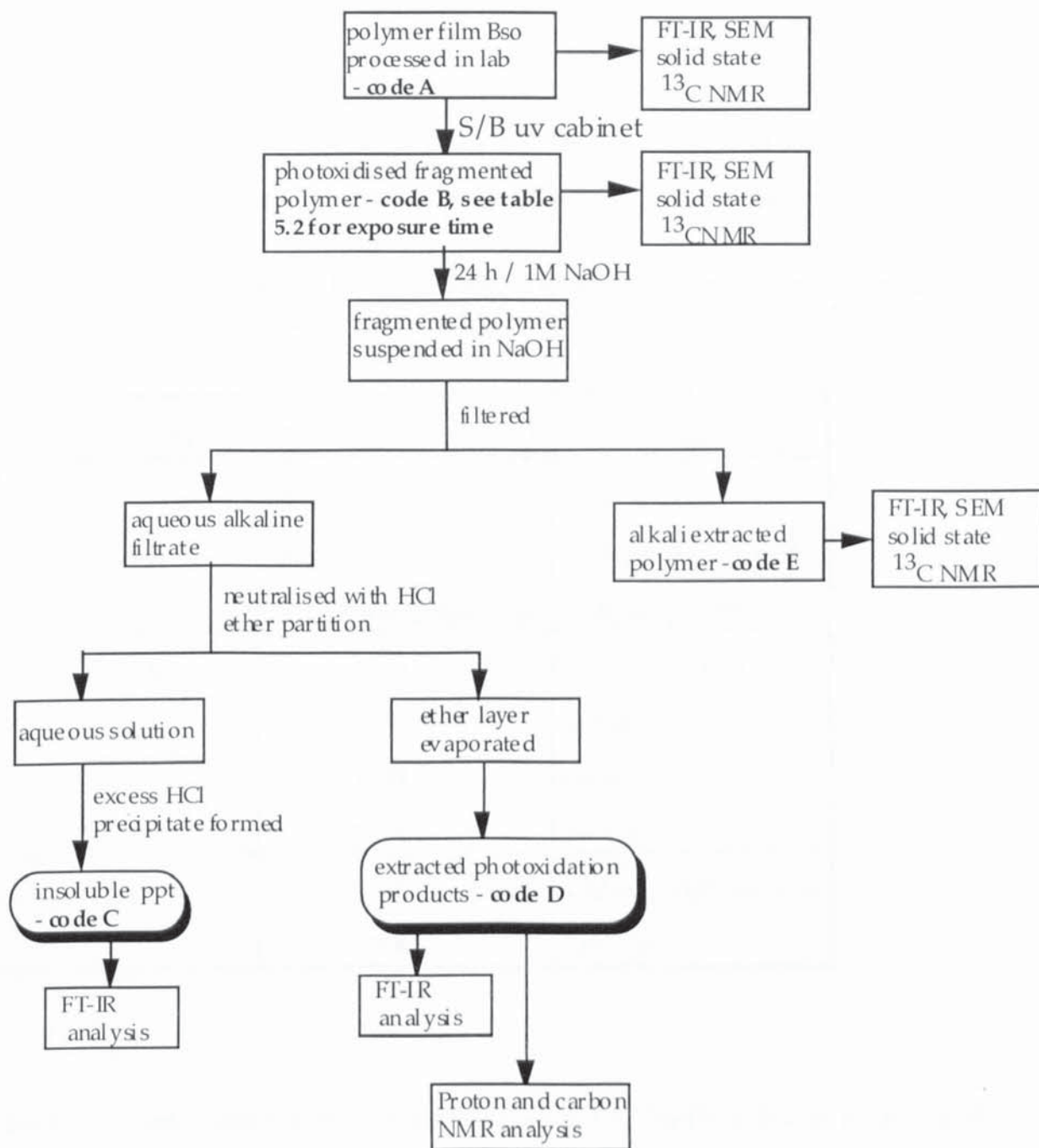
#### 5.2.3.1 Treatment of Photoxidised unstabilised LDPE with 1M Sodium Hydroxide solution.

Scheme 5.2 shows the overall procedure involved during the analysis of this sample. Unstabilised LDPE was photoxidised for eleven months in the S/B UV cabinet.

12.5 grams of the extensively photodegraded polymer fragments (code B) was extracted over twenty-four hours with 250 ml of alkali solution. The addition of the alkali turned the polymer colour from grey to very intense yellow.

12.1 grams of the photodegraded polymer was recovered after treatment with sodium hydroxide, code E in scheme 5.2.

Scheme 5.2: Flow chart of the methodology adopted for analysis of sample Bso



0.15 grams of photoxidised products were leached out from the polymer backbone into the alkali solution (code Bso-D in scheme 5.2) and this was later analysed.

Figure 5.5 shows the FT-IR spectra in the carbonyl region of Bso at various stages of alkali treatment (B and E, in scheme 5.2). Table 5.3 summarises the main absorptions and differences in the polymer at these stages.

Table 5.3: Changes in the FT-IR spectra of sample Bso at various stages of alkali treatment, see scheme 5.2 for codes and figure 5.5.

Stage of treatment	Wavenumber / $\text{cm}^{-1}$	Assignment
Bso-A	FT-IR of unstabilised LDPE before photoxidation	ketones and aldehydes formed during processing
Bso-B	1705	carboxylic acid
	1718	ketone
	1739	ester
	1774	lactone
Bso-E	1567	sodium carboxylate
	1718	ketone

Figure 5.6 and table 5.4 exhibit the solid state  $^{13}\text{C}$  NMR of Bso at stages A, B and E of alkali treatment (see scheme 5.2).

Spectroscopic analysis (FT-IR and  $^{13}\text{C}$  NMR) of the solid polymer confirm that photoxidation of Bso leads to the formation of a variety of carbonyl products (lactones, esters, ketones and carboxylic acids), see figures 5.1, 5.5-5.6 and tables 5.2-5.3. Treatment with 1M sodium hydroxide converts some

Table 5.4: Changes observed in the solid state  $^{13}\text{C}$  NMR of sample Bso at various stages of alkali treatment, see figure 5.6.

Stage of treatment	Chemical shift /ppm	Assignment
Bso-A NMR spectra of unstabilised LDPE before photoxidation	14	-CH <sub>3</sub>
	30	-CH <sub>2</sub> -
Bso-B	11, 14.6	-CH <sub>3</sub>
	24, 31	-CH <sub>2</sub> -
	64, 76, 82	>CH-O- & ≥C-O-
	110	CH <sub>2</sub> =CH-
	172, 177, 180	ester and carboxylic acid
Bso-E	15	-CH <sub>3</sub>
	33	-CH <sub>2</sub> -
	81	≥C-O-
	138	RCH=CH-- /CH <sub>2</sub> =CH-
	181	RCOO Na
	194, 201	aldehyde
	214	ketone

of these carbonyl products in the polymer backbone to their corresponding sodium carboxylate salts, which absorb at  $1567\text{ cm}^{-1}$  in the infrared region and 181 ppm in  $^{13}\text{C}$  NMR. Aldehydes and ketones which are present at stage B, are not affected by treating with the base, as shown in figures 5.5 and 5.6, stage E. In the infrared spectra the ketone/aldehyde absorptions at

1718  $\text{cm}^{-1}$  are still clearly visible and in the NMR spectra of oxidised Bso polymer after it has been treated with alkali (stage E) the peaks confirming the presence of aldehydes and ketones are also visible at 194 ppm, 201 ppm and 214 ppm. NMR analysis also shows the presence of unsaturation in the photoxidised LDPE.

Figure 5.7 is the FT-IR spectra of the precipitate removed from the aqueous layer after it has been neutralised with hydrochloric acid, stage C in scheme 5.2. This precipitate was insoluble in HPLC water, distilled ether, isopropanol and acetonitrile. The main additional infrared absorption features other than those found in LDPE occurred at 1713  $\text{cm}^{-1}$  (carboxylic acid) and 1594  $\text{cm}^{-1}$  (sodium carboxylate). The absorption at 3426  $\text{cm}^{-1}$  had increased in intensity. Infrared analysis suggests that the precipitate is a smaller fragment of oxidised LDPE which is soluble in 1M sodium hydroxide.

#### 5.2.3.2 Treatment of ECO Polymer With 1M Sodium Hydroxide

Scheme 5.3 outlines the procedure used for the analysis of the ECO sample, A3, with alkali solution. The polymer sample was irradiated for eight months. 6.5 grams of photoxidised polymer was used for the extraction process. The addition of the alkali solution immediately turned the grey polymer to pale yellow colour. 6.3 grams of the polymer was recovered after extraction, stage E in scheme 5.3. The total weight of the extracted products at stage D was 0.05 grams.

Figure 5.8 and table 5.5 show the changes in the carbonyl region of the FT-IR spectra of the ECO polymer before and after treatment with sodium hydroxide. Figure 5.9 and table 5.6 reflect the changes in the solid state  $^{13}\text{C}$ NMR of A3 at stages B and E (see scheme 5.3). NMR of A3-A revealed

Scheme 5.3: Flow chart of the methodology adopted for analysis of sample A3

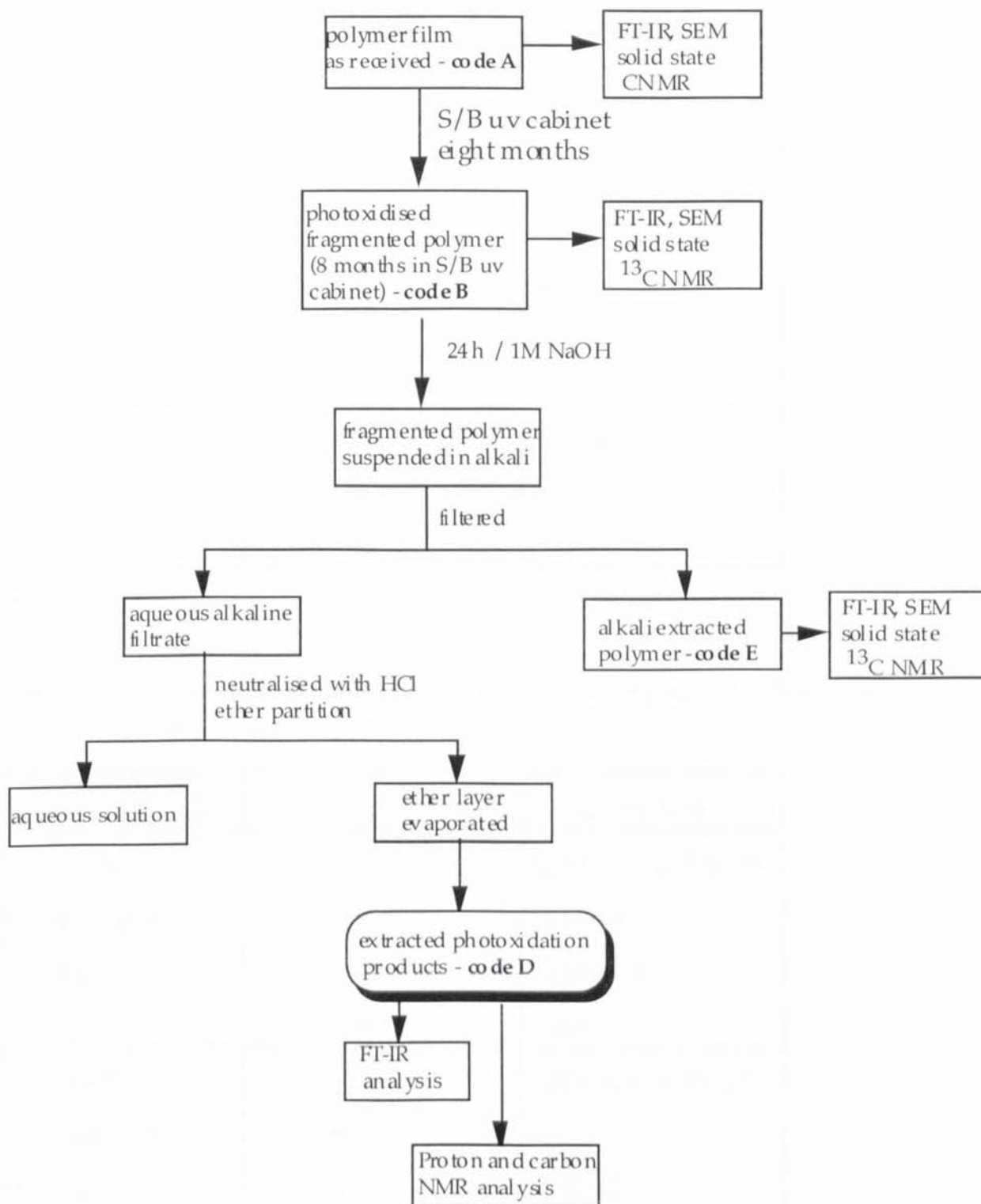


Table 5.5: Main absorptions seen in the FT-IR spectra of sample A3 during alkali extraction, see figure 5.8.

Stage of treatment	Wavenumber / $\text{cm}^{-1}$	Assignment
A3-A	FT-IR of ECO polymer as received (1720)	ketone group in-built into the polymer backbone
A3-B	1640 1715 1740 1786	$>\text{C}=\text{C}<$ ketone ester lactone
A3-E	1574 1716 1740	sodium carboxylate ketone ester

Table 5.6: Chemical shifts ( $^{13}\text{C}$ Carbon) observed for sample A3 during alkali treatment, see figure 5.9.

Stage of treatment	Chemical shift / ppm	Assignment
A3-B	71	$\text{R}_2\text{CH-O-}$ & $\text{R}_3\text{C-O-}$
photoxidised	114	$\text{CH}_2=\text{CH-}$
polymer	135	$\text{RCH}=\text{CH--}$
	169	ester
A3-E	72.85	$\text{R}_2\text{CH-O-}$ & $\text{R}_3\text{C-O-}$
photoxidised	97	
polymer after	114	$\text{CH}_2=\text{CH}$
extraction with	130	$\text{RCH}=\text{CH--}$
alkali	180	$\text{RCOO Na}$

only the alkane carbons and the ketone group which is inbuilt into the system .

FT-IR spectroscopy analysis (figure 5.8) suggests that during photooxidation of the ECO sample the major products are ketones (1715  $\text{cm}^{-1}$ ), esters (1740  $\text{cm}^{-1}$ ) and lactones (1786  $\text{cm}^{-1}$ ). No absorptions at 1705 - 1710  $\text{cm}^{-1}$  are observed in the FT-IR spectra of sample A3 suggesting none or very little carboxylic acids being formed, see figure 5.8 and table 5.5. However, in A3-B, photoxidised sample, chemical shift at 169 ppm in the  $^{13}\text{C}$  NMR spectra (figure 5.9) is indicative of an ester functional group. In this part of the NMR spectra no other peaks are seen. In A3-E, photoxidised treated, the 1574  $\text{cm}^{-1}$  in FT-IR spectra and 180 ppm in the NMR spectra are due to the sodium carboxylate salts of the ester and lactone groups. The ketone absorption remains unaffected after treatment with the alkali.

#### 5.2.3.3 Treatment of Metal Carboxylate system with 1M sodium Hydroxide

The extraction procedure used for this sample is represented in scheme 5.4. 11.2 grams of the photodegraded polymer (eight months in S/B uv cabinet) was extracted with 1M sodium hydroxide solution. On addition of the alkali the colour of the grey polymer turned yellow. After treatment 10.2 grams of the extracted polymer was recovered.

Figure 5.10 and table 5.7 reveal the changes examined using FT-IR spectroscopy in the photoxidised polymer (stage B in scheme 5.4) and photoxidised polymer that has been treated with sodium hydroxide (stage E in scheme 5.4). Figure 5.11 and table 5.8 show the results of the solid state  $^{13}\text{C}$  NMR analysis of Bo1 at stages B and E (see scheme 5.4). FT-IR analysis shows that photoxidation of sample Bo1 (stage B in scheme 5.4) contains the composite carbonyl peak consisting of lactones, esters,

Scheme 5.4: Flow chart of the methodology adopted for the analysis of sample Bo1

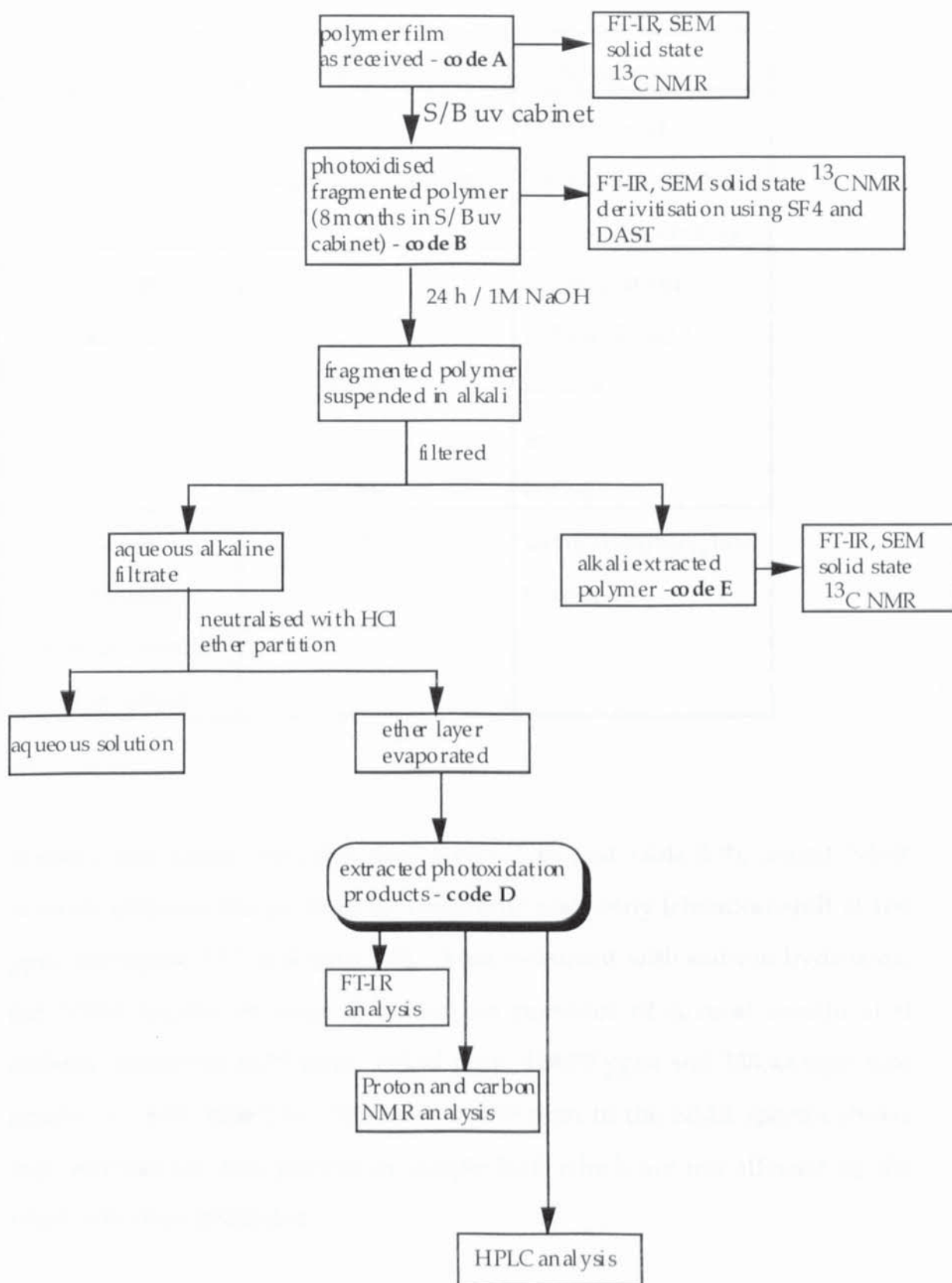


Table 5.7: Changes in FT-IR spectra of sample Bo1 during alkali treatment, see figure 5.10.

Stage of treatment	Wavenumber / $\text{cm}^{-1}$	Assignment
Bo1-A	FT-IR of degradable sample as received	ketones and aldehydes formed during processing
Bo1-B photoxidised polymer	1644	unsaturation
	1710	carboxylic acid
	1718	ketone
	1740	ester
	1784	lactone
Bo1-E photoxidised polymer treated with alkali	1576	sodium carboxylate
	1716	ketone

ketones and carboxylic acids (see figure 5.10 and table 5.7), whilst NMR analysis indicates the presence of carboxylic acids only (chemical shift at 186 ppm, see figure 5.11 and table 5.8). After treatment with sodium hydroxide, the NMR spectra at stage E shows the presence of several unsaturated carbons occurring at 97 ppm, 114.64 ppm, 128.79 ppm and 138.44 ppm (see figure 5.11 and table 5.8). The peak at 205 ppm in the NMR spectra shows that ketones are also present in sample Bo1, which are not affected by the alkali solution treatment.

Table 5.8: Chemical shifts observed for sample Bo1 at various stages of alkali treatment, see scheme 5.4 for codes and figure 5.11.

Stage of treatment	Chemical shift / ppm	Assignment
Bo1-B photoxidised polymer	14.6	-CH <sub>3</sub>
	32.76	-CH <sub>2</sub> -
	96	CH <sub>2</sub> =CH-
	186	carboxylic acid
Bo1-E photoxidised polymer treated with alkali	14	-CH <sub>3</sub>
	32	-CH <sub>2</sub> -
	73.91	≥C-O-
	96.99, 114.64	RCH=CH--
	128.79, 138.44	/CH <sub>2</sub> =CH
	179.91	RCOO Na
204.96	ketone	

#### 5.2.3.4. Treatment of starch-filled PE system with 1M sodium hydroxide

Scheme 5.5 summarises the extraction method carried out on sample C2.

7.3 grams of the photoxidised polymer (exposed for five months in S/B uv cabinet) was used for extraction with 1M sodium hydroxide, code B in scheme 5.5. 6.4 grams was recovered after the alkali treatment, at stage E in scheme 5.5. 0.033 grams of photoxidation products were extracted at stage D in scheme 5.5.

Figure 5.12 and table 5.9 show the changes in the FT-IR spectra of sample C2 at stages B and E of alkali treatment. Figure 5.13 and table 5.10 display the changes in the <sup>13</sup>C NMR spectra after treatment with 1M NaOH solution.

Scheme 5.5: Flow chart of the methodology adopted for the analysis of sample C2

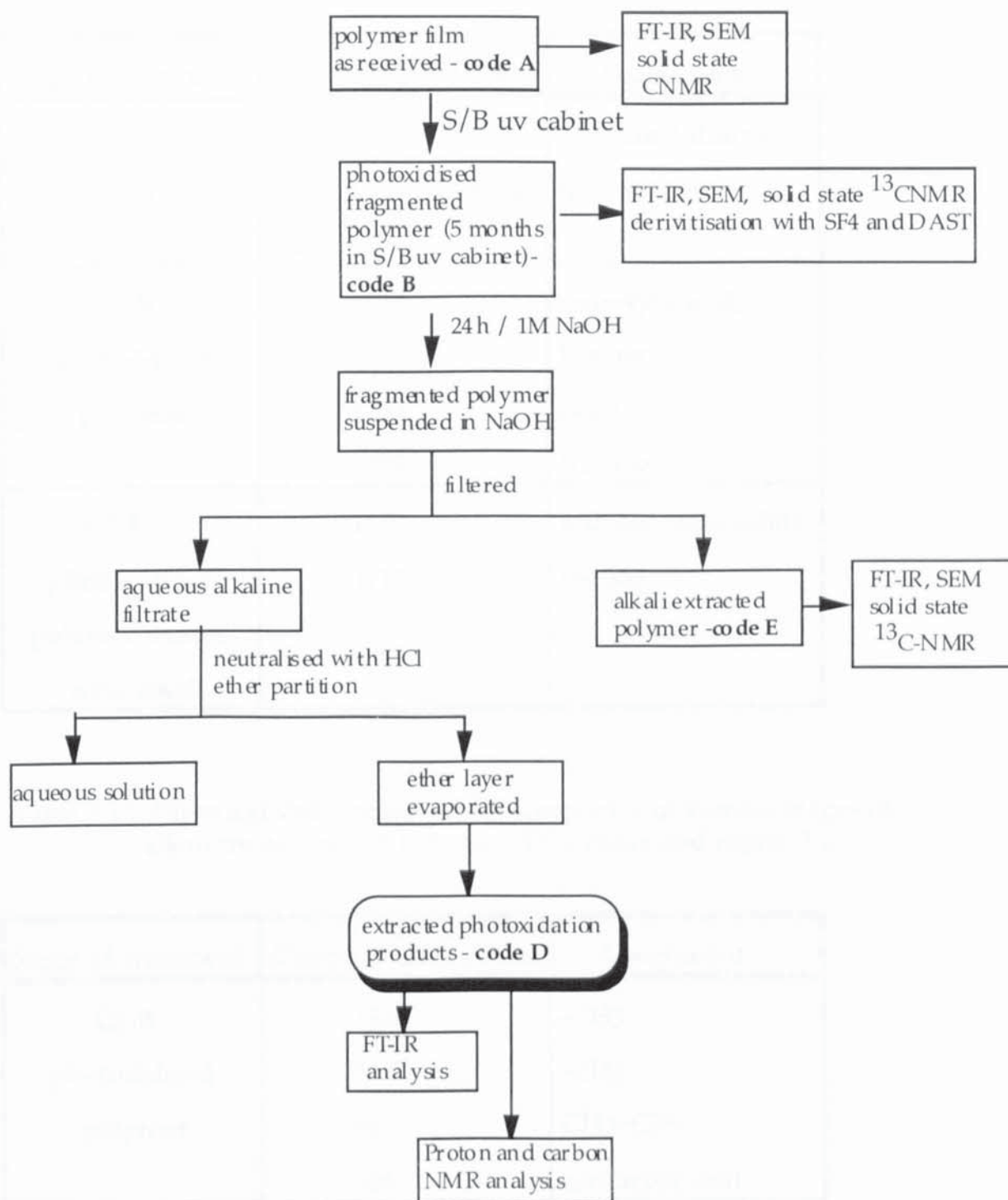


Table 5.9: FT-IR analysis of sample C2 at different stages of alkali extraction, see figure 5.12.

Stage of treatment	Wavenumber / $\text{cm}^{-1}$	Assignment
C2-A	FT-IR of degradable sample as received	$1737 \text{ cm}^{-1}$ due to iron stearate
C2-B photoxidised polymer	1717	carboxylic acid/
	1739	ketone
	1775	ester lactone
C2-E photoxidised polymer treated with alkali	1570	sodium carboxylate
	1715	ketone

Table 5.10: Chemical shifts observed for sample C2 at various stages of alkali treatment, see scheme 5.5 for codes and figure 5.13.

Stage of treatment	Chemical shift / ppm	Assignment
C2-B photoxidised polymer	14.6	-CH <sub>3</sub>
	32.76	-CH <sub>2</sub>
	96	CH <sub>2</sub> =CH-
	186	carboxylic acid
C2-E photoxidised polymer treated with alkali	14	methyl carbon
	32	methylene carbon
	109	RCH=CH--
	185	RCOO Na

Treatment of photoxidised C2 (stage B) with 1M alkali shows the same behaviour observed for the other degradable systems. The carboxylic acids and lactones formed during uv irradiation are converted to their sodium carboxylate salts after extraction with alkali solution, see figures 5.12-5.13 and tables 5.9 and 5.10, stage E.

#### 5.2.4 Derivatisation of Photoxidation Products Still Bound in Polymer Backbone (before Extraction).

The different absorption bands in the infrared spectra of carbonyl groups are generally convoluted. Methods of deconvoluting these bands rely on the selected derivitisation of the various carbonyl groups. Recent derivitisation methods to identify the carbonyl envelope stem from the original work of Carlsson and co-workers, who used sulphur tetrafluoride as the derivitising reagent [89].

In this work, sulphur tetrafluoride and liquid DAST [118] were used to derivitise the carbonyl band. Both classes of compounds convert aldehydes and ketones into geminal difluorides (see reaction 5.1) and carboxylic acids into acid fluorides (see reaction 5.2). The carbonyl species after fluorination show a shift in wavenumbers in the infrared spectra.



Liquid DAST has several advantages over the gas sulphur tetrafluoride. The most important is the ease of handling of liquid DAST. Fluorinations involving DAST require no special apparatus, unlike the sulphur

tetrafluoride gas which requires polyethylene or polytetrafluoroethyl reaction vessels.

Figures 5.14-5.15 show the infrared spectra in the carbonyl region of photoxidised polymers (Bo1 and C2) after derivitisation with liquid DAST and sulphur tetrafluoride gas. Table 5.11 highlights the main similarities and differences in the two figures.

Table 5.11: Changes observed in the FT-IR spectra of samples Bo1 and C2 after derivitisation with DAST and SF<sub>4</sub>, see figures 5.14-5.15.

	WAVENUMBER CM <sup>-1</sup>		
Polymer	Photoxidised polymer (code B)	Photoxidised polymer treated with DAST	Photoxidised polymer treated with SF <sub>4</sub> gas
Bo1	1710 RCO <sub>2</sub> H	--	--
	1720 R'R"CO	1716 R'R"CO	1715 R'R"CO
	1736 R'CO <sub>2</sub> -R"	1735 R'CO <sub>2</sub> -R"	1733 R'CO <sub>2</sub> -R"
	1780 lactones	1777 lactones	1739 R'CO <sub>2</sub> -R"
		1845 acid fluoride	1845 acid fluoride
C2	1710 RCO <sub>2</sub> H	--	1710 RCO <sub>2</sub> H
	1720 R'R"CO	1718 R'R"CO	1720 R'R"CO
	1736 R'CO <sub>2</sub> -R"	1735 R'CO <sub>2</sub> -R"	1735 R'CO <sub>2</sub> -R"
	1780 lactones	1777 lactones	
		1846 acid fluoride	1846 acid fluoride

Table 5.11 and figures 5.14-5.15 show that in both the DAST treated and SF<sub>4</sub> treated polymers, new absorptions at 1845 cm<sup>-1</sup> and 1846 cm<sup>-1</sup> appear which are assigned to acid fluorides. The photoxidised samples, (Bo1-B and C2-B)

treated with DAST show the disappearance of the  $1710\text{ cm}^{-1}$  absorption; however, the other carbonyl absorptions (lactones, esters and ketones) are still present in the polymer. The photoxidised polymer C2 treated with  $\text{SF}_4$  still shows the presence of carboxylic acids, see table 5.11.

It is clear from figures 5.14-5.15 and table 5.11 that under our experimental conditions only partial derivitisation of carbonyl products has been possible. Ketones and aldehydes do not appear to have reacted with either DAST or  $\text{SF}_4$ .

Derivitisation of photoxidised sample Bo1 with DAST was repeated. However, this time the exposure time of the polymer to DAST was increased to 24, 48 and 72 hours. The results are shown in figure 5.16. Increasing the exposure time from ten hours to 24 hours and 48 hours leads to an increase in the absorption at  $1845\text{ cm}^{-1}$  (relative to the carbonyl envelope), indicating more carboxylic acids are converted to their corresponding acid fluorides. The optimum exposure time seems to be 48 hours, since increasing the exposure time to 72 hours does not show any further changes in the acid fluoride absorptions, see figure 5.16.

### 5.2.5 Semi-Quantitative Analysis of Oxidation Products

The commercial photodegradable polymers studied in this work photoxidise via two distinct photochemical reactions (see chapter 3). The ECO polymer appears to degrade via the Norrish II reaction, whereas the other degradable systems studied in this work degrade via the Norrish I reaction. As a consequence, the photoxidation products of the ECO polymer are expected to be slightly different to those of unstabilised LDPE and the other degradable systems. From the results presented in chapter 3, it becomes clear that photoxidised ECO polymers contain predominantly

to a lesser extent carboxylic acids, whereas the other photoxidised degradable systems contain predominantly carboxylic acids and esters, with smaller quantities of ketones. Semi-quantitative analysis of these oxidation products was undertaken and the results are shown in table 5.12.

Table 5.12: Semi-quantitative analysis of photoxidation products formed in samples Bo1 and A3.

Sample	Area of absorption Peak				
	Photoxidised - B		Photoxidised treated with alkali -E		
	C=O area 1845 - 1700	ref peak area 1920-1890	C=O area 1845 - 1700	carboxylate 1570-1530	ref peak area 1920-1890
Bo1	6.92*	1.59	0.78	5.91	1.56
(via Norrish-I)	4.35\$ (100%)	-	0.50 (57%)	3.79 (100%)	
A3	5.23*	1.91	1.71	5.17	1.96
(via Norrish II)	2.74\$ (63%)		0.87 (100%)	2.64 (70%)	

\* peak area; \$ area index

Figure 5.17 compares the total carbonyl and carboxylate contents of Bo1 and A3. Table 5.12 and figure 5.17 demonstrate that after 887 hours of UV exposure, the metal carboxylate sample Bo1 contains higher quantities of photoxidation products compared to the ECO sample (A3). The photoxidised ECO sample (A3) contains approximately 63% of the total carbonyl content of the photoxidised Fe DRC-containing polymer sample (Bo1), see table 5.12 and figure 5.17. However, after treatment with alkali, the measured carbonyl content of the ECO sample is higher (100%) compared to the FeDRC sample (57%), indicating that greater quantities of

ketones are formed in the former (ketones are unaffected by the alkali treatment).

### 5.2.6 Analysis of Extracted Photooxidation Products

Section 5.2.3 showed that the amounts of photooxidation products extracted from the alkali treated polymer ranged from 32.9 mg to 151 mg. The results are summarised in table 5.13. FT-IR and NMR analysis were carried out on the total mixture of extracted products (code D).

Table 5.13: The percent of photooxidation products extracted using 1M alkali.

Sample	STAGE B Weight of photo-oxidised polymer/g	STAGE D weight of extract/ mg	% extracted products
Bso	12.55	151	1.20
A3	6.48	46.1	0.71
Bo1	11.20	83.8	0.75
C2	7.32	32.9	0.45

#### 5.2.6.1 FT-IR Analysis Of Extracted Products

The FT-IR spectra of the extracted photooxidation products of the unstabilised LDPE; Bso, ECO polymer, A3; metal carboxylate system, Bo1 and the starch filled system, C2 are shown in figure 5.18. Table 5.14 summarises the main absorption peaks in the infrared spectra.

#### 5.2.6.2 Proton NMR Analysis

Figure 5.19 shows the <sup>1</sup>H NMR spectra of the extracted degradation products (code D) of unstabilised LDPE, Bso, ECO polymer, A3 and Metal carboxylate system, Bo1. Table 5.15 shows the assigned chemical shifts of the proton

NMR to possible hydrogens of the different functional groups in the extracted degradation products.

Table 5.14: Main FT-IR observations for the extracted photooxidation products of samples Bso, Bo1, C2 and A3, see figure 5.18.

Functional Group	WAVE NUMBER $\text{cm}^{-1}$			
	Bso	A3	Bo1	C2
Hydrogen bonded -OH	3448	3450	3450	3451
>CH stretchings	2929	2929	2927	2932
	2856	2867	2847	2846
saturated carboxylic acid	1712	1714	1715	1716
-C=C-	-	-	1637	-
-C-O-	1463	1472	-	1476
-C-O-	1412	1421	1412	
-C-O-	-	-	1265	1215
-C-O-	1195	1191	1100	

Table 5.15: Chemical shifts observed in the proton NMR of the extracted photooxidation products of samples Bso, Bo1 and A3, see figure 5.19.

Functional Group	CHEMICAL SHIFT PPM		
	Bso	A3	Bo1
-CH <sub>2</sub> -CH <sub>3</sub>	0.81	0.80	0.85
-CH <sub>2</sub> -CH <sub>2</sub> -CH <sub>3</sub>	1.22	1.27	1.30
R'R''CH-CH <sub>3</sub>	1.55	1.58	1.6
-CH <sub>2</sub> -CHO	3.58	3.62	3.62
broad -OH	7.58	6.89	8.12

Figure 5.20 exhibits the  $^{13}\text{C}$ -NMR spectra of the extracted degradation products. The primary and tertiary carbons are shown as positive resonances, whereas the secondary and quaternary carbons as negative resonances. Table 5.16 summarises the information obtained.

Table 5.16: chemical shifts observed in the  $^{13}\text{C}$  NMR of the extracted photooxidation products of samples Bso, Bo1 and A3, see figure 5.20.

Functional Group	resonance position	CHEMICAL SHIFT PPM		
		Bso	A3	Bo1
-CH <sub>2</sub> -CH <sub>3</sub>	positive	14	14.07	7, 14
-CH <sub>2</sub> -CH <sub>2</sub> -CH <sub>3</sub>	negative	25, 29, 34	24.6, 28.9, 34	25, 29, 34
>CH-O-	positive	77, 81	-	77, 81
R-CO <sub>2</sub> H	negative	179	177, 179.6	177, 178, 179

The proton and carbon NMR spectra of the extracted products of polymers Bso, A3 and Bo1 are extremely similar, indicating that the nature of these photooxidation products are also very similar. NMR and FT-IR results suggest that the main functional groups in the extracted degradation products are alkanes and carboxylic acids.  $^{13}\text{C}$  NMR reveals the presence of three different carboxylic acids (177, 178, 179 ppm) in the extracted photooxidation products of Bo1 and two types of carboxylic acids are seen for the ECO polymer, A3 (177, 179.6 ppm).  $^{13}\text{C}$  NMR analysis of the extracted products of the ECO sample does not show the presence of ketones (absence of chemical shifts in the region of 205 - 215 ppm). Table 5.15 and figure 5.19 shows that the broad singlet peak (in proton NMR) assigned to a carboxylic acid increases in frequency in the series A3 < Bso < Bo1.

### 5.2.7 HPLC Analysis

Figure 5.21 shows the HPLC chromatogram obtained for the extracted photooxidation products of sample Bo1. The figure shows at least ten different chromatographic peaks, labelled 1 to 10, indicating that a mixture of photooxidation products are extracted. The UV spectra of these ten individual chromatographic peaks are displayed in figure 5.22 and table 5.17. The UV spectra of the peaks demonstrate clearly that the photooxidation products of Bo1 are very similar carboxylic acids. The UV spectra of a standard dicarboxylic acid (fumaric acid, structural formula  $\text{HO}_2\text{CHC}=\text{CHCO}_2\text{H}$ ) is shown in figure 5.23. It seems more probable that the photooxidation products are more like fumaric acid.

Table 5.17: Retention time and UV spectra of the separated chromatographic peaks for sample Bo1.

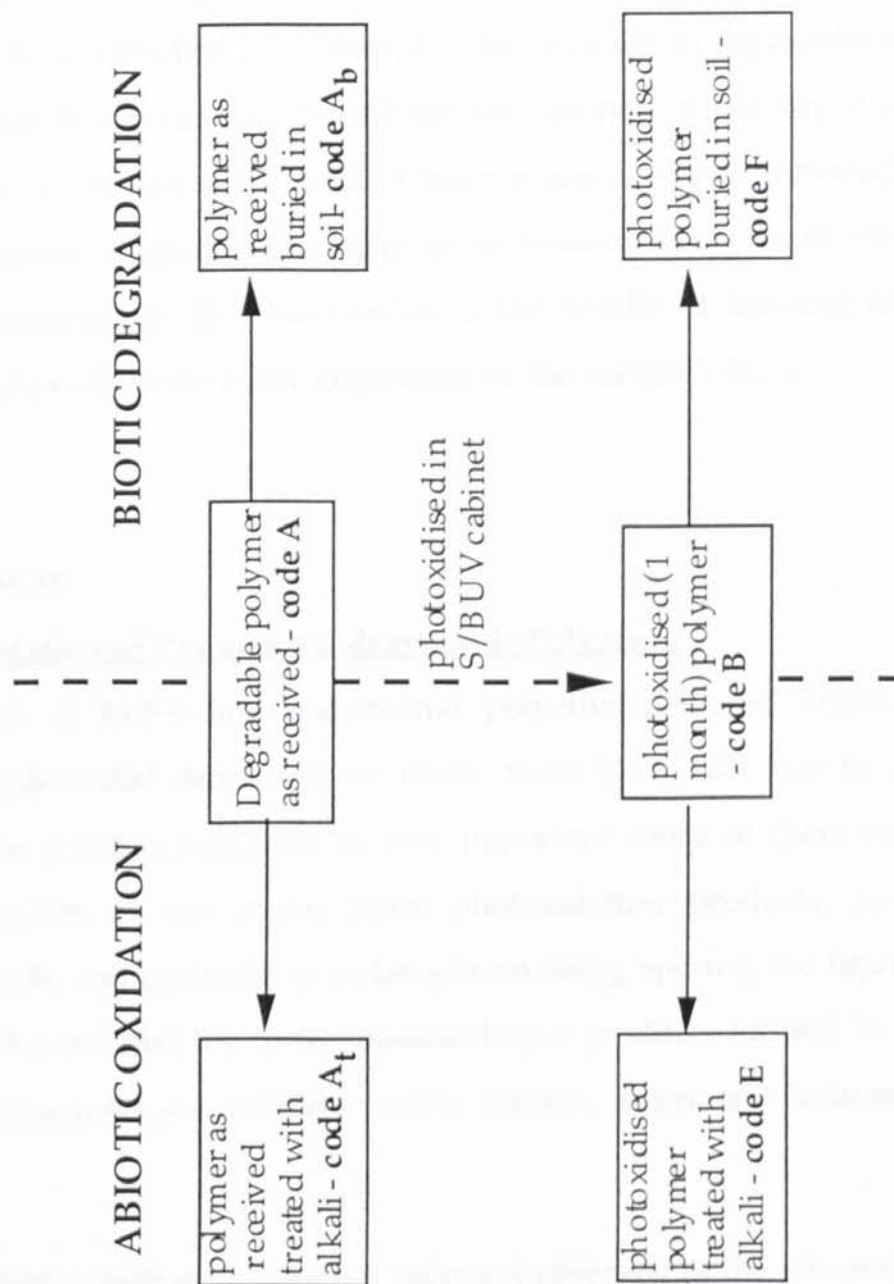
Peak	Retention Time	UV Spectra max(nm)
1	3.37	210 240 270
2	4.31	216 270 295
3	5.19	238
4	7.12	217 240 295
5	8.21	240
6	9.37	210 244
7	13.23	210 265
8	18.50	238
9	24.11	240
10	54.30	243

### 5.2.8 SEM Analysis

Scheme 5.6 shows the methodology involved during the SEM analysis of photodegradable polymers. Figures 5.24-5.30 display the scanning electron micrographs of degradable polymers (A3, B01, C2) and control sample, Bso, taken during the different stages of abiotic (alkali treatment, figures 5.24,5.26,5.28,5.30) and biotic treatments (effect of microorganisms, figures 5.25,5.27,5.29,5.30), see scheme 5.6. SEMs taken before any treatment (non-oxidised non treated) are labelled code A; non-oxidised treated (labelled At), extensively photoxidised polymer, code B; photoxidised treated with alkaline solution (code E) and photoxidised polymer that has been buried in soil (code F), see figures 5.24-5.30.

The SEMs show clearly that for all samples (except C2 buried in soil, see figure 5.29) the non-oxidised polymer samples after abiotic (solvent) and biotic (microorganisms) treatments do not show any morphological changes. The SEMs at this stage, codes At and Ab, are similar to the control samples (figure 5.30) i.e. the non-oxidised non-treated, code A, see figures 5.24-5.30.

SEMs at stage B of all systems show that photoxidation leads to the development of cracks in the polymer matrix. Micrographs of sample C2 photoxidised also reveal cracks in the polymer surface; however, the starch granules which are encapsulated in the PE matrix show no morphological changes. SEMs taken after abiotic treatment (code E) show very different results. All degradable systems at this stage show holes in the polymer matrix, indicating solvent-erosion of the degraded polymer surface. The starch granules in the C2 sample also show large holes and surface pitting, as result of abiotic erosion, see figure 5.28.



Scheme 5.6: Methodology involved during the SEM analysis of degradable polymers.

The results of abiotic treatment were identical to those obtained using biotic treatments at Aston and Clermont-Ferrand [119]. Figures 5.25, 5.27, 5.29 and 5.30 show the micrographs of non-oxidised (code Ab) and oxidised (code F) degradable polymer samples buried in the ground. With the exception of the starch-filled PE system, C2, the commercial degradables and unstabilised LDPE non-oxidised buried samples do not exhibit any changes in the surface (C2 shows small level of bio-erosion in starch granules). All the oxidised buried degradable samples show holes in the polymer surface, confirming bio-erosion. This bio-erosion is the result of leaching of the photooxidation products by micro-organisms in the soil [SC1-SC3].

### 5.3 DISCUSSION

#### 5.3.1 Photooxidation of Commercial degradable Polymers.

Photooxidation of LDPE and commercial polyethylene-based degradables leads to a substantial drop in their molar mass [119, 120] due to chain scission of the polymer backbone. A very important cause of chain scission is the formation of low molar mass photooxidation products, such as alcohols, vinyls, and particularly carbonyl containing species, see figure 5.1. Figure 5.2 showed that the major photooxidation products formed in these commercial samples are carboxylic acids, ketones, esters and lactones (see table 5.18).

Table 5.18: Major carbonyl oxidation products observed in the infrared spectra of LDPE based degradable polymers during photooxidation.

Absorbance Peak (cm <sup>-1</sup> )	Assignment
1780	Lactone
1735- 1738	Ester
1720	Ketone
1710	Carboxylic acids

The photooxidation products shown in table 5.18 and figure 5.2 arise from a series of complex reaction pathways, which result from mechano and photooxidation processes. The overall mechanism of the formation of products is shown in scheme 5.7 (reactions a-u). Mechanooxidation and subsequent storage and use (uv light, heat) of the polymer (reactions a-f) leads to the formation of alkoxy radicals, RO·, which undergo  $\beta$ -scission to give ketones (reaction h) [14,49]. Hence, these photooxidation products (ketones), are to some extent, observed in all degradables examined, see figures 5.1-5.6, 5.8, 5.10-5.11 and tables 5.3-5.4, 5.7-5.8.

During UV irradiation ketones undergo two important photochemical processes, Norrish I and Norrish II reactions (reactions i and s) [21,51]. The products of the Norrish I-process are ultimately esters, lactones and carboxylic acids, with small quantities of aldehydes and ketones (reactions n, j-m, o-q respectively), whereas the products of Norrish II process are mainly ketones and vinyl groups. Tables 5.3-5.11, 5.18 and figures 5.1-5.17 show the presence of these photooxidation species in the degradable systems. Although both photochemical processes may occur to the same extent, a situation arises whereby, one of these photochemical processes dominates. Depending on whether Norrish I or II processes dominate products will be formed at different relative concentrations. Hence, by consideration of the photooxidation products formed in the different degradable polymers (figures 5.2) it is possible to classify the photooxidation mechanisms of the degradables studied into two categories, those that photooxidise mainly via Norrish I and those that photooxidise predominantly via Norrish II process. Figure 5.2, 5.8-5.9 show clearly that the ECO sample, A3, photooxidises predominantly via Norrish II mechanism. The main absorptions observed at  $1716\text{ cm}^{-1}$  (ketone) and  $1640\text{ cm}^{-1}$  (vinyl) in the FT-IR spectra (figure 5.2) provide evidence for the Norrish II mechanism (see scheme reactions s-u).



The formation of other carbonyl products such as esters and lactones (see figure 5.2 and table 5.5-5.6 ) are due to small levels of oxidation that take place via the Norrish I process.

On the other hand, the main photochemical process taking place in unstabilised LDPE, the metal carboxylate system and the starch-filled PE appears to occur via the Norrish I process. Figures 5.2, 5.5-5.6, 5.10-5.11, 5.12-5.16 show implicitly the presence of carboxylic acids being formed as the major photooxidation products in the degradable samples Bo1, C2 and Bso, due to reactions j-m and o-r in scheme 5.7. The formation of esters and lactones in these samples is also due to Norrish I mechanism by virtue of reaction n in scheme 5.7. The small levels of ketones and vinyls in these samples probably arise due to the less dominant Norrish II process (reactions s-u), although, the decomposition of hydroperoxides (reactions d, e) may also account for the formation of vinyl compounds in these samples, see tables 5.4 and 5.7 for Bso and Bo1, respectively.

Figure 5.17 and table 5.12 provide further evidence to suggest that the commercial degradables studied in this work do not degrade by the same mechanisms. The higher concentration of photooxidation products (carbonyl content) observed for sample Bo1 compared to sample A3 is the result of the predominance of the Norrish I mechanism which occurs in the former sample. In the Norrish I process two free radicals are produced for every ketone decomposed (reaction i in scheme 5.7). Hence both radicals can be further oxidised to esters and carboxylic acids, thus giving rise to greater quantities of carbonyls, see table 5.12 and figure 5.17. Therefore, the photooxidation products of A3 are essentially ketones, whereas for samples Bo1, C2 and Bso, carboxylic acids are formed mainly.

Further complementary evidence for the formation of carboxylic acids in samples Bo1 and C2 is observed in figures 5.14-5.16 and table 5.11, which show the derivitisation of carboxylic acids formed in the solid polymer. The shift of the absorption in the IR from  $1710\text{ cm}^{-1}$  to  $1845\text{ cm}^{-1}$  (and  $1846\text{ cm}^{-1}$ ) shows that carboxylic acids are formed in these systems.

### 5.3.2 Analysis of Extracted Photooxidation Products.

The accumulation of the carbonyl-based photooxidation products results in the degradable polymers being more hydrophilic compared to the original polymer prior to oxidation. This is further supported by the swelling of these photoxidised polymers in dilute alkali and even water (section 5.2.2). However, because the products were not extractable using water and dilute alkali, it may be argued that the hydrophilic photooxidation products are not small chain molecules but contain substantially long aliphatic alkyl chains, similar to smaller fragments of PE with photoxidised functional groups, see figure 5.7.

Treatment of the photoxidised degradable polymers with 1M sodium hydroxide converts the majority of carboxylic acids in the solid polymer to their sodium carboxylate salts, indicating that the majority of the photooxidation products are still bound and therefore form part of the main polymer backbone, see tables 5.3-5.9 and figures 5.5-5.6, 5.8-5.13. This suggests that the majority of the carboxylic acids formed consist of long alkane chains and are therefore not leached out from the polymer. Table 5.13 demonstrates this very clearly, as the percentage of extracted products of the total photoxidised polymer is very small (0.45% to 1.20%).

Figures 5.18-5.20 and table 5.14-5.16 of the extracted photooxidation products of Bso, Bo1, C2 and A3 suggest the extracted products to be chemically very

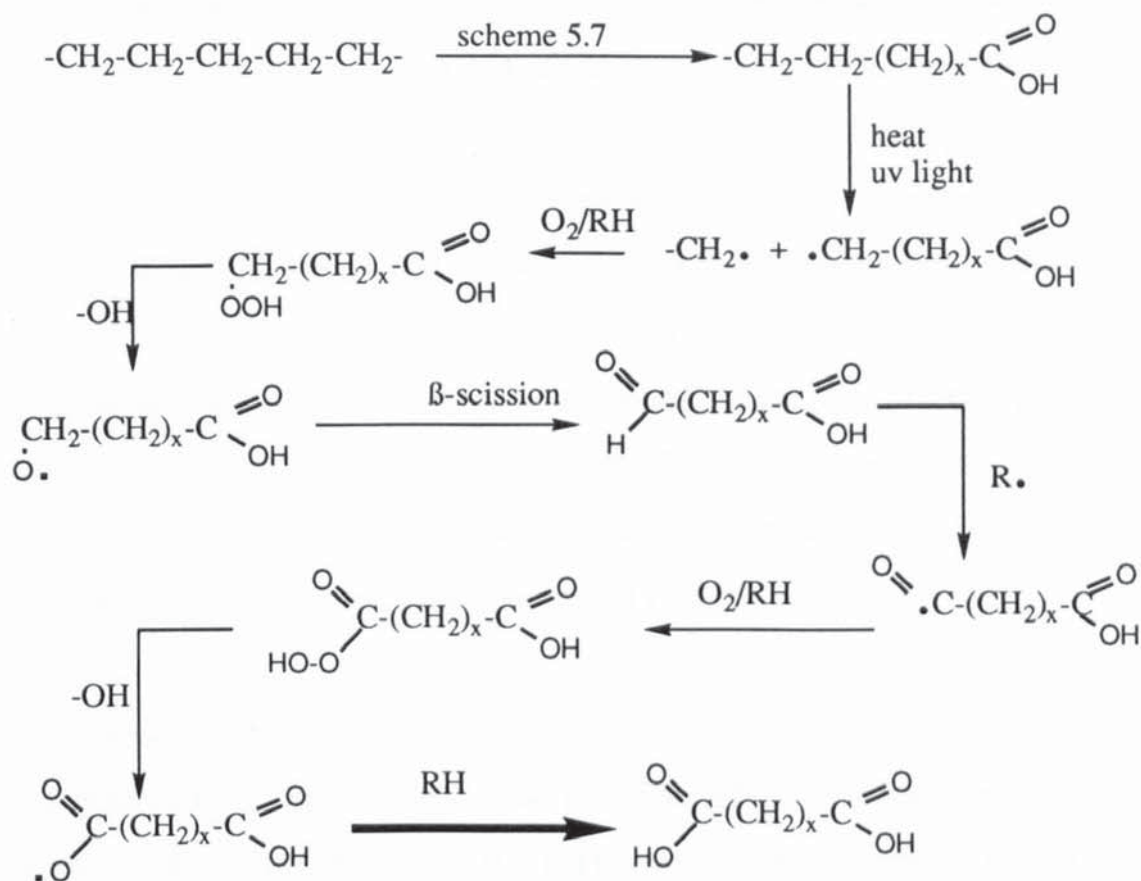
similar to each other. All analytical evidence presented in section 5.2.7 of these extracted products indicates that a mixture of carboxylic acids have been extracted from the photoxidised polymer, see figure 5.20 and table 5.16. Even for sample A3, which appears to degrade via the Norrish II process, the main constituents of the extracted products are carboxylic acids. The broad singlet peak in proton NMR (6.89, 7.58 and 8.12 ppm for samples A3, Bso and Bo1 respectively, see figure 5.19 and table 5.15) which increases in frequency from A3-D < Bso-D < Bo1-D suggests an increase in the degree of hydrogen bonding in the series respectively. One reason for the increased hydrogen bonding in extracted products of samples Bo1 and Bso compared to those of A3 may be the higher concentrations of carboxylic acids extracted in the former samples.

Figure 5.21 and table 5.17 confirmed further that the extracted products consist of a mixture of carboxylic acids. By considering the UV spectra of the extracted carboxylic acids (figure 5.22) and the UV spectra of standard carboxylic acid, fumaric acid, (figure 5.23), it appears that the extracted carboxylic acids may be similar in nature to dicarboxylic acids. Scheme 5.8 shows how dicarboxylic acids may be formed in the degradable polymer samples during photoxidation.

### 5.3.3 Mechanism of Photo-Biodegradation

SEM analysis proved to be a very valuable analytical tool in understanding the mechanism of photobiodegradation. SEM analysis allows any morphological changes in the polymer to be seen, see figures 5.24-5.30.

The non-oxidised hydrophobic degradable polymer samples are not affected by alkali or microorganisms, see figures 5.24-5.30. UV irradiated photoxidised polymer samples containing hydrophilic carbonyl products



Scheme 5.8: Formation of Dicarboxylic acids during uv irradiation.

are more susceptible to abiotic and biotic leaching, see figures 5.24-5.30. In the laboratory (using enriched culture at Clermont Ferrand) the above findings have been substantiated [119]. It was found that microbial growth (fungi, yeast, bacteria) was not supported by the non-oxidised polymer films, not even the starch-filled sample, C2, whereas all the photoxidised polymer films showed microbial activity. Complementary abiotic (alkali) and biotic (microorganisms) studies showed that for the systems examined in this work, biodegradation of the polymers does not occur unless the polymer samples have been first exposed to UV irradiation, see figures 5.24-5.30. Carbonyl products (formed during UV exposure) have a two fold effect on the polymer: they increase the hydrophilicity of the inherent hydrophobic polymer and cause surface swelling.

The hydrophilic nature and the surface swelling of the degradable samples allows solvent and bio-erosion of the polymer surface to take place, see figs 5.24-5.30. Photoxidation of the degradable systems, therefore, appears, to be very important in initiating the biodegradation of the polymers. Even for the starch-filled PE system, C2, which contains a natural biopolymer starch, the photoxidation stage appears to be critical. In the non-oxidised polymer the starch granules are not solvent or bioeroded since they are encapsulated in the polymer matrix, see figs 5.28 and 5.29. UV irradiation, however, breaks down the polymer matrix and releases the starch granules which are then susceptible to solvent and bio-erosion [SC2-SC3].

Many researchers (based on studies by Potts) have argued that biodegradation of degradables is not possible unless the molar mass ( $M_w$ ) has been reduced to 500 or less [121]. However, studies carried out in this work have shown that biodegradation of photoxidised degradables commences when the molar mass ( $M_w$ ) has been reduced to 2000 - 3000 during UV irradiation [120]. Experiments carried out at Clermont Ferrand showed that biodegradation of degradable polymers is even possible on photoxidised LDPE with  $M_w > 10\ 000$  [119]. Contrary to Potts view, the findings of this research suggest that the fundamental contributory factor for biodegradation of degradables to occur is initial photoxidation which creates bioassimilable products that allow microorganisms to get a foothold on the polymer, rather than the decrease of molar mass to a given low value.

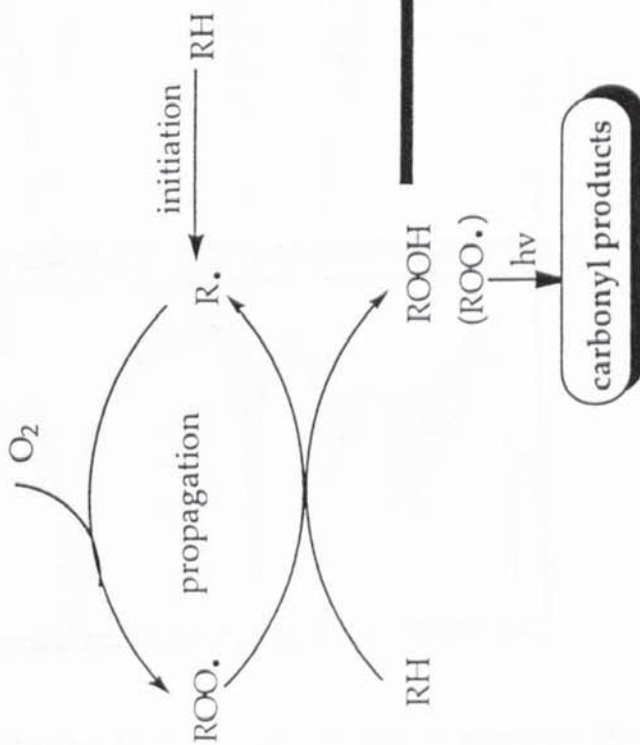
Hence, the mechanism by which the degradable polymer samples biodegrade is a two step process, which is shown in scheme 5.9 [10].

the polymer and the production of a variety of carbonyl species in the polymer surface.

In step 2 these hydrophilic carbonyl products lead to surface swelling of the polymer. As these products are bioassimilable they lead to surface swelling and ultimately biodegradation of the carbonyl products to carbon dioxide and water [84].

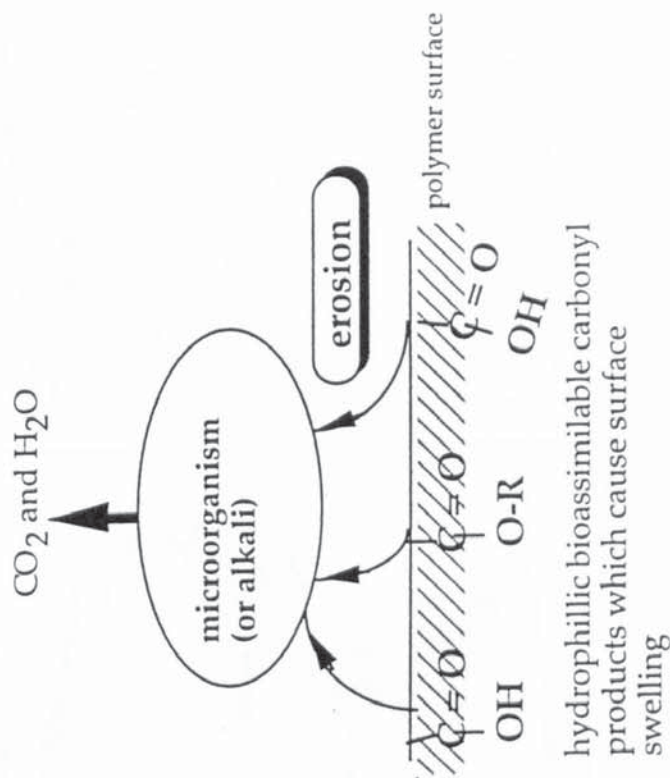
### STEP - 1

#### Abiotic oxidation



### STEP - 2

#### Biodegradation of photoxidised polymer



Scheme 5.9: Mechanism of Photobiodegradation

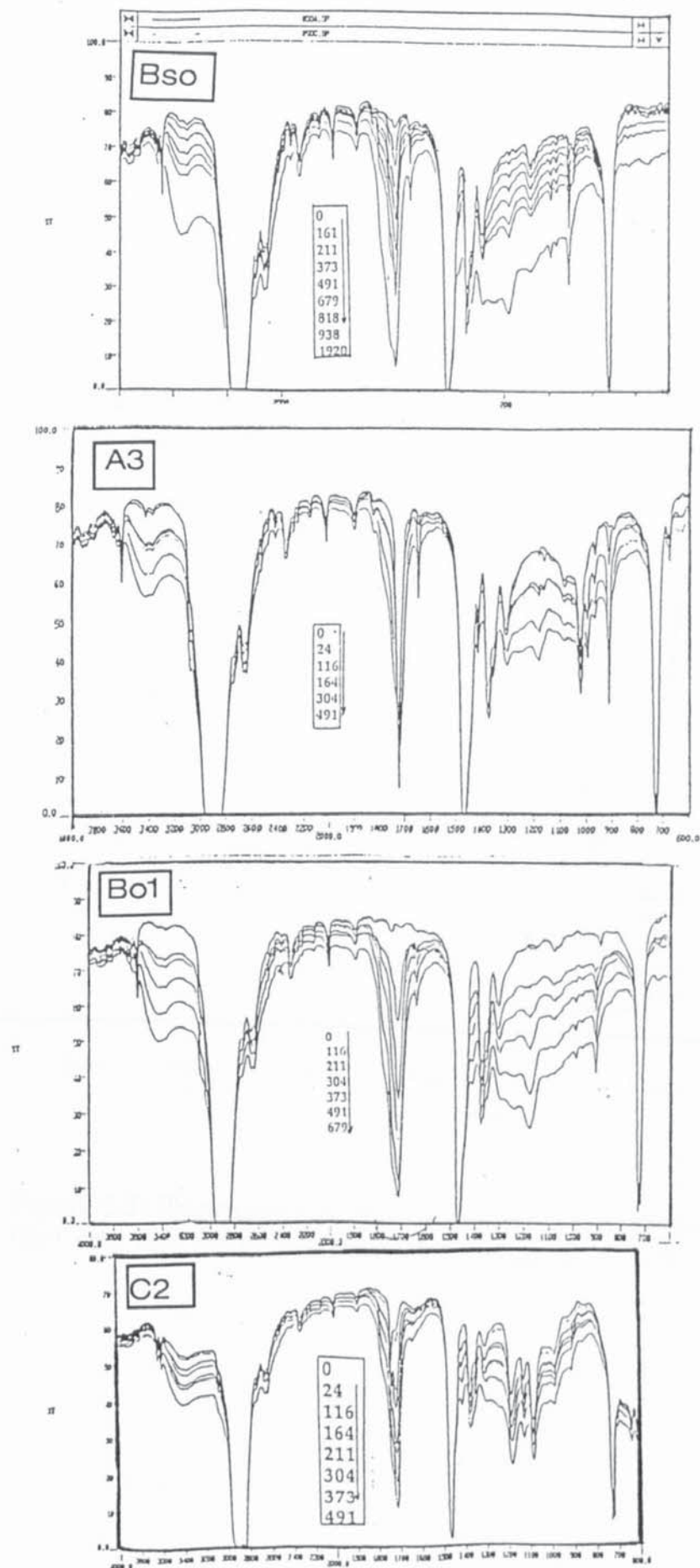


Figure 5.1: Photoxidation in S/B UV cabinet of samples Bso, A3, Bo1 and C2, see table 5.1 for sample codes. Numbers in box are irradiation hours.

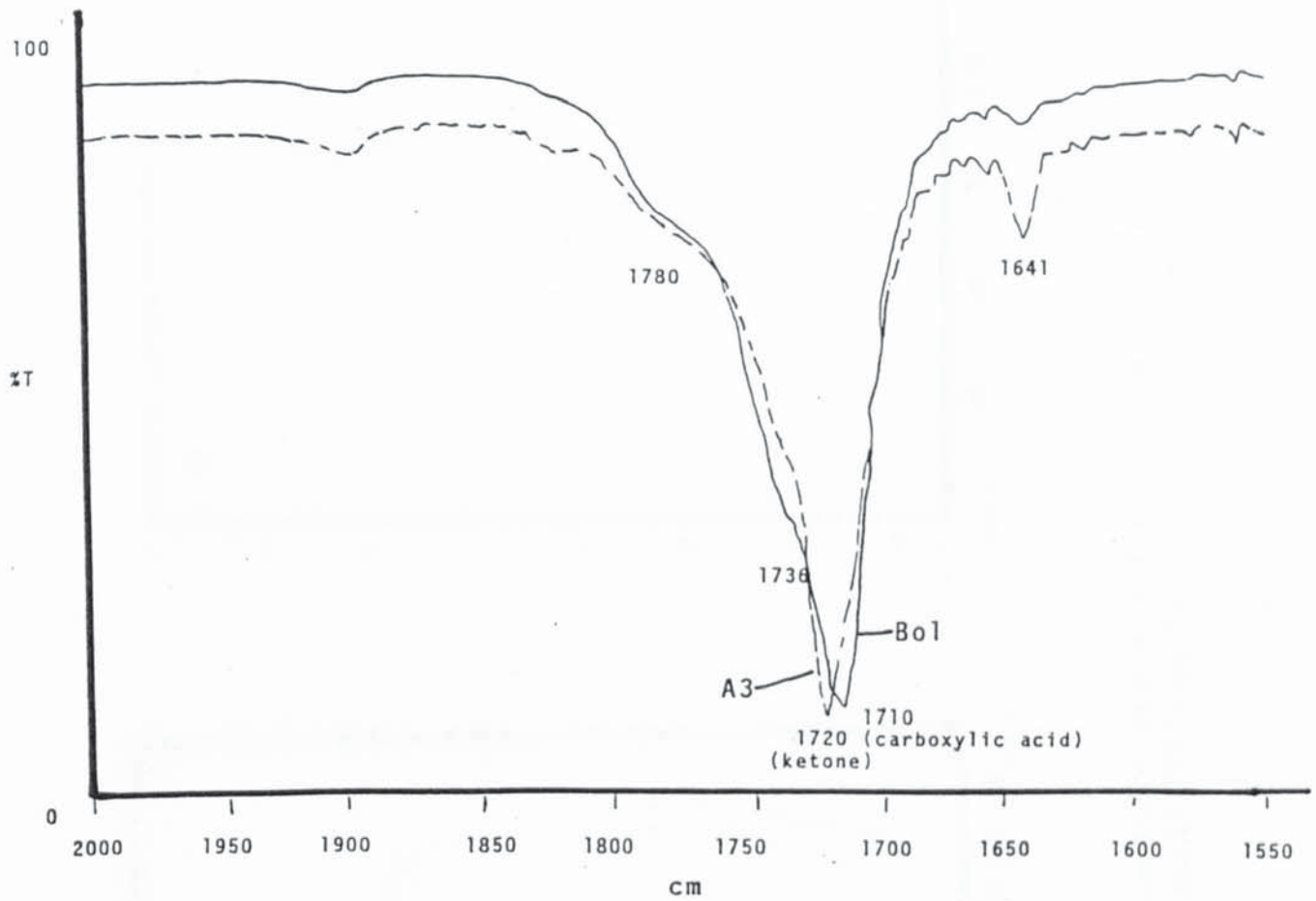


Figure 5.2: Photooxidation products of commercial degradable samples (Bo1 and A3) formed during UV irradiation in S/B cabinet.

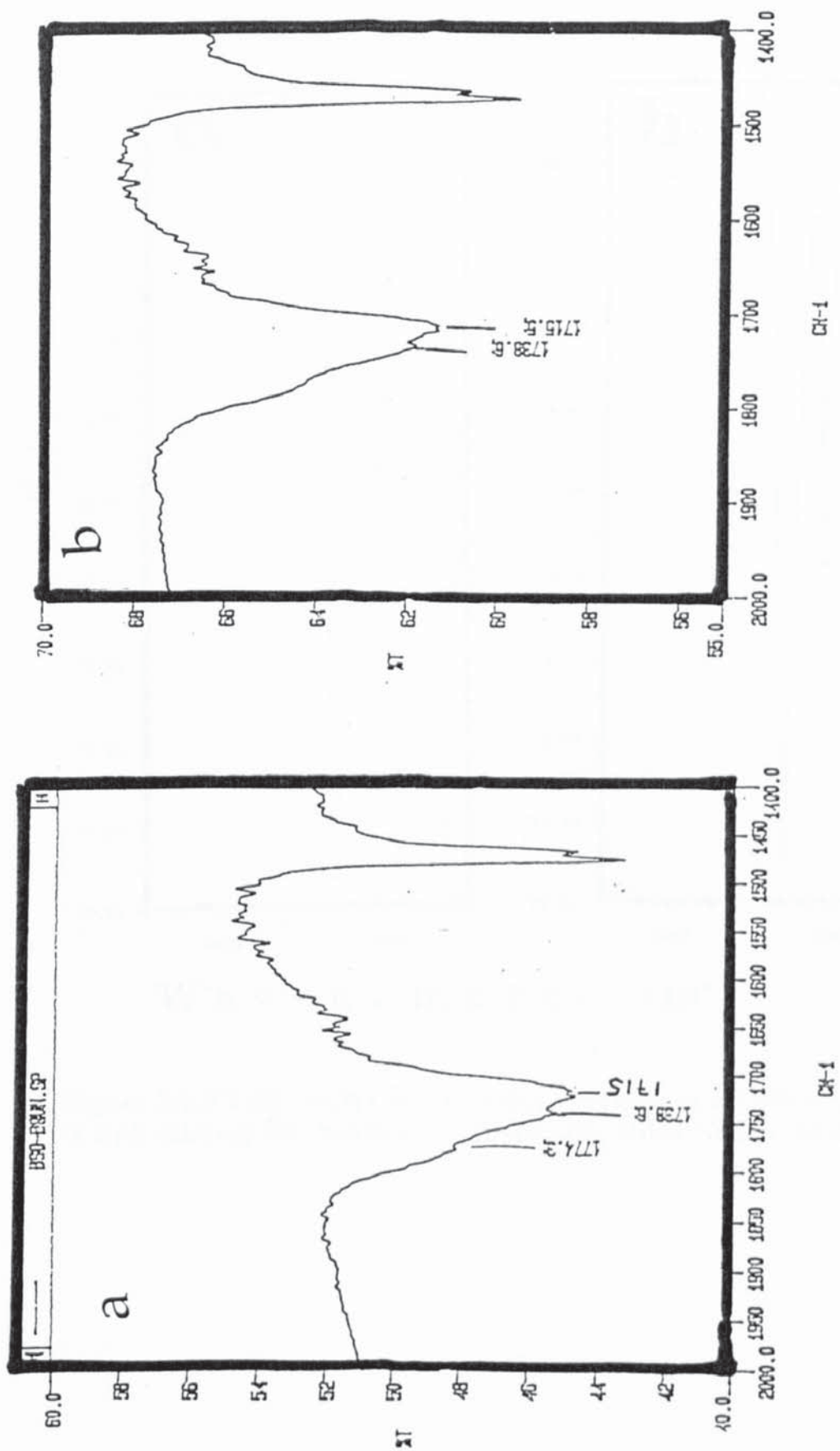


Figure 5.3: FT-IR spectra of photooxidised (in S/B cabinet for 11 months) fragmented unstabilised LDPE before (a) and after (b) water extraction.

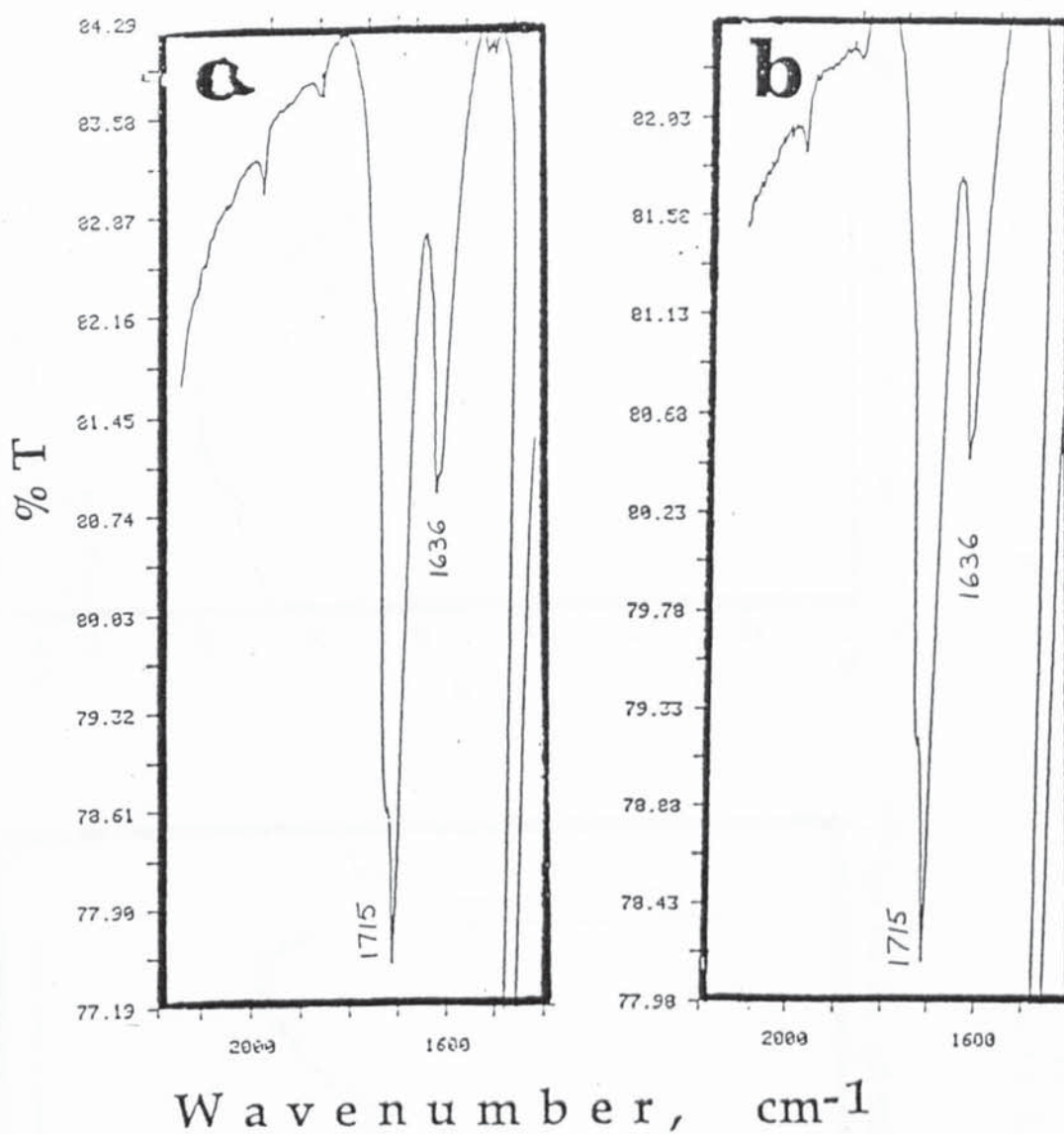
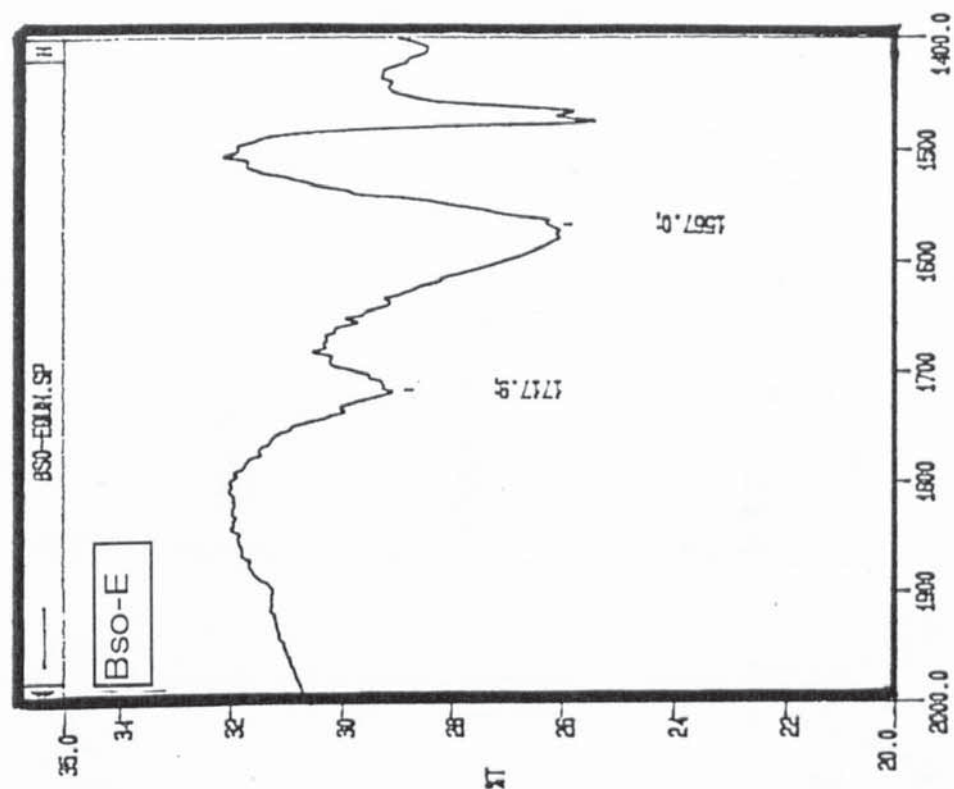
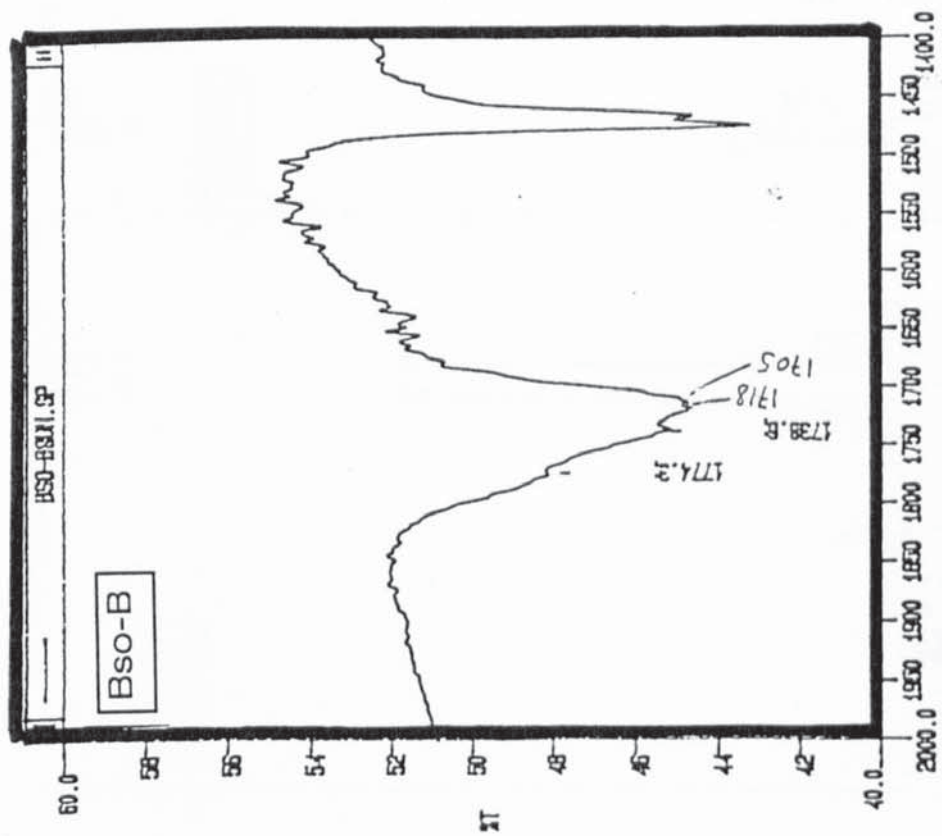


Figure 5.4: FT-IR spectra in the carbonyl region of photoxidised (11 months in S/B cabinet) Bso before (a) and after (b) 0.01M NaOH solution extraction.



CH-1



CH-1

Figure 5.5: FT-IR spectra of photoxidised (II months in S/B cabinet) unstabilised LDPE before (Bso-B) and after (Bso-E) 1M alkali extraction, see table 5.3.

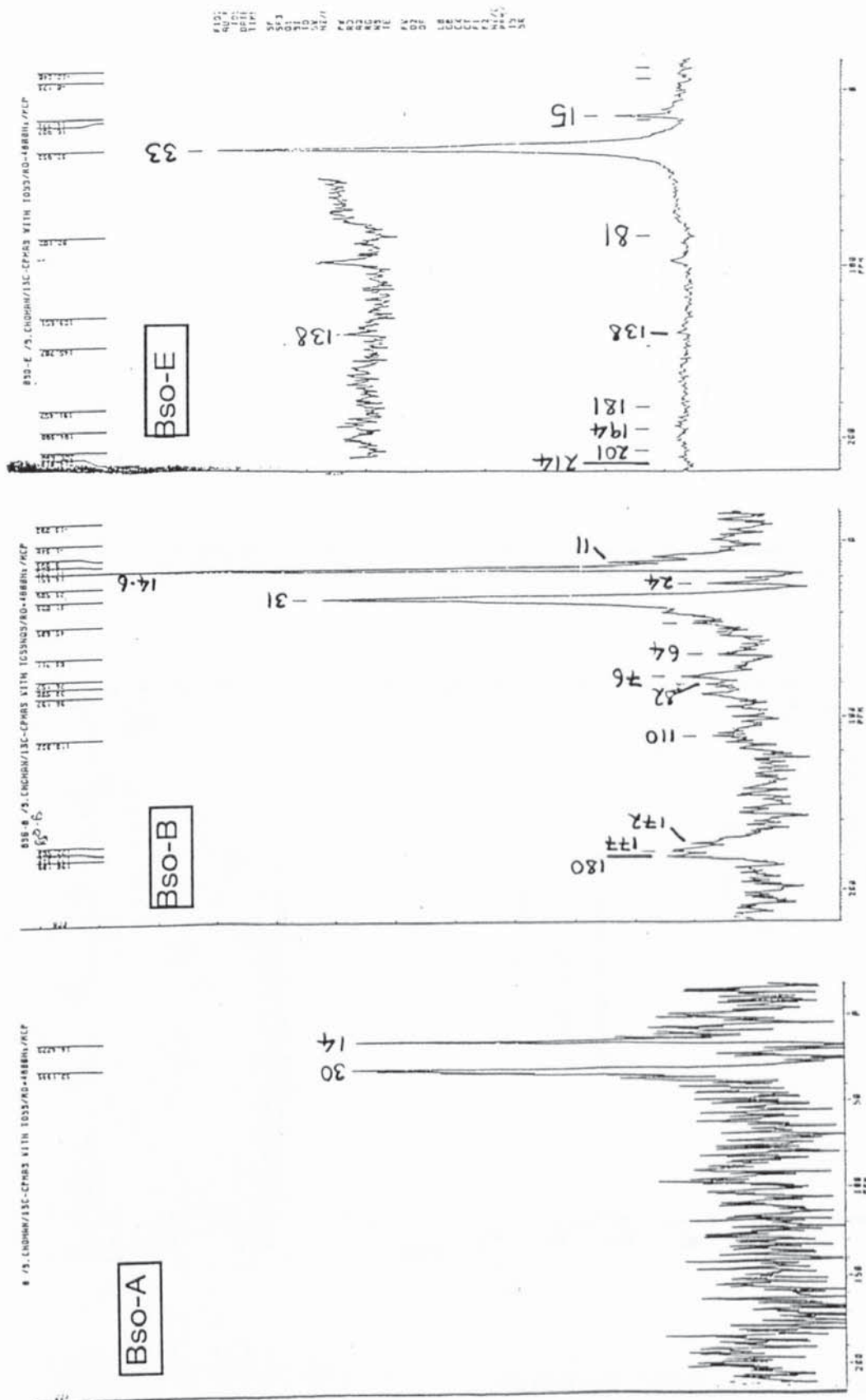
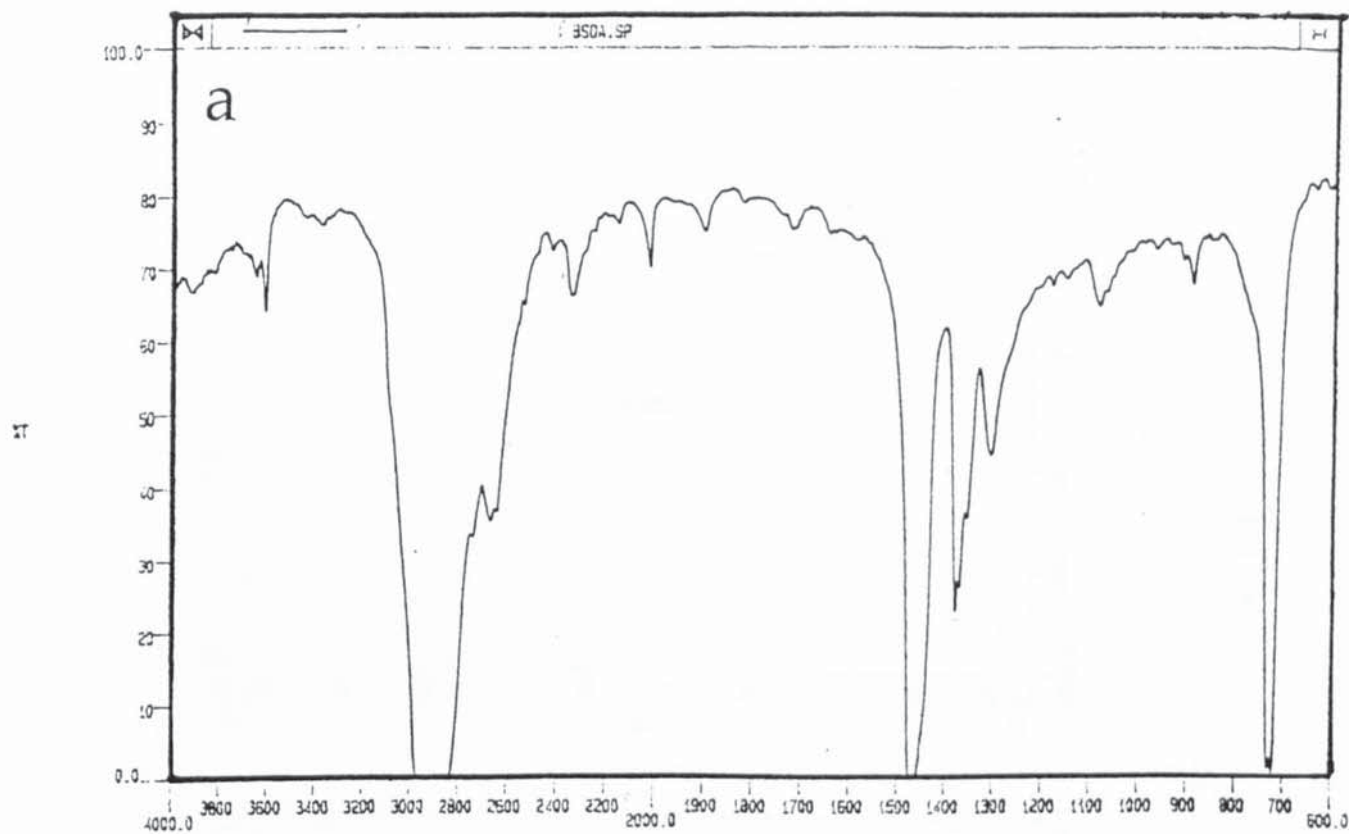
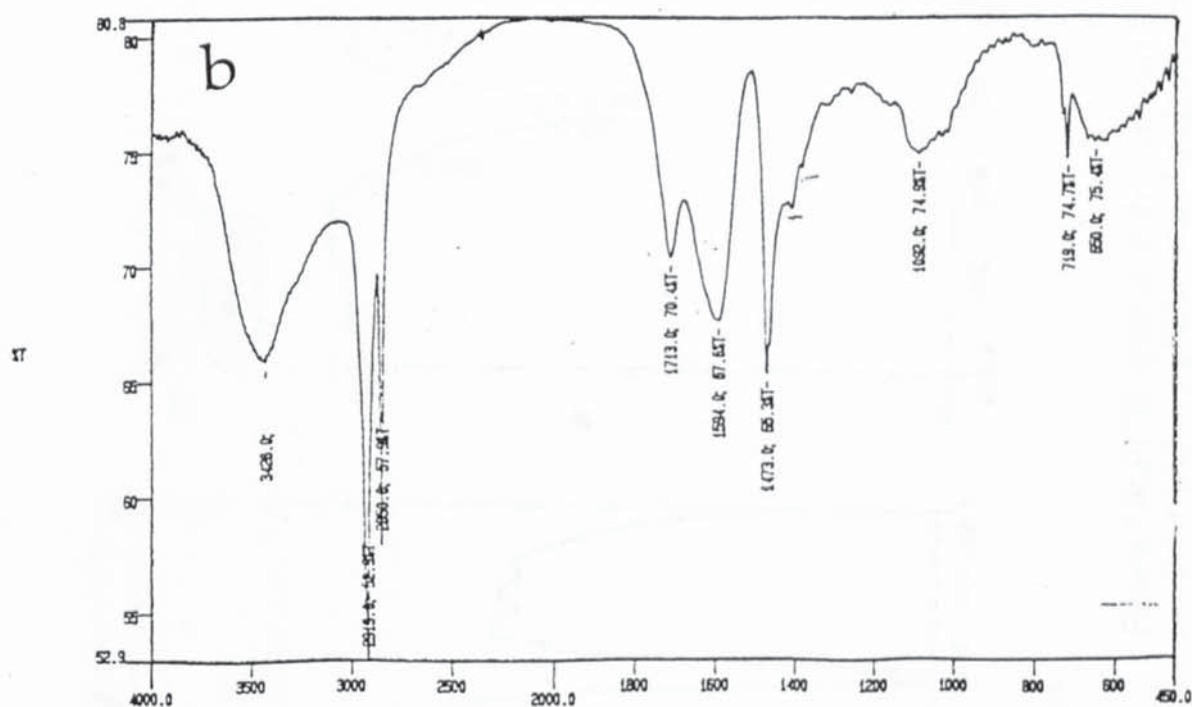


Figure 5.6: Solid state <sup>13</sup>CNMR spectra of unstabilised LDPE as received (Bso-A); photoxidised polymer (11 months in S/B cabinet) before extraction (Bso-B) and the photoxidised polymer after (Bso-E) in alkali extraction, see table 5.4. Numbers on peaks are chemical shifts, ppm.



OK-1



OK-1

Figure 5.7: FT-IR spectra of unstabilised LDPE, Bso (a) and insoluble precipitate (b) formed at stage C during alkali treatment of sample Bso, see scheme 5.2.

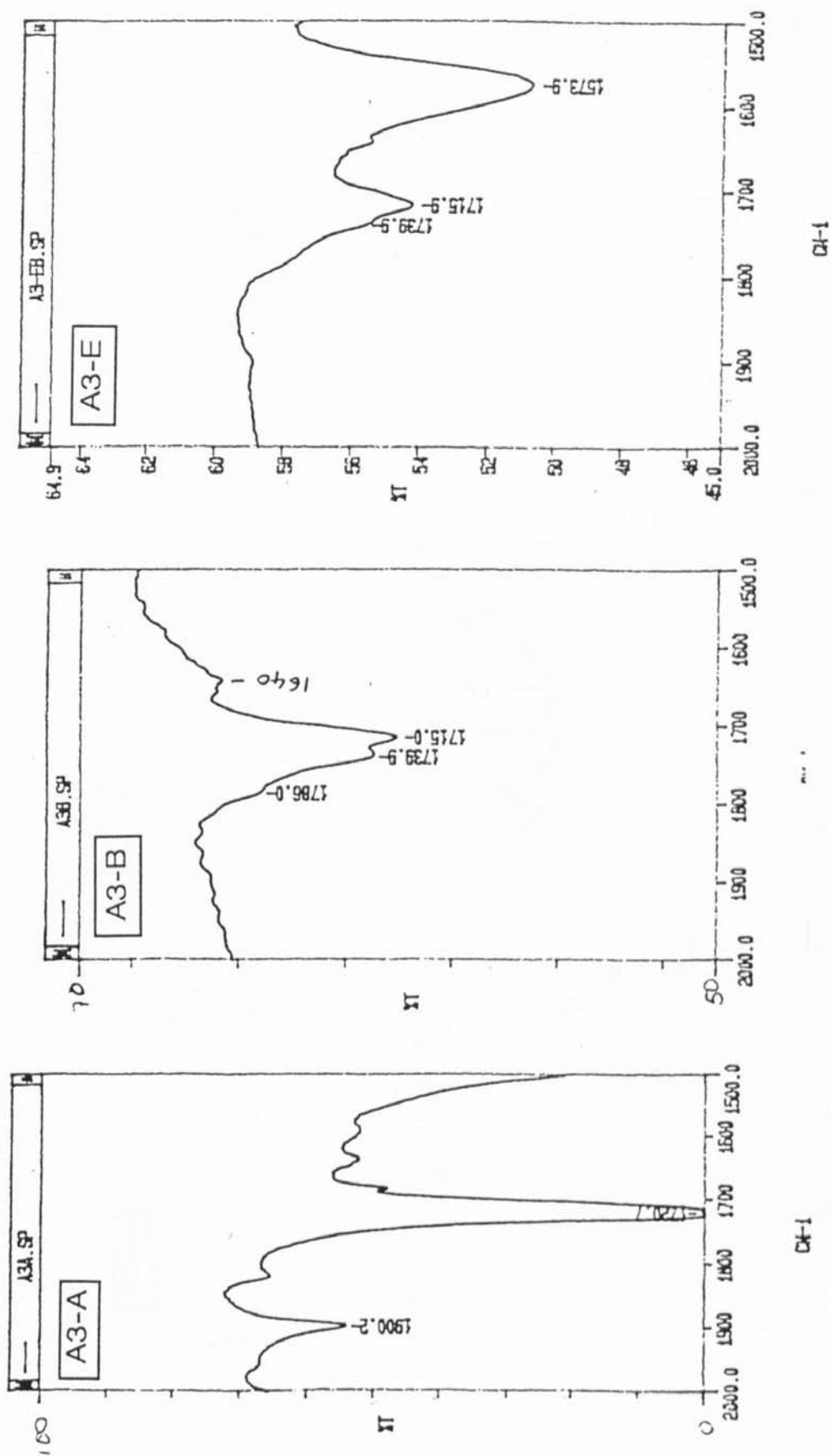


Figure 5.8: FT-IR spectra in the carbonyl region of ECO polymer as received (A3-A); photoxidised polymer before (A3-B) and after 1M alkali (A3-E) extraction, see table 5.5.

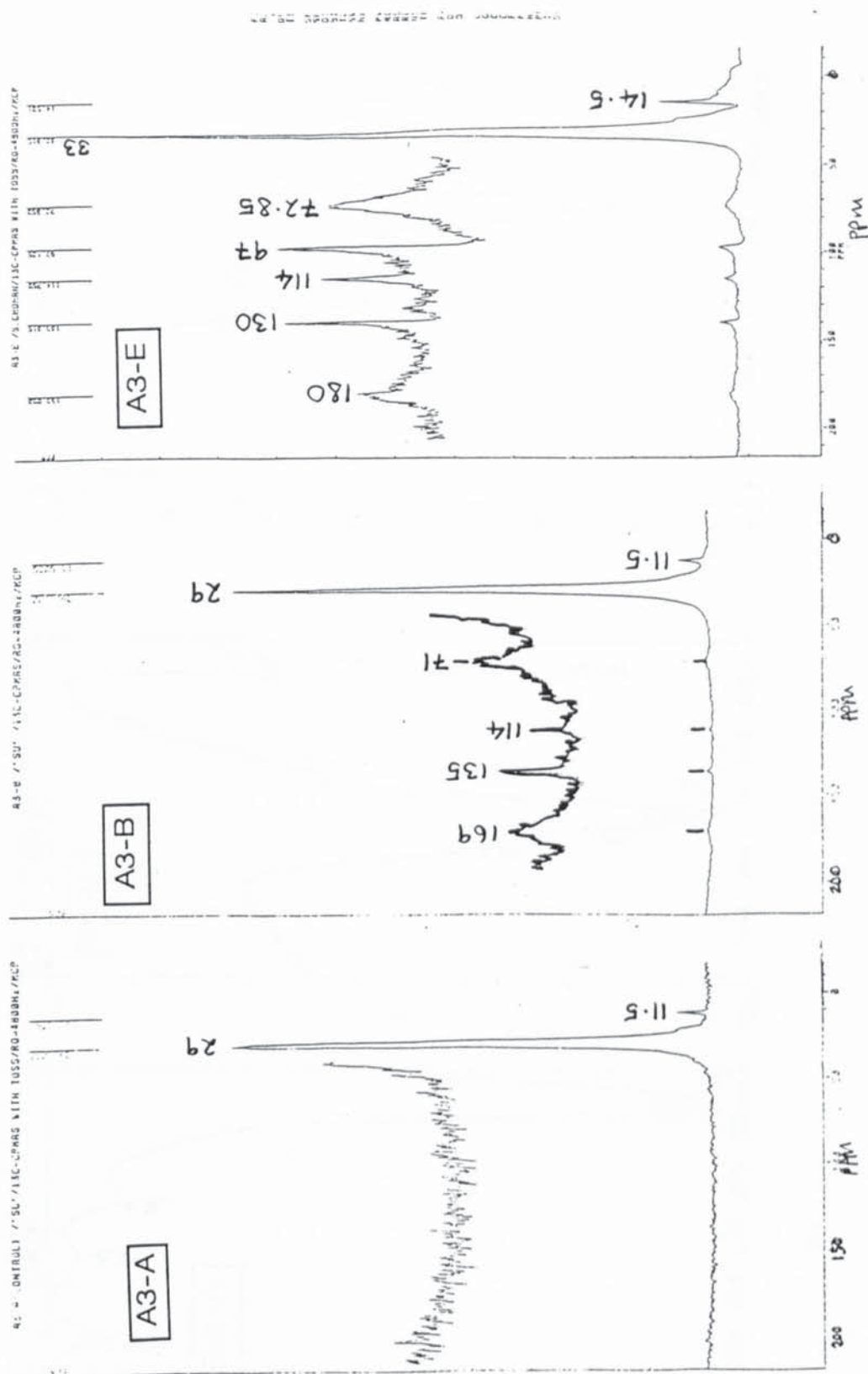


Figure 5.9: Solid state  $^{13}\text{C}$ NMR spectra of ECO polymer as received (A3-A); photoxidised (8 months in S/B cabinet) polymer before (A3-B) and after (A3-E) 1M alkali extraction. See table 5.6. Numbers on peaks are chemical shifts, ppm.

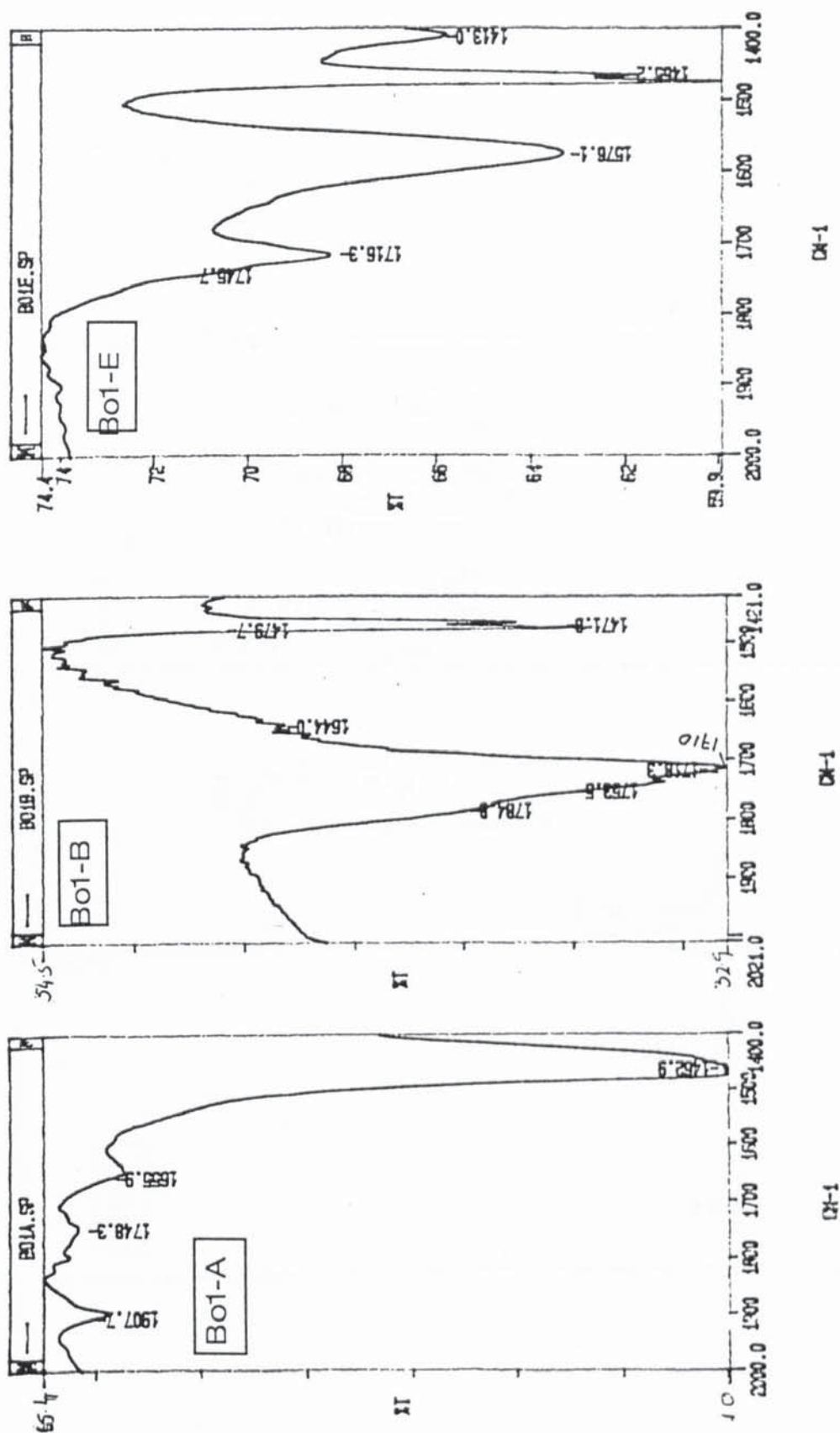


Figure 5.10: FT-IR spectra in the carbonyl region of metal carboxylate polymer as received (Bo1-A); photoxidised polymer before extraction (Bo1-B) and photoxidised after 1M alkali (Bo1-E) extraction, see table 5.7.

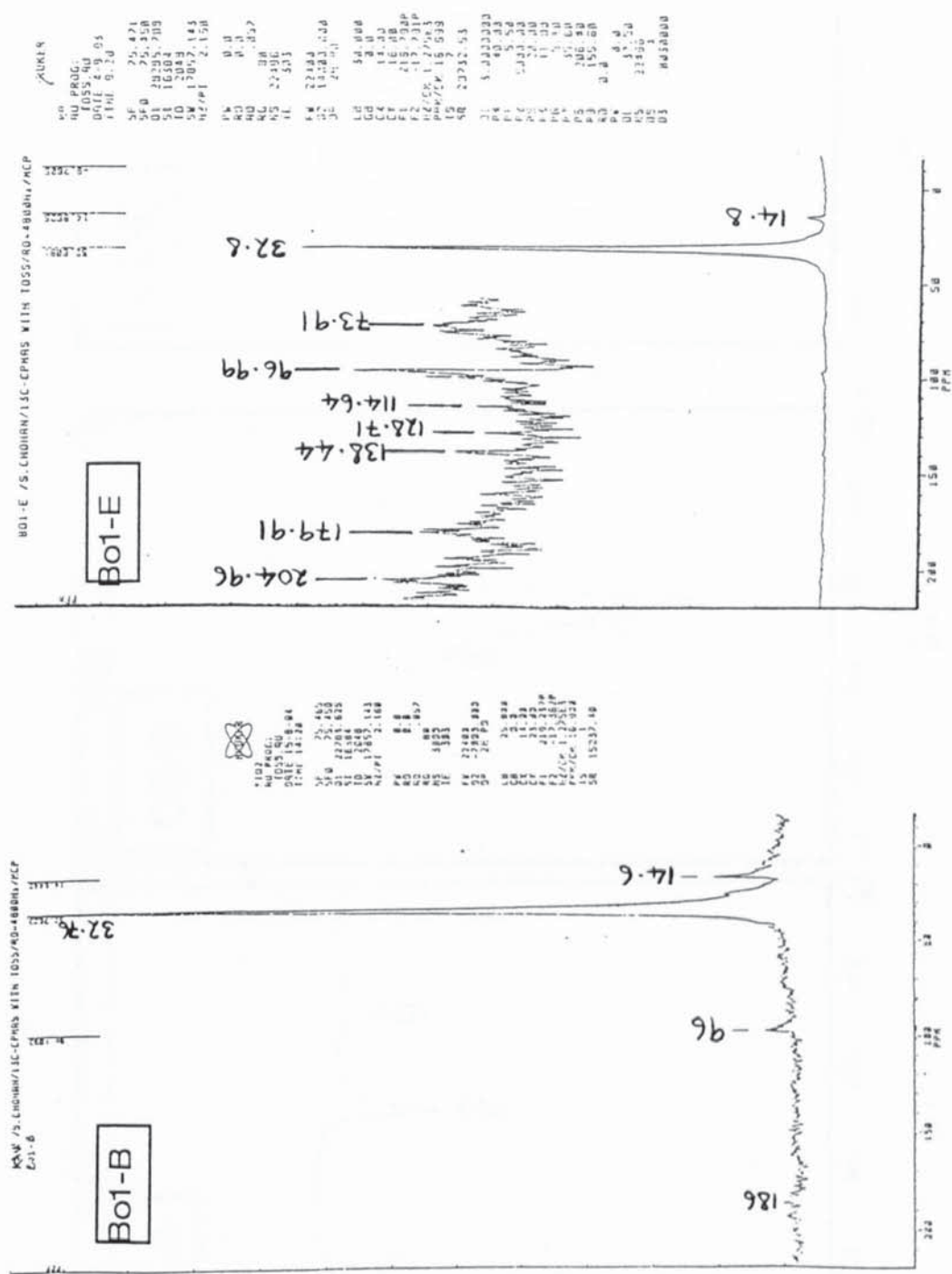


Figure 5.11: Solid state <sup>13</sup>CNMR spectra of Metal carboxylate polymer photoxidised before (Bo1-B) and after (Bo1-E) 1M alkali extraction. See table 5.8. Numbers on peaks are chemical shifts, ppm.

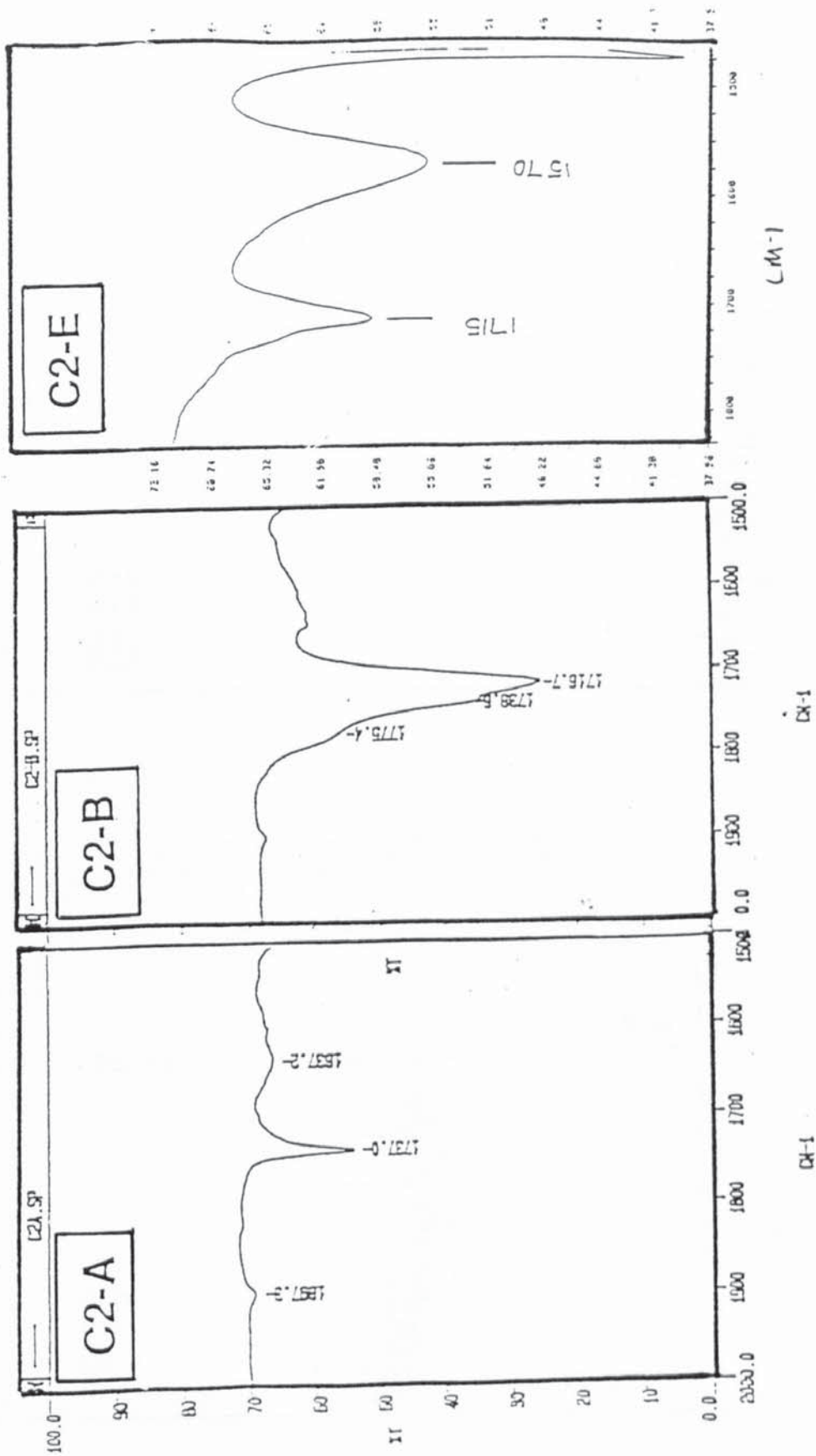


Figure 5.12: FT-IR spectra in the carbonyl region of Starch-filled PE polymer as received (C2-A); photoxidised before (C2-B) and photoxidised after 1M alkali (A3-E) extraction, see table 5.9.

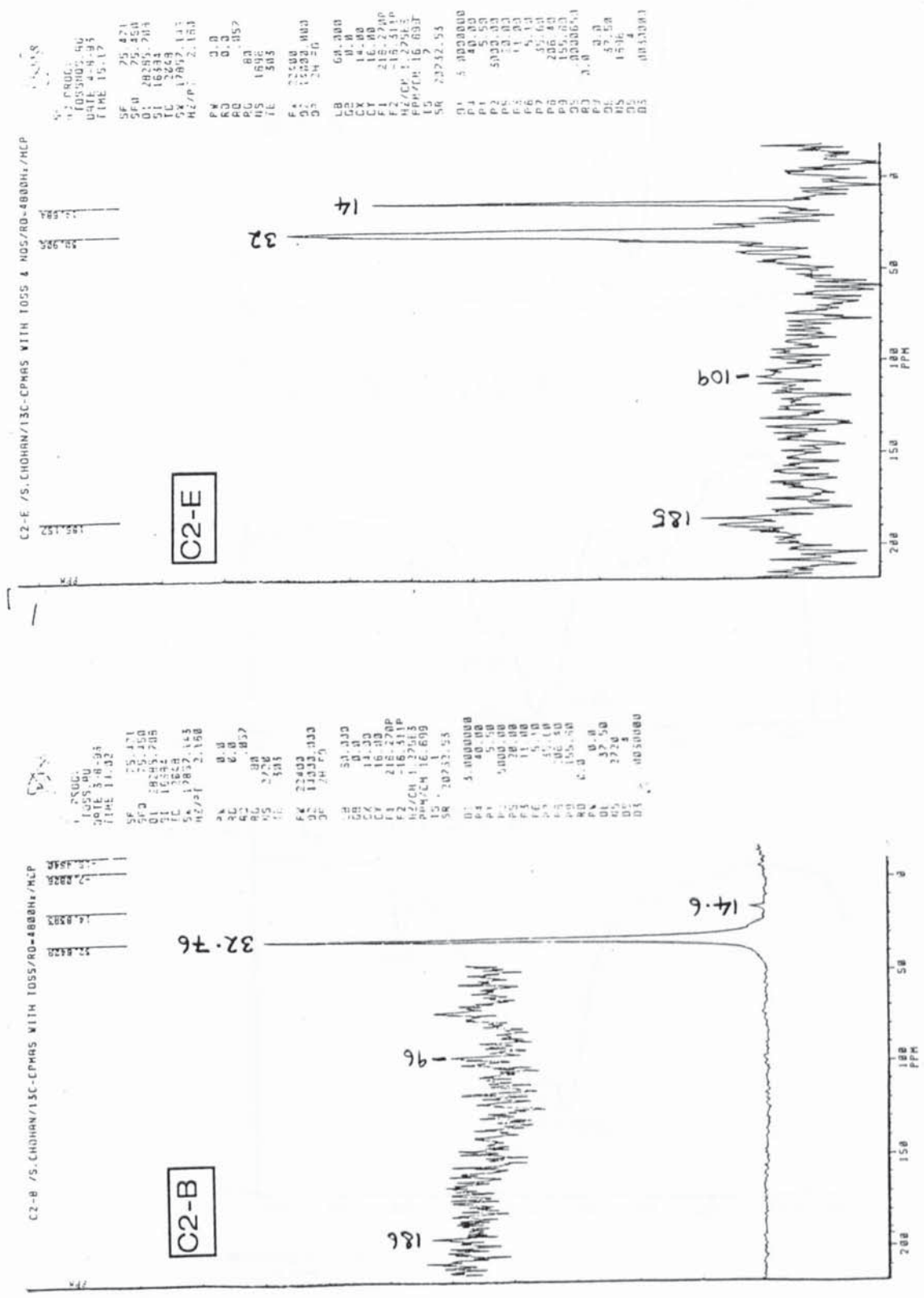


Figure 5.13: Solid state <sup>13</sup>CNMR spectra of Starch-filled PE polymer photoxidised before (C2-B) and photoxidised after (C2-E) 1M alkali extraction, see table 5.10. Numbers on peaks are chemical shifts, ppm.

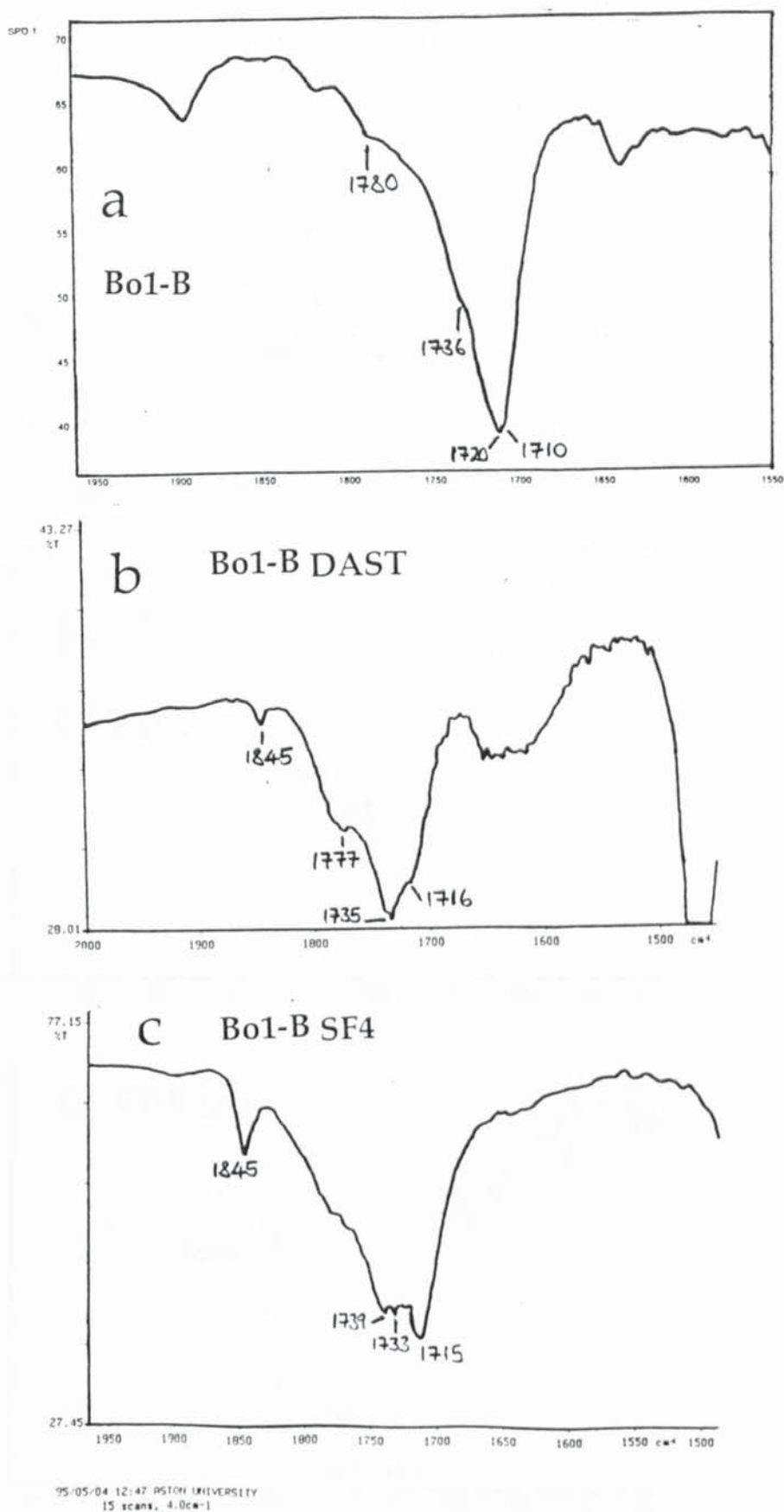


Figure 5.14: FT-IR spectra in the carbonyl region of photoxidised Bo1 (a); photoxidised polymer derivitised with DAST (b) and photoxidised polymer derivitised with SF4 (c) for 10 hours.

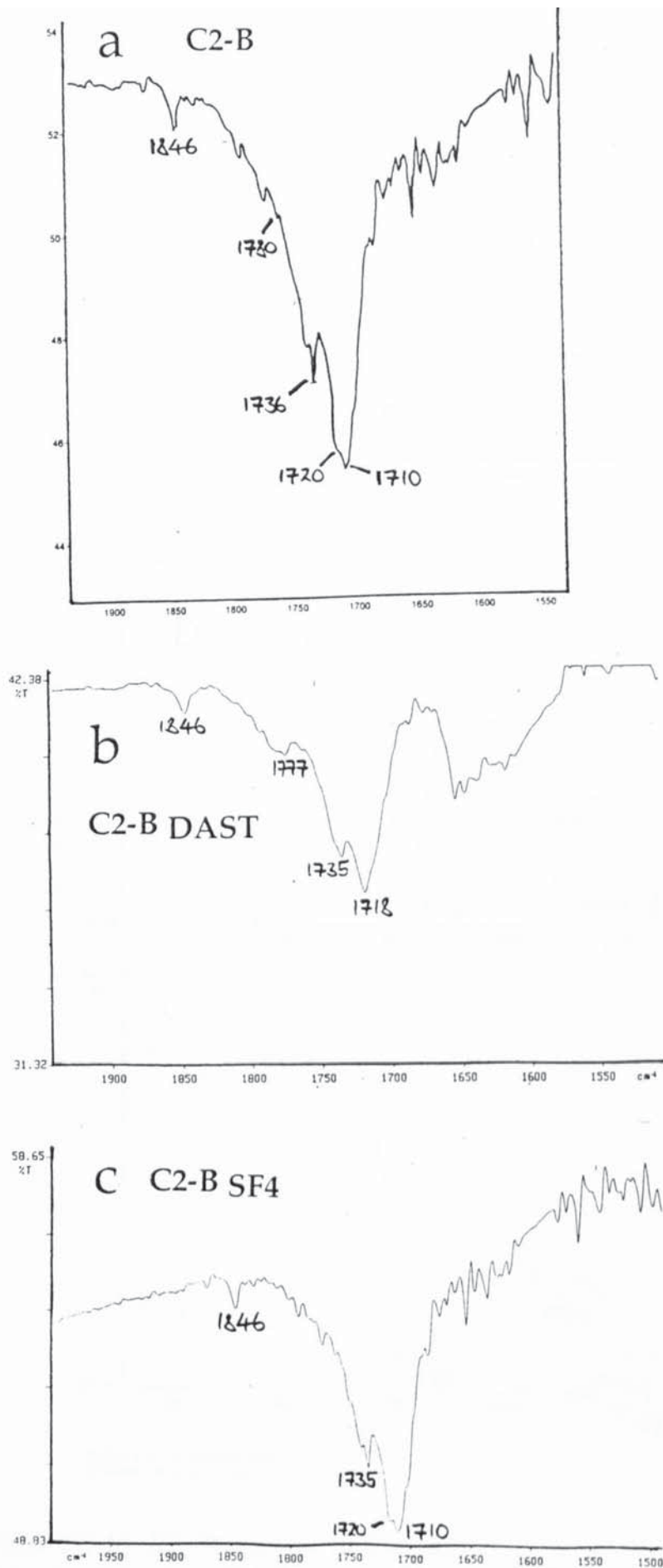


Figure 5.15: FT-IR spectra in the carbonyl region of photooxidised C2 (a); photooxidised polymer derivitised with DAST (b) and photooxidised polymer derivitised with SF4 (c) for 10 hours.

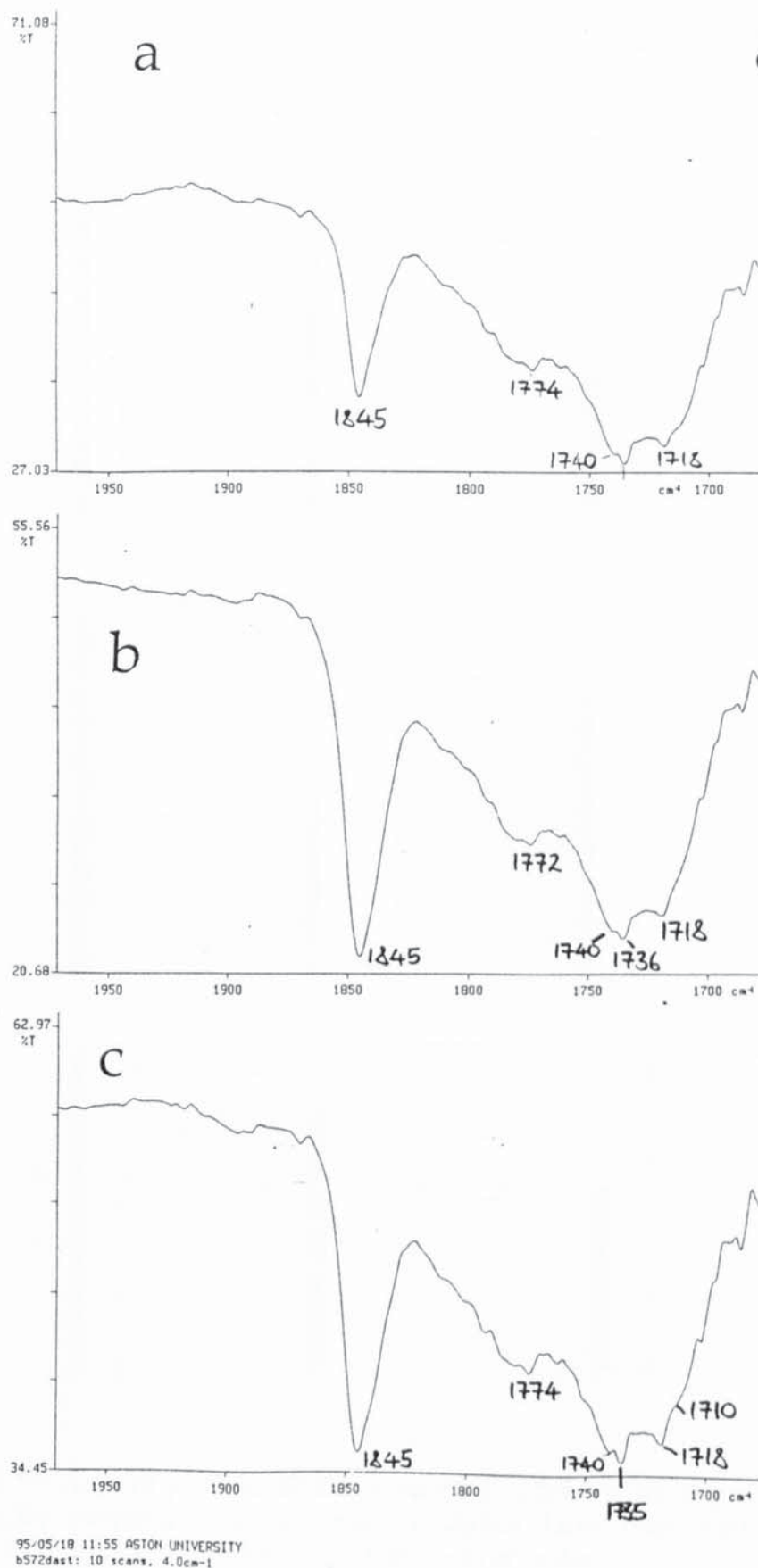


Figure 5.16: FT-IR spectra in the carbonyl region of photooxidised polymer Bo1 derivitised with DAST for 24 hours (a), 48 hours (b) and 72 hours (c).

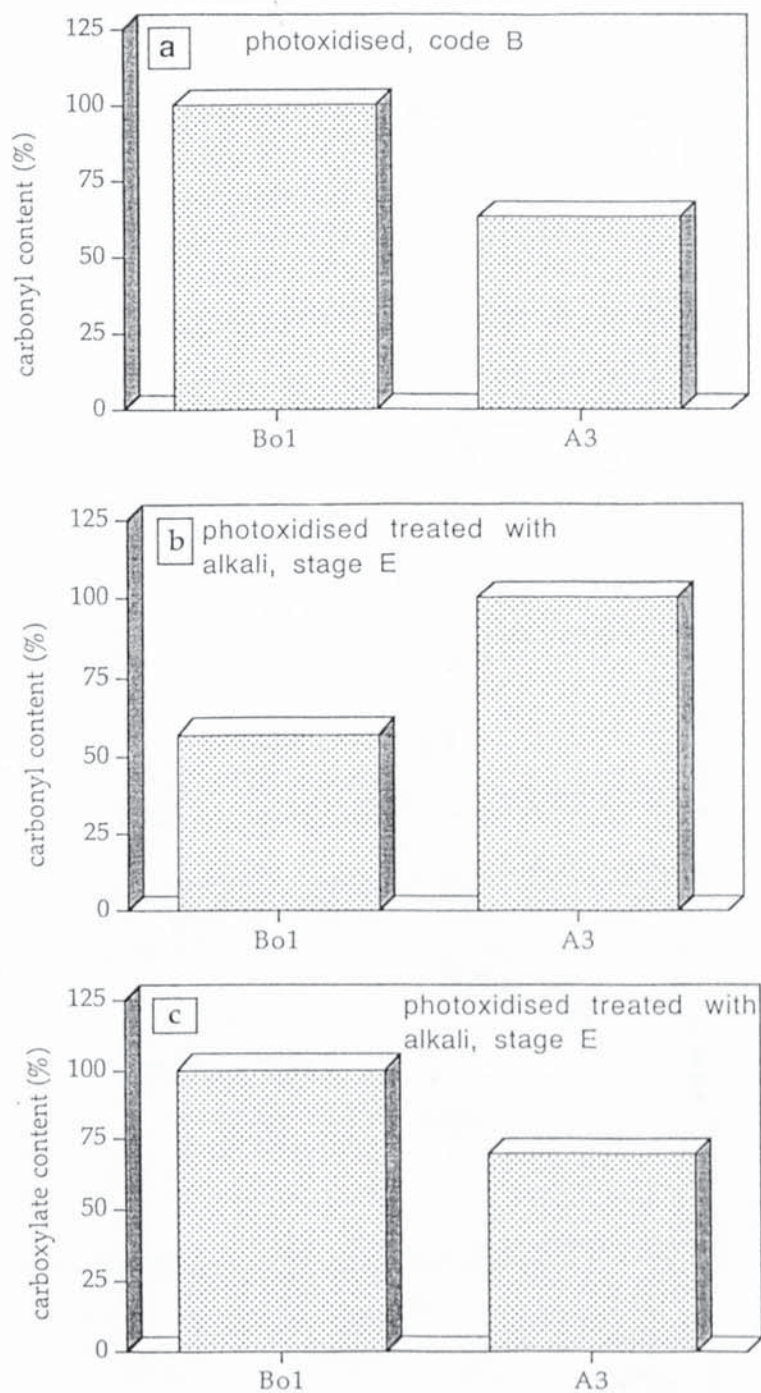


Figure 5.17: Area of photoxidation products (%) before (a) and after 1M NaOH extraction (b=carbonyl, c=carboxylate) measured in samples Bo1 and A3, see schemes 5.3 and 5.4 for codes.

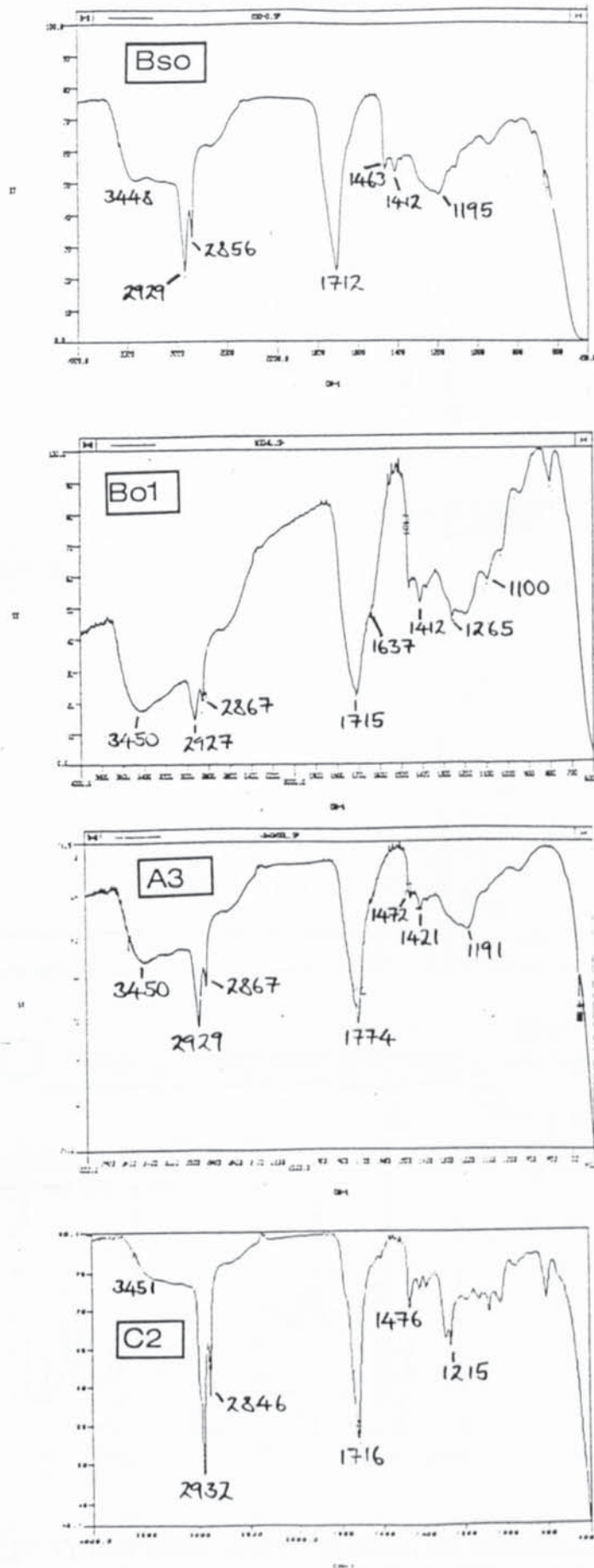


Figure 5.18: FT-IR spectra (NaCl plates) of extracted photooxidation products (code D) of samples Bso, Bo1, A3 and C2 at stage D in schemes 5.1-5.5, see table 5.14.

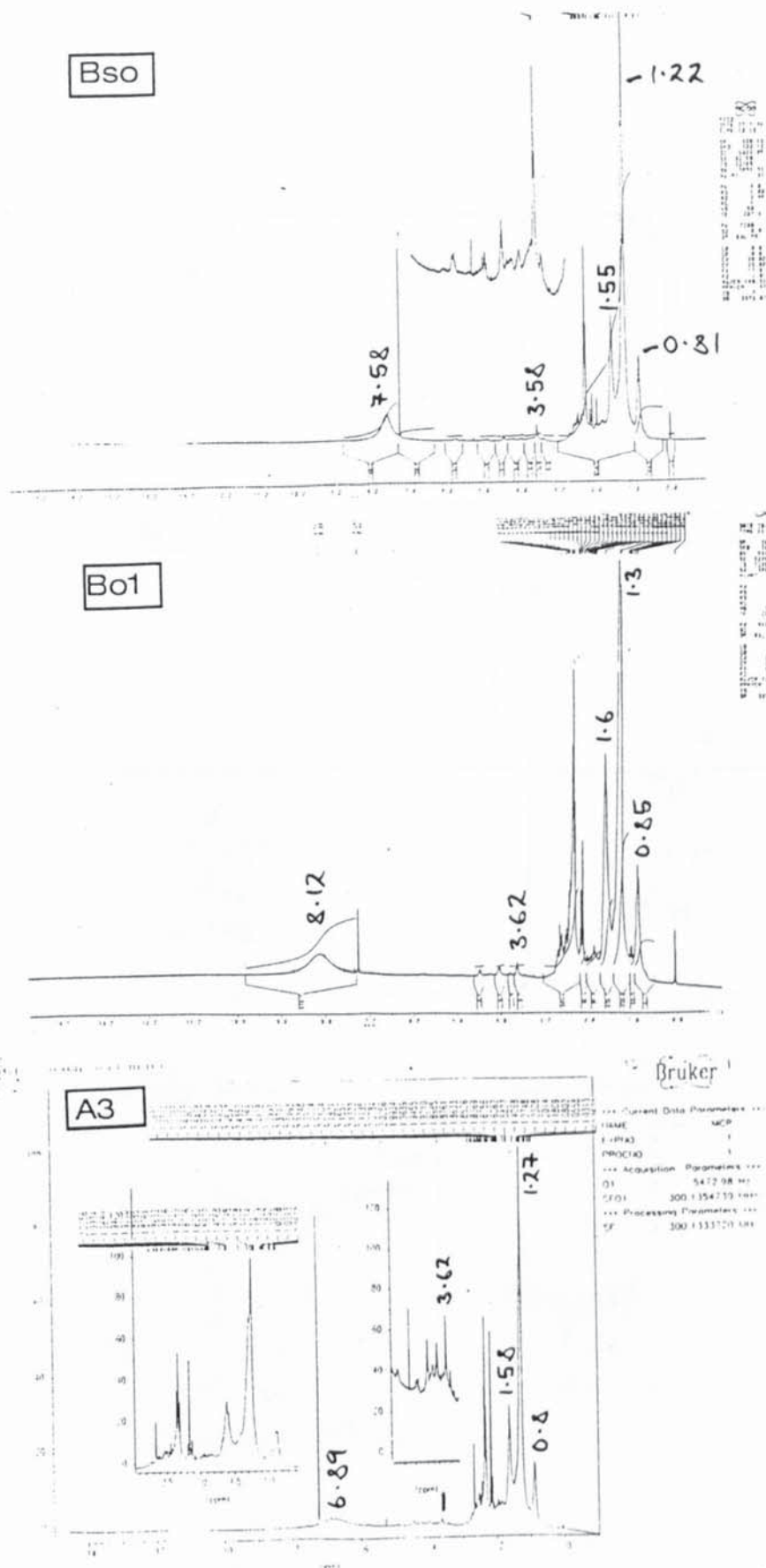


Figure 5.19: Proton NMR spectra of extracted photooxidation products of samples Bso, Bo1 and A3 (code D in schemes 5.1 to 5.5). Numbers on peaks are chemical shifts, ppm.

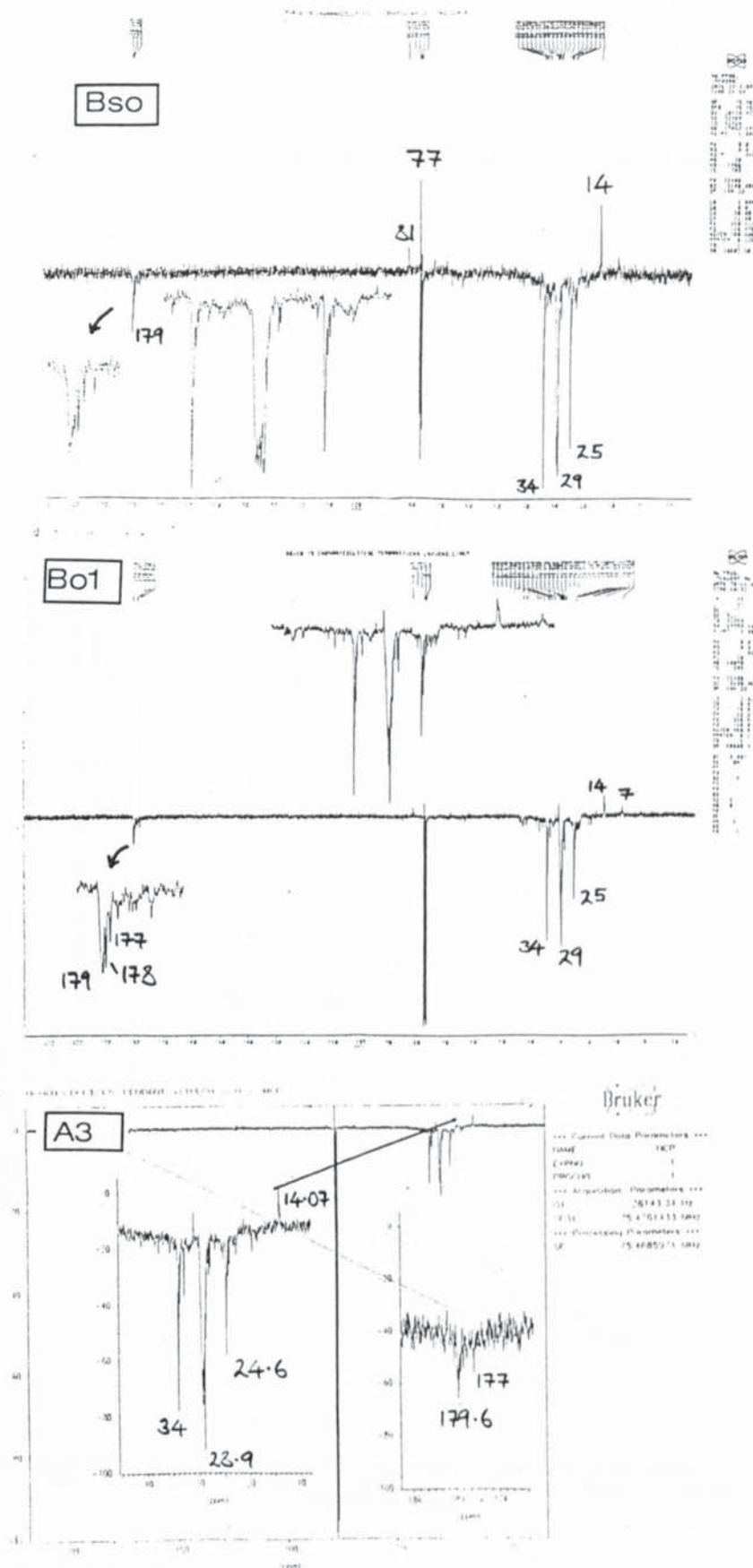


Figure 5.20: Carbon NMR spectra of extracted photooxidation products of samples Bso, Bo1 and A3 (code D in schemes 5.1 to 5.5)  
 Numbers on peaks are chemical shifts, ppm.

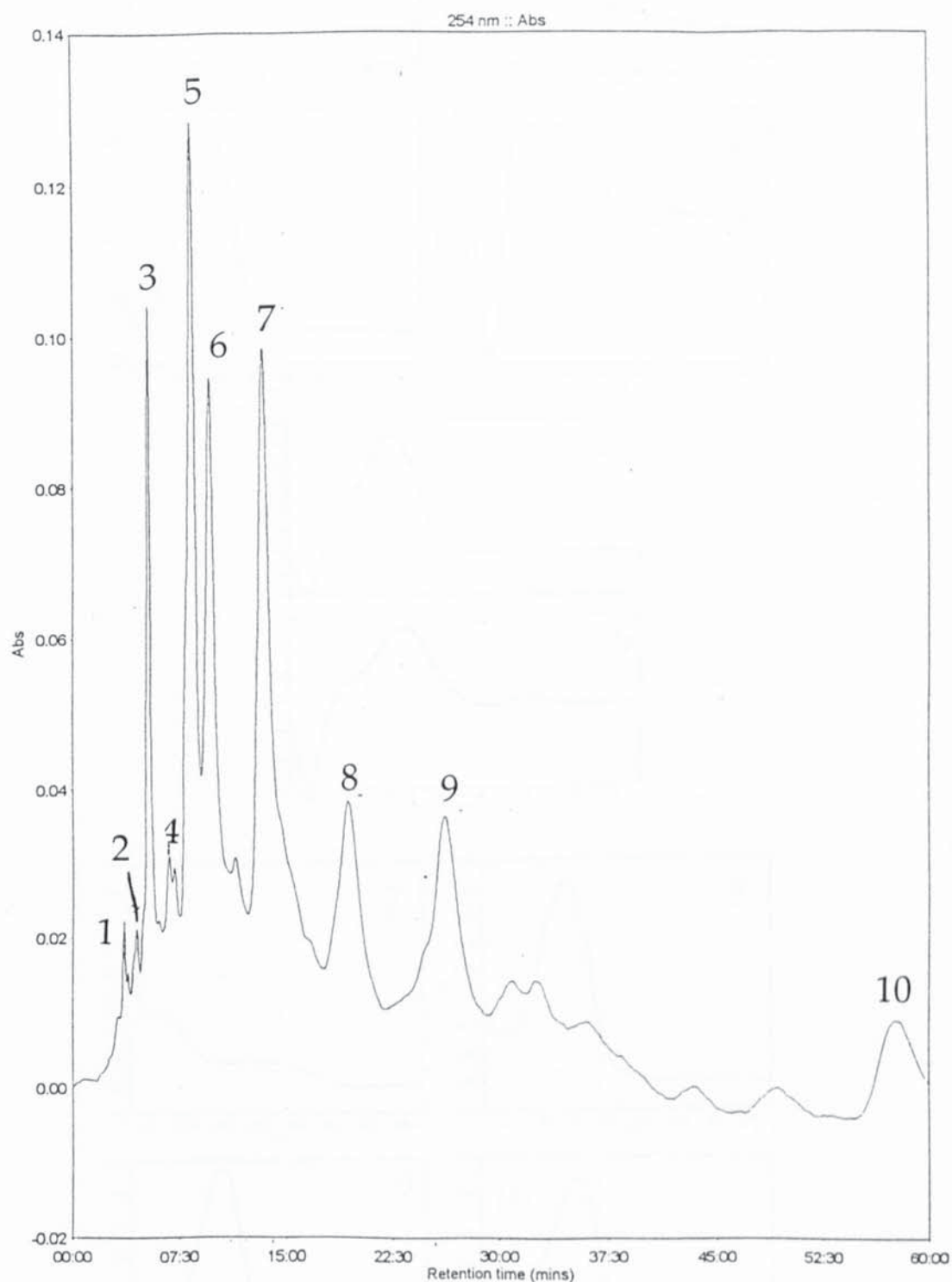


Figure 5.21: HPLC chromatogram of the extracted photooxidation products (code D) of sample Bo1, see scheme 5.4  
conditions: reverse phase Hamiltons PRP-1 column  
85% 1mM Phosphoric acid: 15% acetonitrile  
flowrate = 1ml/min, temp= 19°C  
wavelength of detection = 254 nm

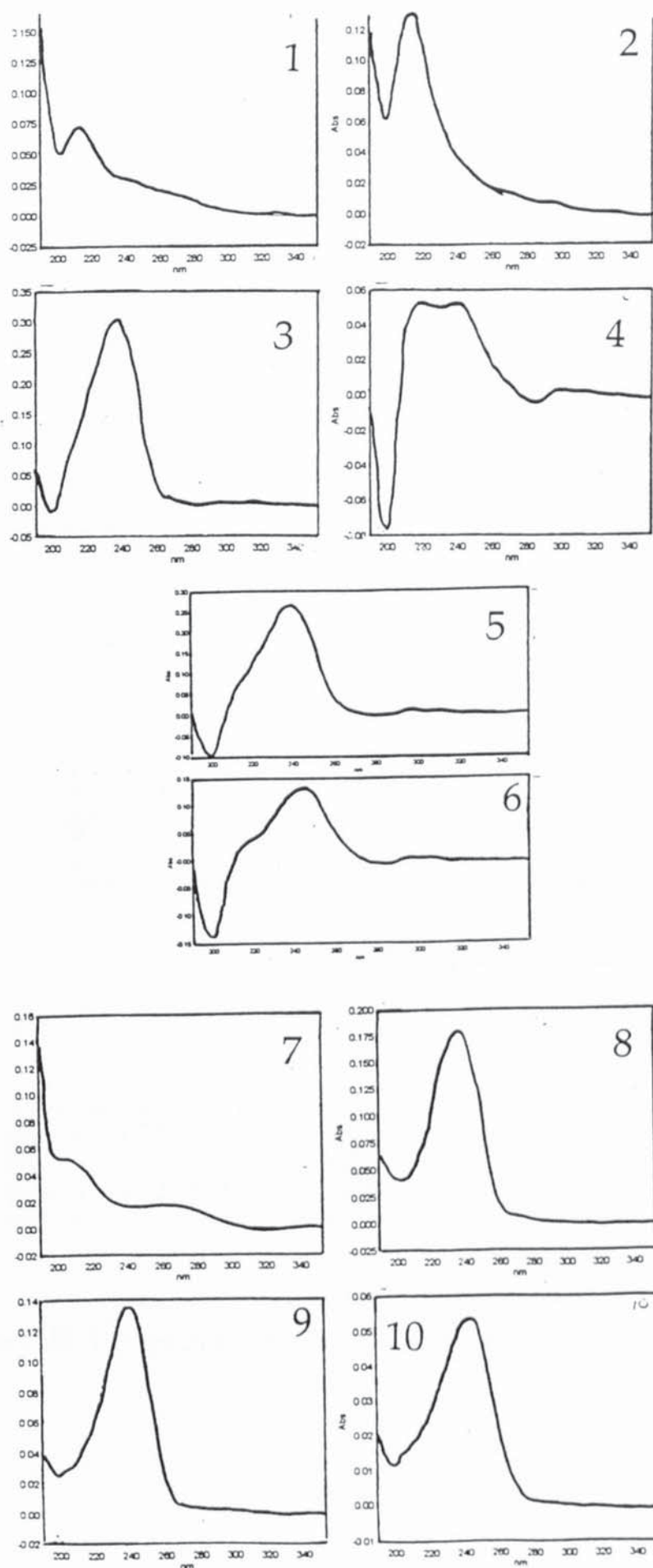
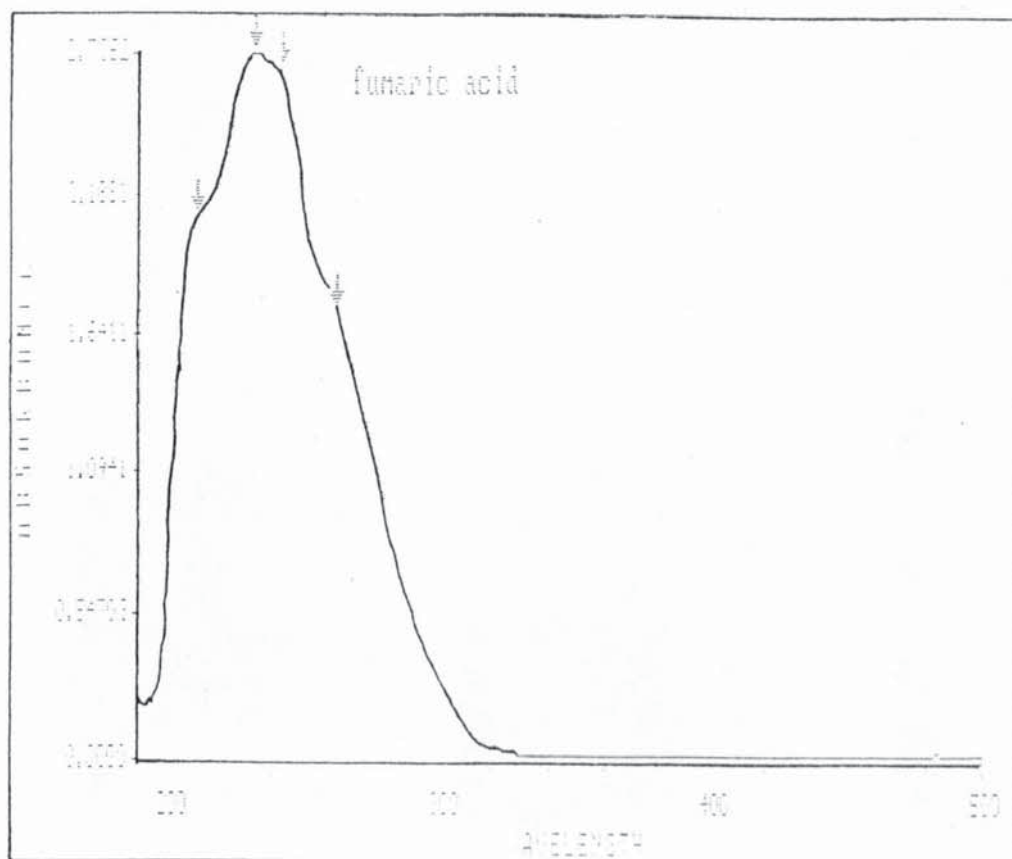


Figure 5.22: UV spectra of the ten chromatographic peaks observed for extracted photooxidation products of sample Bo1.



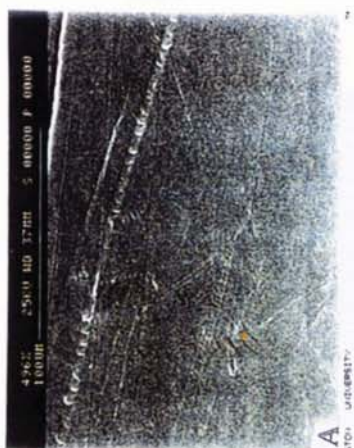
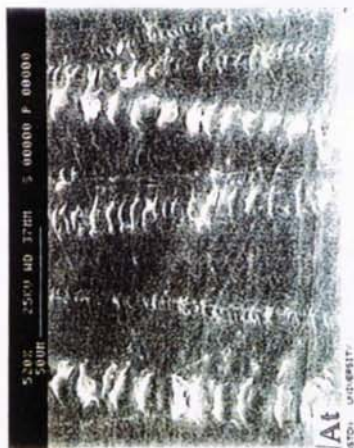
Marked Wavelengths

Reg A: L 262 =	1.7279
Reg A: L 242 =	2.6641
Reg A: L 232 =	2.7352
Reg A: L 210 =	2.0912

Figure 5.23: UV spectra of Fumaric acid.

# A3: PHOTOLYTIC COPOLYMER PE SYSTEM. ABIOTIC OXIDATION

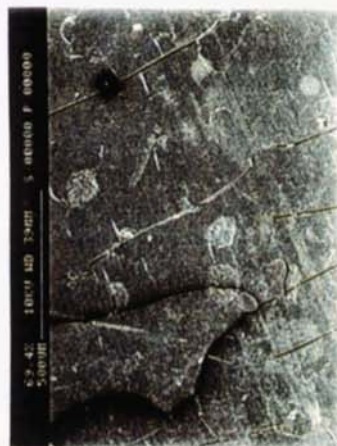
NON-OXIDISED  
NON-TREATED A



PHOTOXIDISED  
NON-TREATED B



PHOTOXIDISED  
TREATED E



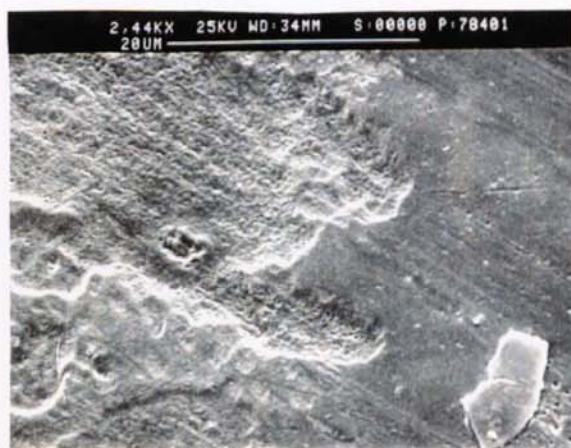
# A3: PHOTOLYTIC COPOLYMER PE SYSTEM

## BIOTIC DEGRADATION

control  
buried  
Ab

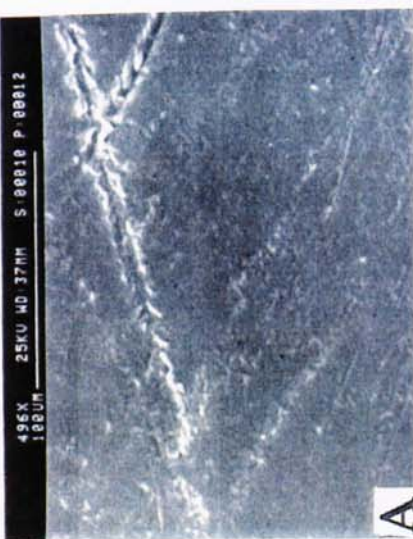


Photo  
oxidised  
buried F

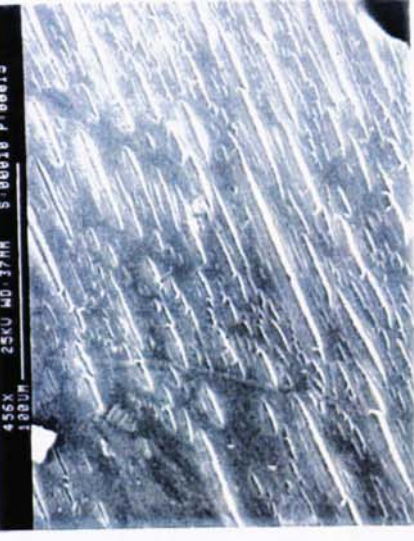


**BO1: PHOTO-ACTIVATOR PE SYSTEM CONTAINING IRON DITHIOCARBAMATE**

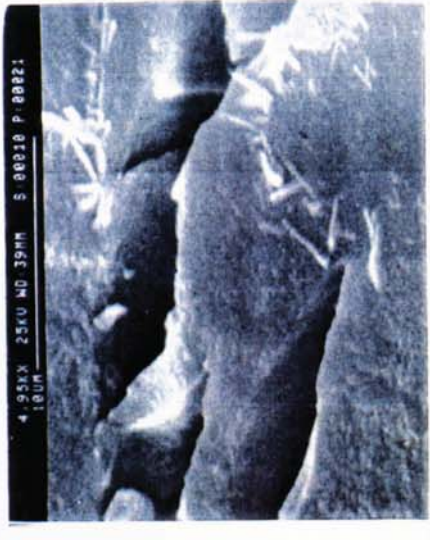
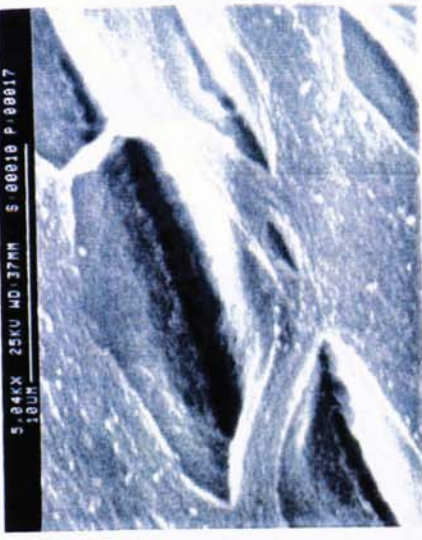
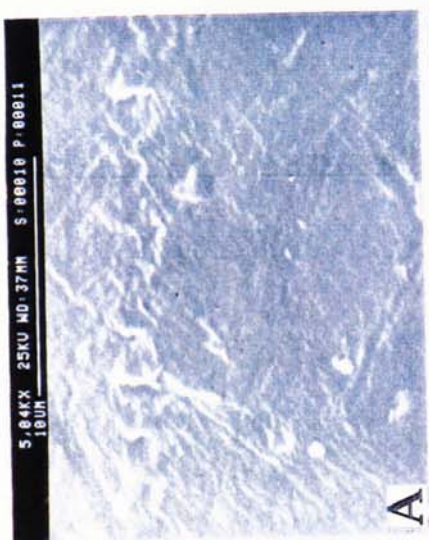
NON-OXIDISED  
NON-TREATED **A**  
NON-OXIDISED  
TREATED **At**



PHOTOXIDISED  
NON-TREATED **B**



PHOTOXIDISED  
TREATED **E**



# BO1: METAL CARBOXYLATE PE SYSTEM

## BIOTIC DEGRADATION

control  
buried  
Ab

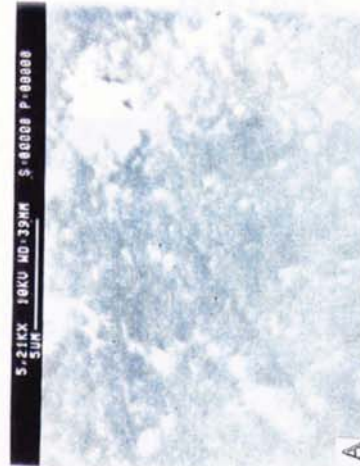
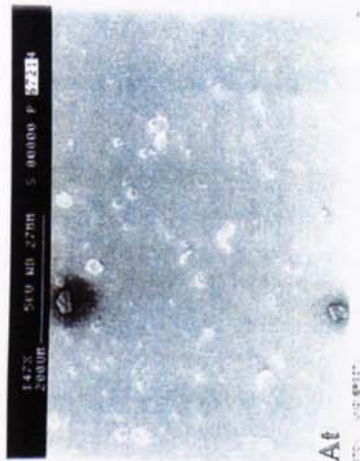
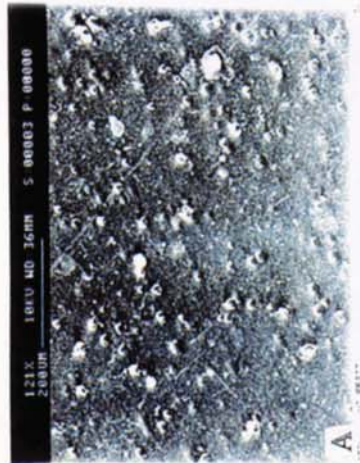


Photo  
oxidised  
buried F



**C2: STARCH FILLED PE SYSTEM CONTAINING IRON  
STEARATE AND TITANIUM DIOXIDE PIGMENT, ABIOTIC OXIDATION**

**NON-OXIDISED  
NON-TREATED A**



**NON-OXIDISED  
NON-TREATED A1**

**PHOTOXIDISED  
NON-TREATED B**



**PHOTOXIDISED  
TREATED E**



## C2: STARCH-FILLED PE SYSTEM

### BIOTIC DEGRADATION

control  
buried

Ab

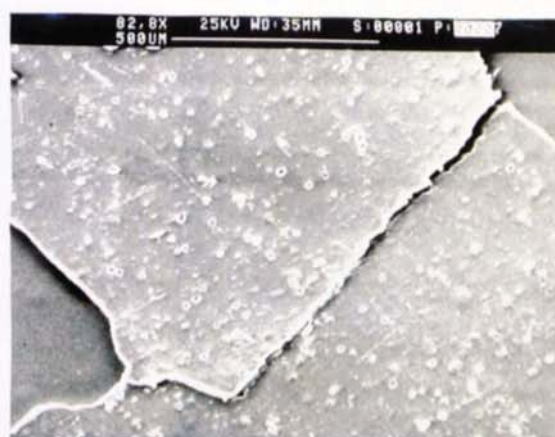
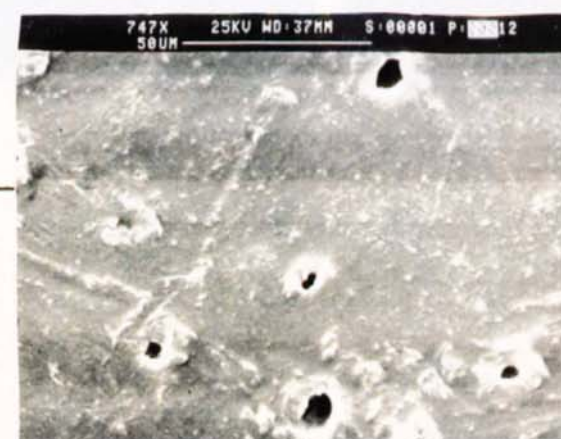


Photo  
oxidised  
buried F



# BSO (control): UNSTABILISED LDPE ABIOTIC AND BIOTIC DEGRADATION

control A



control treated with alkali At



control buried Ab



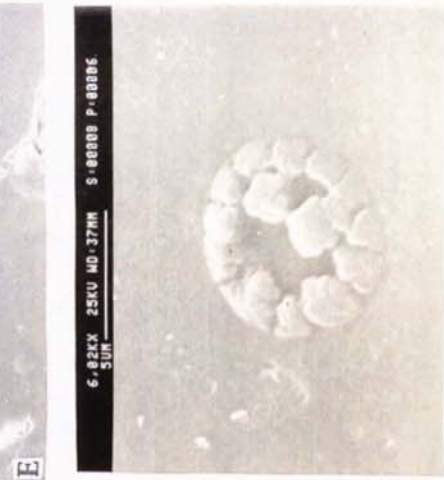
photoxidised B



photoxidised treated with alkali E



photoxidised buried F



## CHAPTER VI

# CONCLUSIONS AND RECOMMENDATIONS FOR FURTHER WORK

## CHAPTER VI

## CONCLUSIONS AND RECOMMENDATIONS FOR FURTHER WORK

## 6.1 CONCLUSIONS

The necessary requirements for the commercial and laboratory extruded polyolefins to degrade were investigated by oxidising the degradable polymer samples in different environments (thermal and photooxidation, natural and accelerated). The nature of the photooxidation products formed in the different degradable polymer samples was examined, and the mechanism of degradation evaluated. The compatibility of the degradables with recycling of other polyolefins was also undertaken.

6.1.1 All the examined degradables showed much faster rates of photooxidation compared to the unstabilised LDPE, the rates being highly dependent on the photooxidation mechanism. However, only the antioxidant photoactivator systems (polymer B5 and Bsx series) showed an induction period and offered time-controlled degradation. The length of the induction period was found to be dependent on the concentration of Ni dithiocarbamate.

6.1.2 Photooxidation and thermal degradation of all degradable polymer samples (and unstabilised LDPE) led to an increase in carbonyl products formed in the polymer. The major carbonyl products identified in all the systems were primarily carboxylic acids (and to a lesser extent ketones, esters and lactones). The build up of these photooxidation products imparts hydrophilicity to the inherent hydrophobic polymer films.

- 6.1.3 The ECO degradable polymer sample (A3) showed much lower levels of carboxylic acids formation compared to the metal carboxylate based degradable system (Bo1). This is due to the predominance of the Norrish II mechanism during photooxidation of the ECO sample, giving rise mainly to ketones and vinyl groups. The metal degradable system, however, was shown to photodegrade mainly via a Norrish I mechanism, resulting in the formation of a variety of carboxylic acids as the major photooxidation products.
- 6.1.4 Experiments have shown that the degradable samples studied in this work are compatible with recycling of other polymers. The addition of representative commercial degradable plastics to PE as homogeneous and heterogeneous blends at the level of 10% by weight (photoxidised and non-photoxidised) has shown that the loss in initial mechanical properties was minimal. Controlling the recycling conditions (for example temperature) led to even smaller loss in mechanical properties. The effects on long term performance (during uv irradiation) were found to be more adverse, and depended largely on the photo sensitisation mechanism of the degradable polymer.
- 6.1.5 The degradable samples degraded in the environment via a two stage mechanism. The primary stage was abiotic, which resulted in the breakdown of the polymer chains into smaller fragments and increased hydrophilicity. The increased surface area and the formation of the hydrophilic bioassimilable photooxidation products allowed the secondary stage of bio-erosion by microorganisms to take place.

## 6.2 RECOMMENDATIONS FOR FURTHER WORK

- 6.2.1 Recyclates of degradables based on metal dithiocarbamates showed least adverse effects on properties, suggesting that degradables can be recycled with a minimal loss if additional melt and photostabilisers are used. Therefore, recycling of degradables using melt and uv stabilisers needs to be examined to substantiate the findings of this work.
- 6.2.2 The importance of the analysis of extracted photooxidation products is apparent in understanding the mechanism of photobiodegradation. Time constraints and limited access to more advanced techniques such as HPLC coupled to mass spectroscopy (HPLC-MS) or NMR (HPLC-NMR) hindered the progress of this part of the research. Hence, this part of the study could easily be continued for further research into the characterisation of degradation products. The chromatographic procedure needs finer tuning to give further baseline resolution, and the individual resolved peaks can then be analysed online using a coupled MS or NMR spectrophotometers. This advanced method of analysis will not only separate the mixture of carboxylic acids but will also allow the identification of the different acids formed.
- 6.2.3 Finally, to complement the understanding of the mechanism of degradation, a particular interest for future work would be the bioassimilation studies of the extracted photooxidation products. This would serve two purposes: the first is to assess if the photooxidation products formed are toxic to microorganisms (and thus alleviate some of the criticisms voiced against degradable polymers on grounds of their unknown toxicity affects on the microorgansims).

The second would be to determine the extent of biodegradation of these photooxidation products.

## REFERENCES

## REFERENCES

1. Scott, G. Chapter 9: "Photobiodegradable Plastics" in Degradable polymers; Principles and applications. Scott, G and Gilead, D (eds.). Chapman and Hall publishers (1994).
2. Gilead, D. Chapter 10: "Photodegradable Plastics in Agriculture" in ref. 1.
3. Tabbari, A. Chapter 11: "The Role of Degradable Polymers in Agricultural Systems" in ref. 1.
4. Guillet, J. Chapter 12: "Plastics and the Environment" in ref. 1.
5. Scott, G and Gilead, D. Chapter 13: "Degradable Polymers in Waste and Litter Control" in ref. 1.
6. Guillet, J. H. Chapter 1: "Polymers with Controlled Lifetimes" in Polymers and Ecological Problems. Plenum Press, New York (1973).
7. Scott, G. "Letter to the Editor" in Int. J. environment. studies, **7**, 131, (1975).
8. Coglan, A. "Most biodegradable Plastics are a Con" in New Scientist 8 February, (1992).
9. Degradable Materials: Perspectives, Issues and Opportunities. Barenberg, S.A; Brash, J.L; Narayan, R and Redpath, A.E (eds.). CRC press, Washington (1990).
10. Biodegradable Polymers and Plastics. Vert, E (eds.). RSC publishers, (1992).
11. Nir, M. M. "Implications of Post Consumer Plastics Waste" in Plastics Eng. **36** (9), 29, (1990).
12. Galante, D. "Degradables Losing 'Green Support'" in Plastics Technology. April (1990).
13. Bolland, J. L. "Kinetics of Olefin Oxidation" in Quart. Review. **3**, 1, (1949).
14. Hawkins, W. L. Chapter 1: " Environmental Deterioration of Polymers" in Polymer Stabilisation-1. W. L. Hawkins (Ed). Wiley-Interscience Publishers, New York, (1972).
15. Carlsson, D. J; Wiles, D. M. "The Photoxidative Degradation of Polypropylene. Part II. Photostabilisation Mechanisms" in Journal Macromolecules sci.- Rev. macromol. Chem. **14**(2), 155, 1976.

- 16 Carlsson, D. J; Wiles, D. M. "The Photoxidative Degradation of Polypropylene. Part I. Photooxidation and Photoinitiation Processes" in Journal Macromolecules sci.- Rev. macromol. Chem. **14**(1), 65, 1976.
- 17 Al-Malaika, S. Chapter 2: "Autoxidation" in Atmospheric Oxidation and Antioxidants, Vol. I. Scott. G. (Ed). Elsevier Science Publishers, (1993).
- 18 Harber, F; Weiss, J. "The Catalytic Decomposition of Hydrogen Peroxides by Iron Salts" in Proceedings of Royal Society, London A. **147**, 332, (1934).
- 19 Chalk, A. J; Smith, J. F. "Catalysis of Cyclohexane Autoxidation by Trace Metals in Non Polar Media" in Transactions of Faraday Society. **53**, 1214, (1957).
- 20 Chien, J. C. W; Vanderberg, E. J; Jabloner, H. "Polymer Reactions III. Structure of Polypropylene Hydroperoxides" in Journal of Polymer Science. Part A1, **6**, 381-392, (1968).
- 21 Rabek, J. F. Chapter 1: "Introduction to Photoxidative Degradation. Mechanisms of Polymers" in Photostabilisation of Polymers: Principles and Applications. Elsevier publishers, London (1990).
- 22 Bateman, L; Morris, A. L. "Initiation Efficiencies in Olefin Autoxidation" in Transactions of Faraday Society. **48**, 1149, (1952).
- 23 Bateman, L; Morris, A. L. "The Autoxidation of 2:6-Dimethylhepta-2:5-diene" in Transactions of Faraday Society. **49**, 1026, (1953).
- 24 Al-Malaika, S; Chakroborty, K. B; Scott, G, Chapter 3: "Peroxidolytic mechanisms" in Developments in Polymer Stabilisation-6. Scott (ed). Applied Science Publishers, London (1983).
- 25 Scott, G. Chapter 1: "Autoxidation and Antioxidants: Historical Perspective" in Atmospheric Oxidation and Antioxidants, Vol. I. Scott. G. (Ed) Elsevier Publishers, (1993).
- 26 Scott, G. Chapter 4: "Antioxidant: and Chain-breaking Mechanisms" in ref. 25.
- 27 Al-Malaika, S. Chapter 5: "Antioxidants - Preventive Mechanisms" in ref. 25.
- 28 Scott, G. Chapter 1: "Mechanisms of Antioxidant Action" in Developments in Polymer Stabilisation-4. Scott, G (ed.). Applied Science Publishers, London (1981).

- 29 Bagheri, R, Chakroborty, K. B; Scott, G. "Mechanisms of Antioxidant Action: Behaviour of a Hindered Piperidine and Related Oxidation Products during Processing and Photoxidation of Polypropylene" in Polymer Degradation and Stability. **4**, no.1, 1-16, (1982).
- 30 Bagheri, R, Chakroborty, K. B; Scott, G. "Mechanisms of Antioxidant Action: Transformation of 4-Hydroxy-2,2,6,6-Tetramethylpiperidine (HTMPO) in Polypropylene during Processing" in Journal of Polymer science. **22**, 1573, (1984).
- 31 Adeniyi, J. B, Al-Malaika, Scott, G. "Mechanisms of Antioxidant Action: The Role of Nitroxyl Radicals in the Stabilisation of PVC" in Journal of Applied Polymer Science. **32**, 6063-6071, (1986).
- 32 Al-Malaika; Omikorede, E. O; Scott, G. "Mechanisms of Antioxidant Action: Mechanochemical Transformation Products of 2,2,6,6-Tetramethyl-4-Hydroxypiperidinoxyl in Polypropylene" in Journal of Applied Polymer Science. **33** (3), 703-714, (1987).
- 33 Bagheri, R; Chakroborty, K. B; Scott, G. "Mechanisms of Antioxidant Action" in Polymer Degradation and Stability. **5**, 81, (1973).
- 34 Pospisil, J. Chapter 1:"Chain breaking Antioxidants in Polymer Stabilisation" in Developments in Polymer Stabilisation-1. Ed. Scott, G. Applied Science Publishers, London (1979).
- 35 Dennison, G. H. "Oxidation of Lubricating oils" in Industrial Engineering Chemistry, **36**, 477, (1944).
- 36 Kennerly, G.W; Patterson, W. L. "Kinetic studies of Petroleum Antioxidants" in Industrial Engineering Chemistry, **48**, 1917, (1956).
- 37 Shelton, J. Chapter 2: "Stabilisation against Thermal Oxidation" in Polymer stabilisation, Hawkins, W.L. Ed, Wiley, New York (1972).
- 38 Hawkins, W; Sautter, H. "Synergistic Antioxidant Combinations. Mechanism of Stabilisation with organo-sulphur Compounds" in Journal of Polymer Science. A1, **Z**, 3499, (1963).
- 39 Al-Malaika; Chakroborty, K.B; Scott, G; Tao, Z. B. "Mechanisms of Antioxidant Action: The Photo antioxidant Mechanism of 4-alkyl-2-MercaptoThiazolines in Polypropylene " in Polymer Degradation and Stability. **13**(3), 261-276, (1985).
- 40 Al-Malaika; Chakroborty, K. B; Scott, G; Tao, Z. B. "Mechanisms of Antioxidant Action: The behaviour of 4-alkyl-2-mercaptothiazolines during Thermal and Photoxidation of Polypropylene " in Polymer Degradation and Stability. **10**(1), 55-66, (1985).

- 41 Al-Malaika; Chakroborty, K. B; Scott, G. Chapter 3: "Peroxidolytic Antioxidants" in Developments in Polymer Stabilisation-6. Scott, G. (ed.). Applied Science Publishers, London (1983).
- 42 Al-Malaika; Marogi, A; Scott, G. "Mechanisms of Antioxidant Action: Transformations Involved in the Antioxidant Function of Zinc Dialkyl Dithiocarbamate. I" in Journal of Applied Polymer Science. **30**, 789-797, (1985).
- 43 Al-Malaika; Marogi, A; Scott, G. "Mechanisms of Antioxidant Action: Transformations Involved in the Antioxidant Function of Metal Dialkyl Dithiocarbamate. III" in Journal of Applied Polymer Science. **33**(5), 1455-1472, (1987).
- 44 Al-Malaika; Marogi, A; Scott, G. "Mechanisms of Antioxidant Action: Transformations Involved in the Antioxidant Function of Zinc Dithiocarbamate. II" in Polymer Degradation and Stability. **10**, 237-245, (1985)
- 45 Al-Malaika. Chapter 3: in Mechanisms of Polymer Degradation and Stability-9. Scott, G. (Ed). Elsevier Applied Science Publishers, London, (1990).
- 46 Al-Malaika; Scott, G: "Mechanisms of Antioxidant Action: Transformations Involved in the Antioxidant Function of Nickel Dithiolates" in European Polymer Journal . **16**, 503-509, (1980).
- 47 Scott, G. Chapter 7: "Photostabilisation of Polyolefins" in Developments in Polymer Degradation-1. Grassie, N. (Ed) Applied Science Publishers, London (1977).
- 48 Amin, M.U; Scott, G. "Photo-initiated Oxidation of Polyethylene - Effect of Photosensitisers" in European Polymer Journal . **10**, 1019-1028, (1974).
- 49 Martin J. T; Norrish, R. G. W. Proceedings of Royal Society A195. 376, 391, (1948-9).
- 50 Norrish, R. G. W; Serbey, M. H. Proceedings of Royal Society A237. 30, (1956).
- 51 Ranby, B; Rabek, J. F Chapter 2: "General Mechanism of Polymer Degradation" in Photodegradation, Photoxidation and Photostabilisation of Polymers. Wiley-Interscience Publishers England (1975).
- 52 Cassidy, P. E; Aminabhavi, T. J. "Enhanced Environmental Degradation of Plastics" in J. Macromolecules science.- Review. macromol. Chemistry. **21**(1), 89, (1981).

- 53 Gilead, D. "Photodegradable Films for Agriculture" in Polymer Degradation and Stability. **29**, 65, (1990).
- 54 Baum, B; Deanim, R. D. "Controlled UV Degradation in Plastics" in Polymer Plastics Technology Eng. **2**(1), 1, (1973).
- 55 Scott, G; "Plastics with Controlled Stability. Their Contribution to Waste Disposal" in Proceedings of American Chemical Society Division of Polymeric materials: Science and Eng. **V.63**, 956, (1990)
- 56 Guillet, J. E; Chapter 55: "Photodegradable Plastics" in 1st Int. Sci. Conc. Workshop on Degradable Materials. CRC press, (1989).
- 57 Lafayette, N; Narayan, R. "Environmentally Degradable. Plastics" in Kunstooffe (ENG), **79**, 92, (1989).
- 58 Griffin, G. J. Chapter I: in ref. 56.
- 59 Stevenson, R. "Biodegradable Polymer" in Chemistry In Britain, June (1990)
- 60 Clavely, J. "Mixed Reception for degradable Biopol" in European Plastics News. June (1990).
- 61 Cox, M. 2nd Int. Sci. Conc. Workshop on Degradable Materials. CRC press, (1991).
- 62 Cox, M. "The effect of Material Parameters on the Properties and Biodegradation of Biopol" in Biodegradable Polymers and Plastics. M. Vert (Ed), (1991).
- 63 Scott, G. "Plastics with Controlled Biodegradability. From concept to Realisation" in Arabian Journal for Science and Engineering **13** (4), (1988).
- 64 Tighe, B; Yasin, M. "Polymers for Biodegradable Medical Devices" in Biomaterials. **vol. 8** July, (1987).
- 65 Griffin. G.J. "Biodegradable Fillers in Thermoplastics" in American Chemical Society, Division Organic Coatings, Plastics Chemistry. **33**, 88, (1973)
- 66 Iannotti, G. "Studies of Environmental Degradation of Starch based Plastics" in ref. 56. p.425
- 67 Maddev, A; Campbell, PD. "Modified Starch based Environmentally Degradable Plastics" in ref. 56 p.237

- 68 Allenza, P; Scollmeyer, J; Rohrbach, R. P. "Evaluating Biodegradable Plastics with in Vitro Enzyme Assays - Additives which Accelerate the Rate of Biodegradation" in ref. 56. p.357
- 69 Gilead, D; Scott, G. Chapter 5: "Time Controlled Stabilisation of Polymers" in Developments in Polymer Stabilisation-5. Applied Science Publishers, London (1982). Scott, G (Ed).
- 70 Albertsson, A.C. "The Shape of the Curve for Low and High Density PE in Prolonged Series of Experiments" in European Polymer Sci. **29**, 623-630, (1980).
- 71 Hartley, G; Guillet, J. "Photochemistry of Ketone Polymers. I. Studies of Ethylene-Carbon Monoxide Copolymers" J. Macromolecules. **1**(2), 165, (1968).
- 72 Americk, Y; Guillet, J. "The Photochemistry Of Ketone Polymers, IV: Photolysis Of Methyl Vinyl Ketone Copolymers " in Macromolecules. **4**, 375, (1971).
- 73 Alexandra, L; Guillet, J. E. "Photochemistry of fibre forming polymers. II. Ketone containing polyethylene terephthalate" in Journal of Applied Polymer Science Chem. ed. **14**, 2791, (1976).
- 74 Cernia, E; Marconi, W; Palladino, N; Bacchin. "Synthesis and Photodegradation Behaviour of PE containing Side chain Keto Ether groups " in Journal of Applied Polymer Science. **18**, 2085-2093, (1974).
- 75 Harper, D. J; McKellar, J. F. "Mechanism of the Benzophenone-Sensitised Photodegradation of PP" in Journal of Applied Polymer Science. **17**, 3503-3508, (1973).
- 76 George, G. A; Hodgeman, D. "Quantitative Phosphorence Spectroscopy of Polystyrene during Photodegradation and the Significance of inchain peroxides" in European. Polymer. J. **9**, 219, (1977).
- 77 Melloir, D. C; Moir, A. B; Scott, G. "The Effect of Processing Conditions on the UV Stability of Polyolefins" in European. Polymer. J. **9**, 219, (1973).
- 78 Al-Malaika, Marogi, A, Scott. G. "Mechanisms of Antioxidant Action: time Controlled Photoantioxidants for PE based on soluble Iron Compounds" in J. Applied Polymer Science. **31**, 685, 1986.
- 79 Al-Malaika, Marogi, A, Scott. G. "Mechanisms of Antioxidant Action: Transformations Involved in the Antioxidant Function of Metal Dialky Dithiocarbamates III" in J. Applied Polymer Science. **33**, 1455, (1987).

- 80 Al-Malaika, Marogi, A, Scott. G. "Mechanisms of Antioxidant Action: Time-Controlled Stabilisation of PP by Transition Metal Dithiocarbamates" in Polymer Degradation and Stability. **18**, 89-98, (1987).
- 81 Adams, J. H; Goodrich. "Analysis of Non-volatile Oxidation of PP, II: Process Degradation" in Journal of Polymer Science. **8**, 1269, (1970).
- 82 David, C; Trojan, M; Daro, A. "Photodegradation of PE: Comparison of various Photoinitiators in Natural Weathering Conditions" in Polymer Degradation and Stability. **37**, 233, (1992).
- 83 Severini. F; Galla, R; Ipsale, S; Ricca, G. "Environmental Degradation of LDPE observed by UV Spectroscopy" in Polymer Degradation and Stability. **41**, 103, (1993).
- 84 Albertsson, A.C; Andersson, S.O; Karlsson, S. "The Mechanism of Biodegradation of Polyethylene". in Polymer Degradation and Stability. **18**, 73, (1987).
- 85 Adams, J. H. "Analysis of the Non-volatile Oxidation Products of Polypropylene I. Thermal Oxidation" in J. of Polymer Science. **8**, 1077, (1970).
- 86 Adams, J. H. "Analysis of the Non-volatile Oxidation Products of Polypropylene III. Photodegradation" in J. of Polymer Science. **8**, 1279, (1970).
- 87 Carlsson, D. J; Brousseau, R; Miles, D. M. "Reaction of Sulphur Dioxide with Oxidised Polyolefins" in Polymer Degradation and Stability. **15**, 67, (1986).
- 88 Carlsson, D. J; Brousseau, R; Zhang, C; Miles, D. M. "Polyolefin Oxidation: Quantification of Alcohol and Hydroperoxide Products by Nitric Oxide Reactions" in Polymer degradation and Stability. **17**, 303, (1987).
- 89 Carlsson, D. J; Brousseau, R; Zhang, C; Miles, D. M. Chapter 27 "Identification of Products from Polyolefin Oxidation by Derivatization Reactions". in Chemical Reactions of Polymers. American Chemical Society Publishers (1988).
- 90 Tidjani, A; Arnaud, R. "Photoxidation of Linear LDPE: A Comparison of Photoproducts Formed Under Natural and Accelerated Exposure" in Polymer Degradation and Stability. **39**, 285, (1993).
- 91 Wilhelm, C; Gardette, J. "Infrared Identification of carboxylic Acids formed in Polymer Photoxidation' in J. Applied Polymer Science. **51**, 1411, (1994).

- 92 Frostling, H; Hoff, A; Jacobsson, S; Pfaffli, P; Vainiotalo, S; Zitting, A; Techn, D. "Analytical, Occupational and Toxicological aspects of the Degradation of Products of Polypropylene Plastics" in Scandinavian. J. Work Environment. health. **10**, 1984, (163).
- 93 Gagman, A; Jacobsson, S. "Analysis of Volatile Organic Compounds in Polymers by Dynamic Headspace-multi-dimensional Gas Chromatography-Mass Spectrometry" in J. of Chromatography. **395**, 271, (1987).
- 94 Albertsson, A. C; Karlsson, S. "Degradation of Polyethylene and Degradation Products" in Proceedings of the American Chemical Society Division of polymeric materials: Science and Eng. **62**, 976, (1990).
- 95 Bravo, A; Hotchkiss, J. H. "Identification of Volatile Compounds Resulting from the Thermal Oxidation of Polyethylene" in J. Applied Polymer Science. **47**, 1741, (1993).
- 96 Albertsson, A. C; Karlsson, S. "Environment-adaptable Polymers" in Polymer Degradation and Stability. **41**, 345, (1993).
- 97 Anon. "Degradable Plastics Generate Controversy in Solid Waste Issues" in Chem. and Eng. Z, June 25, 1990.
- 98 ASTM D882: Tensile properties of thin plastic sheeting.
- 99 Scott, G. Chapter 4:"Oxidation of Polymers" in Polymer Degradation and Stability. Grassie, N and Scott, G (eds.). Cambridge University Press, (1988).
- 100 ASTM G7: Natural weathering of polymers.
- 101 Davies, A; Gardener, D. "Determination of UV Radiation Intensity using Polysulphone Film" in Polymer Testing. **7**, 345-353, (1987).
- 102 Brydson, J. A. Chapter 10 "Polyethylene" in Plastics Materials. 4th Edition. Butterworth Scientific publishers, (1982).
- 103 Homer, J; Perry, M. "New Method for NMR Signal Enhancement by Polarisation Transfer, and Attached Nucleus testing" in J. Chemical Society, Chem. Communication. **373**, (1994).
- 104 Chakroborty, K. C; Scott, G. "The effects of Thermal Processing on the Thermal Oxidative and Photoxidative Stability of LDPE" in European Polymer Journal. **13**, 731-737, (1977).
- 105 Scott, G. Chapter 6: "Substantiative Antioxidants" in Developments in Polymer Stabilisation-4. 1st Edition. Scott (ed.). Applied Science Publishers, (1981).

- 106 Shelton, J. Chapter 2: "Organic Sulphur Compounds as Preventive Antioxidants" in ref 105.
- 107 Al-Malaika, Marogi, A, Scott. G. "Mechanisms of Antioxidant Action: Time Controlled Photoantioxidants for PE based on soluble Iron Compounds" in J. Applied Polymer Science. **31**, 685, (1986).
- 108 Scott, G. "Photobiodegradable Plastics: Their Role in the Protection of the Environment" in Polymer Degradation and Stability. **29**, 131, (1990).
- 109 Allen, N. S; Homer, J; Mckellar, J. F. "Origin and Role of the luminescent species in the Photoxidation of Commercial Polypropylene" in Journal of Applied Polymer Science. **21**, 2261-2267, (1977).
- 110 Day, R. E. "Role of Titanium dioxide Pigments" in Polymer Degradation and Stability. **29**, 73-93, (1990).
- 111 Leonas, K. "Pigments and their Additives that Influence the Degradation Rate of Polyethylene Films" in Textile Chemist and Colorism. **24**(10), 13-16, (1992).
- 112 Al-Malaika, S; Scott, G. Chapter 6: "Thermal Stabilisation of Polyolefins" in Degradation and Stabilisation of Polyolefins. Allen, N. S (ed). Applied Science Publishers, (1983).
- 113 Al-Malaika, S; Scott, G. Chapter 7: "Photostabilisation of Polyolefins" in ref 112.
- 114 Stilvala, S. S; Kimura, J; Gabbay, S. M. Chapter 3: "Thermal Degradation and Oxidative Processes" in ref 112.
- 115 Chakroborty, K. C; Scott, G. "The effects of Thermal Processing on the Thermal Oxidation and Photoxidation Stability of LDPE" in European Polymer Journal. **13**, 731-737, 1977.
- 116 Henman, T. S. Chapter 2 "Controlled Crosslinking and Degradation" in ref 112.
- 117 Sadromohagheh, C; Scott, G. "Effects of Reprocessing on Polymers - Part III: Photoxidation of PE-PP blends" in Polymer Degradation and Stability. **3**, 469, (1980).
- 118 Hudlicky, M. Chapter 3: "Fluorination with DAST and Related Aminofluorosulfuranes" in Organic Reactions (1953).
- 119 Brite Euram Project BE-3120-89. Final Report.
- 120 Dabin, P. PhD thesis, Clermont-Ferrand University, France.
- 121 Potts, J; Clendinning, R; Ackart, W; Niegisch, W. p.61 in ref. 6.

**APPENDIX**  
**PUBLISHED WORK**

Page  
Numbering  
as  
Bound

Pages removed for copyright restrictions.